

UC Berkeley

Research Reports

Title

Integration Of Fault Detection And Identification Into A Fault Tolerant Automated Highway System

Permalink

<https://escholarship.org/uc/item/62t7x79s>

Authors

Douglas, Randal K.
Chung, Walter H.
Malladi, Durga P.
et al.

Publication Date

1997

CALIFORNIA PATH PROGRAM
INSTITUTE OF TRANSPORTATION STUDIES
UNIVERSITY OF CALIFORNIA, BERKELEY

Integration of Fault Detection and Identification into a Fault Tolerant Automated Highway System

**Randal K. Douglas, Walter H. Chung, Durga P. Malladi,
Robert H. Chen, Jason L. Speyer and D. Lewis Mingori**
University of California, Los Angeles

**California PATH Research Report
UCB-ITS-PRR-97-52**

This work was performed as part of the California PATH Program of the University of California, in cooperation with the State of California Business, Transportation, and Housing Agency, Department of Transportation; and the United States Department of Transportation, Federal Highway Administration.

The contents of this report reflect the views of the authors who are responsible for the facts and the accuracy of the data presented herein. The contents do not necessarily reflect the official views or policies of the State of California. This report does not constitute a standard, specification, or regulation.

Report for MOU 291

December 1997

ISSN 1055-1425

Integration of Fault Detection and Identification into a Fault Tolerant Automated Highway System

Randal K. Douglas, Walter H. Chung, Durga P. Malladi, Robert H. Chen,
Jason L. Speyer and D. Lewis Mingori

Mechanical and Aerospace Engineering Department
University of California, Los Angeles
Los Angeles, California 90095

Integration of Fault Detection and Identification into a Fault Tolerant Automated Highway System

**Randal K. Douglas, Walter H. Chung, Durga P. Malladi,
Robert H. Chen, Jason L. Speyer and D. Lewis Mingori**

Mechanical and Aerospace Engineering Department
University of California, Los Angeles
Los Angeles, California 90095

December 5, 1997

Integration of Fault Detection and Identification into a Fault Tolerant Automated Highway System

Randal K. Douglas, Walter H. Chung, Durga P. Malladi, Robert H. Chen, Jason L. Speyer
and D. Lewis Mingori

*Mechanical and Aerospace Engineering Department
University of California, Los Angeles
Los Angeles, California 90095*

December 5, 1997

Abstract

This report is a continuation of the work of (Douglas et al. 1996) which concerns vehicle fault detection and identification and describes a vehicle health management approach based on analytic redundancy. A point design of fault detection filters and parity equations is developed for the vehicle longitudinal mode. Data from analytically redundant sensors and actuators are fused in a way that unique, identifiable static patterns emerge in response to a fault. Sensor noise, process disturbances, system parameter variations, unmodeled dynamics and nonlinearities can distort these static patterns. A Shirayev probability ratio test that has been extended to multiple hypotheses examines the filter and parity equation residuals and generates the probability of the presence of a fault. Tests in a high-fidelity vehicle simulation where nonlinearities and road variations are significant are very encouraging. A preliminary design of a range sensor fault monitoring system is outlined as an application of a new decentralized fault detection filter. This system combines dynamic state information already generated by the existing filter designs with inter-vehicle analytic redundancy.

Keywords. Automated Highway Systems, Automatic Vehicle Monitoring, Fault Detection and Fault Tolerant Control, Reliability, Sensors, Vehicle Monitoring.

Integration of Fault Detection and Identification into a Fault Tolerant Automated Highway System

Award No. 65X817, M.O.U. 291

Executive Summary

This report is a continuation of the work of (Douglas et al. 1996) which concerns vehicle fault detection and identification and describes a vehicle health management approach based on analytic redundancy. A point design of fault detection filters and parity equations is developed for the vehicle longitudinal mode. Data from analytically redundant sensors and actuators are fused in a way that unique, identifiable static patterns emerge in response to a fault. Sensor noise, process disturbances, system parameter variations, unmodeled dynamics and nonlinearities can distort these static patterns. A Shirayev probability ratio test that has been extended to multiple hypotheses examines the filter and parity equation residuals and generates the probability of the presence of a fault. Tests in a high-fidelity vehicle simulation where nonlinearities and road variations are significant are very encouraging. A preliminary design of a range sensor fault monitoring system is outlined as an application of a new decentralized fault detection filter. This system combines dynamic state information already generated by the existing filter designs with inter-vehicle analytic redundancy.

Contents

Abstract	v
Executive Summary	vii
List of Figures	xi
List of Tables	xiii
Chapter 1 Introduction	1
Chapter 2 Vehicle Model	7
2.1 Linear Model	8
2.1.1 Linear Model Reduction	9
2.1.2 Vehicle Measurements	10
2.2 Suspension Model	11
2.2.1 Suspension Model With Suspension Length State	12
2.2.2 Suspension Model With Suspension Force State	13
2.2.3 Example	15
2.3 Manifold Temperature Model	16

Chapter 3	Fault Detection By Analytic Redundancy	17
3.1	Analytic Redundancy	18
3.1.1	Beard-Jones Fault Detection Filter Background	19
3.1.2	Fault Modelling	21
3.1.3	Special Design Considerations	23
	Ill-conditioned fault direction	23
	Output separability	23
	Zero steady-state fault residual	25
3.1.4	Fault Assignment to Multiple Fault Detection Filters	27
3.1.5	Fault Detection Filter Design For Sensors	30
3.1.6	Fault Detection Filter Design For Actuators	35
3.2	Algebraic Redundancy	37
3.3	Structure	38
Chapter 4	Fault Detection Filter Evaluation	41
4.1	Residual Scaling	42
4.2	Smooth Road	42
4.3	Rough Road	44
Chapter 5	Residual Processing	55
5.1	Residual Processor Design	56
5.2	Simulations	58
5.3	Conclusions	60
Chapter 6	A Game Theoretic Fault Detection Filter	63
6.1	The Approximate Detection Filter Design Problem	65
6.1.1	Modeling the Detection Problem	65
6.1.2	Modeling Failures	68
6.1.3	Constructing the Failure Signal	69
6.2	A Game Theoretic Solution to the Approximate Detection Filter Design Problem	74
6.2.1	The Disturbance Attenuation Problem	74
6.2.2	The Differential Game Solution	75
6.2.3	Steady-State Results	79
6.3	Applications	80
6.3.1	Accelerometer Fault Detection in an F16XL	80
	Aircraft Dynamics Model	80
	Full-Order Filter Design	81

Analysis	83
6.3.2 Position Sensor Fault Detection for a Simple Rocket, A Time-Varying System	86
Rocket Dynamics Model	86
Full-Order Filter Design	88
Analysis	90
Chapter 7 The Asymptotic Game Theoretic Fault Detection Filter	93
7.1 Finding the Limiting Solution: Singular Differential Game Theory	94
7.2 Conditions for the Nonpositivity of the Game Cost	95
7.3 The Solution to the Singular Differential Game	98
7.4 The Relationship Between the Limiting Game Filter and Detection Filters .	110
7.4.1 A Reduced-Order Detection Filter from the Limiting Game Solution	110
7.4.2 The Invariant Subspace Structure of the Limiting Case Filter	115
7.5 Revisited: Accelerometer Fault Detection in an F-16XL	121
Chapter 8 A Parameter Robust Game Theoretic Fault Detection Filter	125
8.1 Parameter Robustness and FDI	125
8.2 Parameter Robustness versus FDI	127
8.3 A Disturbance Attenuation Problem with Parameter Variations	128
8.3.1 The Modified Disturbance Attenuation Problem	128
8.3.2 Equivalence to the H_∞ Measurement Feedback Control Problem . .	136
8.4 The Robust Game Theoretic Fault Detection Filter in the Limit	138
8.5 Example: Accelerometer Fault Detection in an F16XL with Model Uncertainty	143
8.5.1 Problem Statement	143
8.5.2 Parameter Robust Filter Design	145
Chapter 9 A Decentralized Fault Detection Filter	151
9.1 Decentralized Estimation Theory and its Application to FDI	152
9.1.1 The General Solution	152
9.1.2 Implications for Detection Filters	156
9.2 Range Sensor Fault Detection in a Platoon of Cars	157
9.2.1 Problem Statement	157
9.2.2 System Dynamics and Failure Modeling	158
9.2.3 Decentralized Fault Detection Filter Design	167

Chapter 10 Multiple Model Adaptive Estimation	171
10.1 Problem Statement	173
10.2 MMAE Algorithm	174
10.2.1 Beta Dominance	176
10.3 Adaptive Kalman Filter Algorithm	177
10.4 Performance of AKF Algorithm	180
10.4.1 Underlying Assumptions of MHSSPRT	181
10.4.2 Convergence of the Posterior Probability	183
10.4.3 Convergence of the Posterior Error Covariance	190
10.5 Simulations	199
10.5.1 Example 1	199
10.5.2 Example 2	200
10.5.3 Example 3	202
10.5.4 Example 4	204
10.6 Conclusions	204
10.7 Proofs	206
10.7.1 Proof A	206
10.7.2 Proof B1	208
10.7.3 Proof B2	209
10.7.4 Proof B3	210
Chapter 11 Fault Detection and Identification Using Linear Quadratic Optimization	213
11.1 Problem Formulation	214
11.2 On Line Filter	219
11.3 The Steady State Filter	220
11.4 Proofs	222
Proof A	222
Proof B	223
Chapter 12 Model Input Reduction	227
12.1 Notation	228
12.2 Input-Output Mappings and Model Input Reduction	229
12.2.1 Output Point of View	229
12.2.2 Input Point of View	230
12.2.3 Output and Input Point of View	232
12.3 Application to Disturbance Direction Estimation	233
12.4 Extension to Parameter Variation Model Reduction	235

12.5 Conclusions	237
Chapter 13 Conclusions	239
Appendix A Fault Detection Filter Design Data	241
References	245

List of Figures

Figure 1.1	A System View of Vehicle Health Management	2
Figure 2.1	Simplified suspension and tire model	11
Figure 3.1	Fault Signatures	25
Figure 3.2	Fault Signatures	27
Figure 3.3	Fault Signatures	28
Figure 3.4	Singular value frequency response from all faults to throttle residual . .	37
Figure 3.5	Fault Signatures	39
Figure 4.1	Residuals for fault detection filter one	45
Figure 4.2	Residuals for fault detection filter one	45
Figure 4.3	Residuals for fault detection filter two	46
Figure 4.4	Residuals for fault detection filter three	46
Figure 4.5	Residual for fault detection filter four	47
Figure 4.6	Residual for fault detection filter five	47
Figure 4.7	Residual for fault detection filter six	48
Figure 4.8	Residuals for fault detection filter one when there is no fault	49

Figure 4.9	Residuals for fault detection filter one when a +2 deg throttle actuator fault occurs	49
Figure 4.10	Residuals for fault detection filter one when a -2 deg throttle actuator fault occurs	50
Figure 4.11	Residuals for fault detection filter one when a brake actuator fault occurs	50
Figure 4.12	Residuals for fault detection filter one when a manifold air mass sensor fault occurs	51
Figure 4.13	Residuals for fault detection filter one when a manifold temperature sensor fault occurs	51
Figure 4.14	Residuals for fault detection filter two	52
Figure 4.15	Residuals for fault detection filter three	52
Figure 4.16	Residual for fault detection filter four	53
Figure 4.17	Residual for fault detection filter five	53
Figure 4.18	Residual for fault detection filter six	54
Figure 5.1	Ramp fault in manifold air mass sensor	60
Figure 5.2	Probability of a fault in the manifold temperature sensor as a ramp fault in manifold air mass sensor is applied	61
Figure 5.3	Ramp fault in throttle actuator	61
Figure 5.4	Ramp fault in Brake actuator	62
Figure 5.5	Ramp fault in Vertical accelerometer	62
Figure 6.1	F-16XL example: singular value plot of accelerometer fault transmission vs. wind gust transmission	84
Figure 6.2	F-16XL example: target fault transmission vs. sensor noise transmission	85
Figure 6.3	Rocket example: failure signal response	90
Figure 7.1	Reduced-Order Detection Filter Performance for the F-16XL Example .	122
Figure 8.1	F-16XL example: signal transmission in the parameter robust game theoretic fault detection filter with a 15% shift in eigenvalues	147
Figure 8.2	F-16XL example: signal transmission in the standard game theoretic fault detection filter with a 15% shift in eigenvalues	148
Figure 9.1	A two-car platoon with a range sensor	157
Figure 9.2	Platoon example: signal transmission in the local detection filter on car # 1	168
Figure 9.3	Platoon example: signal transmission in the local detection filter on car # 2	168

Figure 9.4	Platoon example: signal transmission in the global detection filter	169
Figure 9.5	Platoon example: failure signal response of the decentralized fault detection filter	169
Figure 10.1	Multiple Model Adaptive Estimation - Lainiotis Filters	175
Figure 10.2	Adaptive Kalman Filter Algorithm	177
Figure 10.3	Off-line computation of Λ_{kj} , Λ_{ki} and S_{ki}	200
Figure 10.4	Adaptive Kalman Filter Performance - Change from H_0 to H_1	201
Figure 10.5	$E [\delta P_{ki}]$ vs. t_k	202
Figure 10.6	Adaptive Kalman Filter Performance - Change from H_0 to H_2	203
Figure 10.7	$E [\delta P_{ki}]$ vs. t_k	204
Figure 10.8	Adaptive Kalman Filter Performance - Change from H_0 to H_1	205
Figure 10.9	$E [\delta P_{ki}]$ vs. t_k	206
Figure 10.10	Adaptive Kalman Filter Performance - Change from H_0 to H_2	207
Figure 10.11	$E [\delta P_{ki}]$ vs. t_k	208

List of Tables

Table 5.1	Faults organized into analytically redundant groups	56
Table 5.2	Fault hypotheses for residual processing	57
Table 5.3	Applied faults for residual processor testing	59

CHAPTER 1

Introduction

THIS REPORT is a continuation of the work of (Douglas et al. 1996) which concerns vehicle fault detection and identification and describes a vehicle health management approach based on analytic redundancy. A system view of vehicle health management is summarized by Figure 1.1. Vehicle dynamics, which could be a high-fidelity nonlinear simulation or a real vehicle, are driven by throttle, brake and steering commands, various unmeasured exogenous influences such as road variations and wind and faults. Sensors measure a possible nonlinear function of the dynamic states and are corrupted by noise, biases and faults of their own. A fault detection module uses the sensor measurements and known dynamic inputs to produce a conditional probability of a fault hypothesis. The fault hypothesis is generated in two stages. First, a residual generator formed as a combination of linear observers and algebraic parity equations produces a static pattern uniquely identified with a given fault or no-fault condition. Since the static patterns are only clearly identifiable in nominal operating conditions, the second stage, a residual processor, interrogates the

residual and matches it to one of many known patterns. The pattern matching is done with a probabilistically based algorithm so the residual processor produces a fault hypothesis probability rather than a simple binary announcement. A simple threshold mapping could be added very easily to produce a binary announcement if that were needed. A fault hypothesis probability is passed to a vehicle health monitoring and reconfiguration system. These components determine the impact of the possible fault on safe vehicle operation and adjust control laws if necessary to accommodate a degraded operating condition. These components are being developed by the UC Berkeley team.

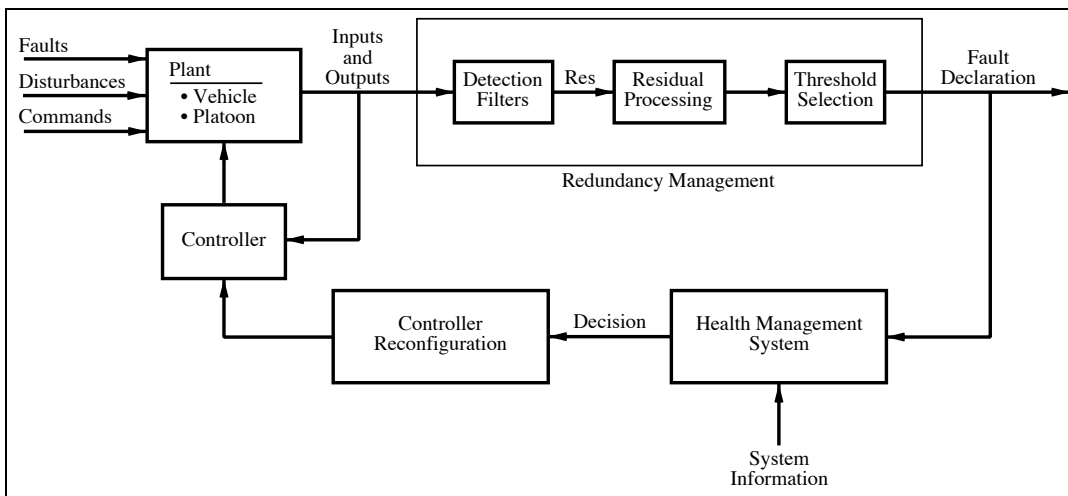


Figure 1.1: A System View of Vehicle Health Management.

Chapters 2, 3, 4 and 5 describe a fault detection and identification system that is designed to meet the requirements of a module in a comprehensive health monitoring and reconfiguration system under development at UC Berkeley. The system is a point design. It is designed to detect faults in sensors and actuators associated with the longitudinal motion of the modeled vehicle. The vehicle has a nominal operating speed of 25 meters per second and is travelling straight ahead. The nonlinear vehicle and road model used for simulation and the reduced-order linear models used for fault detection filter design are described in Chapter 2. The fault detection filter design is discussed in Chapter 3. The performance of the fault detection filter is evaluated in Chapter 4. Finally, a residual processor design

based on a multiple hypothesis Shiriyayev sequential probability ratio test is described in Chapter 5.

In Chapters 6, 7 and 8 a new disturbance attenuation approach to fault detection filter design is described. First reported in chapter 9 of (Douglas et al. 1996), this is a completely rewritten presentation with many improvements. Here, a differential game is defined where one player is the state estimate and the adversaries are all the exogenous signals except for the fault to be detected. By treating faults as disturbances to be attenuated, the usual invariant subspace structure associated with fault detection filters is not present except in the limit. By treating model uncertainty as another element in the differential game, sensitivity to parameter variations can be reduced.

Also introduced is the notion of a fault detection filter for time-varying systems. This is especially important in applications where a vehicle follows a maneuver such as a merge or a split. While first considered in the game theoretic filter derivation, it is expected that the Beard-Jones fault detection filter definition will be extended to time-varying systems in the same way.

In Chapter 9 a decentralized fault detection filter is described. This filter is the result of combining the game theoretic fault detection filter of Chapters 6, 7 and 8 and introduced by Chung in (Chung and Speyer 1996) and (Chung and Speyer 1998) with the decentralized filtering algorithm introduced by Speyer in (Speyer 1979) and extended by Willsky *et al.* in (Willsky et al. 1982). This approach to health monitoring is well suited to large-scale systems as it breaks the problem into smaller pieces and is easily scalable to the dimensions of the problem. For systems of interest to PATH, such as the multi-car platoons which will populate advanced highway systems, a decentralized approach may be the ideal way to monitor sensors that measure quantities defined by relative vehicle motion, for example, the range and range rate between a vehicle and the vehicle immediately ahead of it. An example illustrates the application of a decentralized fault detection filter to the health monitoring of a range sensor.

In Chapter 10 an approach to fault detection is described that combines the residual

generation and residual processing components into a single coherent design. This is a specialization of a class of adaptive estimation problems where a system is an undetermined element of a set of system models.

A common approach to adaptive estimation is the Multiple Model Adaptive Estimation algorithm as first proposed by (Magill 1965) and later generalized by (Lainiotis 1976) to form the framework of partitioned algorithms. Here the problem domain is restricted to linear stochastic systems with time-invariant parametric uncertainty. With the parametric uncertainty expressed as a set of hypotheses, the multiple model estimation algorithm is formed as a joint estimation and system identification algorithm consisting of a bank of Kalman filters, each matched to one hypothesis, and an identification subsystem, which may be interpreted as a sub-optimal multiple hypothesis Wald's sequential probability ratio test. In addition to a system state estimate, a product of the algorithm is a set of probabilities, conditioned on the measurement history, that the hypotheses match the true system, that is, the system underlying the measurement history. As shown in (Athans 1977), there is no proof that the probability of the hypothesis associated with the 'true' system will converge to one. Furthermore, the algorithm exhibits *beta dominance* (Menke and Maybeck 1995), which arises out of incorrect system modeling and leads to irregular residuals. Finally, the algorithm is computationally intensive since filters for each hypothesis are propagated.

A new approach to adaptive estimation is based on a single adaptive Kalman filter where time-varying system model parameters are updated by feeding back the posterior probability of each hypothesis conditioned on the residual process. It is shown that the expected value of the true posterior probability converges to one and, under certain assumptions, the expected value of the norm of the difference between the constructed error covariance and the true posterior error covariance converges to a lower bound. It is also shown that in the presence of modeling errors, the filter converges to the hypothesis which maximizes a certain information function. The application to fault detection and identification follows the use the dynamics of a multiple hypothesis Shiriyayev sequential probability ratio test, an algorithm that explicitly allows for parametric transitions in the system model.

In Chapter 11 a new approach to the residual generation problem for fault detection and identification based on linear quadratic optimization is presented. A quadratic cost encourages the input observability of a fault that is to be detected and the unobservability of disturbances, sensor noise and a set of faults that are to be isolated. Since the filter is not constrained to form unobservability subspace structures, adjustment of the quadratic cost could realize improved performance as reduced sensor noise and dynamic disturbance components in the residual and reduced sensitivity to parametric variations. In the present form, the filter detects a single fault so the structure could also be described as that of an unidentified input observer. A bank of filters are constructed when multiple faults are to be detected.

In Chapter 12 a new model input reduction algorithm is presented. This work was motivated by the need for improved disturbance direction modeling for fault detection filter design. Another application is to control blending but that is not used here. In disturbance decoupling problems where the disturbance is meant to model neglected higher-order or nonlinear dynamics, determination of the direction from first principles is not always possible or practical. When the disturbance direction is found empirically, typically several directions are found, each one associated with a different operating point, and a suitable representative direction must be chosen. The problem is complicated further when the rank of the disturbance map is not known, that is, when it is not clear how many directions should be chosen from the empirically derived set.

CHAPTER 2

Vehicle Model

IN THIS CHAPTER, vehicle models are developed for the design and evaluation of fault detection filters. A high-fidelity six degree of freedom nonlinear vehicle model described in last year's report (Douglas et al. 1996) allows for arbitrary variations in road slope and road noise. An object-oriented vehicle simulation is implemented in C++ and is currently hosted on an Apple Macintosh PowerPC 8100 computer.

Linear models for the longitudinal vehicle dynamics are derived numerically from the nonlinear vehicle simulation using a central differences method. The models are described in Section 2.1 and the derivation method is described in (Douglas et al. 1996). Model order reduction issues related to the suspension model are discussed in Section 2.2.

The manifold temperature measurement model is discussed in Section 2.3. To monitor the health of the manifold temperature sensor, an analytically redundant relationship for the manifold temperature has to be found. Since the temperature enters the engine model as a constant, a state model would introduce an unobservable integrator. An alternative is to let the temperature be a known, that is measured, input to the engine.

2.1 Linear Model

The linearized longitudinal dynamics of the vehicle are derived numerically from high-fidelity nonlinear simulation using a central differences method. The nonlinear model and the central differences method are described in detail in (Douglas et al. 1996). The linearization is done at a single nominal operating point of 25 meters per second, about 56 miles per hour, where the car is travelling straight ahead. Since the car is not in a turn, the linear longitudinal dynamics decouple completely from the linear lateral dynamics. The longitudinal model has thirteen states and three inputs. Two of the inputs, throttle and brake actuator commands are regarded as controls. The third input is the manifold temperature and is regarded as a known, that is measured, exogenous input.

States:	m_a : Manifold air mass.
	ω_e : Engine speed.
	v_x : Longitudinal velocity.
	z : Vertical position.
	v_z : Vertical velocity.
	θ : Pitch angle.
	q : Pitch rate.
	$\bar{\omega}_f$: Sum of front wheel speeds.
	$\bar{\omega}_r$: Sum of rear wheel speeds.
	\bar{F}_f : Sum of front suspension forces.
	\bar{F}_r : Sum of rear suspension forces.
	α : Throttle state.
	T_b : Brake state.
Control inputs:	u_α : Throttle command.
	u_{T_b} : Brake command.

Exogenous input: ω_{T_m} : Manifold temperature.

The lateral model states and inputs are given for completeness although they are not used.

States: v_y : Lateral velocity.
 ϕ : Roll angle.
 p : Roll rate.
 r : Yaw rate.
 $\tilde{\omega}_f$: Difference of front wheel speeds.
 $\tilde{\omega}_r$: Difference of rear wheel speeds.
 \tilde{F}_f : Difference of front suspension forces.
 \tilde{F}_r : Difference of rear suspension forces.
 γ : Steering state.

Control inputs: u_γ : Steering command.

2.1.1 Linear Model Reduction

The thirteenth-order longitudinal model has eigenvalues: -215.62 , -160.79 , $-136.03 \pm 1.67i$, -90.91 , -31.56 , -26.26 , $-2.00 \pm 6.55i$, $-1.32 \pm 5.56i$, -1.25 and -0.0418 . Observe that five of these eigenvalues are significantly faster than the rest. By inspection of the eigenvectors, it is determined that the fast eigenvalues are associated with the states $\bar{\omega}_f$, $\bar{\omega}_r$, \bar{F}_f , \bar{F}_r and α .

A model order reduction is done by dynamic truncation with a steady-state correction. First, the derivatives of the fast states $\bar{\omega}_f$, $\bar{\omega}_r$, \bar{F}_f , \bar{F}_r and α are set to zero. Then, the linear dynamic equations are solved for the fast states in terms of the remaining states: m_a , ω_e , v_x , z , v_z , θ , q and T_b . The result is substituted into the state equations of the remaining states. This process is described in more detail in Section 2.3 of (Douglas et al. 1996). The eigenvalues of the eighth-order reduced-order longitudinal model are -33.01 , -25.87 , $-2.08 \pm 6.45i$, $-1.44 \pm 5.47i$, -1.25 and -0.0451 which are close to the eigenvalues of the

full-order longitudinal model. Also the frequency responses of the reduced and full-order models are close to each other.

The reduced-order linear longitudinal dynamics data are given in Appendix A.

2.1.2 Vehicle Measurements

There are thirteen sensors on the car.

y_{m_a} : Manifold air mass sensor.

y_{ω_e} : Engine speed sensor.

y_{T_m} : Manifold temperature sensor.

y_{p_m} : Manifold pressure sensor.

y_{v_x} : Longitudinal velocity sensor.

y_{a_x} : Longitudinal accelerometer.

y_{a_z} : Vertical accelerometer.

$y_{\omega_{fl}}$: Front left wheel speed sensor.

$y_{\omega_{fr}}$: Front right wheel speed sensor.

$y_{\omega_{rl}}$: Rear left wheel speed sensor.

$y_{\omega_{rr}}$: Rear right wheel speed sensor.

y_{α} : Throttle sensor.

y_{T_b} : Brake sensor.

Since the dynamics naturally decompose into longitudinal and lateral components, the following processed wheel speed sensors form a more natural set of measurements:

$y_{\bar{\omega}_f}$: Sum of front wheel speeds.

$y_{\bar{\omega}_r}$: Sum of rear wheel speeds.

$y_{\tilde{\omega}_f}$: Difference of front wheel speeds.

$y_{\tilde{\omega}_r}$: Difference of rear wheel speeds.

For the longitudinal dynamics, the wheel speed difference sensors $y_{\bar{\omega}_f}$ and $y_{\bar{\omega}_r}$ are not relevant. Also, the throttle and brake sensors y_α and y_{T_b} measure control inputs rather than states. The manifold temperature sensor y_{T_m} measures an exogenous input. Finally, the manifold pressure y_{pm} and manifold air mass y_{m_a} are linearly dependent. Thus, there are only seven sensors that provide measurements linearly related to the vehicle longitudinal states: y_{m_a} , y_{ω_e} , y_{v_x} , y_{a_x} , y_{a_z} , $y_{\bar{\omega}_f}$ and $y_{\bar{\omega}_r}$.

The reduced-order linear longitudinal measurement data are given in Appendix A.

2.2 Suspension Model

The suspension system is modelled as a nonlinear spring and linear damper. The tire is a mass and linear spring. Since the mass of the tire is very small relative to the car, the tire model is simplified to a linear spring as shown in Figure 2.1. It is possible to

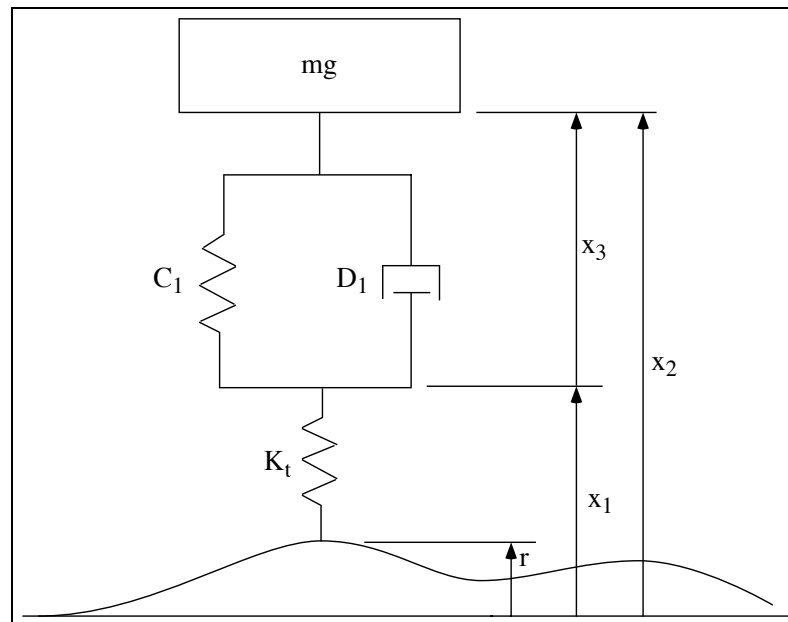


Figure 2.1: Simplified suspension and tire model.

express the dynamics of the suspension model using either suspension force or suspension length as states. Although both realizations are meant to model the same physical system, their reduced-order linearized dynamics can be very different. In the following sections,

two representations of the suspension model and their reduced-order linearized models are derived. In Section 2.2.1, suspension length is used as the suspension state. In Section 2.2.2, suspension force is used as the suspension state. Section 2.2.3 provides more discussion and a numerical example is given to illustrate the modelling difficulty.

2.2.1 Suspension Model With Suspension Length State

In this section, the suspension model uses suspension length as the state. The suspension force F_s acting on each wheel is given by

$$F_s = -C_1(x_3 - x_{30})[1 + C_2(x_3 - x_{30})^4] - D_1\dot{x}_3 + mg \quad (2.1)$$

where x_{30} is the length of the suspension system when a nominal load mg is applied. Compare this with Equation 2.3 of (Douglas et al. 1996).

The force F_t transmitted to the suspension by the tire spring is given by

$$F_t = -K_t(x_2 - x_3 - r - x_{10}) \quad (2.2)$$

where K_t is the tire spring stiffness and x_{10} is the nominal tire radius. Since the tire is massless, the tire spring force is equal to the suspension force.

$$F_t = F_s \quad (2.3)$$

Put (2.1) and (2.2) into (2.3),

$$\dot{x}_3 = \frac{1}{D_1}[-(K_t + C_1)x_3 + K_t x_2 - C_1 C_2 (x_3 - x_{30})^5 - K_t r + (mg + C_1 x_{30} - K_t x_{10})] \quad (2.4)$$

An equation of motion for the chassis given by

$$m\ddot{x}_2 = K_t(-x_2 + x_3 + r + x_{10}) \quad (2.5)$$

provides another relation between x_2 and x_3 .

The dynamics (2.4, 2.5) after a linearization become

$$\frac{d}{dt} \begin{bmatrix} x_2 \\ \dot{x}_2 \\ x_3 \end{bmatrix} = \begin{bmatrix} 0 & 1 & 0 \\ -\frac{K_t}{D_1} & 0 & \frac{K_t}{D_1} \\ \frac{K_t}{D_1} & 0 & -\frac{K_t + C_1}{D_1} \end{bmatrix} \begin{bmatrix} x_2 \\ \dot{x}_2 \\ x_3 \end{bmatrix} + \begin{bmatrix} 0 \\ \frac{K_t}{D_1} \\ -\frac{K_t}{D_1} \end{bmatrix} r$$

with the characteristic equation

$$s^3 + \frac{K_t + C_1}{D_1} s^2 + \frac{K_t}{m} s + \frac{K_t C_1}{m D_1} = 0 \quad (2.6)$$

The linearized dynamics order is reduced by noting that the suspension length state x_3 is fast. See the example in Section 2.2.3. Let $\dot{x}_3 = 0$ and algebraically eliminate x_3 as a linear combination of x_2 and \dot{x}_2 .

$$\frac{d}{dt} \begin{bmatrix} x_2 \\ \dot{x}_2 \end{bmatrix} = \begin{bmatrix} 0 & 1 \\ -\frac{K_t C_1}{m(K_t + C_1)} & 0 \end{bmatrix} \begin{bmatrix} x_2 \\ \dot{x}_2 \end{bmatrix} + \begin{bmatrix} 0 \\ \frac{K_t C_1}{m(K_t + C_1)} \end{bmatrix} r$$

The reduced-order dynamics characteristic equation is

$$s^2 + \frac{K_t C_1}{m(K_t + C_1)} = 0 \quad (2.7)$$

Clearly, the reduced-order dynamics (2.7) are very different from the full-order dynamics (2.6) since the reduced-order dynamics exhibit no damping. The eigenvalues of the full and reduced-order linearized models are evaluated in the example of Section 2.2.3.

2.2.2 Suspension Model With Suspension Force State

In this section, the suspension model uses suspension force as the state. Start with (2.1, 2.2, 2.3) of the last section

$$F_s = -C_1(x_2 - x_1 - x_{30})[1 + C_2(x_2 - x_1 - x_{30})^4] - D_1(\dot{x}_2 - \dot{x}_1) + mg \quad (2.8a)$$

$$F_t = -K_t(x_1 - r - x_{10}) \quad (2.8b)$$

$$F_t = F_s \quad (2.8c)$$

The tire spring force F_t is eliminated by rearranging (2.5) to get

$$x_1 = r + x_{10} - \frac{F_t}{K_t} \quad (2.9a)$$

$$\dot{x}_1 = \dot{r} - \frac{\dot{F}_t}{K_t} \quad (2.9b)$$

and then combining (2.8a), (2.8c) and (2.9) as

$$\dot{F} = \frac{K_t}{D_1} \left\{ -F + mg - C_1(x_2 - r - x_{10} - x_{30} + \frac{F}{K_t}) \right. \\ \left. [1 + C_2(x_2 - r - x_{10} - x_{30} + \frac{F}{K_t})^4] - D_1(\dot{x}_2 - \dot{r}) \right\}$$

where $F \triangleq F_s$. An equation of motion for the chassis is given by combining (2.5) with (2.8b) and (2.8c)

$$m\ddot{x}_2 = F$$

The linearized model is

$$\frac{d}{dt} \begin{bmatrix} x_2 \\ \dot{x}_2 \\ F \end{bmatrix} = \begin{bmatrix} 0 & 1 & 0 \\ 0 & 0 & \frac{1}{m} \\ -\frac{K_t C_1}{D_1} & -K_t & -\frac{K_t + C_1}{D_1} \end{bmatrix} \begin{bmatrix} x_2 \\ \dot{x}_2 \\ F \end{bmatrix} + \begin{bmatrix} 0 & 0 \\ 0 & 0 \\ \frac{K_t C_1}{D_1} & K_t \end{bmatrix} \begin{bmatrix} r \\ \dot{r} \end{bmatrix}$$

with the characteristic equation

$$s^3 + \frac{K_t + C_1}{D_1} s^2 + \frac{K_t}{m} s + \frac{K_t C_1}{m D_1} = 0 \quad (2.10)$$

which is the same as (2.6) as expected.

Again, since the suspension force state F is fast, the reduced-order linearized model is derived by letting $\dot{F} = 0$ and algebraically eliminating F as a linear combination of x_2 and \dot{x}_2 .

$$\frac{d}{dt} \begin{bmatrix} x_2 \\ \dot{x}_2 \end{bmatrix} = \begin{bmatrix} 0 & 1 \\ -\frac{K_t C_1}{m(K_t + C_1)} & -\frac{K_t D_1}{m(K_t + C_1)} \end{bmatrix} \begin{bmatrix} x_2 \\ \dot{x}_2 \end{bmatrix} + \begin{bmatrix} 0 & 0 \\ \frac{K_t C_1}{m(K_t + C_1)} & \frac{K_t D_1}{m(K_t + C_1)} \end{bmatrix} \begin{bmatrix} r \\ \dot{r} \end{bmatrix}$$

The reduced-order dynamics characteristic equation is

$$s^2 + \frac{K_t D_1}{m(K_t + C_1)} s + \frac{K_t C_1}{m(K_t + C_1)} = 0 \quad (2.11)$$

This reduced-order model includes a damping term and is probably a more realistic model than the reduced-order model of Section 2.2.1. However, note that this model regards road displacement r and road displacement rate \dot{r} as two independent inputs. In the physical system being modelled, they are not independent. The eigenvalues of this model are also evaluated in Section 2.2.3.

2.2.3 Example

Here is a numerical example of a suspension model. The parameters are obtained from the vehicle simulation code from U.C. Berkeley.

$$\begin{aligned}
 m &= 393.25 \text{ kg} && \text{Mass of a quarter car.} \\
 K_t &= 190632 \frac{\text{N}}{\text{m}} && \text{Tire spring constant.} \\
 C_1 &= 17000 \frac{\text{N}}{\text{m}} && \text{Suspension spring constant.} \\
 D_1 &= 1500 \frac{\text{N} \cdot \text{s}}{\text{m}} && \text{Suspension damper constant.}
 \end{aligned}$$

The eigenvalues of both full-order models in Section 2.2.1 and 2.2.2 are the same: -135.13 , $-1.64 \pm 6.16i$. The eigenvalues of the reduced-order model in Section 2.2.1 are $\pm 6.30i$ and the eigenvalues of the reduced-order model in Section 2.2.2 are $-1.75 \pm 6.05i$. The light damping of the force-state model of Section 2.2.2 is more realistic so this model is considered to be a better representation of the suspension dynamics.

Remark 1. If the model reduction is done by balanced realization and truncation, the length-state and force-state realizations should have similar reduced-order linear models. Balanced realization and truncation, discussed in detail in (Douglas et al. 1996), truncates the least observable and controllable modes as determined by inspection of the observability and controllability Grammians. By this method, the truncated modes are not necessarily the fast modes so that the eigenvalues of the reduced-order model might be very different from those of the full-order model. Further, when fast modes are truncated, the simple state truncation with steady-state correction method illustrated in Sections 2.2.1 and 2.2.2 produces results that are dependent on the state basis. Regarding a balanced realization as just another basis, it is possible that for some problems, a balanced realization does not provide a best reduced-order model. Best is problem dependent but is generally determined by comparing the full and reduced-order frequency responses and eigenstructures. ◀

2.3 Manifold Temperature Model

In the engine model the manifold temperature is taken to be a constant. If a manifold temperature sensor is to be monitored for a fault, two sensor models are possible. One model has the manifold temperature as an engine state and appends an integrator to the engine dynamics. Another model considers the manifold temperature as a measured exogenous input.

Since manifold temperature changes are on a much longer time scale than the engine dynamics, it is a natural choice to model the manifold temperature as a constant. With a constant manifold temperature as an engine state, an integrator is appended to the engine dynamics.

$$\begin{aligned} \begin{bmatrix} \dot{x} \\ \dot{x}_{T_m} \end{bmatrix} &= \begin{bmatrix} A & B_{T_m} \\ 0 & 0 \end{bmatrix} \begin{bmatrix} x \\ x_{T_m} \end{bmatrix} + \begin{bmatrix} B \\ 0 \end{bmatrix} u \\ y &= \begin{bmatrix} C & 0 \\ 0 & 1 \end{bmatrix} \begin{bmatrix} x \\ x_{T_m} \end{bmatrix} \end{aligned}$$

where x_{T_m} is the manifold temperature state and x are the rest of the states. A problem with this model is that the observability Grammian is ill-defined because the eigenvalue at the origin is associated with a measured state, the temperature x_{T_m} .

An alternate model has the temperature as a known, that is measured, input to the engine.

$$\begin{aligned} \dot{x} &= Ax + Bu + B_{T_m} \omega_{T_m} \\ y_x &= Cx \\ y_\omega &= \omega_{T_m} \end{aligned}$$

This approach avoids the observability Grammian problem and seems more reasonable in that the manifold temperature is an environmental factor which cannot be controlled.

Fault Detection By Analytic Redundancy

ANALYTIC REDUNDANCY is an approach to health monitoring that compares dissimilar instruments using a detailed system model. The approach is to find dynamic or algebraic relationships between sensors and actuators. That is, information provided by a monitored sensor is, in some form, also provided by other sensors or, through the dynamics, by actuator commands. In automated vehicles, these requirements preclude monitoring nonredundant sensors such as obstacle detection or lane position sensors. The information provided by a radar or infrared sensor designed to detect objects in the vehicle's path has no dynamic correlation with other sensors on the vehicle. A sensor that detects the vehicle's position in a lane is the only sensor that can provide this information. Actuators that do no observable action are also difficult to monitor. For example, the health of a power window actuator is easily monitored by the driver. But, unless specialized sensors are installed, no other part of the car is affected by the operation of this actuator and there is no analytic redundancy.

A range sensor is another example of a sensor for which a vehicle has no redundant information. In some configurations, range information is provided by several different

types of sensors, for example, radar and optical range sensors. In this type of design, the sensor measurements are fused at the vehicle regulation layer. So, for the purposes of vehicle control and fault detection, the range sensors are regarded as providing a single synthesized, and nonredundant, measurement.

Analytic dynamic redundancy requires a detailed model of the dynamic relationship between sensors and actuator commands. This information is encoded in a fault detection filter that detects and isolates faults by producing a static pattern in a linear observer residual. Most sensors and actuators associated with the vehicle longitudinal dynamics are monitored this way. Fault detection filter design is described in Section 3.1. Algebraic redundancy provides a simple algebraic parity equation that must be satisfied. For example, since the throttle actuator dynamics are very fast, the throttle actuator command minus the throttle actuator position is nominally zero. Parity equation design is described in 3.2. The fault detection and isolation system is summarized in Section 3.3.

3.1 Analytic Redundancy

Eleven sensors and two actuators are to be monitored. The sensors are the manifold air mass sensor y_{m_a} , engine speed sensor y_{ω_e} , manifold temperature sensor y_{T_m} , manifold pressure sensor y_{p_m} , longitudinal velocity sensor y_{v_x} and accelerometer y_{a_x} , vertical accelerometer y_{a_z} , the sum of front wheel speed sensors $y_{\bar{\omega}_f}$, the sum of rear wheel speed sensors $y_{\bar{\omega}_r}$, throttle sensor y_{α} and brake sensor y_{T_b} . The two actuators are the throttle u_{α} and brake u_{T_b} . Three of the sensors y_{α} , y_{T_b} and y_{p_m} , are monitored with algebraically redundant information. Hence, eight sensors and two actuators are included in the fault detection filter design.

A very brief review of the fault detection filter is provided in Section 3.1.1. Section 3.1.2 describes the sensor and actuator fault models. Section 3.1.3 discusses several design considerations that are specific to the longitudinal vehicle dynamics health monitoring problem. Section 3.1.4 discusses how multiple faults are grouped among several filters. The fault detection filter designs are sensor and actuator fault groups described in Sections 3.1.5

and 3.1.6.

3.1.1 Beard-Jones Fault Detection Filter Background

A detailed review of fault detection filter design is provided in Appendix A of last year's report (Douglas et al. 1996). For a thorough background, several references are available, a few of which are (Douglas 1993), (White and Speyer 1987) and (Massoumnia 1986).

Consider a linear time-invariant system with q failure modes and no disturbances or sensor noise

$$\dot{x} = Ax + Bu + \sum_{i=1}^q F_i m_i \quad (3.1a)$$

$$y = Cx + Du \quad (3.1b)$$

The system variables x , u , y and the m_i belong to real vector spaces and the system maps A , B , C , D and the F_i are of compatible dimensions. Assume that the input u and the output y both are known. The F_i are the failure signatures. They are known and fixed and model the directional characteristics of the faults. The m_i are the failure modes and model the unknown time-varying amplitude of faults. The m_i do not have to be scalar values.

A fault detection filter is a linear observer that, like any other linear observer, forms a residual process sensitive to unknown inputs. Consider a full-order observer with dynamics and residual

$$\dot{\hat{x}} = (A + LC)\hat{x} + Bu - Ly \quad (3.2a)$$

$$r = C\hat{x} + Du - y \quad (3.2b)$$

Form the state estimation error $e = \hat{x} - x$ and the dynamics and residual are

$$\dot{e} = (A + LC)e - \sum_{i=1}^q F_i m_i$$

$$r = Ce$$

In steady-state, the residual is driven by the faults when they are present. If the system is (C, A) observable, and the observer dynamics are stable, then in steady-state and in the

absence of disturbances and modeling errors, the residual r is nonzero only if a fault has occurred, that is, if some m_i is nonzero. Furthermore, when a fault does occur, the residual is nonzero except in certain theoretically relevant but physically unrealistic situations. This means that any stable observer can detect the presence of a fault. Simply monitor the residual and when it is nonzero a fault has occurred.

In addition to detecting a fault, a fault detection filter provides information to determine which fault has occurred. An observer such as (3.2) becomes a fault detection filter when the observer gain L is chosen so that the residual has certain directional properties that immediately identify the fault. The gain is chosen to partition the residual space where each partition is uniquely associated with one of the design fault directions F_i . A fault is identified by projecting the residual onto each of the residual subspaces and then determining which projections are nonzero.

In a detection filter, the state estimation error in response to a fault in the direction F_i remains in a state subspace \mathcal{T}_i^* , an unobservability subspace or detection space. See Appendix A of last year's report (Douglas et al. 1996) for details. The ability to identify a fault, to distinguish one fault from another, requires, for an observable system, that the detection spaces be independent. Thus, the number of faults that can be detected and identified by a fault detection filter is limited by the size of the state space and the sizes of the detection spaces associated with each of the faults. If the problem considered has more faults than can be accommodated by one fault detection filter, then a bank of filters will have to be constructed.

For a fault F_i , the approach to finding the detection space \mathcal{T}_i^* is to find the minimal (C, A) -invariant subspace \mathcal{W}_i^* that contains F_i and then to find the invariant zero directions of the triple (C, A, F_i) , if any. With the invariant zero directions denoted by \mathcal{V}_i , the minimal unobservability subspace \mathcal{T}_i^* is given by

$$\mathcal{T}_i^* = \mathcal{W}_i^* + \mathcal{V}_i$$

Before the fault detection filter design (3.2) can begin, a system model with faults has to be found with the form (3.1). This is discussed in the next section.

3.1.2 Fault Modelling

This section describes sensor and actuator fault models used for fault detection filter design. Two classes of sensor fault are considered. One measures a linear combination of states. For the longitudinal vehicle dynamics these include y_{m_a} , y_{ω_e} , y_{v_x} , y_{a_x} , y_{a_z} , $y_{\bar{\omega}_f}$ and $y_{\bar{\omega}_r}$. Another class of sensor fault is one that measures exogenous inputs. The manifold temperature sensor is the only sensor in this class.

The fault of a sensor which measures system states can be modelled as an additive term in the measurement equation

$$y = Cx + E_i\mu_i \quad (3.3)$$

where E_i is a column vector of zeros except for a one in the i^{th} position and where μ_i is an arbitrary time-varying scalar. This is explained in last year's report (Douglas et al. 1996) but is included here for completeness. Since, for fault detection filter design, faults are expressed as additive terms to the system dynamics, a way must be found to convert the E_i sensor fault form of (3.3) to an equivalent F_i form as in (3.1). Let F_i satisfy

$$CF_i = E_i$$

and define a state estimation error e as

$$e = x - \hat{x} + F_i\mu_i$$

Using (3.2), the error dynamics are

$$\dot{e} = (A + LC)e + F_i\dot{\mu}_i - AF_i\mu_i \quad (3.4)$$

and a sensor fault E_i in (3.3) is equivalent to a two-dimensional fault F_i

$$\dot{x} = Ax + Bu + F_i m_i \quad \text{with } F_i = [F_i^1, F_i^2]$$

where the directions F_i^1 and F_i^2 are given by

$$E_i = CF_i^1 \quad (3.5a)$$

$$F_i^2 = AF_i^1 \quad (3.5b)$$

An interpretation of the effect of a sensor fault on observer error dynamics follows from (3.4) where F_i^1 is the sensor fault rate $\dot{\mu}_i$ direction and F_i^2 is the sensor fault magnitude μ_i direction. This interpretation suggests a possible simplification when information about the spectral content of the sensor fault is available. If it is known that a sensor fault has persistent and significant high frequency components, such as in the case of a noisy sensor, the fault direction could be approximated by the F_i^1 direction alone. Or, if it is known that a sensor fault has only low frequency components, such as in the case of a bias, the fault direction could be approximated by the F_i^2 direction alone. For example, if a sensor were to develop a bias, a transient would be likely to appear in all fault directions but, in steady-state, only the residual associated with the faulty sensor should be nonzero.

A linear model partitioned to isolate first-order actuator dynamics can be expressed as

$$\begin{bmatrix} \dot{x} \\ \dot{x}_a \end{bmatrix} = \begin{bmatrix} A & B \\ 0 & -\omega \end{bmatrix} \begin{bmatrix} x \\ x_a \end{bmatrix} + \begin{bmatrix} 0 \\ \omega \end{bmatrix} u + B_\omega \omega$$

where x_a is a vector of actuator states and ω is an exogenous input. Typically, exogenous inputs are dynamic disturbances such as road noise and wind gusts and are not known or measured. However, as described in Section 2.3, the manifold temperature is modelled as a dynamic input and is measured. A fault in this sensor is modelled as a direction given by the associated column of the B_ω matrix.

A fault in a control input is also modeled as an additive term in the system dynamics. In the case of a fault appearing at the input of an actuator, that is the actuator command, the fault has the same direction as the associated column of the $[0, \omega]^T$ matrix. A fault appearing at the output of an actuator, the actuator position, has the same direction as the associated column of the $[B^T, 0]^T$ matrix. In the vehicle model, the actuator dynamics are relatively fast and, in an approximation made here, are removed from the system model. Thus, the control inputs are applied directly to the system through a column of the B matrix.

3.1.3 Special Design Considerations

Several design considerations arise that are specific to the longitudinal vehicle dynamics health monitoring problem. One problem is a conditioning problem that arises from the model order reduction done in Section 2.1. Another concerns the output separability of the modeled faults. A third problem concerns a reasonable expectation that a fault detection filter should produce a nonzero fault residual for as long as a modeled fault is present.

Ill-conditioned fault direction

For all sensor and throttle actuator faults described in Section 3.1.2, the detection or minimal unobservability subspaces are given by the fault directions themselves, that is,

$$\mathcal{T}_i^* = \mathcal{W}_i^* + \mathcal{V}_i = \text{Im } F_i$$

For example, for the brake actuator, $\mathcal{T}_i^* = \text{Im } F_i$ because $CF_{u_{T_b}} \neq 0$, (Douglas et al. 1996). However, $CF_{u_{T_b}} \neq 0$ only holds for the reduced, eighth-order model. For the full-order model, $CF_{u_{T_b}} = 0$ so $F_{u_{T_b}}$ should be considered as a very weakly observable direction. For fault detection filter design, the brake actuator unobservability subspace is taken to be the second-order space given by

$$\mathcal{T}_{u_{T_b}}^* = \text{Im} \left[F_{u_{T_b}}, AF_{u_{T_b}} \right]$$

Output separability

The output separability design requirement states that the residuals produced by design faults be pairwise linearly independent. Faults that are not output separable generate co-linear residuals and cannot be isolated. Output separability of two faults F_i and F_j is determined by

$$CT_i^* \cap CT_j^* = 0 \tag{3.6}$$

which may be checked by the column independence of realizations for CT_i and CT_j .

Performing the check (3.6) reveals that two pairs of faults are not output separable. The throttle actuator u_α and manifold air mass sensor y_{m_a} faults are not output separable and the manifold temperature sensor y_{T_m} and manifold air mass sensor y_{m_a} faults are not output separable. The problem is summarized as

$$\begin{aligned} \mathcal{T}_{u_\alpha}^* &= F_{u_\alpha} \\ \mathcal{T}_{y_{T_m}}^* &= F_{y_{T_m}} \\ \mathcal{T}_{y_{m_a}}^* &= [F_{y_{m_a}} \quad AF_{y_{m_a}}] \\ F_{u_\alpha} &= F_{y_{m_a}} \\ F_{y_{T_m}} &= AF_{y_{m_a}} \end{aligned}$$

First, consider the throttle actuator and manifold air mass sensor faults where $CF_{u_\alpha} = CF_{y_{m_a}}$ indicates that they cannot be isolated. As explained in Section 3.1.2, the direction of the air mass sensor fault magnitude is $AF_{y_{m_a}}$ while the direction of the fault rate is $F_{y_{m_a}}$. The throttle actuator and air mass sensor faults become output separable if only the sensor fault magnitude direction is used. This design decision could allow a noisy but zero mean sensor fault to remain undetected through the direction $CAF_{y_{m_a}}$. Also, since the throttle fault detection space is spanned by $F_{u_\alpha} = F_{y_{m_a}}$, an air mass sensor fault rate will stimulate the throttle fault residual. However, a throttle actuator fault could never stimulate the air mass sensor fault residual. In summary, as long as the air mass sensor fault spectral components are low frequency, the throttle actuator and manifold air mass sensor faults should be detectable and isolatable.

Next, consider the manifold temperature and air mass sensor faults where $CF_{y_{T_m}} = CAF_{y_{m_a}}$ indicates that they cannot be isolated. Since $AF_{y_{m_a}}$ represents the fault magnitude direction, this direction can not be dropped from the detection space. One remedy is to design a second fault detection filter that does not take the manifold air mass as a measurement. Such a filter will be unaffected by air mass sensor faults but will respond to manifold temperature sensor faults. A problem with this fix is that the throttle actuator and temperature sensor faults are not output separable without an air mass sensor measurement.

Responses of the two filter designs are summarized in Figure 3.1. Each row represents a bias (hard) fault in either the throttle actuator, the air mass sensor or the temperature sensor. The columns are the residual responses to the given fault conditions. The first column is the response of the throttle actuator fault residual of the first filter. The second column is the response of the air mass sensor and temperature sensor fault residuals also from the first filter. The third column is the response of the throttle actuator and temperature sensor fault residuals of the second filter.

Figure 3.1 shows that neither filter alone can detect and isolate the three faults: the throttle actuator, the air mass sensor and the temperature sensor. Taken together, the two filters produce a pattern unique to each fault so that the faults may be isolated. However, the picture is not yet complete. A problem with the second fault detection filter is described in the next section.

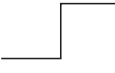

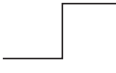






Residual Fault	Detection Filter #1		Detection Filter #2
	Throttle Actuator	Manifold Air Mass and Temperature	
Throttle Actuator			
Manifold Air Mass			
Manifold Temperature			

Figure 3.1: Fault Signatures.

Zero steady-state fault residual

It is a reasonable expectation that a fault detection filter should produce a nonzero fault residual for as long as a modeled fault is present. A necessary and sufficient condition is given in the following theorem.

Theorem 3.1. A necessary and sufficient condition for a fault detection filter residual to hold a non-zero steady-state value in response to a bias fault is $CA^{-1}F \neq 0$, that is,

$$C(sI - A - LC)^{-1}F|_{s=0} = 0 \quad \Leftrightarrow \quad CA^{-1}F = 0$$

Proof. Let $\bar{F} \triangleq (A + LC)^{-1}F$. (\Rightarrow)

$$\begin{aligned} F &= (A + LC)\bar{F} = A\bar{F} \quad \text{because } C\bar{F} = C(A + LC)^{-1}F = 0. \\ \Rightarrow \bar{F} &= A^{-1}F \\ \Rightarrow CA^{-1}F &= C\bar{F} = 0 \end{aligned}$$

(\Leftarrow)

$$\begin{aligned} A\bar{F} + LC\bar{F} &= F \\ \Rightarrow \bar{F} &= A^{-1}F \quad \text{because } CA^{-1}F = 0 \text{ and } (A + LC) \text{ is unique.} \\ \Rightarrow C(A + LC)^{-1}F &= C\bar{F} = CA^{-1}F = 0 \end{aligned}$$

Since $CA^{-1}F_{y_{T_m}} = 0$, the second fault detection filter will not see the temperature sensor faults in the steady state. When a temperature bias fault occurs, the residual responds with only a transient. Figure 3.1 is corrected in Figure 3.2 to illustrate the transitory response. Once again, the fault patterns for the three faults are not unique, at least not in steady-state.

Since a second fault detection filter no longer fixes the output separability problem, another fix is needed. An algebraic relation between the manifold pressure and manifold air mass is useful

$$\text{manifold pressure} - 19.9635 * \text{manifold air mass} = 0 \quad (3.7)$$

This convenient relation arises from the perfect gas law. The magic number 19.9635 includes the gas constant, a nominal temperature and the manifold volume. Equation (3.7) is a










Residual Fault	Detection Filter #1		Detection Filter #2
	Throttle Actuator	Manifold Air Mass and Temperature	
Throttle Actuator			
Manifold Air Mass			
Manifold Temperature			

Figure 3.2: Fault Signatures.

parity equation that is satisfied when the manifold pressure and manifold air mass sensors are working and is not satisfied when either sensor has failed. The parity equation by itself cannot isolate a fault.

By combining the parity equation (3.7) with the first fault detection filter of the last section, a residual pattern unique to each fault is formed and the faults may be isolated. The faults are the throttle actuator, the air mass sensor, the temperature sensor and the manifold pressure sensor. The residual patterns are summarized in Figure 3.3 Each row represents a bias (hard) fault in either the throttle actuator, the air mass sensor, the temperature sensor or the manifold pressure sensor. The columns are the residual responses to the given fault conditions. The first column is the response of the throttle actuator fault residual of the first filter. The second column is the response of the air mass sensor and temperature sensor fault residuals also from the first filter. The third column is the response of the parity equation for the manifold air mass and pressure sensors. The parity equation is discussed further in Section 3.2.

3.1.4 Fault Assignment to Multiple Fault Detection Filters

The ability to identify a fault, to distinguish one fault from another, requires for an observable system that the detection spaces be independent. Therefore, the number of

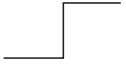











Residual Fault	Detection Filter		Parity Equation
	Throttle Actuator	Manifold Air Mass And Temperature	
Throttle Actuator			
Manifold Air Mass			
Manifold Temperature			
Manifold Pressure			

Figure 3.3: Fault Signatures.

faults that can be detected and identified by a fault detection filter is limited by the size of the state space and the sizes of the detection spaces associated with each of the faults. If the problem considered has more faults than can be accommodated by one fault detection filter, then a bank of filters will have to be constructed. The health monitoring system described in this section for a vehicle going straight, considers nine system faults: seven sensor faults and two actuator faults. Since the reduced-order longitudinal model has eight states and seven measurements, clearly more than one fault detection filter is needed. The dimension of the throttle actuator, the manifold air mass sensor and the manifold temperature sensor detection spaces is one. The dimension of the brake actuator and the rest of the sensor faults is two. Therefore, for this problem at least three filters are needed.

One consideration in grouping the faults among the fault detection filters is to group faults which are robust to system nonlinearities. Note that an actuator fault changes the vehicle operating point possibly introducing nonlinear effects into all measurements. The nonlinear effect is small if the residual response is small compared to that for some nominal fault. Also, sensor faults that are open-loop are easily isolated since they do not stimulate any dynamics. One approach to fault grouping is to always group actuator and sensor faults

with different fault detection filters.

Usually an attempt is made to group as many faults as possible in each filter. When full-order filters are used, this approach minimizes the number of filters needed. When reduced-order filters are used, this approach minimizes the order of each complementary space and, therefore, the order of each reduced-order filter. Note that each fault included in a fault detection filter design imposes more constraints on the filter eigenvectors. Sometimes, the objective of obtaining well-conditioned filter eigenvectors imposes a tradeoff between robustness and the reduced-order filter size.

With all the considerations above in mind, now we should decide how many fault detection filters are needed and which faults should go together. Robustness to nonlinearities requires all the actuator faults to be in the same filter. The output separability consideration of Section 3.1.3 requires the throttle actuator and manifold air mass sensor fault to be in the same filter. Thus, one fault detection filter has the throttle actuator u_α , brake actuator u_{T_b} and manifold air mass sensor y_{m_a} . Note that this filter is also sensitive to faults in the manifold temperature sensor y_{T_m} since manifold temperature and manifold air mass sensor faults are not output separable.

The six remaining sensor faults, y_{ω_e} , y_{v_x} , y_{a_x} , y_{a_z} , $y_{\bar{\omega}_f}$ and $y_{\bar{\omega}_r}$ are assigned to two more fault detection filters. Each filter has three faults. There are ten different combinations for these two filters and they are all non-mutually detectable which means the invariant zeros arising from the fault combinations will be the eigenvalues of the filters, that is, some poles of the filters cannot be assigned. In six of these cases, the invariant zeros, hence the fixed poles, are in the right-half plane resulting in an unstable fault detection filter. The remaining four configurations are stable. Each stable case has been designed and tested. The most robust combination is to put y_{ω_e} , y_{a_x} and $y_{\bar{\omega}_f}$ into the second filter and put y_{v_x} , y_{a_z} and $y_{\bar{\omega}_r}$ into the third filter. Here, *most robust* is taken to mean the filter with left eigenvectors that are least ill-conditioned. This hedges against eigenstructure sensitivity to small variations in system parameters. The three fault detection filters are

Fault detection filter 1.

u_α : Throttle actuator.

u_{T_b} : Brake actuator.

y_{m_a} : Manifold air mass sensor.

y_{T_m} : Manifold temperature sensor.

Fault detection filter 2.

y_{ω_e} : Engine speed sensor.

y_{a_x} : Longitudinal accelerometer.

$y_{\bar{\omega}_f}$: Sum of front wheel speed sensors.

Fault detection filter 3.

y_{v_x} : Longitudinal velocity sensor.

y_{a_z} : Vertical accelerometer.

$y_{\bar{\omega}_r}$: Sum of rear wheel speed sensors.

3.1.5 Fault Detection Filter Design For Sensors

In this and the following sections, Beard-Jones fault detection filters have been designed using eigenstructure assignment while ensuring that the eigenvectors are not ill-conditioned. The essential feature of a fault detection filter is the detection space structure embedded in the filter dynamics. A left eigenvector assignment design algorithm explicitly places eigenvectors to span these subspaces. An eigenvector assignment design algorithm also has to balance the objective of having well-conditioned eigenvectors for robustness against the objective of each fault being highly input observable for fault detection performance. System disturbances, sensor noise and system parameter variations are not considered in the fault detection filter designs described in this report. Note that they are considered in performance evaluation. For such a benign environment, the filter designs are based on

spectral considerations only; there is little else that can be used to distinguish a good design from a bad design.

Since the calculations are somewhat long and they are the similar for each detection filter, the calculation details are given for only the first and third fault detection filters. In this section, the fault detection filter is designed for the third fault group which has the longitudinal velocity sensor y_{v_x} , the vertical accelerometer y_{a_z} and the sum of rear wheel speed sensors $y_{\bar{\omega}_r}$. In next section, a filter is designed for the first fault group which has the throttle actuator u_α , the brake actuator u_{T_b} and the manifold air mass sensor y_{m_a} . Note once again that the manifold air mass sensor y_{m_a} is not output separable with respect to the manifold temperature sensor y_{T_m} .

The eight state reduced-order longitudinal model derived in Section 2.1 is used. The dimension of each detection space was found in Section 3.1.4 as

$$\begin{aligned}\nu_{y_{v_x}} &= \dim \mathcal{T}_{y_{v_x}}^* = 2 \\ \nu_{y_{a_z}} &= \dim \mathcal{T}_{y_{a_z}}^* = 2 \\ \nu_{y_{\bar{\omega}_r}} &= \dim \mathcal{T}_{y_{\bar{\omega}_r}}^* = 2\end{aligned}$$

The dimension of the fault detection filter complementary space \mathcal{T}_0 is also needed. The complementary space is any subspace independent of the detection spaces that completes the state-space.

$$\mathcal{X} = \mathcal{T}_{y_{v_x}}^* \oplus \mathcal{T}_{y_{a_z}}^* \oplus \mathcal{T}_{y_{\bar{\omega}_r}}^* \oplus \mathcal{T}_0$$

Thus the dimension of \mathcal{T}_0 is two

$$\begin{aligned}\nu_0 &= n - \nu_{y_{v_x}} - \nu_{y_{a_z}} - \nu_{y_{\bar{\omega}_r}} \\ &= 8 - 2 - 2 - 2 \\ &= 2\end{aligned}$$

Next define the complementary faults sets. There are three faults $F_{y_{v_x}}$, $F_{y_{a_z}}$ and $F_{y_{\bar{\omega}_r}}$

so there are four complementary fault sets which are:

$$\hat{F}_{y_{vx}} = [F_{y_{az}}, F_{y_{\bar{\omega}_r}}] \quad (3.8a)$$

$$\hat{F}_{y_{az}} = [F_{y_{vx}}, F_{y_{\bar{\omega}_r}}] \quad (3.8b)$$

$$\hat{F}_{y_{\bar{\omega}_r}} = [F_{y_{vx}}, F_{y_{az}}] \quad (3.8c)$$

$$\hat{F}_0 = [F_{y_{vx}}, F_{y_{az}}, F_{y_{\bar{\omega}_r}}] \quad (3.8d)$$

Now choose the filter closed-loop eigenvalues. As discussed in Section 3.1.4, these three faults are not mutually detectable. Therefore the invariant zero -14.52 has to be one of the eigenvalues of the complementary subspace. Since the system model includes no sensor noise, no disturbances and no parameter variations, there is little basis for preferring one set of detection filter closed-loop eigenvalues over another. The poles are chosen here to give a reasonable response time but are not unrealistically fast. The assigned eigenvalues are

$$\Lambda_{y_{vx}} = \{-3, -4\}$$

$$\Lambda_{y_{az}} = \{-3, -4\}$$

$$\Lambda_{y_{\bar{\omega}_r}} = \{-3, -4\}$$

$$\Lambda_0 = \{-3, -14.52\}$$

The next step is to find the closed-loop fault detection filter left eigenvectors. For each eigenvalue $\lambda_{i_j} \in \Lambda_i$, the left eigenvectors v_{i_j} generally are not unique and must be chosen from a subspace as $v_{i_j} \in V_{i_j}$ where V_{i_j} and another space W_{i_j} are found by solving

$$\begin{bmatrix} A^T - \lambda_{i_j} I & C^T \\ \hat{F}_i^T & 0 \end{bmatrix} \begin{bmatrix} V_{i_j} \\ W_{i_j} \end{bmatrix} = \begin{bmatrix} 0 \\ 0 \end{bmatrix} \quad (3.9)$$

There are eight V_{i_j} associated with eight eigenvalues. To help desensitize the fault detection filter to parameter variations, the left eigenvectors are chosen from $v_{i_j} \in V_{i_j}$ as the set with the greatest degree of linear independence. The degree of linear independence is indicated by the smallest singular value of the matrix formed by the left eigenvectors. Upper bounds

on the singular values of the left eigenvectors are given by the singular values of

$$V = [V_{0_1}, V_{0_2}, V_{y_{v_{x1}}}, V_{y_{v_{x2}}}, V_{y_{a_{z1}}}, V_{y_{a_{z2}}}, V_{y_{\bar{\omega}_{r1}}}, V_{y_{\bar{\omega}_{r2}}}]$$

These singular values are

$$\sigma(V) = \{2.83, 2.50, 1.69, 1.41, 1.32, 0.333, 0.080, 0.0088\} \quad (3.10)$$

If the left eigenvector singular value upper bounds were small, then all possible combinations of detection filter left eigenvectors would be ill-conditioned and the filter eigenstructure would be sensitive to small parameter variations. Since (3.10) indicates that the upper bounds are not small, continue by looking for a set of fault detection filter left eigenvectors that are reasonably well-conditioned. For this case, one possible set of left eigenvectors from the set V nearly meets the upper bound and should be well-conditioned. The singular values of this set of left eigenvectors are

$$\sigma(\tilde{V}) = \{1.95, 1.12, 1.00, 1.00, 0.92, 0.285, 0.063, 0.00691\}$$

Since the difference between the largest and the smallest singular values is only three orders of magnitude, the detection filter gain will be reasonably small and the filter eigenstructure should not be sensitive to small parameter variations.

The fault detection filter gain L is found by solving

$$\tilde{V}^T L = \tilde{W}^T \quad (3.11)$$

where \tilde{V} is the matrix of left eigenvectors as found above, and \tilde{W} is a matrix of vectors w_{i_j}

$$\begin{bmatrix} A^T - \lambda_{i_j} I & C^T \\ \hat{F}_i^T & 0 \end{bmatrix} \begin{bmatrix} v_{i_j} \\ w_{i_j} \end{bmatrix} = \begin{bmatrix} 0 \\ 0 \end{bmatrix}$$

If the left eigenvector v_{i_j} is a linear combination of the columns of V_{i_j} , w_{i_j} is the same linear combination of the columns of W_{i_j} where V_{i_j} and W_{i_j} are from (3.9).

To complete the detection filter design, output projection matrices $\hat{H}_{y_{v_x}}$, $\hat{H}_{y_{a_z}}$ and $\hat{H}_{y_{\bar{\omega}_r}}$ are needed to project the residual along the respective output subspaces $C\hat{T}_{y_{v_x}}^*$, $C\hat{T}_{y_{a_z}}^*$ and

$C\hat{T}_{y\bar{\omega}_r}^*$. What this means is that, for example, $\hat{T}_{y_{v_x}}^*$ becomes the unobservable subspace of the pair $(\hat{H}_{y_{v_x}}C, A + LC)$. Remember that by the definition of the complementary faults (3.8), faults $F_{y_{a_z}}$ and $F_{y_{\bar{\omega}_r}}$ lie in $\hat{T}_{y_{v_x}}^*$ and fault $F_{y_{v_x}}$ does not. The effect is that the projected residual is driven by fault $F_{y_{v_x}}$ and only fault $F_{y_{v_x}}$.

A projection \hat{H}_i is computed by first finding a basis for the range space of $C\hat{T}_i^*$ where again, \hat{T}_i^* is any basis for the detection space \hat{T}_i^* . This is done by finding the left singular vectors of $C\hat{T}_i^*$. Denote this basis for now as h_i . Then \hat{H}_i is given by

$$\hat{H}_i = I - h_i h_i^T$$

In summary, a fault detection filter for the system with sensor faults $E_{y_{v_x}}$, $E_{y_{a_z}}$ and $E_{y_{\bar{\omega}_r}}$

$$\begin{aligned}\dot{x} &= Ax + Bu + B_{T_m}\omega_{T_m} \\ y &= Cx + Du + E_{y_{v_x}}\mu_{y_{v_x}} + E_{y_{a_z}}\mu_{y_{a_z}} + E_{y_{\bar{\omega}_r}}\mu_{y_{\bar{\omega}_r}}\end{aligned}$$

is equivalent to a fault detection filter for the system with faults $F_{y_{v_x}}$, $F_{y_{a_z}}$ and $F_{y_{\bar{\omega}_r}}$

$$\begin{aligned}\dot{x} &= Ax + Bu + B_{T_m}\omega_{T_m} + F_{y_{v_x}}m_{y_{v_x}} + F_{y_{a_z}}m_{y_{a_z}} + F_{y_{\bar{\omega}_r}}m_{y_{\bar{\omega}_r}} \\ y &= Cx + Du\end{aligned}$$

and has the form

$$\begin{aligned}\dot{\hat{x}} &= (A + LC)\hat{x} + (B + LD)u + B_{T_m}y_{T_m} - Ly \\ z_{y_{v_x}} &= \hat{H}_{y_{v_x}}(C\hat{x} + Du - y) \\ z_{y_{a_z}} &= \hat{H}_{y_{a_z}}(C\hat{x} + Du - y) \\ z_{y_{\bar{\omega}_r}} &= \hat{H}_{y_{\bar{\omega}_r}}(C\hat{x} + Du - y)\end{aligned}$$

where L , $\hat{H}_{y_{v_x}}$, $\hat{H}_{y_{a_z}}$ and $\hat{H}_{y_{\bar{\omega}_r}}$ are shown in Appendix A.

A fault detection filter design for the second fault group is carried out in the similar way and is not shown here. However, the filter gain L and projections $\hat{H}_{y_{\omega_e}}$, $\hat{H}_{y_{a_x}}$ and $\hat{H}_{y_{\bar{\omega}_f}}$ are shown in Appendix A.

3.1.6 Fault Detection Filter Design For Actuators

In next section, a fault detection filter is designed for the first fault group which has the throttle actuator u_α , the brake actuator u_{T_b} and the manifold air mass sensor y_{m_a} . Note once again that the manifold air mass sensor y_{m_a} is not output separable with respect to the manifold temperature sensor y_{T_m} .

The design procedure is similar to the previous section but does have a twist. As discussed in Section 3.1.3, a reduced-order manifold air mass sensor fault is used to achieve output separability with the throttle actuator fault. Also manifold air mass and manifold temperature sensor faults cannot be isolated.

The dimension of each detection space was found in Section 3.1.4 as

$$\nu_{u_\alpha} = \dim \mathcal{T}_{u_\alpha}^* = 1$$

$$\nu_{u_{T_b}} = \dim \mathcal{T}_{u_{T_b}}^* = 2$$

$$\nu_{y_{m_a}} = \dim \mathcal{T}_{y_{m_a}}^* = 1$$

and the dimension of the fault detection filter complementary space \mathcal{T}_0 where

$$\mathcal{X} = \mathcal{T}_{u_\alpha}^* \oplus \mathcal{T}_{u_{T_b}}^* \oplus \mathcal{T}_{y_{m_a}}^* \oplus \mathcal{T}_0$$

is four

$$\begin{aligned} \nu_0 &= n - \nu_{u_\alpha} - \nu_{u_{T_b}} - \nu_{y_{m_a}} \\ &= 8 - 1 - 2 - 1 \\ &= 4 \end{aligned}$$

Next define the complementary faults sets. There are three faults F_{u_α} , $F_{u_{T_b}}$ and $F_{y_{m_a}}$ so there are four complementary fault sets which are:

$$\hat{F}_{u_\alpha} = [F_{u_{T_b}}, F_{y_{m_a}}] \quad (3.12a)$$

$$\hat{F}_{u_{T_b}} = [F_{u_\alpha}, F_{y_{m_a}}] \quad (3.12b)$$

$$\hat{F}_{y_{m_a}} = [F_{u_\alpha}, F_{u_{T_b}}] \quad (3.12c)$$

$$\hat{F}_0 = [F_{u_\alpha}, F_{u_{T_b}}, F_{y_{m_a}}] \quad (3.12d)$$

Now choose the fault detection filter closed-loop eigenvalues. Since these three faults are mutually detectable, all eigenvalues are freely assignable.

$$\begin{aligned}\Lambda_{u_\alpha} &= \{-3\} \\ \Lambda_{u_{T_b}} &= \{-3, -4\} \\ \Lambda_{y_{m_a}} &= \{-3\} \\ \Lambda_0 &= \{-3, -4, -5, -6\}\end{aligned}$$

The next step is to find the closed-loop fault detection filter left eigenvectors. The left eigenvectors v_{i_j} for each eigenvalue $\lambda_{i_j} \in \Lambda_i$ generally are not unique and must be chosen from a subspace as $v_{i_j} \in V_{i_j}$ where V_{i_j} is found by solving

$$\begin{bmatrix} A^T - \lambda_{i_j} I & C^T \\ \hat{F}_i^T & 0 \end{bmatrix} \begin{bmatrix} V_{i_j} \\ W_{i_j} \end{bmatrix} = \begin{bmatrix} 0 \\ 0 \end{bmatrix} \quad (3.13)$$

There are eight V_{i_j} associated with eight eigenvalues. Upper bounds on the singular values of the left eigenvectors are given by the singular values of

$$V = [V_{0_1}, V_{0_2}, V_{0_3}, V_{0_4}, V_{u_\alpha}, V_{u_{T_{b1}}}, V_{u_{T_{b2}}}, V_{y_{m_a}}]$$

These singular values are

$$\sigma(V) = \{2.83, 2.83, 2.82, 1.98, 1.41, 0.290, 0.174, 0.021\} \quad (3.14)$$

Since (3.14) indicates that the upper bounds are not small, continue by looking for a set of fault detection filter left eigenvectors that are reasonably well-conditioned. One possible choice has the following singular values

$$\sigma(\tilde{V}) = \{1.46, 1.41, 1.35, 1.00, 1.00, 0.235, 0.056, 0.0028\}$$

Since these singular values are quite close to their respective upper bounds, the detection filter gain should not be large and the filter eigenstructure should not be sensitive to small parameter variations. As in Section 3.1.5, the fault detection filter gain L is found by solving

$$\tilde{V}^T L = \tilde{W}^T \quad (3.15)$$

where the columns of \tilde{V} and \tilde{W} are found from (3.13). Output projection matrices \hat{H}_{u_α} , $\hat{H}_{u_{T_b}}$, $\hat{H}_{y_{m_a}}$ and $\hat{H}_{y_{T_m}}$ are found in the same way as for the sensor fault example of Section 3.1.5. The filter gain L and projections \hat{H}_{u_α} , $\hat{H}_{u_{T_b}}$, $\hat{H}_{y_{m_a}}$ and $\hat{H}_{y_{T_m}}$ are shown in Appendix A

A note should be made regarding the throttle actuator fault residual. By the definition of the complementary faults (3.12), $F_{u_{T_b}}$ and $F_{y_{m_a}}$ lie in $\hat{T}_{u_\alpha}^*$ while F_{u_α} does not. The effect is that the projected residual is not driven by fault $F_{u_{T_b}}$ or $F_{y_{m_a}}$. Now recall that $F_{y_{m_a}}$ is a reduced-order approximation for $E_{y_{m_a}}$ so the throttle actuator residual is not only driven by F_{u_α} , but also the part of $E_{y_{m_a}}$ not modeled by $F_{y_{m_a}}$. As shown in Figure 3.4, the throttle actuator residual can only isolate faults well at low frequency while other residuals isolate all faults.

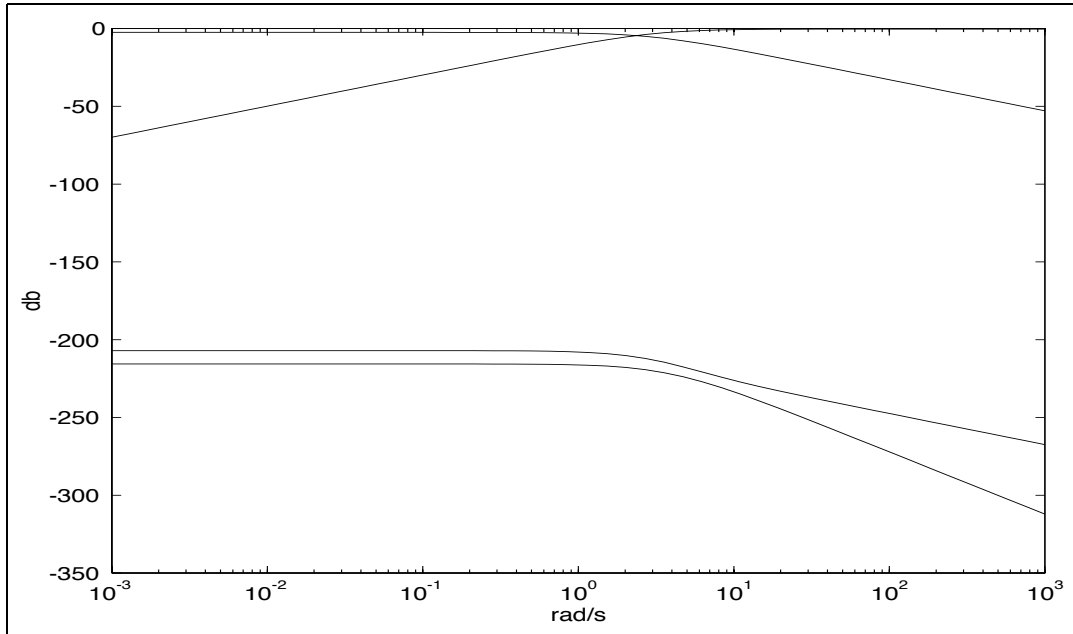


Figure 3.4: Singular value frequency response from all faults to throttle residual.

3.2 Algebraic Redundancy

Algebraic parity equations provide a second component to the fault detection and isolation system. The following algebraically redundant pairs are available: the throttle sensor y_α

and throttle actuator, the brake sensor y_{T_b} and brake actuator u_{T_b} and the manifold pressure sensor y_{pm} and manifold air mass sensor y_{ma} . Three parity equations are defined:

1. $0 = \text{Throttle sensor } y_\alpha - \text{Throttle actuator } u_\alpha$
2. $0 = \text{Brake sensor } y_{T_b} - \text{Brake actuator } u_{T_b}$
3. $0 = \text{Manifold pressure sensor } y_{pm} - \text{Manifold air mass sensor } y_{ma} * 19.9635$

None of the parity equations can by itself identify a fault. But by combining the parity equations with the first fault group detection filter of Section 3.1.4, a unique residual pattern is presented allowing each fault to be isolated. The patterns are summarized in Figure 3.5.

Each row of Figure 3.5 represents a bias (hard) fault in either the throttle actuator, the throttle sensor, the brake actuator, the brake sensor, the manifold air mass sensor, the manifold temperature sensor or the manifold pressure sensor. The columns are the residual responses to the given fault conditions. The first column is the response of the throttle actuator fault residual of the first filter. The second column is the response of the brake actuator fault residual of the first filter. The third column is the response of the air mass sensor and temperature sensor residuals of the first filter. The fourth, fifth and sixth columns are responses of the first, second and third parity equations.

3.3 Structure

Combining the fault detection filters of Section 3.1 and parity equations in Section 3.2, a set of six analytic redundancy relationships either dynamic or algebraic are presented. The designs are given in Appendix A.

Fault detection filter 1.

u_α : Throttle actuator.

u_{T_b} : Brake actuator.

y_{m_a} : Manifold air mass sensor.

y_{T_m} : Manifold temperature sensor.


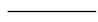
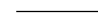






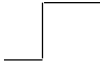










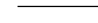
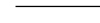



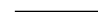










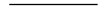
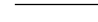




Residual Fault	Beard-Jones Fault Detection Filter #1			Parity Equation #1	Parity Equation #2	Parity Equation #3
	Throttle Actuator	Brake Actuator	Air Mass and Temperature			
Throttle Actuator						
Throttle Sensor						
Brake Actuator						
Brake Sensor						
Manifold Air Mass						
Manifold Temperature						
Manifold Pressure						

Figure 3.5: Fault Signatures.

Fault detection filter 2.

y_{ω_e} : Engine speed sensor.

y_{a_x} : Longitudinal accelerometer.

$y_{\bar{\omega}_f}$: Sum of front wheel speed sensors.

Fault detection filter 3.

y_{v_x} : Longitudinal velocity sensor.

y_{a_z} : Vertical accelerometer.

$y_{\bar{\omega}_r}$: Sum of rear wheel speed sensors.

Parity equation 1.

y_α : Throttle sensor.

u_α : Throttle actuator.

Parity equation 2.

y_{T_b} : Brake sensor.

u_{T_b} : Brake actuator.

Parity equation 3.

y_{pm} : Manifold pressure sensor.

y_{ma} : Manifold air mass sensor.

Fault Detection Filter Evaluation

FAULT DETECTION FILTER PERFORMANCE is evaluated using the nonlinear simulation discussed in Section 2. The fault detection filters designed in Sections 3 are tested on smooth and rough roads and at an off-nominal condition. The off-nominal operating condition is with the vehicle travelling straight ahead at 27 meters per second. Recall that the fault detection filters were designed for the vehicle traveling straight ahead at 25 meters per second. Performance is evaluated with respect to robustness to model nonlinearities and road noise. A smooth road model has no irregularities at all and a rough road model has roughness similar to what would be found on a reasonably well maintained freeway.

With the filters operating at an off-nominal condition, it is expected that the residuals will be nonzero but small even when no fault is present. Section 4.1 discusses the issue of when a residual is small and when a residual is large enough to indicate that a fault has occurred. Section 4.2 discusses the detection filter performance when the vehicle operates on smooth roads. Section 4.3 discusses the detection filter performance when the vehicle operates on rough roads.

4.1 Residual Scaling

Since most residuals are not zero, as is to be expected, the natural question to ask is what magnitude residual should be considered small. The answer lies in comparing the size of a nonzero residual due to non-linearities and the size of a nonzero residual due to a fault. A residual scaling factor is chosen such that when a fault is introduced into the linearized dynamics the magnitude of the corresponding reduced-order fault detection filter residual is one. Since all residuals generated by the off-nominal operating condition have magnitude less than 0.12, they should not be easily mistaken for residuals generated by a fault.

Of course, the size of the residual is proportional to the size of the fault. The size of the fault used for finding the residual scaling factors is determined as follows. For most sensors, the size of the fault is given by the difference in magnitude between the sensor output at the nominal and off-nominal steady state operating conditions. For accelerometers, the output is zero in any steady state condition and another method has to be used. The value $0.5 \frac{\text{m}}{\text{sec}^2} \approx 0.05\text{g}$ is chosen as a reasonable value for an accelerometer bias fault.

4.2 Smooth Road

In this section, the fault detection filters of Section 3 are tested on smooth, flat roads at an off-nominal operating point, that is, the vehicle operates in a steady state condition but not the same one used to generate the linearized dynamics. This is achieved by letting the car run at 27 meters per second rather than the nominal 25 meters per second. The road is flat and smooth so only vehicle nonlinearities corrupt the filter residuals. If the vehicle dynamics were linear, the increased throttle setting would have only a transient effect, if any, on the linear fault detection filter state estimates. The state estimate errors and the filter residuals would asymptotically go to zero. Since the vehicle dynamics are not linear and the vehicle operating condition is not the same as it would be if the dynamics were linear, the filter state estimates and the residuals are not zero.

The performance of the fault detection filter for the first fault group which includes throttle and brake actuator faults, manifold air mass and temperature sensor faults is shown

in Figures 4.1 and 4.2. A throttle fault is simulated by sending a two-degree incremental or decremental step throttle command after two seconds to the nonlinear simulation but not to the fault detection filter. This increases or decreases the speed of the car by about 2 meters per second or 4.5 miles per hour. Even though a throttle fault stimulates the vehicle nonlinear dynamics and the residuals associated with other faults, Figure 4.1 shows that both positive and negative throttle faults are clearly identifiable from other faults.

A brake fault is simulated by applying a brake torque just large enough to slow the vehicle from 25 meters per second to 23 meters per second. This changes the vehicle steady state operating point by the same amount as a minus two degree throttle fault. Figure 4.1 shows that the brake fault is clearly identified. It is important to note that when any of the faults from the first fault design group occur, the residuals associated with a fault detection filter designed for other faults have no meaning. This is why only four residuals are shown in each plot of Figures 4.1 and 4.2.

A few interesting observations that follow from the discussion of Section 3.1.3 are illustrated in Figure 4.2. First, since one direction of the throttle actuator fault corresponds to the air mass sensor fault rate, a bias fault in the air mass sensor causes a transient response in the throttle actuator residual. Because the transient dies out quickly, there should be no problem distinguishing throttle actuator and air mass sensor faults as long as the air mass sensor faults have only low frequency components. Second, since manifold air mass and temperature sensor faults are not output separable, the fault detection filter has the same residual response for both faults. However, the throttle actuator and manifold temperature sensor faults are output separable so there is no transient in the throttle residual when a manifold temperature fault occurs. Finally, note that the fault detection filter does not respond to the manifold pressure sensor fault because the filter does not use a manifold pressure measurement.

Figure 4.3 shows the magnitudes of the residuals for the fault detection filter derived from the second fault design group: the engine speed sensor, the longitudinal accelerometer and the sum of front wheel speed sensors. For each test, a sensor bias fault is added after two

seconds. Only one sensor fault is added at a time since simultaneous faults are not allowed. As with the first detection filter tests, when any of the sensor faults from the second fault design group occur, the residuals of fault detection filters designed for other faults have no meaning. This is why only three residuals are shown in each plot of Figures 4.3 and 4.4. Distinguishing a meaningful residual from a non-meaningful residual is left to the residual processing system. The residual associated with the fault quickly approaches one and other residuals in the fault group remain unaffected.

Figure 4.4 shows the residuals for the three fault detection filters derived from the third fault design group: the longitudinal velocity sensor, the vertical accelerometer and the sum of the rear wheel speed sensors. Residual scaling factors are chosen in the same way as for the first fault design group. The fault detection filter performance indicated by Figure 4.4 is the same as that indicated by Figure 4.3.

Figure 4.5 shows the residual from the parity equation derived for the fourth fault design group: the throttle actuator and throttle sensor. Note that there is only one residual. The scaling factor is chosen in the same way as for the other fault design groups. As discussed in Section 3.1, a nonzero residual could mean that either or both components have failed.

Figures 4.6 and 4.7 show the residuals from parity equations derived for the fifth, the brake actuator and brake sensor, and sixth, manifold air mass and temperature sensor, fault design groups. They are similar to Figure 4.5.

4.3 Rough Road

Tests performed on the fault detection filters in this section closely follow those of the last section except that the road is no longer smooth. The same types and sizes of faults are used here as in Section 4.2.

To start, residuals for fault detection filter one in the no-fault case are illustrated in Figure 4.8. Since actuator faults stimulate the nonlinear vehicle dynamics, alter the operating point and cause all residuals to respond, plots of all residuals are provided when actuator faults are simulated. Figures 4.9, 4.10, 4.11, 4.12 and 4.13 show each residual as a

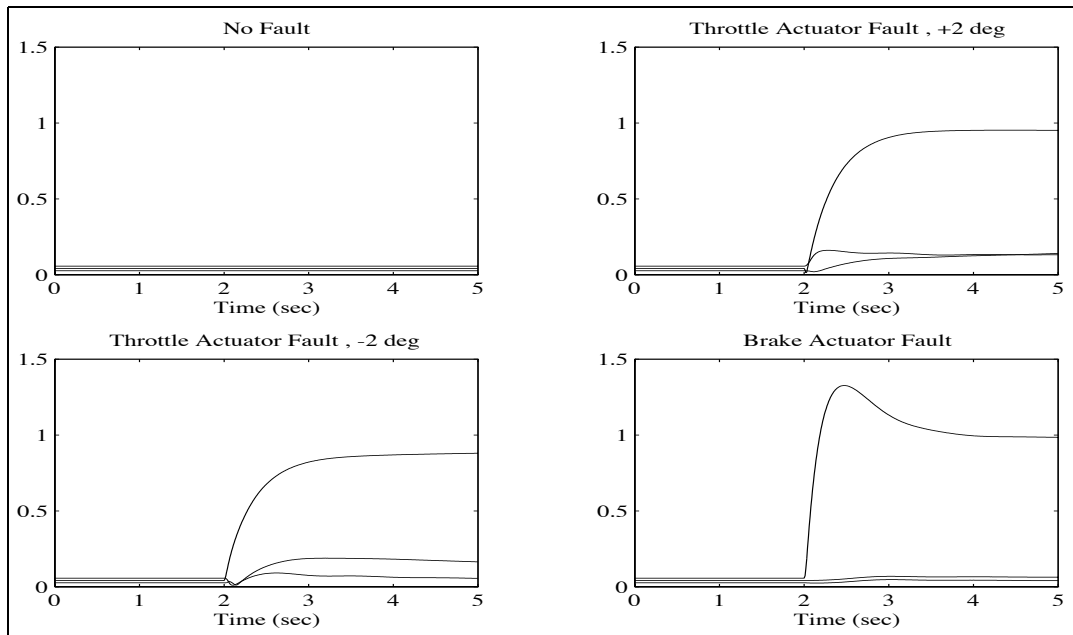


Figure 4.1: Residuals for fault detection filter one.

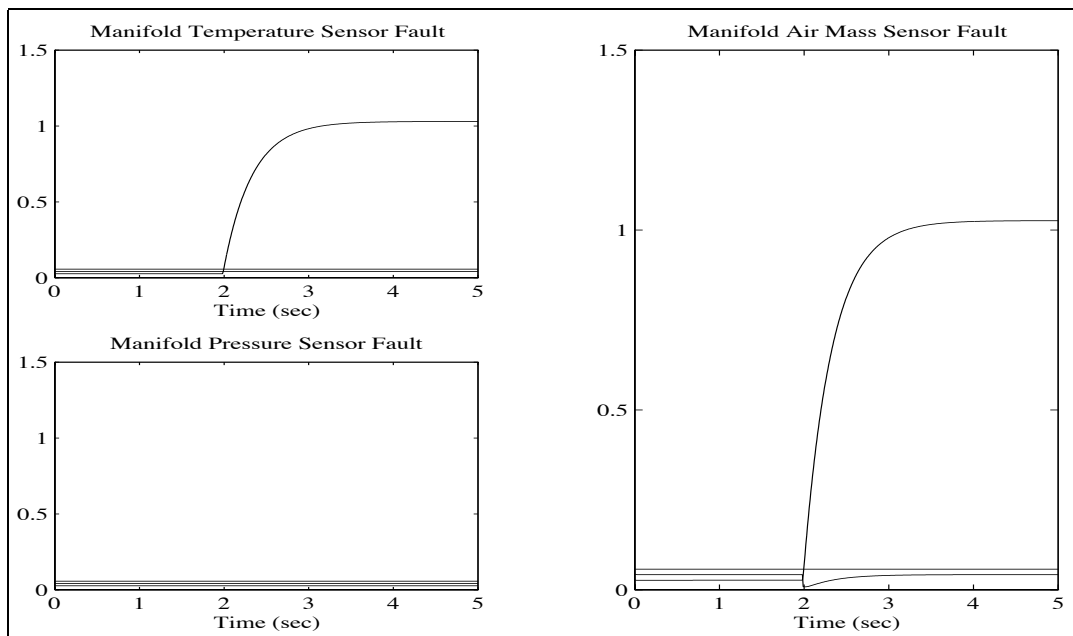


Figure 4.2: Residuals for fault detection filter one.

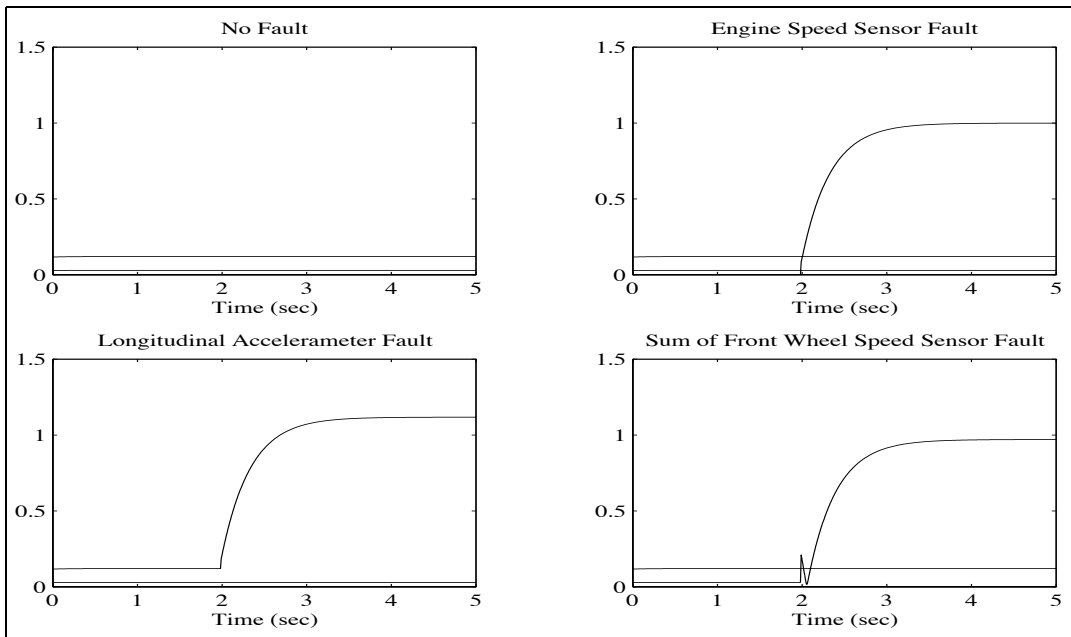


Figure 4.3: Residuals for fault detection filter two.

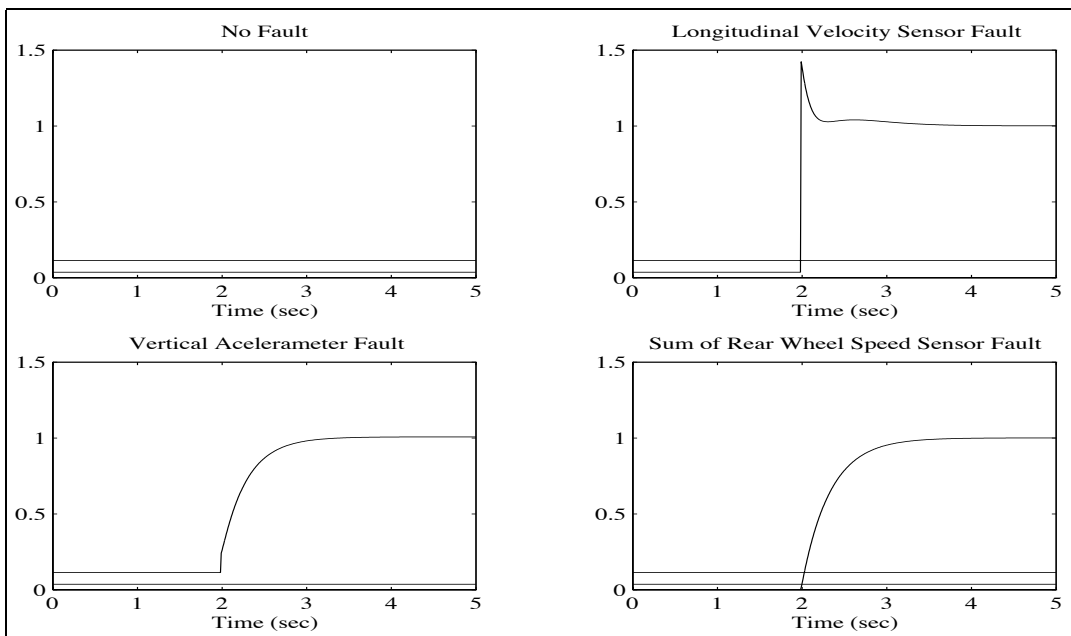


Figure 4.4: Residuals for fault detection filter three.

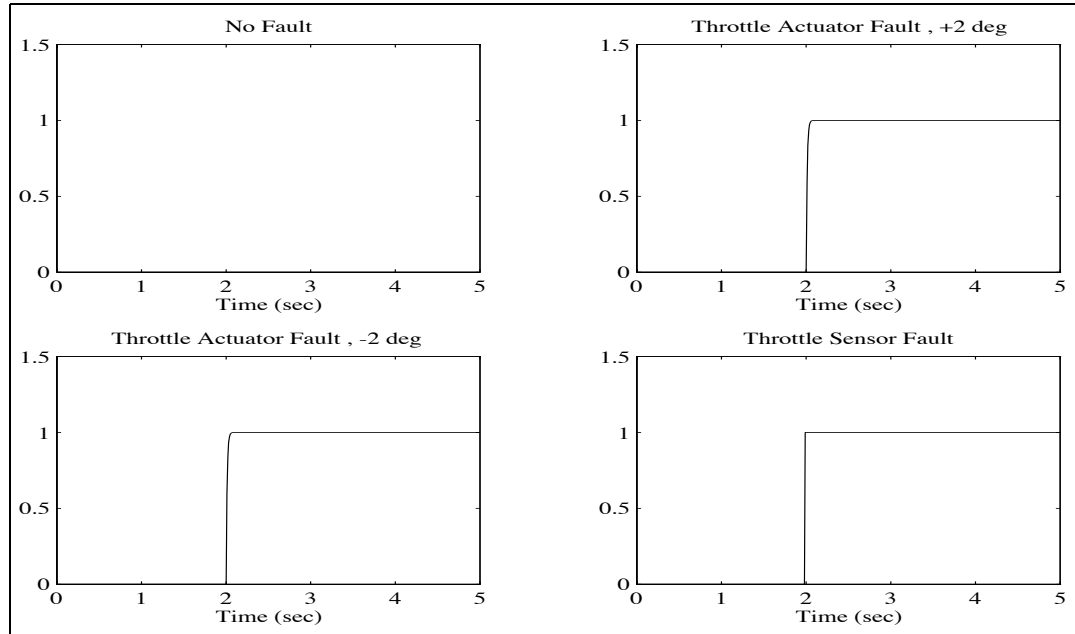


Figure 4.5: Residual for fault detection filter four.

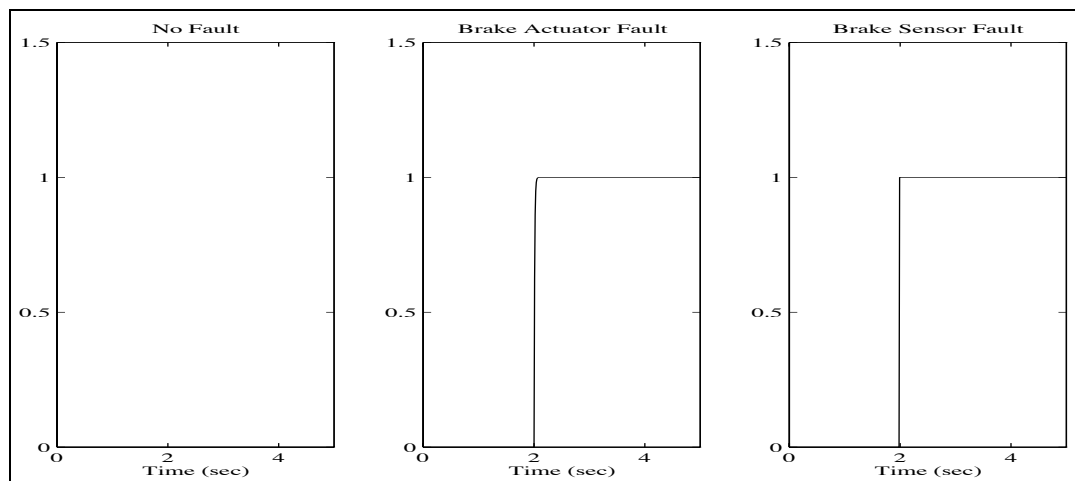


Figure 4.6: Residual for fault detection filter five.

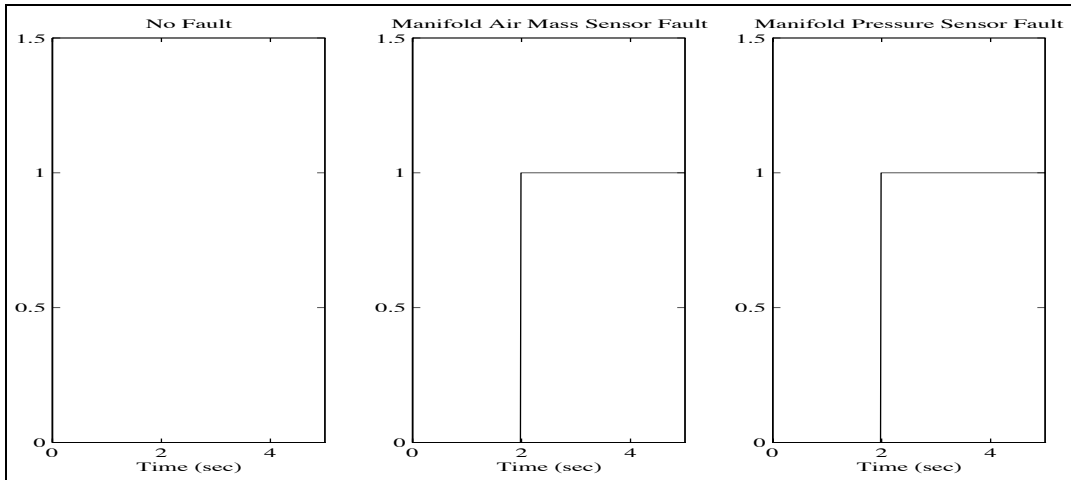


Figure 4.7: Residual for fault detection filter six.

separate plot for clarity.

Figure 4.14 shows the residuals for fault detection filter two derived from the second fault group. Figure 4.14 illustrates a visually obvious contrast between cases where no fault occurs and where a step fault occurs in the engine speed sensor, longitudinal accelerometer and the sum of front wheel speed sensors.

Figure 4.15 shows the residuals for fault detection filter three derived from the third fault group. Figures 4.16, 4.17 and 4.18 show the residuals for parity equations derived for the third, fourth and sixth fault groups. They are the same as on a smooth road.

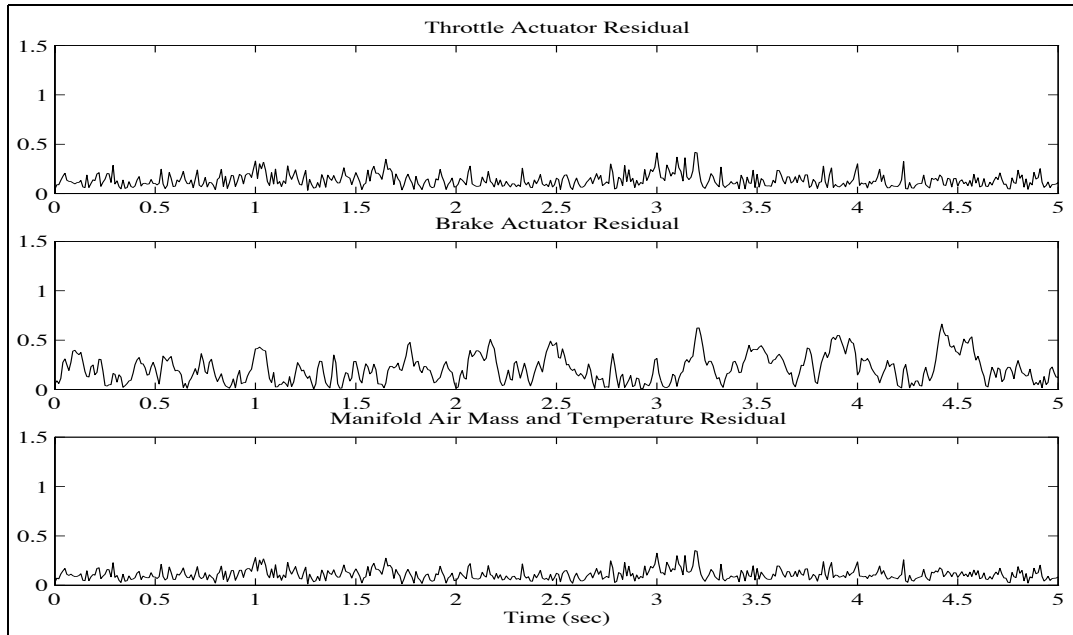


Figure 4.8: Residuals for fault detection filter one when there is no fault.

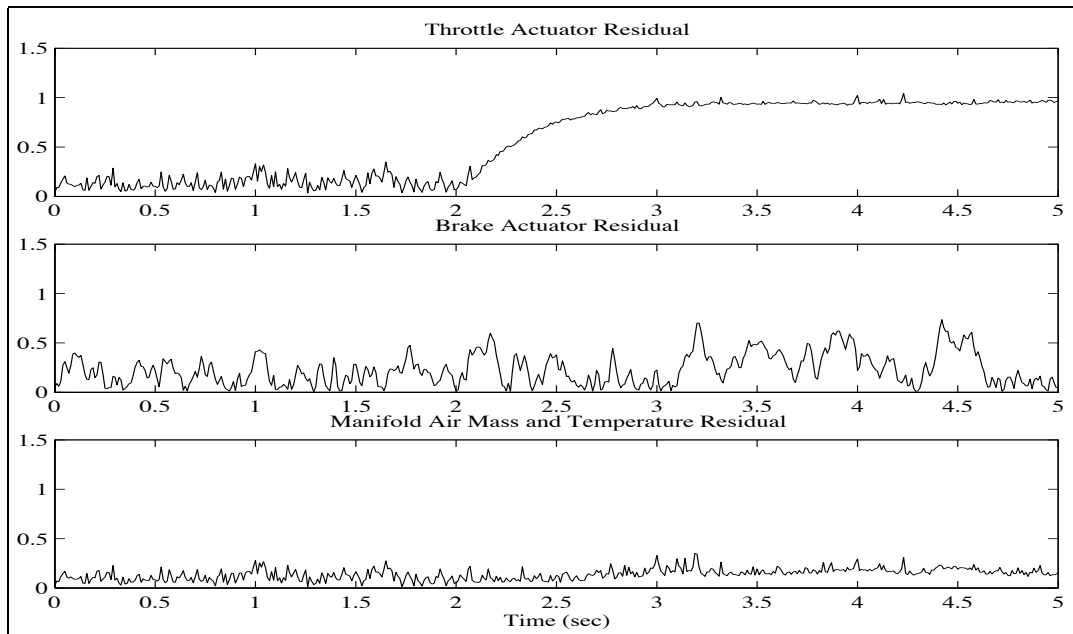


Figure 4.9: Residuals for fault detection filter one when a +2 deg throttle actuator fault occurs.

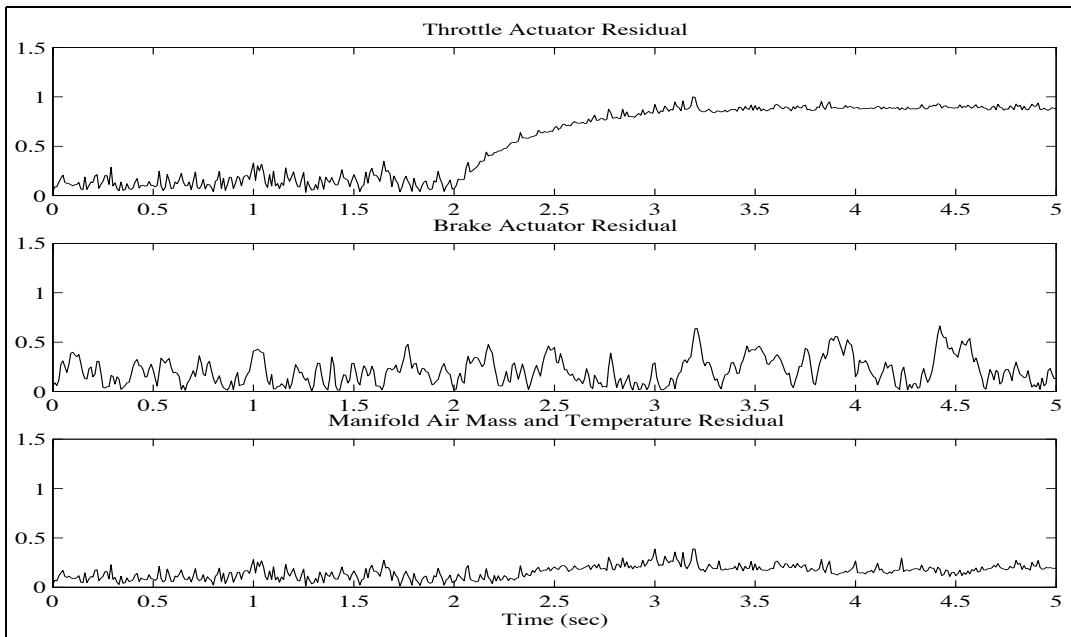


Figure 4.10: Residuals for fault detection filter one when a -2 deg throttle actuator fault occurs.

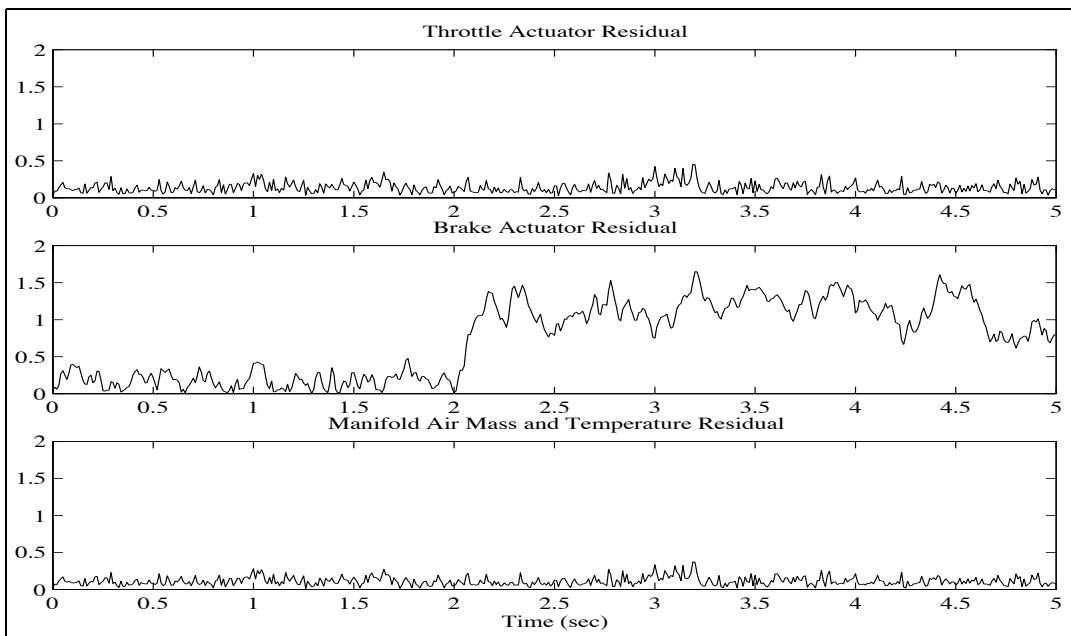


Figure 4.11: Residuals for fault detection filter one when a brake actuator fault occurs.

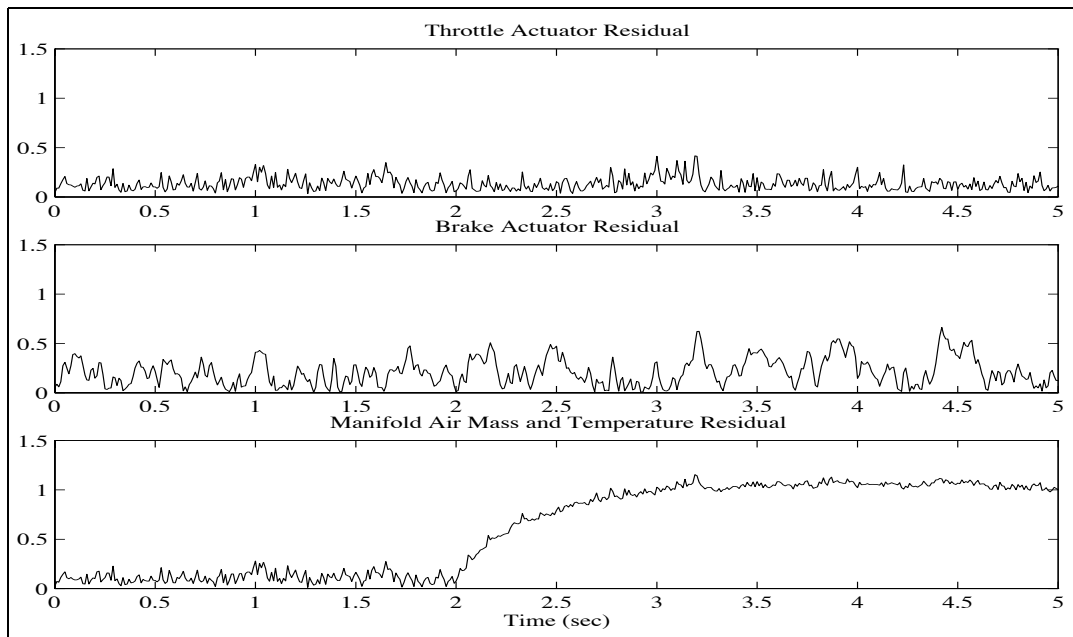


Figure 4.12: Residuals for fault detection filter one when a manifold air mass sensor fault occurs.

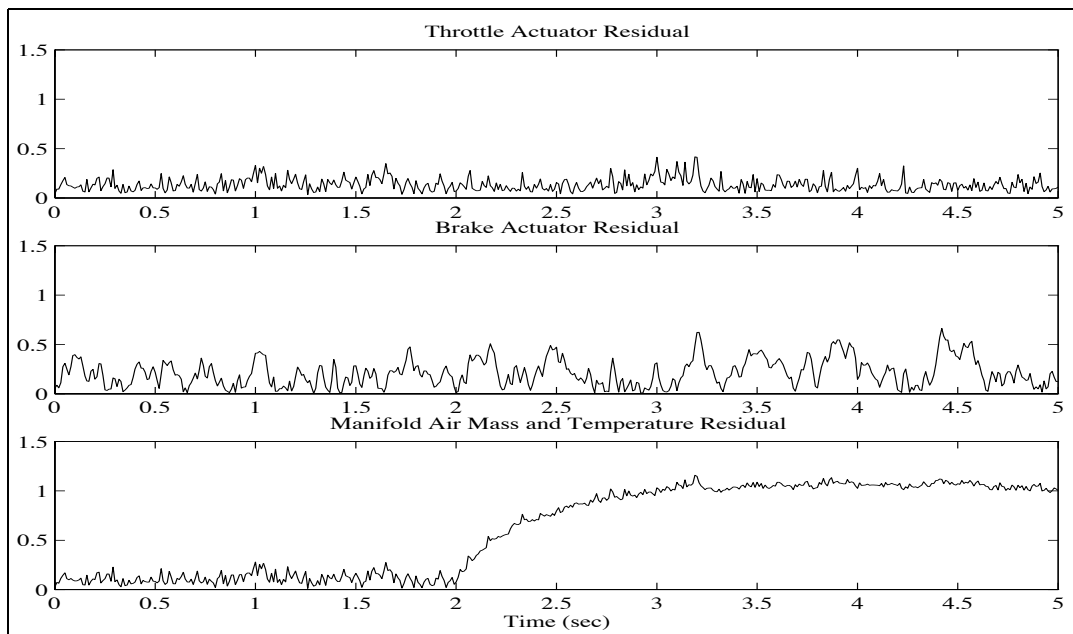


Figure 4.13: Residuals for fault detection filter one when a manifold temperature sensor fault occurs.

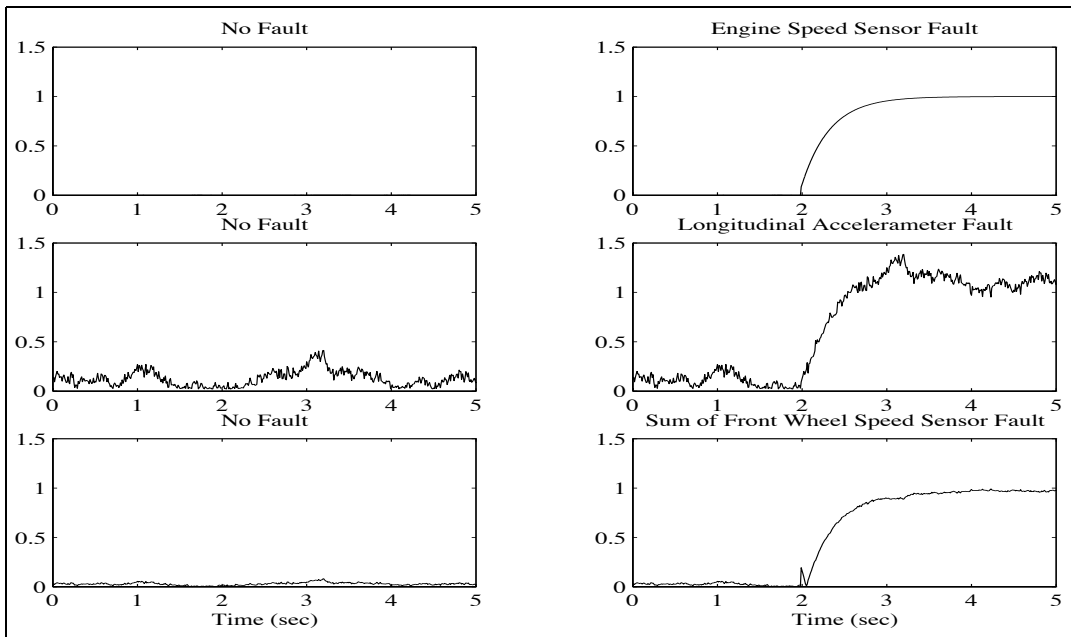


Figure 4.14: Residuals for fault detection filter two.

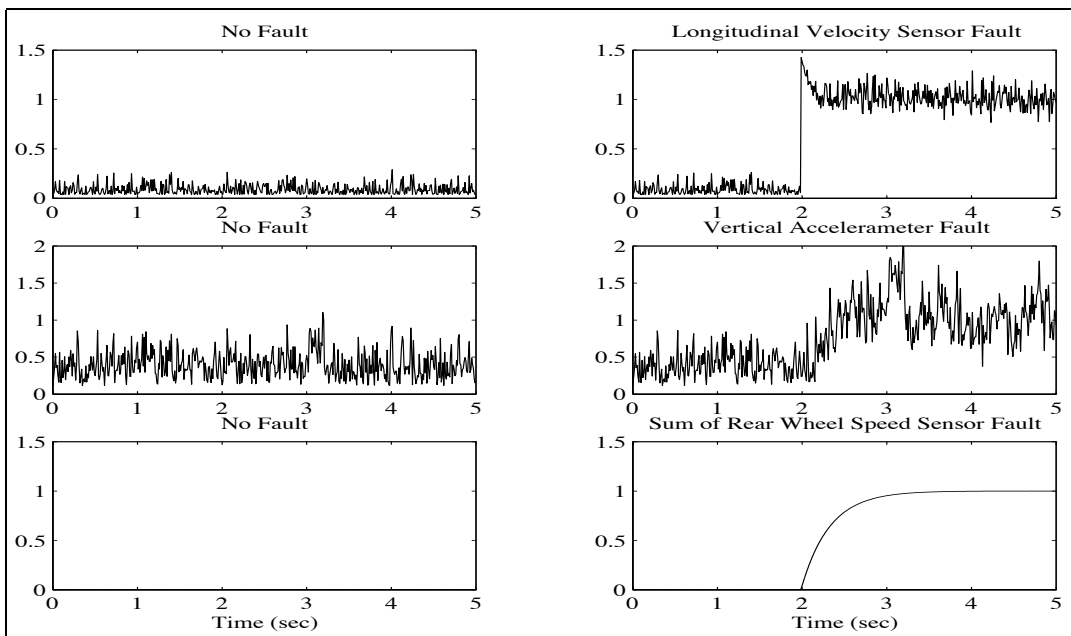


Figure 4.15: Residuals for fault detection filter three.

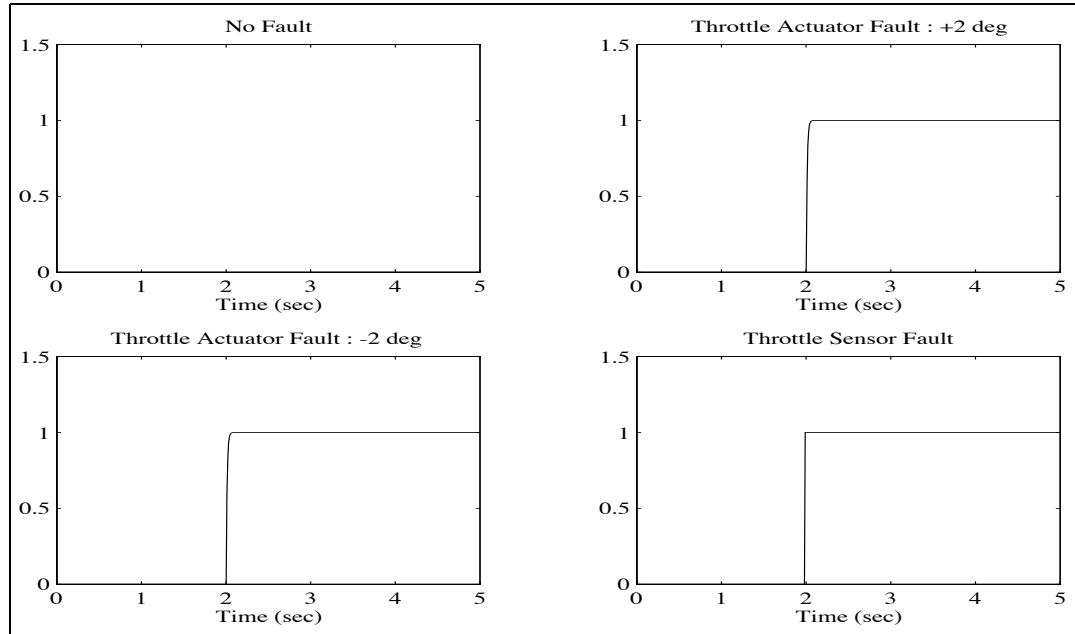


Figure 4.16: Residual for fault detection filter four.

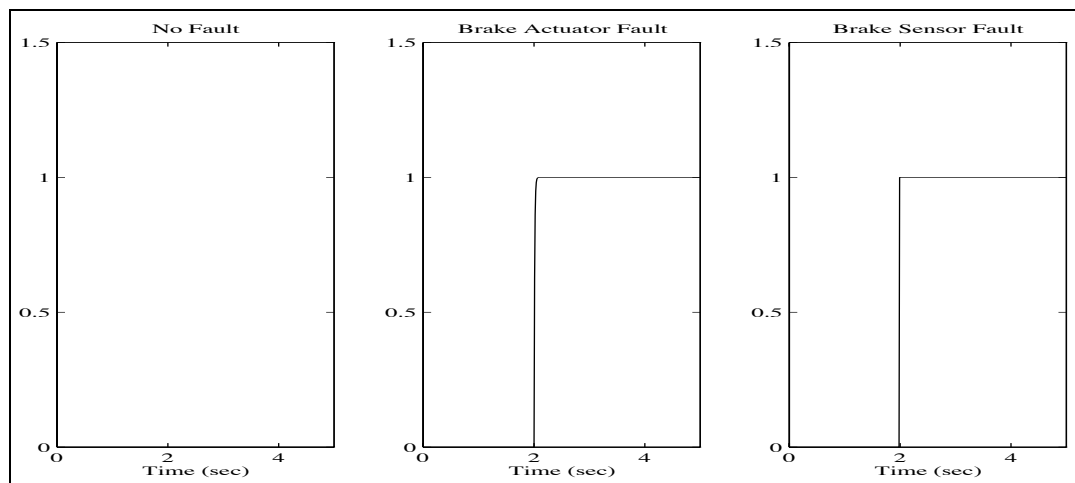


Figure 4.17: Residual for fault detection filter five.

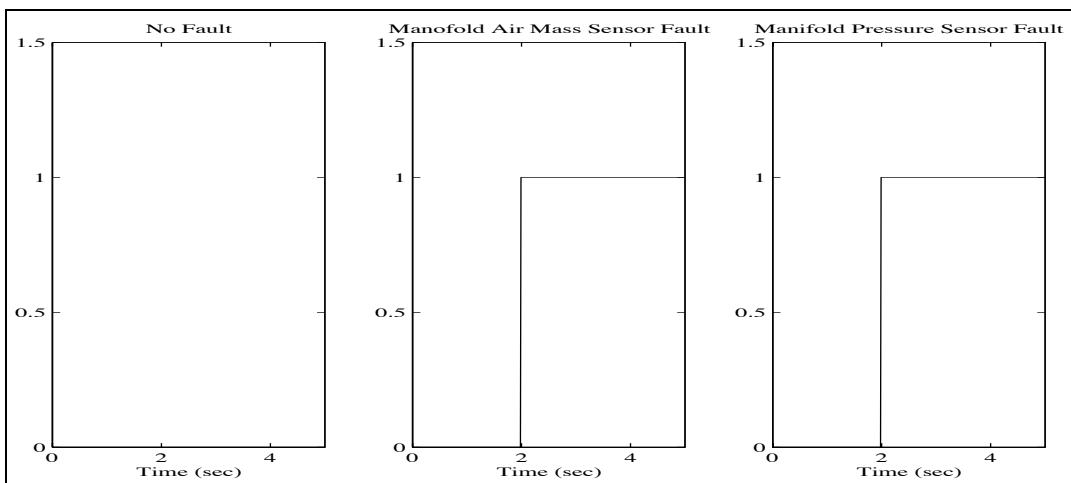


Figure 4.18: Residual for fault detection filter six.

CHAPTER 5

Residual Processing

A PRIMARY OBJECTIVE of any analytic redundancy management scheme is to generate residuals with sufficient statistics and to analyze these signals. The fault detection filters perform this task by constraining the residual to respond in a known and fixed direction for each fault, thereby aiding the fault isolation process. However, in the presence of nonlinearities and process uncertainties, the directional properties of the residual process are no longer well defined. Further analysis of the signals is needed.

In this scenario, fault isolation may be viewed as a pattern recognition problem. The residual processor could be a Bayesian neural network whose input is the residual process and the outputs, in some sense, approximate the posteriori probabilities of each fault (Douglas et al. 1995). However, the Bayesian neural network, while easy to implement, is not easily amenable to mathematical analysis. Moreover, due to feedback, the performance deteriorates in the presence of noise at the input.

A better approach is to use a Sequential Probability Ratio Test (SPRT). We derived a multiple hypothesis Shiriyayev SPRT by adopting a dynamic programming viewpoint and

Fault detection filter 1:	Throttle actuator Brake actuator Manifold air mass sensor Manifold temperature sensor
Fault detection filter 2:	Engine speed sensor Longitudinal accelerometer Front wheel symmetric speed sensor
Fault detection filter 3:	Longitudinal velocity sensor Vertical accelerometer Rear wheel symmetric speed sensor
Parity equation 1:	Throttle actuator Throttle sensor
Parity equation 2:	Brake actuator Brake sensor
Parity equation 3:	Manifold air mass sensor Manifold pressure sensor

Table 5.1: Faults organized into analytically redundant groups.

showed that for a certain criterion of optimality, it detects and isolates a fault in minimum time (Malladi and Speyer 1996, Malladi and Speyer 1997). The fault isolation problem is now solved by assuming that each fault corresponds to a particular hypothesis. The multiple hypothesis Shiryayev SPRT is described in detail in last year's report (Douglas et al. 1996) and in (Malladi and Speyer 1996) and (Malladi and Speyer 1997). The notation of this chapter is the same as in Chapter 7 of (Douglas et al. 1996).

5.1 Residual Processor Design

As discussed in Sections 3.1.4 and 3.2, sensor and actuator faults are organized into the analytically redundant groups of Table 5.1. The combined residual processes, $x_k \in \mathbb{R}^{12}$, from the fault detection filters and parity equations are considered to be the measurement sequence for the Shiryayev sequential probability ratio test. The measurement sequence is assumed to have a Gaussian distribution and be conditionally independent, that is, once a fault occurs, the measurement process is independent.

There are 14 hypotheses $\{\mathcal{H}_0 \dots \mathcal{H}_{13}\}$, including the no-fault case. For convenience,

\mathcal{H}_0 : No fault	\mathcal{H}_1 : Manifold air mass sensor
\mathcal{H}_2 : Manifold temperature sensor	\mathcal{H}_3 : Manifold pressure sensor
\mathcal{H}_4 : Throttle sensor	\mathcal{H}_5 : Throttle actuator
\mathcal{H}_6 : Brake sensor	\mathcal{H}_7 : Brake actuator
\mathcal{H}_8 : Engine speed sensor	\mathcal{H}_9 : Front wheel speed sensor
\mathcal{H}_{10} : Rear wheel speed sensor	\mathcal{H}_{11} : Longitudinal velocity sensor
\mathcal{H}_{12} : Longitudinal accelerometer	\mathcal{H}_{13} : Vertical accelerometer

Table 5.2: Fault hypotheses for residual processing.

they are listed below. Each hypothesis is a given residual probability density function. The density functions for all hypotheses are constructed as follows. First, since the residuals are assumed to have Gaussian distribution, the only required statistics are the mean and covariance. Next, model a step fault as a sudden increase in the mean of the residual process. While a ramp fault could be modelled as a gradual increase in the mean, no hypothesis models this type of fault signature directly. Using the nonlinear simulation, apply a design step fault of some particular size to one component at a time and compute the resulting residual mean and covariance matrix.

It is important to state that while the hypothesis statistics are associated with a given design step fault, the statistics remain fixed throughout all residual processor testing. The hypothesis statistics are not recomputed when the size of an applied fault does not match the design fault or when ramp faults are applied.

As an example, the bias vector for the design fault size in the manifold air mass sensor, hypothesis $\{\mathcal{H}_1\}$, is

$$[0.197 \ 5.226 \ 1.799 \ 6.595 \ 1.639 \ 5.504 \ 0.448 \ 0.533 \ 6.620 \ -0.001 \ 0.012 \ 1.392]$$

while the covariance matrix is

$$\begin{bmatrix}
 0.011 & 0.016 & 0.008 & 0.018 & -0.001 & 0.008 & 0.002 & 0.005 & \dots \\
 0.016 & 11.26 & 0.113 & 0.070 & 0.104 & 0.135 & -0.003 & -0.015 & \dots \\
 0.008 & 0.113 & 0.158 & 0.575 & 0.205 & 0.721 & 0.033 & 0.037 & \dots \\
 0.018 & 0.070 & 0.575 & 2.142 & 0.756 & 2.668 & 0.121 & 0.132 & \dots \\
 -0.001 & 0.104 & 0.205 & 0.756 & 0.318 & 1.074 & 0.043 & 0.042 & \dots \\
 0.008 & 0.135 & 0.721 & 2.668 & 1.074 & 3.692 & 0.151 & 0.156 & \dots \\
 0.002 & -0.003 & 0.033 & 0.121 & 0.043 & 0.151 & 0.008 & 0.008 & \dots \\
 0.005 & -0.015 & 0.037 & 0.132 & 0.042 & 0.156 & 0.008 & 0.013 & \dots \\
 0.018 & 0.072 & 0.577 & 2.148 & 0.758 & 2.675 & 0.121 & 0.132 & \dots \\
 0.0001 & -0.001 & 0.0004 & -0.0001 & 0.001 & 0.002 & 0.0001 & 0.001 & \dots \\
 0.001 & -0.017 & 0.001 & 0.003 & 0.002 & 0.007 & 0.0002 & 0.001 & \dots \\
 -0.001 & -0.026 & -0.003 & -0.010 & -0.002 & -0.011 & -0.001 & -0.001 & \dots \\
 \dots & \dots & \dots & \dots & \dots & \dots & \dots & \dots & \dots \\
 \dots & 0.018 & 0.0001 & 0.001 & -0.001 & \dots & \dots & \dots & \dots \\
 \dots & 0.072 & -0.001 & -0.017 & -0.026 & \dots & \dots & \dots & \dots \\
 \dots & 0.577 & 0.0004 & 0.001 & -0.003 & \dots & \dots & \dots & \dots \\
 \dots & 2.148 & -0.0001 & 0.003 & -0.010 & \dots & \dots & \dots & \dots \\
 \dots & 0.758 & 0.001 & 0.002 & -0.002 & \dots & \dots & \dots & \dots \\
 \dots & 2.675 & 0.002 & 0.007 & -0.011 & \dots & \dots & \dots & \dots \\
 \dots & 0.121 & 0.0001 & 0.0002 & -0.001 & \dots & \dots & \dots & \dots \\
 \dots & 0.132 & 0.001 & 0.001 & -0.001 & \dots & \dots & \dots & \dots \\
 \dots & 2.154 & -0.0001 & 0.003 & -0.010 & \dots & \dots & \dots & \dots \\
 \dots & -0.0001 & 0.010 & 0.001 & 0.0002 & \dots & \dots & \dots & \dots \\
 \dots & 0.003 & 0.001 & 0.010 & -0.001 & \dots & \dots & \dots & \dots \\
 \dots & -0.010 & 0.0002 & -0.001 & 0.010 & \dots & \dots & \dots & \dots
 \end{bmatrix}$$

5.2 Simulations

The statistics of the residual process $\{x\}$ are exactly modeled by the Shiriyayev sequential probability ratio test as

$$\text{Under } \mathcal{H}_i : x \sim \mathcal{N}(m_i, \Lambda_i)$$

where m_i and Λ_i are a known mean and covariance. Therefore it is not surprising that when a hard fault of the same magnitude as the design step fault is applied in the nonlinear simulation, the residual processor isolates the fault almost immediately. However, real faults have an unknown magnitude and never match the design case so it seems reasonable to evaluate the residual processor by applying ramp faults to the nonlinear simulation.

Manifold air mass sensor:	x_3 derived from fault detection filter 1
Throttle actuator:	x_1 derived from fault detection filter 1
Brake actuator:	x_{11} derived from parity equation 2
Vertical accelerometer:	x_8 derived from fault detection filter 3

Table 5.3: Applied faults for residual processor testing.

To illustrate typical results, ramp faults in the manifold air mass sensor, throttle actuator, vertical accelerometer and brake actuator are considered. Figures 5.1, 5.3, 5.4 and 5.5 show the residuals given in Table 5.3.

Figure 5.1 shows a 10 second simulation of a ramp fault applied to the manifold air mass sensor. The size of the fault is gradually increased from zero at two seconds to the design size of 0.07 kg/s at seven seconds. It is seen that the posteriori probability of a fault in the manifold air mass sensor, hypothesis \mathcal{H}_1 , becomes one at around five seconds.

Figure 5.2 shows the posteriori probability of a fault in the manifold temperature sensor, hypothesis \mathcal{H}_2 . The probability increases initially, but goes back to zero as the fault size in the manifold air mass sensor increases.

Figure 5.3 shows a ten second simulation of a ramp fault applied to the throttle actuator. The size of the fault is gradually increased from zero at two seconds to the design size of two degrees at seven seconds. In this case, the posteriori probability of a fault in the throttle actuator, hypothesis \mathcal{H}_5 , increases to one at around three seconds.

Figure 5.4 shows a ten second simulation of a ramp fault applied to the brake actuator. The size of the fault is gradually increased from zero at two seconds to the design size of fifty at seven seconds. Here, the posteriori probability of a fault in the brake actuator, hypothesis \mathcal{H}_7 , increases to one at around three seconds.

In Figure 5.5, a ten second simulated ramp fault is applied to the vertical accelerometer. The size of the fault is gradually increased from zero at two seconds to the design size of $0.5 \frac{\text{m}}{\text{sec}^2}$ at seven seconds. Here, the posteriori probability of a fault in the vertical

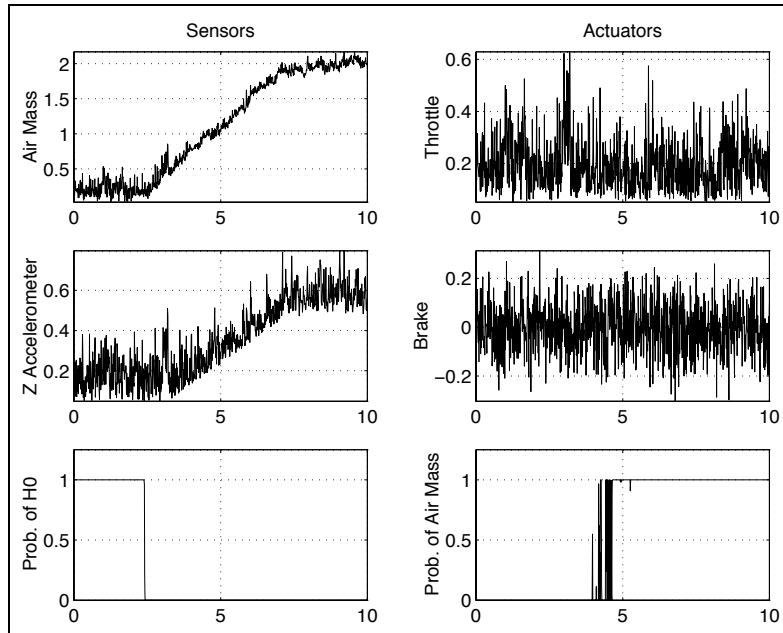


Figure 5.1: Ramp fault in manifold air mass sensor.

accelerometer, hypothesis \mathcal{H}_{13} , increases to one at around three seconds.

5.3 Conclusions

The simulation studies clearly illustrate the efficacy of a health monitoring scheme which blends a classical fault detection filters approach with hypothesis testing ideas.

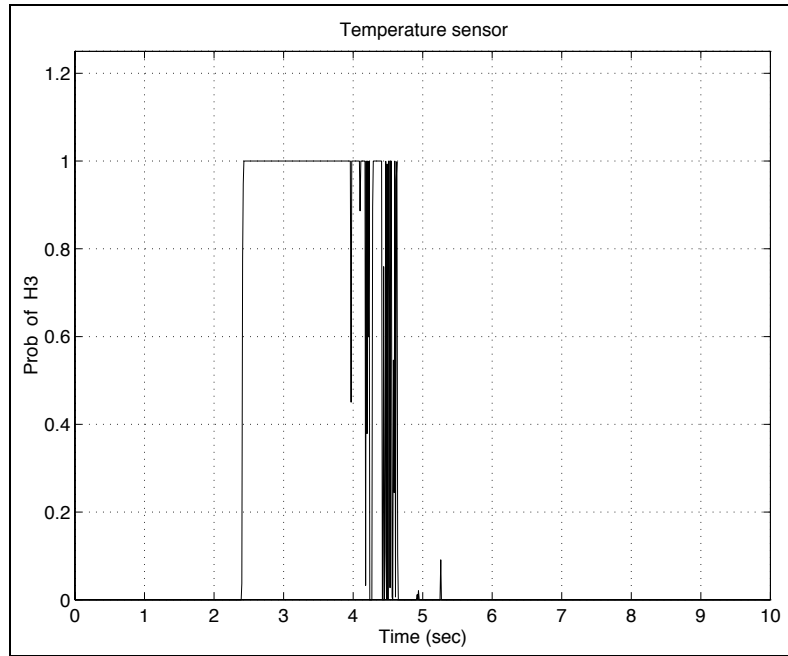


Figure 5.2: Probability of a fault in the manifold temperature sensor as a ramp fault in manifold air mass sensor is applied.

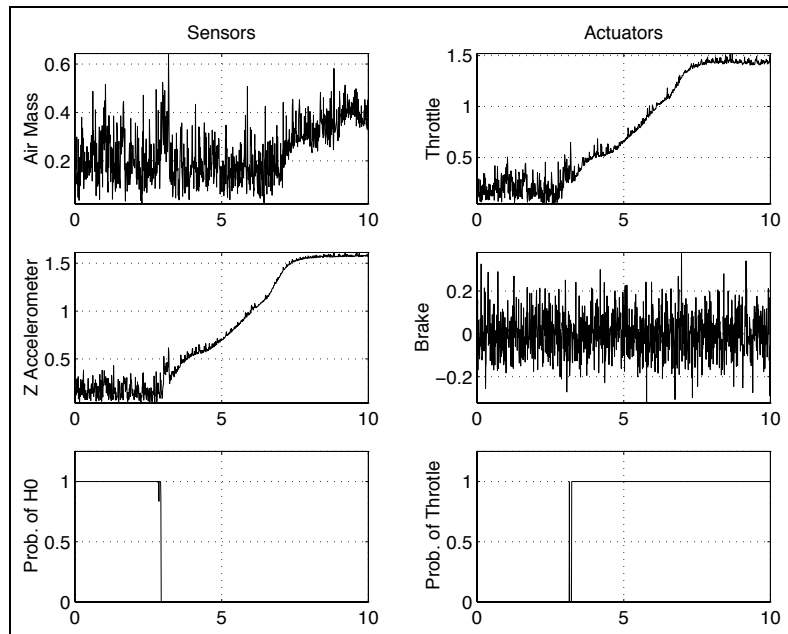


Figure 5.3: Ramp fault in throttle actuator.

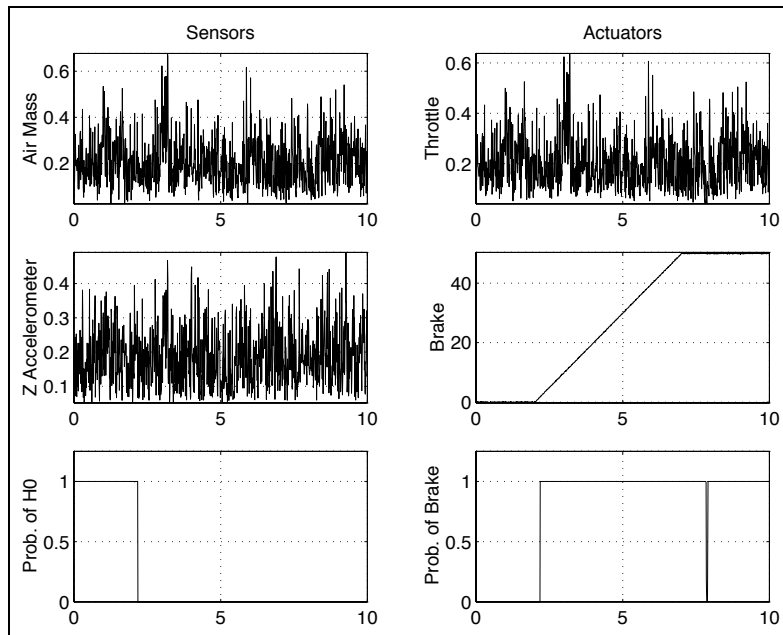


Figure 5.4: Ramp fault in Brake actuator.

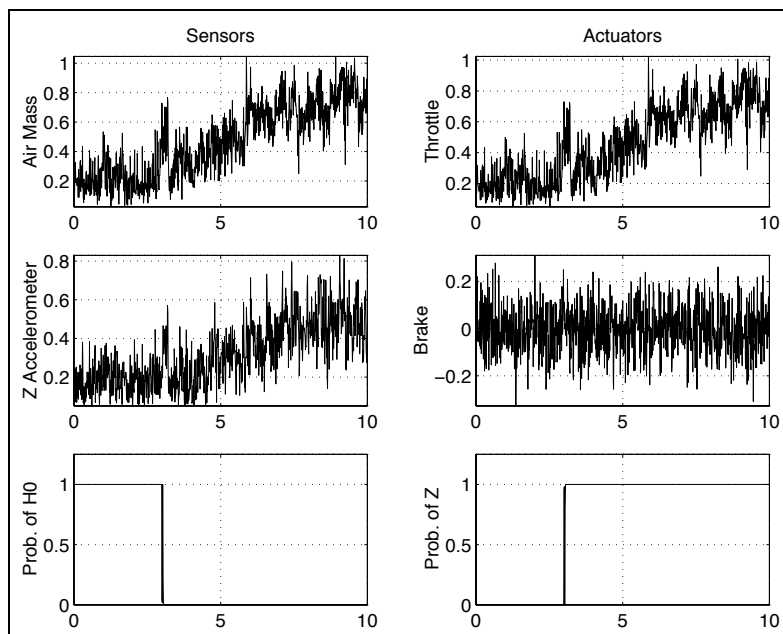


Figure 5.5: Ramp fault in Vertical accelerometer.

A Game Theoretic Fault Detection Filter

THE FAULT DETECTION FILTER was introduced by Beard (Beard 1971) in his doctoral thesis and later refined by Jones (Jones 1973) who gave it a geometric interpretation. Since then, the fault detection filter has undergone many refinements. White (White and Speyer 1987) derived an eigenstructure assignment design algorithm. Massoumnia (Massoumnia 1986) used advances in geometric theory to derive a complete and elegant geometric version of a fault detection filter and derived a reduced-order fault detector (Massoumnia et al. 1989). Most recently, Douglas robustified the filter to parameter variations (Douglas 1993) and (Douglas and Speyer 1996) and also derived a version of the filter which bounds disturbance transmission (Douglas and Speyer 1995). The fault detection filter background and design methods discussed in Appendices A,B and C of last year's report (Douglas et al. 1996) as well as the application to vehicle fault detection of Sections 2 through 4 all follow from these sources.

Common to all of these sources is an underlying structure of independent, invariant subspaces. Most design algorithms, an exception being (Douglas and Speyer 1995), rely

on spectral methods, that is, specifying eigenvalues and eigenvectors, since these methods lead directly to the needed filter structure. Spectral methods, however, also limit the applicability of fault detection filters to linear, time-invariant systems and filters designed by these methods can have poor robustness to parameter variations (Lee 1994).

For these reasons, we take a different approach to detection filter design. We look at the fault detection process as a disturbance attenuation problem and convert the process into a differential game which leads to the final design. The game is one in which the player is a state estimate and the adversaries are all of the exogenous signals, save the fault to be detected. The player attempts to exclude the adversaries from a specified portion of the state-space much in the same way that the invariant subspace structure of the fault detection filter restricts state trajectories when driven by faults. The end result is an \mathcal{H}_∞ -type filter which bounds disturbance transmission.

Since fault detection filters block transmission, it would seem reasonable to expect that in the limiting case when the \mathcal{H}_∞ transmission bound is brought to zero, the game filter no longer approximates, but actually becomes a fault detection filter. We will prove that this is indeed the case. For linear time-invariant (LTI) systems, we will show, in fact, that the game filter becomes a Beard-Jones fault detector in the sense of (Douglas 1993): faults other than the one to be detected are restricted to a subspace which is invariant and unobservable.

The method developed here has wider applicability than current techniques since time-invariance is never assumed in the game solution. Thus, for a class of time-varying systems, results analogous to the LTI case exist in the limit as disturbance bounds are taken to zero. It is also possible with this method to deal with model uncertainty by treating it as another element in the differential game (Chichka and Speyer 1995, Mangoubi et al. 1994). In this manner, sensitivity to parameter variations can be reduced. Finally, by using a game theoretic approach, the designer has the freedom to choose the extent to which the game filter behaves as an \mathcal{H}_∞ filter and the extent to which it behaves like a detection filter. This flexibility is unique to this method of fault detection filter design.

The development of game theoretic estimation closely followed the development of game theoretic control theory. The most notable and the most cited (and most unreadable) work in the latter was the paper by Doyle *et al.* (Doyle et al. 1989). The ascendant of the work presented here is the paper by Rhee and Speyer (Rhee and Speyer 1991) which derived the two Riccati solution of (Doyle et al. 1989) via the calculus of variations. It is hard to credit the first derivation of the game theoretic estimator, though (Banavar and Speyer 1991) or (Yaesh and Shaked 1993) are probable candidates.

In Section 6.1, we motivate the disturbance attenuation approach to FDI by showing how it approximates the actions of a detection filter. In Section 6.2, we solve a disturbance attenuation problem patterned after the fault detection process. The game theoretic fault detection filter is a product of this solution. In Sections 6.3.1 and 6.3.2, we demonstrate the effectiveness of the new filter with a pair of examples.

6.1 The Approximate Detection Filter Design Problem

6.1.1 Modeling the Detection Problem

The general class of systems that we will look at are linear, observable, possibly time-varying, and driven by noisy measurements:

$$\begin{aligned}\dot{x}(t) &= Ax(t) + Bu(t), \\ y(t) &= Cx(t) + v.\end{aligned}\tag{6.1}$$

We will also assume that our state matrices have sufficient smoothness to guarantee the existence of derivatives various order.

Beard (Beard 1971) showed that failures in the sensors and actuators, and unexpected changes in the plant dynamics can be modeled as additive signals:

$$\dot{x} = Ax + Bu + F_1\mu_1 + \cdots + F_q\mu_q.\tag{6.2}$$

Let n be the dimension of the state-space. The $n \times p_i$ matrix, F_i , $i = 1 \cdots q$, is called a *failure map* and represents the directional characteristics of the i th fault. The $p_i \times 1$ vector,

μ_i , is the *failure signal* and represents the time dependence of the failure. It will always be assumed that each F_i is monic, i.e. $F_i\mu_i \neq 0$ for $\mu_i \neq 0$. We will look at F_i and μ_i in more detail in Section 6.1.2, and we will show the importance of the monicity assumption in Section 6.1.3. Throughout this paper, we will refer to μ_1 as the “target fault” and the other faults, μ_j , $j = 2 \cdots q$, as the “nuisance faults”. Without loss of generality, we can represent the entire set of nuisance faults with a single map and vector:

$$\dot{x} = Ax + Bu + F_1\mu_1 + F_2\mu_2.$$

Suppose that it is desired to detect the occurrence of the failure, μ_1 , in spite of the measurement noise, v , and the possible presence of the nuisance faults, μ_2 . As described earlier, a detection filter-based solution to this problem,

$$\dot{\hat{x}} = A\hat{x} + L(y - C\hat{x}), \quad (6.3)$$

works by keeping the reachable subspaces of μ_1 and μ_2 in separate and nonintersecting invariant subspaces. Thus, with a properly chosen projector, H , we can project the filter residual, $(y - C\hat{x})$, onto the orthogonal complement of the invariant subspace containing μ_2 and get a signal,

$$z = H(y - C\hat{x}), \quad (6.4)$$

such that

$$z = 0 \quad \text{when } \mu_1 = 0 \text{ and } \mu_2 \text{ is arbitrary.} \quad (6.5)$$

To be useful for FDI, z must also be such that

$$z \neq 0 \quad \text{when } \mu_1 \neq 0. \quad (6.6)$$

If we restrict ourselves to time-invariant systems, (6.6) will be equivalent to requiring that the transfer matrix between $\mu_1(s)$ and $z(s)$ ¹ be *left-invertible*. Left-invertibility, however, is

¹ $\mu_1(s)$ and $z(s)$ are the Laplace transforms of the time-domain signals $\mu_1(t)$ and $z(t)$.

a severe restriction, and has no analog for the general time-varying systems that considered here. Previous researchers (Douglas 1993, Massoumnia et al. 1989) have, in fact, only required that the mapping from $\mu_1(t)$ to $z(t)$ be *input observable*, i.e. $z \neq 0$ for any μ_1 that is a step input. It is then argued (Massoumnia et al. 1989) that with input observability z will be nonzero for “almost any” μ_1 , since μ_1 is unlikely to remain in the kernel of the mapping to z for all time.

We formulate the approximate detection filter problem by requiring input observability and relaxing the requirement for strict blocking that is implied by (6.5). We, instead, only require that the transmission of the nuisance fault be bounded above by a pre-set level, $\gamma > 0$:

$$\frac{\|z\|^2}{\|\mu_2\|^2} \leq \gamma. \quad (6.7)$$

Equation (6.7) is clearly a disturbance attenuation problem, and it is an H^∞ problem if we assume L_2 norms for μ_2 and z in (6.7). We refer to the solution to the approximate detection filter problem as the *game theoretic fault detection filter*.

Remark 2. Detection filters typically make no assumptions about the time dependence of nuisance faults. The L_2 assumption that we make above is, thus, a new restriction. We will, however, recover the full generality of the detection filter in the limiting case when we take the disturbance attenuation bound to zero. ◀

Remark 3. The terms, “ H_∞ ” and “game theoretic,” are used interchangeably throughout this chapter. Doyle (Doyle et al. 1989) showed that the solution to the infinite-horizon linear quadratic game (Mageirou 1976) provides a fundamental solution to many H_∞ -norm minimizing problems, all other solutions being expressible in terms of this solution and a free parameter², Q . Other researchers established a direct equivalence between the two problems by using a disturbance attenuation interpretation of the H_∞ problem to recover Doyle’s result with the calculus of variations (Rhee and Speyer 1991) and with dynamic

²The free parameter, Q , is a real rational transfer function matrix.

programming (Başar and Bernhard 1995)³. These researchers, moreover, derive significant extensions of the H_∞ result, obtaining solutions for finite-horizon problems and time-varying systems. The differential game approach to solving H_∞ problems has since been revisited by a number of researchers (Limebeer et al. 1992, Mills and Bryson 1994) and has led to new results in estimation (Banavar and Speyer 1991, Yaesh and Shaked 1993), robust control (Ghaoui et al. 1992), robust estimation (DeSouza et al. 1992, Mangoubi 1995), and adaptive control (Chichka and Speyer 1995). The differential game approach has even made its way into textbooks such as (Green and Limebeer 1995). ◀

6.1.2 Modeling Failures

In this section, we will show how to construct failure maps and signals for each type of failure. Existing methods (Beard 1971, Douglas 1993, White and Speyer 1987) exist for time-invariant systems. For actuator faults and plant changes, these methods can be extended “as is” to time-varying systems. In the actuator fault case, this means that the map is taken to be the corresponding column of the input matrix. In the plant fault case, the map is similarly derived by pulling out the corresponding entries in the state matrix. The failure signals in both cases can be found by choosing an appropriate time function⁴.

Sensor faults require a generalization of the time-invariant result. Because these failures enter the system through the measurements, we can initially model them as an additive input in the measurement equation:

$$y = Cx + E_j\mu_j. \quad (6.8)$$

C is an $m \times n$ matrix, and E_j is an $m \times 1$ unit vector with a one at j th position, which corresponds to a failure in the j th sensor.

Following (Douglas 1993), we determine the sensor failure map by finding the input to the plant which drives the error state in the same way that μ_j will in (6.8). This is elegantly accomplished by a Goh transformation on the error space (Jacobson 1971). Defining the

³This approach was significantly extended by Chichka and Speyer in (Chichka and Speyer 1995).

⁴For example, hard failures or saturation failures can be modeled as step inputs.

estimation error, e , as $x - \hat{x}$, the filter residual is then

$$r \triangleq y - C\hat{x} = Ce$$

when there is no sensor noise (6.1). When a sensor failure occurs,

$$r = Ce + E_j\mu_j. \quad (6.9)$$

Let f_j be the solution to $E_j = Cf_j$. The transformation begins by defining a new error state,

$$\bar{e} \triangleq e + f_j\mu_j, \quad (6.10)$$

which allows us to rewrite (6.9) as $r = C\bar{e}$. Assuming a generic form for the observer, (6.3), and a homogeneous dynamic system, $\dot{x} = Ax$, we differentiate \bar{e} ,

$$\begin{aligned} \dot{\bar{e}} &= \dot{e} + \dot{f}_j\mu_j + f_j\dot{\mu}_j \\ &= Ae + LC\bar{e} + Af_j\mu_j - Af_j\mu_j + \dot{f}_j\mu_j + f_j\dot{\mu}_j \\ &= (A + LC)\bar{e} + \begin{bmatrix} f_j & (Af_j - \dot{f}_j) \end{bmatrix} \begin{Bmatrix} \dot{\mu}_j \\ -\mu_j \end{Bmatrix}, \end{aligned}$$

to get a differential equation for the transformed error trajectory. Clearly, the equivalent input is one which enters the system through

$$F_j = \begin{bmatrix} f_j & f_j^* \end{bmatrix}, \quad (6.11)$$

where $f_j^* = Af_j - \dot{f}_j$. When the system is time-invariant, $\dot{f}_j = 0$ and (6.11) will match the time-invariant failure map given in (Beard 1971) and (White and Speyer 1987). For our purposes, finding F_j is the key result. The actual time history of the failure signal is not important and so undue importance should not be attached to the “equivalent” input, $\begin{bmatrix} \dot{\mu}_j^T & -\mu_j^T \end{bmatrix}^T$.

6.1.3 Constructing the Failure Signal

We complete our formulation of the disturbance attenuation problem for fault detection by constructing a projector, H , which determines the failure signal, z , (6.4). For time-invariant

systems, this projector is constructed to map the reachable subspace of the fault signal μ_2 to zero (Beard 1971, Douglas 1993), i.e.

$$H = I - C\hat{F} \left[(C\hat{F})^T C\hat{F} \right]^{-1} (C\hat{F})^T, \quad (6.12)$$

where

$$\hat{F} = [A^{\beta_1} f_1, \dots, A^{\beta_{p_2}} f_{p_2}]. \quad (6.13)$$

The vector, f_i , $i = 1 \cdots p_2$, is the i th column of F_2 , and the integer, β_i , is the smallest natural number such that $CA^{\beta_i} f_i \neq 0$. The time-varying extension of this result is

$$H = I - C\hat{F}(t) \left[(C\hat{F}(t))^T C\hat{F}(t) \right]^{-1} (C\hat{F}(t))^T. \quad (6.14)$$

The columns of the matrix,

$$\hat{F}(t) = [b_1^{\beta_1}(t), \dots, b_{p_2}^{\beta_{p_2}}(t)],$$

are constructed with the Goh transformation:

$$b_i^1(t) = f_i(t), \quad (6.15)$$

$$b_i^j(t) = A(t)b_i^{j-1}(t) - \dot{b}_i^{j-1}. \quad (6.16)$$

In the time-varying case, β_i is the smallest integer for which the iteration above leads to a vector, $b_i^{\beta_i}(t)$, such that $C(t)b_i^{\beta_i}(t) \neq 0$ for all $t \in [t_0, t_1]$. It will be assumed that $A(t), C(t)$, and $F_2(t)$ are such that β_i exists. Since the state-space has dimension n , β_i is such that $0 \leq \beta_i \leq n - 1$. This restricts the class of admissible systems, but such assumptions seem to be unavoidable when dealing with the time-varying case (see, for example, (Clements and Anderson 1978)). The Goh transformation will be introduced explicitly in Section 7.3, where we will also give an alternate representation of (6.12) and (6.14).

We are now ready to discuss the conditions under which the solution to (6.7) will also generate an input observable mapping from μ_1 to z . The key requirement is that the system

be *output separable*. That is, F_1 and F_2 must be linearly independent and remain so when mapped to the output space by C and A . For time-invariant systems, the test for output separability is

$$\text{rank} \left[CA^{\delta_1} \tilde{f}_1, \dots, CA^{\delta_{p_1}} \tilde{f}_{p_1}, CA^{\beta_1} f_1, \dots, CA^{\beta_{p_2}} f_{p_2} \right] = p_1 + p_2. \quad (6.17)$$

As in (6.13), f_i is the i th column of F_2 , and β_i is the smallest integer such that $CA^{\beta_i} f_i \neq 0$. Similarly, \tilde{f}_j is the j th column of F_1 , and δ_j is the smallest integer such that $A^{\delta_j} \tilde{f}_j \neq 0$. The integer sum, $p_1 + p_2$, is the total number of columns in F_1 and F_2 .

For time-varying systems, the output separability test becomes

$$\begin{aligned} \text{rank} \left[C(t) \tilde{b}_1^{\delta_1}(t), \dots, C(t) \tilde{b}_{p_1}^{\delta_{p_1}}(t), C(t) b_1^{\beta_1}(t), \dots, C(t) b_{p_2}^{\beta_{p_2}}(t) \right] \\ = p_1 + p_2, \quad \forall t \in [t_0, t_1], \end{aligned} \quad (6.18)$$

where the vectors, $b_i^{\beta_i}$ and $\tilde{b}_j^{\delta_j}$, are found from the iteration defined by (6.15) and (6.16). The initial vector, \tilde{b}_j^1 , is set equal to the j th column of F_1 , and b_i^1 is initialized as the i th column of F_2 .

The following proposition connects output separability to input observability and shows the importance of the monicity assumption:

Proposition 6.1. Suppose that we have an approximate detection filter which satisfies (6.7) and generates the failure signal, z , given by (6.4). If F_1 and F_2 are output separable and F_1 is monic, then the mapping, $\mu_1(t) \mapsto z(t)$, is input observable.

Proof. The input observability of the mapping, $\mu_1(t) \mapsto z(t)$, is equivalent (Douglas 1993, Massoumnia et al. 1989) to requirement that F_1 be monic and that its image not intersect the unobservable subspace of (HC, A) . We have already assumed the former. To show the latter, let us assume the converse, i.e. that there exists a vector,

$$\xi_1(t) = \sum_{i=1}^{p_1} \alpha_i \tilde{f}_i(t), \quad (6.19)$$

such that

$$H(t)C(t)\Phi(t, \tau)\xi_1(\tau) = 0, \quad \forall t \text{ and } \tau \leq t. \quad (6.20)$$

The vector, \tilde{f}_i , is the i th column of F_1 , and the coefficient, α_i , is a real number. At least one α_i is nonzero. $\Phi(t, \tau)$ is the state transition matrix of $A(\cdot)$ from τ to t .

Equation (6.20) implies that $\xi_1(t) \in \text{Ker } H(t)C(t)$, since we can set $\tau = t$ and get $\Phi(t, t) = I$. Since the vectors, \tilde{f}_i , are independent by the monicity assumption, this implies that

$$\tilde{f}_i(t) \in \text{Ker } H(t)C(t), \quad \forall i = 1, \dots, p_1. \quad (6.21)$$

Now, if one of these vectors, say $\tilde{f}_{i_0}(t)$, is not also in $\text{Ker } C(t)$, then (6.21) can hold only if $C\tilde{f}_{i_0}(t)$ is linearly dependent upon the vectors, $Cb_i^{\beta_i}$, which form the projector, $H(t)$. This, in turn, would imply that the output separability test, (6.18), will fail, which implies the proposition. Thus, for argument's sake, let us suppose that all the \tilde{f}_i lie in $\text{Ker } C(t)$, so that we can continue with the proof.

Now, because we have assumed that the underlying matrices are smooth enough to allow for derivatives of arbitrary order, a necessary and sufficient condition for (6.20) is that the derivatives of $HC\Phi\xi_1$ be zero for all t and τ . Thus,

$$\begin{aligned} \frac{d}{d\tau} [H(t)C(t)\Phi(t, \tau)\xi_1(\tau)] &= H(t)C(t)\Phi(t, \tau) \left[-A(\tau)\xi_1(\tau) + \dot{\xi}_1(\tau) \right] \\ &= H(t)C(t)\Phi(t, \tau)\xi_2(\tau) = 0, \quad \forall t, \tau, \end{aligned} \quad (6.22)$$

where $\xi_2 \triangleq -A\xi_1 + \dot{\xi}_1$. Again, setting $\tau = t$ in (6.22) implies that $\xi_2(t) \in \text{Ker } H(t)C(t)$. From the definition of ξ_1 and the iteration formulas (6.15,6.16), we can rewrite ξ_2 as

$$\xi_2 = \alpha_1 \tilde{b}_1^2 + \dots + \alpha_{p_1} \tilde{b}_{p_1}^2. \quad (6.23)$$

The same arguments as before will lead us to the conclusion that either $\tilde{b}_j^2(t) \in \text{Ker } C(t), \forall j, t$ or that our proposition holds. We will again assume the former for argument's sake.

In the general case, we consider the vector, ξ_k , which is the k th iteration of formula,

$$\xi_j = -A\xi_{j-1} + \dot{\xi}_{j-1}, \quad (6.24)$$

in which the initial vector, ξ_1 , is given by (6.19)⁵. We can also write ξ_k as

$$\xi_k = \sum_{i=1}^{p_1} \alpha_i \tilde{b}_i^k(t),$$

where \tilde{b}_i^k is the k th step of the iteration (6.15,6.16) with \tilde{b}_i^1 taken to be \tilde{f}_i , the i th column of F_1 . Previously, we saw for the case, $k = 1$, that

$$H(t)C(t)\Phi(t,\tau)\xi_k(\tau) = 0, \quad \forall t \text{ and } \tau \leq t \quad (6.25)$$

implies

$$C(t)\tilde{b}_i^k(t) = 0, \quad \forall i, t, \quad (6.26)$$

$$H(t)C(t)\Phi(t,\tau)\xi_{k+1}(\tau) = 0, \quad \forall t \text{ and } \tau \leq t, \quad (6.27)$$

where $\xi_{k+1} \triangleq -A\xi_k + \dot{\xi}_k$ is the next step in the iteration (6.24). The arguments used for $k = 1$ are independent of the particular value of k , which means that (6.26,6.27) hold for all k . Thus, by induction, we can claim that ξ_1 unobservable through (HC, A) implies that all of the vectors $\tilde{b}_k^i(t)$, $i = 1 \dots n-1$, $k = 1 \dots p_1$ from (6.15,6.16) lie in the kernel of $C(t)$. This, implies that the output separability test matrix,

$$\left[C\tilde{b}_1^{\delta_1}, \dots, C\tilde{b}_{p_1}^{\delta_{p_1}}, Cb_1^{\beta_1}, \dots, Cb_{p_2}^{\beta_{p_2}} \right],$$

will fail to be full-rank. Therefore, the contrapositive argument,

$$\text{image } F_2 \cap \text{Ker } HC \neq 0 \implies F_1 \text{ and } F_2 \text{ not output separable,}$$

implies our proposition. ◀

⁵Note that this formula is simply the Goh transformation.

Remark 4. Although output separability is a necessary condition for the existence of Beard-Jones filters (Beard 1971, Douglas 1993), Edelmayer *et al.* (Edelmayer et al. 1996), show that even without output separability it is still possible to find approximate detection filters which can distinguish the target input from nuisance inputs. There is no guarantee, however, that this will always be the case, and our example in Chapter 8 will show that the loss of output separability severely reduces our ability to distinguish the two faults. ◀

Remark 5. A property of the unknown input observer such as described by (Frank 1990, Patton and Chen 1992, Saif and Guan 1993), and its approximations, such as the filter we are about to derive, is the ability to distinguish only one fault out of a set of faults. In general, this is a disadvantage when compared to the Beard-Jones Fault Detection Filter which can identify several faults. An exception to this rule, however, is in the number of faults which can be included in the nuisance set. In the unknown input observer, any fault which is output separable from the target fault can be included, though a minimal set that spans the range of the nuisance set may have to be used as the failure map in order to preserve monicity. In a Beard-Jones Filter, all of the faults in the model will be target faults at one point or another and so they must be pairwise output separable. This severely limits the number of faults which can be included in a single Beard-Jones Filter⁶. ◀

6.2 A Game Theoretic Solution to the Approximate Detection Filter Design Problem

6.2.1 The Disturbance Attenuation Problem

We now turn our attention to the disturbance attenuation problem implied by (6.7). We begin by defining a disturbance attenuation function,

$$D_{af} = \frac{\int_{t_0}^{t_1} \|HC(x - \hat{x})\|_Q^2 dt}{\int_{t_1}^{t_2} [\|\mu_2\|_{M^{-1}}^2 + \|v\|_{V^{-1}}^2] dt + \|x(t_0) - \hat{x}_0\|_{P_0}^2}, \quad (6.28)$$

⁶In general, one can include, at most, only as many faults as there are measurements in the system (Douglas 1993, Massoumnia et al. 1989).

which is a ratio of the outputs to the disturbances (Rhee and Speyer 1991). Equation (6.28) is patterned roughly after (6.7). We have added the sensor noise, v , and the initial error, $x(t_0) - \hat{x}_0$, to the set of disturbance signals to incorporate tradeoffs for noise rejection and settling time into the problem. M, V, Q , and P_0 are weighting matrices. Note that we do not include the target fault, μ_1 , at this stage of the design problem, since we are now focusing on nuisance blocking. Our only concern with μ_1 is that it be visible at the output, which is what Proposition 6.1 guarantees.

The disturbance attenuation problem is to find the estimate, \hat{x} , so that for all μ_2 , $v \in L_2[t_1, t_2]$, $x(t_0) \in \mathbb{R}^n$,

$$D_{af} \leq \gamma,$$

where $\gamma \in \mathbb{R}$ is called the *disturbance attenuation bound*. Since D_{af} is defined with L_2 norms, the disturbance attenuation problem is equivalent to a suboptimal H_∞ problem. (C, A) will always be assumed to be an observable pair.

To solve this problem, we convert (6.28) into a cost function,

$$J = \int_{t_0}^{t_1} \left[\|HC(x - \hat{x})\|_Q^2 - \gamma(\|\mu_2\|_{M^{-1}}^2 + \|y - Cx\|_{V^{-1}}^2) \right] dt - \|x(t_0) - \hat{x}_0\|_{\Pi_0}^2, \quad (6.29)$$

where we have used (6.1) to rewrite the measurement noise term. Note that we have also rewritten the initial error weighting, defining $\Pi_0 \triangleq \gamma^{-1}P_0$. The disturbance attenuation problem is then solved via the differential game,

$$\min_{\hat{x}} \max_y \max_{\mu_2} \max_{x(t_0)} J \leq 0, \quad (6.30)$$

subject to

$$\begin{aligned} \dot{x} &= Ax + F_2\mu_2, \\ y &= Cx + v. \end{aligned} \quad (6.31)$$

6.2.2 The Differential Game Solution

We will solve the differential game in two steps beginning with the subproblem,

$$\max_{\mu_2} \max_{x(t_0)} J \leq 0,$$

subject to (6.31) with y and \hat{x} fixed. The first step in this solution is to append the problem constraints, which are the system dynamics, (6.31), to the cost, (6.29), through a Lagrange multiplier, λ^T :

$$J = \int_{t_0}^{t_1} \left[\|HC(x - \hat{x})\|_Q^2 - \gamma(\|\mu_2\|_{M^{-1}}^2 + \|y - Cx\|_{V^{-1}}^2) + \lambda^T(Ax + F_2\mu_2 - \dot{x}) \right] dt - \|x(t_0) - \hat{x}_0\|_{\Pi_0}^2.$$

Integrate $\lambda^T \dot{x}$ by parts,

$$J = \int_{t_0}^{t_1} \left[\|HC(x - \hat{x})\|_Q^2 - \gamma(\|\mu_2\|_{M^{-1}}^2 + \|y - Cx\|_{V^{-1}}^2) + \lambda^T(Ax + F_2\mu_2) + \dot{\lambda}^T x \right] dt - \|x(t_0) - \hat{x}_0\|_{\Pi_0}^2 + \lambda(t_0)^T x(t_0) - \lambda(t_1)^T x(t_1), \quad (6.32)$$

and then take the variation of (6.32) with respect to μ_2 and $x(t_0)$:

$$\begin{aligned} \delta J = \int_{t_0}^{t_1} \left\{ \left[(x - \hat{x})^T C^T H Q H C + \gamma(y - Cx)^T V^{-1} C + \dot{\lambda}^T + \lambda^T A \right] \delta x \right. \\ \left. + \left[-\gamma \mu_2^T M^{-1} + \lambda^T F_2 \right] \delta \mu_2 \right\} dt - \lambda(t_1)^T \delta x(t_1) \\ - \left[(x(t_0) - \hat{x}_0)^T \Pi_0 - \lambda(t_0)^T \right] \delta x(t_0). \quad (6.33) \end{aligned}$$

Note that since H is a projector, $H = H^T = H^2$. Equation (6.33) implies that the first-order necessary conditions to maximize (6.29) with respect to $x(t_0)$ and μ_2 are

$$\mu_2^* = \frac{1}{\gamma} M F_2^T \lambda, \quad (6.34)$$

$$-\dot{\lambda} = A^T \lambda + C^T H Q H C (x - \hat{x}) + \gamma C^T V^{-1} (y - Cx), \quad (6.35)$$

$$\lambda(t_1) = 0, \quad (6.36)$$

$$\lambda(t_0) = \Pi_0 [x^*(t_0) - \hat{x}_0]. \quad (6.37)$$

The asterisks in (6.34) and (6.37) denote that the extremizing value for the given variable is being used. By substituting the maximizing strategy for μ_2 , (6.34), into the state equation (6.31), we get a nonhomogeneous two-point boundary value problem (TPBVP),

$$\begin{aligned} \begin{Bmatrix} \dot{x} \\ \dot{\lambda} \end{Bmatrix} = \begin{bmatrix} A & \frac{1}{\gamma} F_2 M F_2^T \\ -C^T (H Q H - \gamma V^{-1}) C & -A^T \end{bmatrix} \begin{Bmatrix} x \\ \lambda \end{Bmatrix} \\ + \begin{Bmatrix} 0 \\ C^T H Q H C \hat{x} - \gamma C^T V^{-1} y \end{Bmatrix}, \end{aligned} \quad (6.38)$$

by coupling (6.31) with (6.35). We will assume solutions x^* and λ^* to (6.38) such that

$$\lambda^* = \Pi(x^* - x_p). \quad (6.39)$$

The vector, x_p , is a measurement-dependent variable which will reduce to the optimal state estimate in the second-half of this game. If we take

$$\Pi(t_0) = \Pi_0, \quad (6.40)$$

$$x_p(t_0) = \hat{x}_0, \quad (6.41)$$

then (6.39) will match the boundary condition for λ at t_0 , (6.37). By differentiating (6.39) and substituting in the equations for \dot{x} and $\dot{\lambda}$ from (6.38), we get

$$\begin{aligned} 0 = \left[\dot{\Pi} + A^T \Pi + \Pi A + \frac{1}{\gamma} \Pi F_2 M F_2^T \Pi + C^T (H Q H - \gamma V^{-1}) C \right] x^* \\ - \dot{\Pi} x_p - \Pi \dot{x}_p - A^T \Pi x_p - C^T H Q H C \hat{x} + \gamma C^T V^{-1} y. \end{aligned} \quad (6.42)$$

Now, add and subtract $\gamma C^T V^{-1} C \hat{x}$ and $[\Pi A + C^T (H Q H - \gamma V^{-1}) C] x_p$ to (6.42) and collect terms:

$$0 = \left[\dot{\Pi} + A^T \Pi + \Pi A + \frac{1}{\gamma} \Pi F_2 M F_2^T \Pi + C^T (H Q H - \gamma V^{-1}) C \right] (x^* - x_p) \\ - \Pi \dot{x}_p + \Pi A x_p - \left[C^T (H Q H - \gamma V^{-1}) C \right] (\hat{x} - x_p) + \gamma C^T V^{-1} (y - C \hat{x}). \quad (6.43)$$

We, thus, find that (6.39) solves the TPBVP identically if

$$-\dot{\Pi} = A^T \Pi + \Pi A + \frac{1}{\gamma} \Pi F_2 M F_2^T \Pi + C^T (H Q H - \gamma V^{-1}) C, \quad (6.44)$$

$$\Pi \dot{x}_p = \Pi A x_p - \left[C^T (H Q H - \gamma V^{-1}) C \right] (\hat{x} - x_p) + \gamma C^T V^{-1} (y - C \hat{x}). \quad (6.45)$$

Equation (6.44) is clearly a Riccati equation, and its boundary condition is given by (6.40). Equation (6.45) looks like an estimator equation, except that it propagates the intermediate variable, x_p , and not the state estimate, \hat{x} .

Substituting the maximizing values for μ_2 and $x(t_0)$, (6.34,6.37), into the original cost function, (6.29), gives us

$$\bar{J} = \int_{t_0}^{t_1} \left[\|x - \hat{x}\|_{C^T H Q H C}^2 - \|\lambda\|_{\frac{1}{\gamma} F_2 M F_2^T}^2 - \gamma \|y - Cx\|_{V^{-1}}^2 \right] dt - \|\lambda(t_0)\|_{\Pi_0^{-1}}^2. \quad (6.46)$$

The second half of the game is then

$$\min_{\hat{x}} \max_y \bar{J} \leq 0,$$

subject to (6.45). By adding the identically zero term,

$$\|\lambda(t_0)\|_{\Pi(t_0)^{-1}}^2 - \|\lambda(t_1)\|_{\Pi(t_1)^{-1}}^2 + \int_{t_0}^{t_1} \frac{d}{dt} \|\lambda(t)\|_{\Pi^{-1}}^2 dt = 0,$$

to (6.46) and applying the boundary conditions for λ , (6.36,6.37), we get

$$\bar{J} = \int_{t_0}^{t_1} \left[\|x - \hat{x}\|_{C^T H Q H C}^2 - \|\lambda\|_{\frac{1}{\gamma} F_2 M F_2^T}^2 - \gamma \|y - Cx\|_{V^{-1}}^2 \right. \\ \left. + \dot{\lambda}^T \Pi^{-1} \lambda^T + \lambda^T \dot{\Pi}^{-1} \lambda + \lambda^T \Pi^{-1} \dot{\lambda} \right] dt. \quad (6.47)$$

If we substitute the differential equation for λ from (6.38) into (6.47), we then have

$$\begin{aligned} \bar{J} = \int_{t_0}^{t_1} \left\{ & \|x - \hat{x}\|_{C^T H Q H C}^2 + \lambda^T (-A \Pi^{-1} - \Pi^{-1} A^T - F_2 M F_2^T + \dot{\Pi}^{-1}) \lambda \right. \\ & - (x - \hat{x})^T C^T H Q H C \Pi^{-1} \lambda - \lambda^T \Pi^{-1} C^T H Q H C (x - \hat{x}) \\ & \left. - \gamma \left[\|y - Cx\|_{V^{-1}}^2 + (y - Cx)^T V^{-1} C \Pi^{-1} \lambda + \lambda^T \Pi^{-1} C^T V^{-1} (y - Cx) \right] \right\} dt. \end{aligned} \quad (6.48)$$

From (6.44), the differential equation for Π^{-1} is

$$\begin{aligned} \dot{\Pi}^{-1} = -\Pi^{-1} \dot{\Pi} \Pi^{-1} = \Pi^{-1} A^T + A \Pi^{-1} + \frac{1}{\gamma} F_2 M F_2^T \\ + \Pi^{-1} C^T (H Q H - \gamma V^{-1}) C \Pi^{-1}, \end{aligned} \quad (6.49)$$

which, when substituted into the second term in (6.48), gives us

$$\bar{J} = \int_{t_0}^{t_1} \left[\|\Pi^{-1} \lambda - (x - \hat{x})\|_{C^T H Q H C}^2 - \gamma \|C \Pi^{-1} \lambda + (y - Cx)\|_{V^{-1}}^2 \right] dt. \quad (6.50)$$

Substituting the optimal value for λ , (6.39), into (6.50) then leads to

$$\bar{J} = \int_{t_0}^{t_1} \left[\|\hat{x} - x_p\|_{C^T H Q H C}^2 - \gamma \|y - Cx_p\|_{V^{-1}}^2 \right] dt. \quad (6.51)$$

From (6.51), the minimizing strategy for \hat{x} and the maximizing strategy for y are clearly

$$\begin{aligned} \hat{x}^* &= x_p, \\ y^* &= Cx_p. \end{aligned} \quad (6.52)$$

This implies that our game optimal estimate, \hat{x} , is found from

$$\dot{\hat{x}} = A \hat{x} + \gamma \Pi^{-1} C^T V^{-1} (y - C \hat{x}), \quad \hat{x}(t_0) = \hat{x}_0, \quad (6.53)$$

which is simply the extremizing value of \hat{x} , (6.52), applied to (6.45) and (6.41). Π is found by propagating (6.44) with the initial condition, (6.40).

Remark 6. The derivation presented in this section follows that presented by Banavar and Speyer (Banavar and Speyer 1991). ◀

6.2.3 Steady-State Results

In many cases, it is desired to extend finite-time solutions of game theoretic problems to the steady-state condition. Whenever it is possible to find a steady-state solution to the disturbance attenuation problem, the optimal estimator will be given by (6.53) with Π being the solution of the algebraic Riccati equation (Green and Limebeer 1995),

$$0 = A^T \Pi + \Pi A + \frac{1}{\gamma} \Pi F_2 M F_2^T \Pi + C^T (H Q H - \gamma V^{-1}) C. \quad (6.54)$$

However, unlike the algebraic Riccati equation of linear-quadratic optimal control problems, there are no conditions which guarantee the existence of a unique, nonnegative definite, stabilizing solution to the steady-state Riccati equation (6.54), except in the special case where A is asymptotically stable (Green and Limebeer 1995).

6.3 Applications

This section demonstrates the effectiveness of the new game theoretic fault detection filter with a pair of examples.

6.3.1 Accelerometer Fault Detection in an F16XL

In this application, the F16XL example of (Douglas and Speyer 1996) is re-examined. The objective is to detect a normal accelerometer fault in the presence of wind gusts and sensor noise.

Aircraft Dynamics Model

The aircraft dynamics are linearized about trimmed level flight at 10,000 ft altitude and Mach 0.9. For simplicity, a reduced-order, five-state model of the longitudinal dynamics (including a first-order wind gust model) is considered:

$$\begin{aligned} \dot{x} &= Ax + B_{wg} w_{wg}, \\ y &= Cx + v. \end{aligned}$$

The five components of the state vector are

$$x = \begin{cases} u \\ w \\ q \\ \theta \\ w_g \end{cases} \begin{array}{l} \text{long. velocity (ft/sec)} \\ \text{normal velocity (ft/sec)} \\ \text{pitch rate (deg/sec)} \\ \text{pitch (deg)} \\ \text{wind gust (ft/sec)} \end{array}$$

with the measurements,

$$y = \begin{cases} q \\ \theta \\ A_z \\ A_x \end{cases} \begin{array}{l} \text{pitch rate (deg/sec)} \\ \text{pitch (deg)} \\ \text{long. acceleration (ft/sec}^2\text{)} \\ \text{normal acceleration (ft/sec}^2\text{)}. \end{array} \quad (6.55)$$

The input, w_{wg} , is windgust and v is the sensor noise. The system matrices are

$$A = \begin{bmatrix} -.0674 & .0430 & -.8886 & -.5587 & .0430 \\ .0205 & -1.4666 & 16.5800 & -.0299 & -1.4666 \\ .1377 & -1.6788 & -.6819 & 0 & -1.6788 \\ 0 & 0 & 1 & 0 & 0 \\ 0 & 0 & 0 & 0 & -1.1948 \end{bmatrix}, \quad (6.56)$$

$$B_{wg}^T = [0 \ 0 \ 0 \ 0 \ 2.0156], \quad (6.57)$$

and

$$C = \begin{bmatrix} 0 & 0 & 1 & 0 & 0 \\ 0 & 0 & 0 & 1 & 0 \\ 0.0139 & 1.0517 & 0.1485 & -0.0299 & 0 \\ -0.0677 & 0.0431 & 0.0171 & 0 & 0 \end{bmatrix}. \quad (6.58)$$

Full-Order Filter Design

Following the modeling techniques described in Section 6.1, we convert the accelerometer fault into an input to the system,

$$\dot{x} = Ax + F_{A_z}\mu_{A_z} + F_{wg}\mu_{wg},$$

$$y = Cx + v,$$

where

$$F_{A_z} = \begin{bmatrix} 0.6003 & 0 \\ 0.9429 & -1.3706 \\ 0 & -1.5003 \\ 0 & 0 \\ 0 & 0 \end{bmatrix}.$$

In order to distinguish the accelerometer fault from the windgust disturbance, we model the windgust as the nuisance fault. Hence, F_{wg} is simply B_{wg} and μ_{wg} is the wind gust input, w_{wg} . A quick check shows that F_{A_z} and F_{wg} are output separable. Finally, we generate the residual projector, H . Since $CF_{wg} = 0$, we must go through the Goh iteration one time to find that

$$\hat{F} = AF_{wg}.$$

The projector is then

$$\begin{aligned} H &= I - CAF_{wg} \left[(CAF_{wg})^T CAF_{wg} \right]^{-1} (CAF_{wg})^T \\ &= \begin{bmatrix} 0.5330 & 0 & -0.4982 & -0.0264 \\ 0 & 1 & 0 & 0 \\ -0.4982 & 0 & 0.4685 & -0.0281 \\ -0.0264 & 0 & -0.0281 & 0.9985 \end{bmatrix}. \end{aligned} \quad (6.59)$$

The full-order filter design problem boils down to finding a solution to the game Riccati equation, (6.44), that leads to acceptable filter performance. Acceptable, in this example, means that the filter transmits the target fault and attenuates the nuisance fault so that there is good separation between the respective transmission levels. Since the inverse of Π is used in the filter gain, we directly solve for this inverse using the steady-state version of (6.49),

$$0 = \Pi^{-1}A^T + A\Pi^{-1} + \frac{1}{\gamma}F_2MF_2^T + \Pi^{-1}C^T(HQH - \gamma V^{-1})C\Pi^{-1}, \quad (6.60)$$

with

$$\gamma = 5 \times 10^{-7}, \quad Q = M = I, \quad \gamma^{-1}V = \begin{bmatrix} 1 & 0 & 0 & 0 \\ 0 & 1 & 0 & 0 \\ 0 & 0 & 10,000 & 0 \\ 0 & 0 & 0 & 1 \end{bmatrix}. \quad (6.61)$$

The solution to (6.60) is

$$\Pi^{-1} = 10^5 \times \begin{bmatrix} 0.000001 & -0.000050 & -0.000053 & -0.000000 & 0.002291 \\ -0.000050 & 0.001603 & 0.001661 & 0.000009 & -0.077892 \\ -0.000053 & 0.001661 & 0.001704 & 0.000010 & -0.088760 \\ -0.000000 & 0.000009 & 0.000010 & 0.000000 & -0.000020 \\ 0.002291 & -0.077892 & -0.088760 & -0.000020 & 9.219357 \end{bmatrix}. \quad (6.62)$$

The peculiar form of $\gamma^{-1}V$ is necessitated by the fact that, in the true system, the target fault is a sensor fault which appears in the measurements,

$$y = Cx + E_{A_z}\mu_{A_z},$$

and, as a result, directly feeds through to the failure signal:

$$z = H(y - C\hat{x}) = HCe + HE_{A_z}\mu_{A_z}.$$

Analysis

The effect of this feedthrough can be seen in Figure 6.1, which is a plot of the singular values of the transfer function matrix between μ_{A_z} and μ_{wg} and the failure signal, z . As Figure 6.1 shows, the direct feedthrough of the target fault prevents its transmission from rolling off at higher frequencies and detrimentally effects its DC gain, as evidenced by the dashed-dot line which depicts the performance of a filter designed with $\gamma^{-1}V = I$. By choosing $\gamma^{-1}V$ as in (6.61), the contribution of the accelerometer channel is minimized because its gain and bandwidth are kept small. In terms of detection performance, it can be seen that that the filter does a good job of separating the target fault from nuisance fault transmissions when the filter is designed with the weightings, (6.61).

Our choice of γV^{-1} , (6.61), and the solution Π^{-1} , (6.62), to (6.60) also result in high-gain feedback for the other sensor channels (see Remark 6.3.1). High gain means high bandwidth

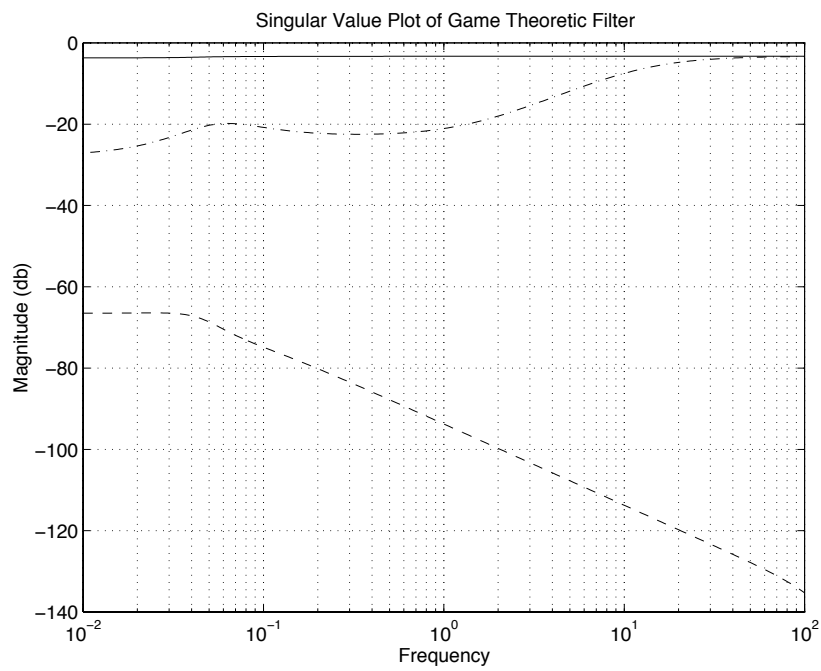


Figure 6.1: F-16XL example: singular value plot of accelerometer fault transmission vs. wind gust transmission (solid line - output due to μ_{A_z} ; dashed line - output due to μ_{wg} ; dashed-dot line - output due to μ_{A_z} for filter with $\gamma V^{-1} = I$).

which works against our ability to quench noise coming through these channels. As shown in Figure 6.2, sensor noise is transmitted to the failure signal at distressingly amplified levels. Ideally, we would like to be able to reverse this situation, i.e. keep the high gain on the accelerometer channel and turn down the gain on the other channels to reject noise.

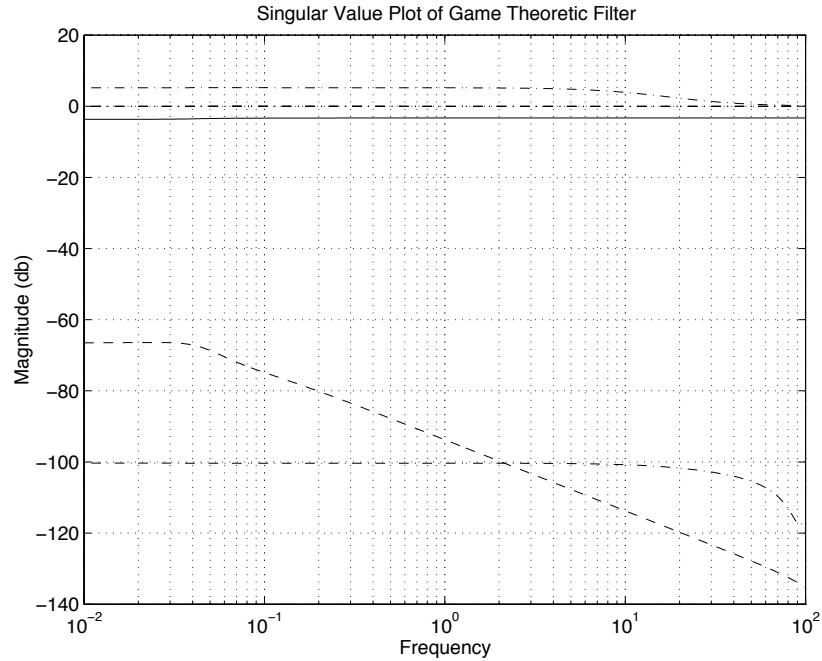


Figure 6.2: F-16XL example: target fault transmission vs. sensor noise transmission (The solid line represents the accelerometer fault and the dash-dot line represents sensor noise from all four channels. The dashed line is the windgust input).

It should be noted that, with a different measurement suite, we might be able to mitigate the detrimental effects of the direct feedthrough term. With our current measurement set, (6.55), there are no other sensors that can observe the portion of the state-space covered by accelerometer, and so there is nothing to compensate for the loss of this measurement. Thus, augmenting the sensor set may be needed to improve our ability to health monitor the system. This, of course, reduces some of the advantage to using analytical redundancy.

Finally, we note that we may not always be able to choose such an extreme form for $\gamma^{-1}V$ and still get a solution to the game Riccati equation. In those cases, one simply

has to do the best that one can and rely on residual post-processing to help with failure identification.

Remark 7. The result that our solution is a high-gain filter, while not predicted, should not be altogether surprising; since, as we will show in Chapter 7, we are asymptotically imposing an invariant subspace structure on our filter. Previous work on asymptotic structures, such as “almost invariant subspaces” (Willems 1981) and “almost disturbance decoupling” (Ozçetin et al. 1992), also report high-gain feedback. ◀

6.3.2 Position Sensor Fault Detection for a Simple Rocket, A Time-Varying System

In this section, we present, quite likely, the first example ever given for detection filtering applied to a time-varying system. Our example is taken from (Rugh 1996) and is a rocket moving in the vertical plane. The problem is to detect a fault in the rocket position sensor without triggering a false alarm due to uncertainty in the rocket motor mass rate.

Rocket Dynamics Model

Consider a rocket moving in the vertical plane with height, $h(t)$, and velocity, $v(t)$. The rocket is propelled against gravity, g , by thrust generated from expelled fuel mass:

$$\begin{aligned} F_{\text{thrust}} &= -V_e u(t), \\ u(t) &= \dot{m}(t). \end{aligned}$$

The variable, \dot{m} , is the rate of change of the mass due to spent fuel, and V_e is the exit velocity of the fuel through the nozzle.

Kinematics gives us $\dot{h}(t) = v(t)$, and Newton’s Second Law of Motion gives us

$$\dot{v}(t) = -g + \frac{V_e u(t)}{m(t)}.$$

Defining $x_1 \triangleq h$, $x_2 \triangleq v$, and $x_3 \triangleq m$, we get

$$\begin{Bmatrix} \dot{x}_1(t) \\ \dot{x}_2(t) \\ \dot{x}_3(t) \end{Bmatrix} = f(t) = \begin{bmatrix} x_2(t) \\ -g + V_e u(t)/x_3(t) \\ u(t) \end{bmatrix} \quad (6.63)$$

as our state equation. If we assume that the mass rate, $u(t)$, is nominally a constant, i.e. $\bar{u}(t) = u_0$, then integrating each of the state equations in turn gives us

$$\begin{Bmatrix} \bar{x}_1(t) \\ \bar{x}_2(t) \\ \bar{x}_3(t) \end{Bmatrix} = \begin{bmatrix} -\frac{g}{2}t^2 + \frac{m_0 V_e}{u_0} \left[\left(1 + \frac{u_0}{m_0}t\right) \ln\left(1 + \frac{u_0}{m_0}t\right) - \frac{u_0}{m_0}t \right] \\ -gt + V_e \ln\left(1 + \frac{u_0}{m_0}t\right) \\ m_0 + u_0 t \end{bmatrix} \quad (6.64)$$

as the nominal solution to (6.63). The scalar constant, m_0 , is the initial mass of the rocket. If the true mass rate of the rocket, however, is $u(t) = u_0 + \delta u(t)$ (where δu is some “small”, time-varying perturbation), then the system will be perturbed away from the nominal state, i.e. $x(t) = \bar{x}(t) + \delta x(t)$. Using a Taylor expansion of (6.63) about (6.64) and neglecting terms higher than first-order, we find that the behavior of the system about the nominal trajectory can be described by

$$\delta \dot{x} = \begin{bmatrix} 0 & 1 & 0 \\ 0 & 0 & -\frac{V_e u_0}{(m_0 + u_0 t)^2} \\ 0 & 0 & 0 \end{bmatrix} \delta x(t) + \begin{Bmatrix} 0 \\ \frac{V_e}{m_0 + u_0 t} \\ 1 \end{Bmatrix} \delta u(t).$$

For this example, we will assume that we have sensors that measure the height and velocity of the rocket so that

$$y(t) = \begin{bmatrix} 1 & 0 & 0 \\ 0 & 1 & 0 \end{bmatrix} \delta x.$$

With these measurements, our system is observable.

Full-Order Filter Design

Suppose that we want to detect a position sensor fault in spite of uncertainty about the mass rate input, $u(t)$. We can apply the game theoretic detection filter to this problem by treating the perturbation, $\delta u(t)$, as the nuisance fault:

$$F_2(t) = \left\{ \begin{array}{c} 0 \\ \frac{V_e}{m_0+u_0t} \\ 1 \end{array} \right\}, \quad \mu_2(t) = \delta u(t).$$

To check for output separability, we also need to find the failure map for the position sensor fault. As described in Section 6.1.2, we begin with

$$y = Cx + E\mu_1,$$

where $E^T = [1 \ 0]$. The first column of the sensor failure map is found as the solution to the equation,

$$E = Cf.$$

It can easily be verified that $f^T = [1 \ 0 \ 0]$. The second column is found from $Af - \dot{f}$, which in this case turns out to be zero. Thus, we only need a single column failure map for the position sensor. The output separability test is then

$$M(t) = [CF_2 \ Cf] = \left[\begin{array}{cc} 0 & 1 \\ \frac{V_e}{m_0+u_0t} & 0 \end{array} \right]$$

which is full rank so long $u_0t \neq -m_0$ (note that u_0 is a negative quantity since it represents the rate of mass loss). Finally, we get

$$\begin{aligned} H &= I - CF_2 \left[(CF_2)^T CF_2 \right]^{-1} F_2^T C^T \\ &= \left[\begin{array}{cc} 1 & 0 \\ 0 & 1 \end{array} \right] - \left\{ \begin{array}{c} 0 \\ \frac{V_e}{m_0+u_0t} \end{array} \right\} \frac{(m_0 + u_0t)^2}{V_e^2} \left[\begin{array}{cc} 0 & \frac{V_e}{m_0+u_0t} \end{array} \right] \\ &= \left[\begin{array}{cc} 1 & 0 \\ 0 & 0 \end{array} \right] \end{aligned}$$

as the failure signal projector.

The detection filter is obtained by propagating the equations,

$$\begin{aligned} \dot{\delta \hat{x}} &= A\delta \hat{x} + PC^T V^{-1}(y - C\delta \hat{x}), \\ \dot{P} &= PA^T + AP - C^T(V^{-1} - HQH)C + \frac{1}{\gamma} F_2 M F_2^T. \end{aligned}$$

A failure is then declared whenever the failure signal,

$$z = H(y - C\delta\hat{x}),$$

exceeds some *a priori* chosen threshold. After some trial and error, the following values for the weighting matrices were chosen:

$$V = \begin{bmatrix} .2 & 0 \\ 0 & .045 \end{bmatrix}, \quad Q = \begin{bmatrix} .01 & 0 \\ 0 & 1 \end{bmatrix}, \quad P(t_0) = \begin{bmatrix} 10 & 0 & 0 \\ 0 & 10 & 0 \\ 0 & 0 & 10 \end{bmatrix}, \quad M = 10,000,$$

along with $\gamma = 0.25$. The initial conditions were arbitrarily picked to be

$$\delta x(t_0) = \begin{Bmatrix} 0 \\ 0 \\ 0 \end{Bmatrix}, \quad e(t_0) = \begin{Bmatrix} 0 \\ -0.3 \\ 0.2 \end{Bmatrix}. \quad (6.65)$$

A nonzero initial error state was chosen to demonstrate the filter's convergence properties. The physical parameters of the rocket were taken from (Sutton 1986, pg. 263–264) and are the characteristics of the first-stage Minuteman Missile Motor:

$$m_0 = 50,550 \text{ lb} - \text{mass}, \quad u_0 = -855 \frac{\text{lb} - \text{mass}}{\text{sec}}, \quad V_e = -5180 \frac{\text{ft}}{\text{sec}}.$$

Q and V were chosen to maximize the low frequency transmission of the target fault; though, in this example, we were limited in our choices for Q and V by the existence of a finite escape time for the Riccati solution. The escape time turned out to be a function of these weightings.

Analysis

The rocket dynamics along with the filter were simulated from $t_0 = 0$ seconds to $t_1 = 25$ seconds. In Figure 6.3, the response of the failure signal generated by the time-varying game theoretic fault detection filter is displayed for a hard failure of the position sensor at $t = 10$ seconds and for a step bias in the mass rate also occurring at $t = 10$ seconds.

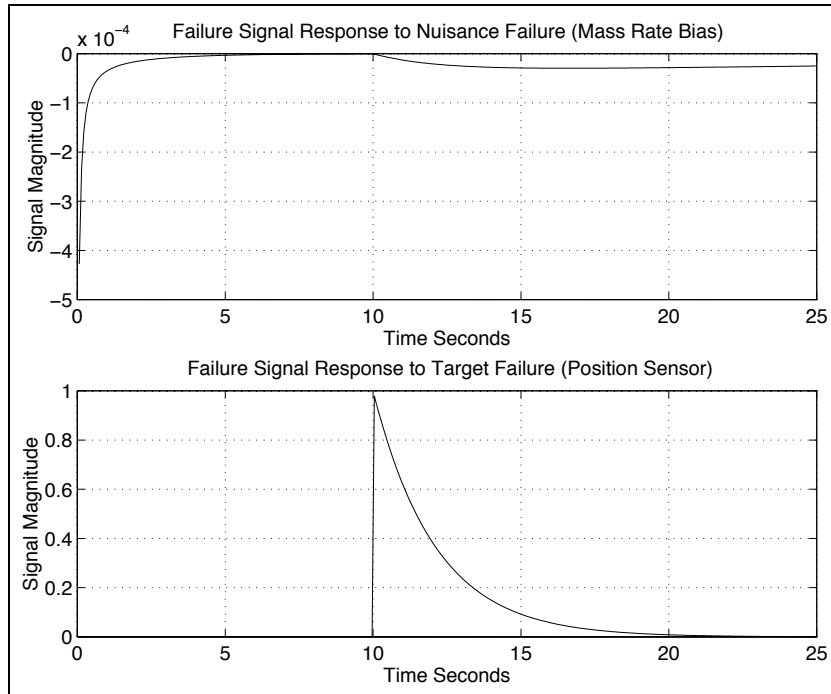


Figure 6.3: Rocket example: failure signal response (failures occur at $t = 10$ seconds).

The detrimental effect of the direct feedthrough can clearly be seen in this figure. The response to the target fault has a transient quality which dies away noticeably after $t = 15$ seconds. The magnitude of the target fault response, however, is still quite a bit greater than the nuisance fault transmission and remains so for a substantial period of time. Thus, a reasonably designed post-processing scheme should be able to detect and declare a sensor fault. We should note that, as with the previous example, a different sensor suite might improve our ability to detect a position sensor fault; since, with the current set, the position bias is unobservable to the velocity sensor.

The initial response at the beginning of Figure 6.3 is the transient response of the filter to the nonzero initial condition, (6.65). It must be noted that in this example the Riccati matrix loses definiteness past $t = 50$ seconds. For this application, however, this may not be a liability, since the rocket motor is on for only a brief period of time.

CHAPTER 7

The Asymptotic Game Theoretic Fault Detection Filter

THE ASYMPTOTIC PROPERTIES of the game theoretic fault detection filter are examined in this chapter. In Section 7.1, we show how the limiting case disturbance attenuation problem can be made into a singular differential game. In Section 7.2, we derive sufficient conditions for a nonpositive cost in the original game and in the singular game. These conditions turn out to be the key to our understanding of the asymptotic game theoretic fault detection filter. In Section 7.3, we solve the singular game; and, in Section 7.4, we explore the relationship between this solution and a pair of long standing detection filter structures: the unknown input observer and the reduced-order residual generator. The latter we accomplish by deriving our own reduced-order filter out of the singular game solution. We conclude in Section 7.5 by returning to the example of Section 6.3.1 and applying the new reduced-order filter.

7.1 Finding the Limiting Solution: Singular Differential Game Theory

We motivated the disturbance attenuation problem of Chapter 6 by formulating it in such a way as to approximate the detection filter problem. It is clear, however, that when the disturbance attenuation bound is zero the two problems are equivalent. It is logical to then ask whether the solution to the disturbance attenuation problem likewise becomes a detection filter at this limit. The answer to this question is by no means obvious, since it is not clear that a limiting case solution even exists.

It is a well-known phenomena of game Riccati equations such as (6.44) that positive semi-definite, symmetric solutions exist only for values of γ larger than a critical value, γ_{crit} . This would seem to immediately imply the nonexistence of limiting solutions. However, we can prevent the onset of the γ_{crit} phenomenon by taking the weighting, V , to zero along with γ so that their product, γV^{-1} , does not disappear in the limit. This, in and of itself, does not resolve the existence question, but it does turn the limiting case problem into a singular optimization problem since the game cost loses the input term, $\gamma \|\mu_2\|_{M^{-1}}^2$, i.e.

$$J^* = \lim_{\gamma \rightarrow 0} J = \int_{t_0}^{t_1} \left[\|x - \hat{x}\|_{C^T H Q H C}^2 - \|y - Cx\|_{\bar{V}^{-1}}^2 \right] dt - \|x(t_0) - \hat{x}\|_{\bar{\Pi}_0}^2. \quad (7.1)$$

We define $\bar{V}^{-1} \triangleq \lim_{\gamma \rightarrow 0} \gamma V^{-1}$ and $\bar{\Pi}_0 \triangleq \lim_{\gamma \rightarrow 0} \Pi_0$. This is a problem that we can solve.

Remark 8. Singular optimization theory has a rich legacy dating back to the beginning of the modern control period. Much of the work from this period is summarized nicely in the book by Bell and Jacobson (Bell and Jacobsen 1973), which is the source for many of the singular optimal control techniques that we will use in this chapter. We should note that a significant portion of this book originally appeared in (Jacobson and Speyer 1971). Other important summaries from this period can be found in the survey article by Jacobson (Jacobson 1971) and in the book by Bryson and Ho (Bryson and Ho 1975). The original work on singular estimation, is due to Bryson and his students (Bryson and Johansen 1965, Mehra and Bryson 1968). In more recent times, singular optimal control theory has taken on a geometric flavor, e.g (Schumacher 1985, Stoorvogel 1991, Willems et al. 1986). ◀

7.2 Conditions for the Nonpositivity of the Game Cost

In this section, we will determine the properties of the limiting case filter by converting the nonpositivity condition on the game cost, (6.30), into an equivalent linear matrix inequality condition. The latter falls out when we manipulate the cost function to look like a simple quadratic,

$$J(\hat{x}, x(t_0), \mu_2, v) = \int_{t_0}^{t_1} \xi^T W \xi dt.$$

The vector, ξ , consists of linear combinations of the game elements. Nonpositivity of the cost then hinges on the sign definiteness of W . In singular optimal control theory, W is called the “dissipation matrix,” because its nonnegative definiteness ensures that the system will be dissipative (Bell and Jacobsen 1973, Clements and Anderson 1978, Schumacher 1983). For our purposes, W needs to be *nonpositive definite*, or opposite in sign to the dissipation matrix, in order to guarantee a nonpositive game cost. A nonpositive game cost, in turn, implies that the disturbance attenuation objective is satisfied, giving us a sufficiency condition for an attenuating solution.

This sufficiency condition, however, is strongly tied to the game solution. Results from the game solution are used¹ in several places to construct W , and the sufficiency condition is really nothing more than the first half of the saddle point inequality that is implicit in every differential game,

$$J(\hat{x}^*, x(t_0), \mu_2, \mu_3, v) \leq J(\hat{x}^*, x^*(t_0), \mu_2^*, \mu_3^*, v^*) = 0 \leq J(\hat{x}, x^*(t_0), \mu_2^*, \mu_3^*, v^*).$$

As before, the asterisk indicates that the game optimal strategy is being used for that element.

We begin by appending the dynamics of the system, (6.31), to the cost, (6.29), through the Lagrange multiplier², $(x - \hat{x})^T \Pi$:

¹One can think of this as \hat{x} playing its optimal strategy before the adversaries get to play theirs.

²Note that this form of the Lagrange multiplier comes from the TPBVP solution in Section 6.2, (6.39).

$$J = \int_{t_0}^{t_1} \left[\|x - \hat{x}\|_{C^T H Q H C}^2 - \gamma \|\mu_2\|_{M^{-1}}^2 - \gamma \|y - Cx\|_{V^{-1}}^2 + (x - \hat{x})^T \Pi (Ax + F_2 \mu_2 - \dot{x}) \right] dt - \|x(t_0) - \hat{x}_0\|_{\Pi_0}^2. \quad (7.2)$$

Add and subtract $(x - \hat{x})^T \Pi A \hat{x}$ and $(x - \hat{x})^T \Pi \dot{\hat{x}}$ to (7.2) and collect terms to get

$$J = \int_{t_0}^{t_1} \left\{ \|x - \hat{x}\|_{\Pi A + C^T H Q H C}^2 - \gamma \|\mu_2\|_{M^{-1}}^2 - \gamma \|y - Cx\|_{V^{-1}}^2 + (x - \hat{x})^T \Pi F_2 \mu_2 - (x - \hat{x})^T \Pi (\dot{x} - \dot{\hat{x}}) + (x - \hat{x})^T \left[\Pi A \hat{x} - \Pi \dot{\hat{x}} \right] \right\} dt - \|x(t_0) - \hat{x}_0\|_{\Pi_0}^2.$$

Integrate $(x - \hat{x})^T \Pi (\dot{x} - \dot{\hat{x}})$ in the above by parts and substitute the state equation, (6.31), into the appropriate places. Add and subtract $\hat{x}^T A^T \Pi (x - \hat{x})$ to the result and collect terms to get

$$J = \int_{t_0}^{t_1} \left\{ \|x - \hat{x}\|_{\Pi + \Pi A + A^T \Pi + C^T H Q H C}^2 - \gamma \|\mu_2\|_{M^{-1}}^2 + (x - \hat{x})^T \Pi F_2 \mu_2 + \mu_2^T F_2^T \Pi (x - \hat{x}) - \gamma \|y - Cx\|_{V^{-1}}^2 + (x - \hat{x})^T \left[-\Pi \dot{\hat{x}} + \Pi A \hat{x} \right] + \left[-\Pi \dot{\hat{x}} + \Pi A \hat{x} \right]^T (x - \hat{x}) \right\} dt - \|x(t_0) - \hat{x}_0\|_{\Pi_0 - \Pi(t_0)}^2 - \|x(t_1) - \hat{x}(t_1)\|_{\Pi(t_1)}^2. \quad (7.3)$$

Finally, by expanding $\|y - Cx\|_{V^{-1}}^2$ into $\|(y - C\hat{x}) - C(x - \hat{x})\|_{V^{-1}}^2$ and collecting terms, (7.3) can be rewritten as

$$J = \int_{t_0}^{t_1} \left\{ \|x - \hat{x}\|_{\Pi + \Pi A + A^T \Pi + C^T H Q H C}^2 - \gamma \|\mu_2\|_{M^{-1}}^2 + (x - \hat{x})^T \Pi F_2 \mu_2 + \mu_2^T F_2^T \Pi (x - \hat{x}) - \gamma \|y - C\hat{x}\|_{V^{-1}}^2 + (x - \hat{x})^T \left[-\Pi \dot{\hat{x}} + \Pi A \hat{x} + \gamma C^T V^{-1} (y - C\hat{x}) \right] + \left[-\Pi \dot{\hat{x}} + \Pi A \hat{x} + \gamma C^T V^{-1} (y - C\hat{x}) \right]^T (x - \hat{x}) \right\} dt - \|x(t_0) - \hat{x}_0\|_{\Pi_0 - \Pi(t_0)}^2 - \|x(t_1) - \hat{x}(t_1)\|_{\Pi(t_1)}^2. \quad (7.4)$$

Using the estimator equation, (6.53), we can eliminate the third and fourth lines in (7.4).

The remainder can then be compactly written as

$$J = \int_{t_0}^{t_1} \left[\xi^T W(\Pi) \xi - \gamma \|y - C\hat{x}\|_{V^{-1}}^2 \right] dt - \|x(t_0) - \hat{x}_0\|_{\Pi_0 - \Pi(t_0)}^2 - \|x(t_1) - \hat{x}(t_1)\|_{\Pi(t_1)}^2,$$

where

$$\xi \triangleq \begin{Bmatrix} (x - \hat{x}) \\ \mu_2 \end{Bmatrix}$$

and

$$W(\Pi) \triangleq \begin{bmatrix} \dot{\Pi} + A^T \Pi + \Pi A + C^T (H Q H - \gamma V^{-1}) C & \Pi F_2 \\ F_2^T \Pi & -\gamma M^{-1} \end{bmatrix}. \quad (7.5)$$

Thus, for matrices $\Pi \geq 0$ such that

$$W(\Pi) \leq 0,$$

$$\Pi_0 - \Pi(t_0) \geq 0, \quad (7.6)$$

$$\Pi(t_1) \geq 0, \quad (7.7)$$

we will have $J \leq 0$. For $\gamma > 0$, it is easy to see that the Riccati equation, (6.44), of the previous section is embedded in $W(\Pi)$ ³; but, unlike (6.44), $W(\Pi)$ can be evaluated in the limit, $\gamma \rightarrow 0$. In fact, from (7.5), it is clear that the sufficient conditions for the limiting case cost, J^* (7.1), to be nonpositive are:

$$\Pi F_2 = 0, \quad (7.8)$$

$$\dot{\Pi} + A^T \Pi + \Pi A + C^T (H Q H - \bar{V}^{-1}) C \leq 0. \quad (7.9)$$

The boundary conditions are (7.7) and a modification of (7.6) to account for a possible jump in the value of Π from t_0 to t_0^+ (we will show this in the next section).

³In fact, the solution of (6.44) is the solution of $W(\Pi)$ which minimizes its rank (Schumacher 1983).

Equation (7.8) clearly shows that, in the limit, the Riccati matrix, Π , obtains a nontrivial null space which contains the image of the nuisance map, F_2 . Moreover, those familiar with singular optimal control theory will recognize (7.8) and (7.9) as conditions seen previously for the singular linear quadratic regulator (Bell and Jacobsen 1973).

7.3 The Solution to the Singular Differential Game

In this section, we solve the singular differential game obtained in Section 7.1. The key result will be a Riccati equation for the limiting case problem. We will find, in subsequent sections, that the solution to this equation is central to understanding the structure of the limiting case game theoretic fault detection filter.

To get our Riccati equation, we must recast the limiting case problem to look like the differential game solved in Section 6.2. This is done with the Goh transformation, which is the same technique that was used in Section 6.1 to construct various elements of the disturbance attenuation problem. The transformation begins when we define a new nuisance fault vector, ϕ_1 , and a new state vector, α_1 :

$$\phi_1(t) \triangleq \int_{t_0}^t \mu_2(\tau) d\tau, \quad (7.10)$$

$$\alpha_1 \triangleq x - F_2\phi_1. \quad (7.11)$$

Differentiating (7.11) gives us

$$\dot{\alpha}_1 = A\alpha_1 + B_1\phi_1, \quad (7.12)$$

$$B_1 \triangleq AF_2 - \dot{F}_2. \quad (7.13)$$

Equation (7.12) is the new state equation. The need for the subscript on B_1 will become obvious later. Substituting (7.10) and (7.11) into the limiting case game cost (7.1) gives us

$$\begin{aligned} J^* = \int_{t_0}^{t_1} & \left[\|\alpha_1 - \hat{x}\|_{C^T H Q H C}^2 - \|y - C\alpha_1\|_{\bar{V}^{-1}}^2 \right. \\ & + (y - C\alpha_1)^T \bar{V}^{-1} C F_2 \phi_1 + \phi_1^T F_2^T C^T \bar{V}^{-1} (y - C\alpha_1) \\ & \left. - \|\phi_1\|_{F_2^T C^T \bar{V}^{-1} C F_2}^2 \right] dt - \|\alpha_1(t_0) + F_2\phi_1(t_0^+) - \hat{x}_0\|_{\bar{I}_0}^2. \quad (7.14) \end{aligned}$$

At first glance, the term, $\phi_1(t_0^+)$, may seem odd, since $\phi_1(t)$ is defined to be the integral of μ_2 from t_0 to t . However, μ_2 need not be an L_2 function, or even a function at all, since it no longer appears in the game cost, (7.1). Thus, we must be able to account for impulsive jumps in ϕ_1 at t_0 . Classical results from singular optimization theory, in fact, contain many examples of control inputs (Bell and Jacobsen 1973) or state estimates (Bryson and Johansen 1965, Mehra and Bryson 1968) that are impulsive at the initial time.

If $F_2^T C^T \bar{V}^{-1} C F_2 > 0$, we have a new differential game,

$$\min_{\hat{x}} \max_y \max_{\phi_1} \max_{\alpha_1(t_0)} J^* \leq 0,$$

subject to (7.12). This is the essentially the same game that we examined in Section 6.2, the only difference being new cross-terms between the nuisance input and measurement noise. We should note that we are only able to recover the game from Section 6.2, because the projector, H , (6.12,6.14), has been constructed so that $H C F_2 = 0$. Without this property, there would be cross-terms involving \hat{x} and ϕ_1 in the cost, (7.14), which changes the game.

Begin by appending the state dynamics (7.12) to the cost (7.14) with a Lagrange multiplier λ^T :

$$\begin{aligned} J^* = \int_{t_0}^{t_1} & \left[\|\alpha_1 - \hat{x}\|_{C^T H Q H C}^2 - \|y - C\alpha_1\|_{\bar{V}^{-1}}^2 - \|\phi_1\|_{F_2^T C^T \bar{V}^{-1} C F_2}^2 \right. \\ & + (y - C\alpha_1)^T \bar{V}^{-1} C F_2 \phi_1 + \phi_1^T F_2^T C^T \bar{V}^{-1} (y - C\alpha_1) \\ & \left. + \lambda^T (A\alpha_1 + B_1\phi_1 - \dot{\alpha}_1) \right] dt - \|\alpha_1(t_0) + F_2\phi_1(t_0^+) - \hat{x}_0\|_{\bar{\Pi}_0}^2. \end{aligned} \quad (7.15)$$

By maximizing (7.15) with respect to $\alpha_1(t_0)$ and ϕ_1 , the first-order necessary conditions are

$$\dot{\lambda} = -A^T \lambda + C^T \bar{V}^{-1} C F_1 \phi_1 - C^T \bar{V}^{-1} (y - C\alpha_1) - C^T H Q H C (\alpha_1 - \hat{x}), \quad (7.16)$$

$$\phi_1 = (F_2^T C^T \bar{V}^{-1} C F_2)^{-1} B_1^T \lambda + (F_2^T C^T \bar{V}^{-1} C F_2)^{-1} F_2^T C^T \bar{V}^{-1} (y - C\alpha_1), \quad (7.17)$$

$$\lambda(t_0^+) = \bar{\Pi}_0 [\alpha_1(t_0) + F_2 \phi_1(t_0) - \hat{x}_0], \quad (7.18)$$

$$\lambda(t_1) = 0,$$

$$\phi_1(t_0^+) = (F_2^T \bar{\Pi}_0 F_2)^{-1} F_2^T \bar{\Pi}_0 [\alpha_1(t_0) - \hat{x}_0]. \quad (7.19)$$

Note that (7.19) results when we maximize the initial error term, $\|\alpha_1(t_0) + F_2\phi_1(t_0^+) - \hat{x}_0\|_{\bar{\Pi}_0}^2$, with respect to $\phi_1(t_0^+)$. Substituting this term into (7.18) gives us

$$\lambda(t_0^+) = \left[\bar{\Pi}_0 - \bar{\Pi}_0 F_2 (F_2^T \bar{\Pi}_0 F_2)^{-1} F_2^T \bar{\Pi}_0 \right] (\alpha_1(t_0) - \hat{x}_0). \quad (7.20)$$

Using (7.17), we can rewrite our state equation, (7.12), and our co-state equation, (7.16), as

$$\begin{aligned} \dot{\alpha}_1 = & \left[A - B_1 (F_2^T C^T \bar{V}^{-1} C F_2)^{-1} F_2^T C^T \bar{V}^{-1} C \right] \alpha_1 \\ & + B_1 (F_2^T C^T \bar{V}^{-1} C F_2)^{-1} B_1^T \lambda + B_1 (F_2^T C^T \bar{V}^{-1} C F_2)^{-1} F_2^T C^T \bar{V}^{-1} y, \end{aligned} \quad (7.21)$$

$$\begin{aligned} \dot{\lambda} = & - \left[A - B_1 (F_2^T C^T \bar{V}^{-1} C F_2)^{-1} F_2^T C^T \bar{V}^{-1} C \right]^T \lambda - C^T H Q H C (\alpha - \hat{x}) \\ & - C^T \left[\bar{V}^{-1} - \bar{V} C F_2 (F_2^T C^T \bar{V}^{-1} C F_2)^{-1} F_2^T C^T \bar{V}^{-1} \right] (y - C\alpha). \end{aligned} \quad (7.22)$$

It will turn out that our notation can be greatly simplified if we rearrange the term in front of $(y - C\alpha)$ in (7.22),

$$\begin{aligned} & \bar{V}^{-1} - \bar{V}^{-1} C F_2 (F_2^T C^T \bar{V}^{-1} C F_2)^{-1} F_2^T C^T \bar{V}^{-1} \\ & = \bar{V}^{-\frac{1}{2}} \left[I - \bar{V}^{-\frac{1}{2}} C F_2 (F_2^T C^T \bar{V}^{-1} C F_2)^{-1} F_2^T C^T \bar{V}^{-\frac{1}{2}} \right] \bar{V}^{-\frac{1}{2}}. \end{aligned} \quad (7.23)$$

Since the term inside the square brackets on the right hand side of (7.23) is a projector, we can rewrite (7.23) as

$$\begin{aligned} & \bar{V}^{-1} - \bar{V}^{-1} C F_2 (F_2^T C^T \bar{V}^{-1} C F_2)^{-1} F_2^T C^T \bar{V}^{-1} \\ & = \bar{V}^{-\frac{1}{2}} \left[I - \bar{V}^{-\frac{1}{2}} C F_2 (F_2^T C^T \bar{V}^{-1} C F_2)^{-1} F_2^T C^T \bar{V}^{-\frac{1}{2}} \right] \\ & \quad \times \left[I - \bar{V}^{-\frac{1}{2}} C F_2 (F_2^T C^T \bar{V}^{-1} C F_2)^{-1} F_2^T C^T \bar{V}^{-\frac{1}{2}} \right] \bar{V}^{-\frac{1}{2}}. \end{aligned}$$

Pulling the $\bar{V}^{-\frac{1}{2}}$ terms through the projectors and in towards the center gives us

$$\begin{aligned}
& \bar{V}^{-1} - \bar{V}^{-1} C F_2 (F_2^T C^T \bar{V}^{-1} C F_2)^{-1} F_2^T C^T \bar{V}^{-1} \\
&= \left[I - \bar{V}^{-1} C F_2 (F_2^T C^T \bar{V}^{-1} C F_2)^{-1} F_2^T C^T \right] \\
&\quad \times \bar{V}^{-1} \left[I - C F_2 (F_2^T C^T \bar{V}^{-1} C F_2)^{-1} F_2^T C^T \bar{V}^{-1} \right] \\
&= \bar{H}^T \bar{V}^{-1} \bar{H},
\end{aligned}$$

where we have defined

$$\bar{H} \triangleq I - C F_2 (F_2^T C^T \bar{V}^{-1} C F_2)^{-1} F_2^T C^T \bar{V}^{-1}. \quad (7.24)$$

Aside from greatly condensing our equations, \bar{H} has the same effect as a projector since it is idempotent, i.e. $\bar{H}^2 = \bar{H}$. Thus, its eigenvalues will be either one or zero. \bar{H} , in fact, maps vectors onto the same subspace as H , since $\bar{H} C F_2 = 0$. If V is of the form, νI , then \bar{H} is identically H . This becomes evident if one looks at (6.14) or (6.12) and substitutes F_2 in for \hat{F} .

Using (7.24), we can write (7.21) and (7.22) compactly as a two-point boundary value problem,

$$\begin{aligned}
\begin{Bmatrix} \dot{\alpha}_1 \\ \lambda \end{Bmatrix} &= \begin{bmatrix} \bar{A} & B_1 (F_2^T C^T \bar{V}^{-1} C F_2)^{-1} B_1^T \\ C^T (\bar{H}^T \bar{V}^{-1} \bar{H} - H Q H) C & -\bar{A}^T \end{bmatrix} \begin{Bmatrix} \alpha_1 \\ \lambda \end{Bmatrix} \\
&\quad + \begin{Bmatrix} B_1 (F_2^T C^T \bar{V}^{-1} C F_2)^{-1} F_2^T C^T \bar{V}^{-1} y \\ -C^T (\bar{H})^T \bar{V}^{-1} \bar{H} y + C^T H Q H C \hat{x} \end{Bmatrix}.
\end{aligned}$$

The matrix \bar{A} is defined to be

$$\bar{A} \triangleq A - B_1 (F_2^T C^T \bar{V}^{-1} C F_2)^{-1} F_2^T C^T \bar{V}^{-1} C.$$

If we assume a solution of the form,

$$\lambda = S(\alpha_1 - \alpha_p), \quad (7.25)$$

where α_p is analogous to x_p from Section 6.2, then differentiating (7.25) gives us

$$\begin{aligned}
-\dot{S} = S & \left[A - B_1(F_2^T C^T \bar{V}^{-1} C F_2)^{-1} F_2^T C^T \bar{V}^{-1} C \right] \\
& + \left[A - B_1(F_2^T C^T \bar{V}^{-1} C F_2)^{-1} F_2^T C^T \bar{V}^{-1} C \right]^T S \\
& + C^T (H Q H - \bar{H}^T \bar{V}^{-1} \bar{H}) C + S B_1 (F_2^T C^T \bar{V}^{-1} C F_2)^{-1} B_1^T S \quad (7.26)
\end{aligned}$$

and

$$\begin{aligned}
S \dot{\alpha}_p = S A \alpha_p + S B_1 (F_2^T C^T \bar{V}^{-1} C F_2)^{-1} F_2^T C^T \bar{V}^{-1} (y - C \alpha_p) \\
+ C^T H Q H C (\alpha_p - \hat{x}) + C^T (\bar{H})^T \bar{V}^{-1} \bar{H} (y - C \alpha_p) \quad (7.27)
\end{aligned}$$

with the boundary conditions,

$$\begin{aligned}
S(t_0^+) &= \bar{\Pi}_0 - \bar{\Pi}_0 F_2 (F_2^T \bar{\Pi}_0 F_2)^{-1} F_2^T \bar{\Pi}_0, \quad (7.28) \\
\alpha_p(t_0^+) &= \hat{x}_0.
\end{aligned}$$

The boundary conditions fall out when we match (7.25) with the boundary condition for λ at t_0^+ , (7.20). Note that

$$S(t_0^+) F_2 = \bar{\Pi}_0 F_2 - \bar{\Pi}_0 F_2 (F_2^T \bar{\Pi}_0 F_2)^{-1} F_2^T \bar{\Pi}_0 F_2 = \bar{\Pi}_0 F_2 - \bar{\Pi}_0 F_2 = 0, \quad (7.29)$$

which shows that $S(t)$ takes an impulsive jump at t_0 . Equation (7.26) is sometimes referred to in singular optimal control literature as the *Goh Riccati equation*. The existence of the game optimal estimator, (7.27), will hinge upon the existence of a nonnegative definite, symmetric solution to this equation. To get the final form of (7.27), we need to solve the second half of the game,

$$\min_{\hat{x}} \max_y \bar{J}^* \leq 0,$$

$$\begin{aligned}
\bar{J}^* = \int_{t_0}^{t_1} & \left[\|\alpha_1 - \hat{x}\|_{C^T H Q H C} - \|y - C \alpha_1\|_{\bar{H}^T \bar{V}^{-1} \bar{H}} \right. \\
& \left. - \|\alpha_1 - \alpha_p\|_{S B_1 (F_2^T C^T \bar{V}^{-1} C F_2)^{-1} B_1^T S} \right] dt \\
& - \|\alpha_1(t_0^+) - \hat{x}_0\|_{\bar{\Pi}_0 - \bar{\Pi}_0 F_2 (F_2^T \bar{\Pi}_0 F_2)^{-1} F_2^T \bar{\Pi}_0}.
\end{aligned}$$

\bar{J}^* is the singular game cost, (7.14), with the extremizing value of ϕ_1 - including $\phi_t(t_0^+)$ - substituted into the appropriate places. For simplicity, we define

$$\begin{aligned}\hat{e} &= \alpha_1 - \hat{x}, \\ \hat{v} &= y - C\alpha_1, \\ \hat{r} &= \alpha_1 - \alpha_p,\end{aligned}$$

so that the game is now

$$\min_{\hat{e}} \max_{\hat{v}} \bar{J}^* \leq 0,$$

$$\begin{aligned}\bar{J}^* &= \int_{t_0}^{t_1} \left[\|\hat{e}\|_{C^T H Q H C} - \|\hat{v}\|_{\bar{H}^T \bar{V}^{-1} \bar{H}} - \|\hat{r}\|_{S B_1 (F_2^T C^T \bar{V}^{-1} C F_2)^{-1} B_1^T S} \right] dt \\ &\quad - \|\hat{r}(t_0^+)\|_{\bar{\Pi}_0 - \bar{\Pi}_0 F_2 (F_2^T \bar{\Pi}_0 F_2)^{-1} F_2^T \bar{\Pi}_0}, \quad (7.30)\end{aligned}$$

subject to

$$\begin{aligned}S\dot{\hat{r}} &= S(\dot{\alpha}_1 - \dot{\alpha}_p) \\ &= \left\{ S \left[A - B_1 (F_2^T C^T \bar{V}^{-1} C F_2)^{-1} F_2^T C^T \bar{V}^{-1} C \right] + S B_1 (F_2^T C^T \bar{V}^{-1} C F_2)^{-1} B_1^T S \right. \\ &\quad \left. + C^T (H Q H - \bar{H}^T \bar{V}^{-1} \bar{H}) C \right\} \hat{r} - C^T (\bar{H})^T \bar{V}^{-1} \bar{H} \hat{v} - C^T H Q H C \hat{e}. \quad (7.31)\end{aligned}$$

After appending (7.31) to (7.30) through the Lagrange multiplier, ψ^T , and taking the first variation, we find that the first-order necessary conditions to extremize the cost with respect to \hat{e} and \hat{r} are

$$0 = C^T H Q H C (\hat{e} - \hat{r}), \quad (7.32)$$

$$0 = \bar{H}^T \bar{V}^{-1} \bar{H} (\hat{v} + C \hat{r}), \quad (7.33)$$

$$\begin{aligned}S\dot{\psi} &= S \left[A - B_1 (F_2^T C^T \bar{V}^{-1} C F_2)^{-1} F_2^T C^T \bar{V}^{-1} C \right] \psi \\ &\quad + S B_1 (F_2^T C^T \bar{V}^{-1} C F_2)^{-1} B_1^T S \hat{r}, \quad (7.34)\end{aligned}$$

$$0 = \left(\bar{\Pi}_0 - \bar{\Pi}_0 F_2 (F_2^T \bar{\Pi}_0 F_2)^{-1} F_2^T \bar{\Pi}_0 \right) \left[\psi(t_0^+) - \hat{r}(t_0^+) \right] \quad (7.35)$$

Because of (7.28), (7.35) can be rewritten as

$$0 = S(t_0^+) [\psi(t_0^+) - \hat{r}(t_0^+)]. \quad (7.36)$$

Using (7.31–7.33), we get

$$\begin{aligned} S\dot{\hat{r}} = & \left\{ S \left[A - B_1 (F_2^T C^T \bar{V}^{-1} C F_2)^{-1} F_2^T C^T \bar{V}^{-1} C \right] \right. \\ & \left. + S B_1 (F_2^T C^T \bar{V}^{-1} C F_2)^{-1} B_1^T S \right\} \hat{r} \\ & + \left[C^T (\bar{H})^T \bar{V}^{-1} \bar{H} C - C^T H Q H C \right] (\hat{r} - \psi). \quad (7.37) \end{aligned}$$

Equations (7.36) tells us that

$$\psi = \hat{r} \quad \text{mod Ker } S \quad \text{at } t = t_0^+$$

which implies that

$$\psi = \hat{r} \quad \text{mod Ker } HC \quad (= \text{Ker } \bar{H}C) \quad \text{at } t = t_0^+,$$

since $\text{Ker } S = \text{Ker } HC$ at $t = t_0^+$ (7.29). Equation (7.37), therefore, simplifies to

$$\begin{aligned} S\dot{\hat{r}} = & S \left[A - B_1 (F_2^T C^T \bar{V}^{-1} C F_2)^{-1} F_2^T C^T \bar{V}^{-1} C \right. \\ & \left. + S B_1 (F_2^T C^T \bar{V}^{-1} C F_2)^{-1} B_1^T S \right] \hat{r} \quad (7.38) \end{aligned}$$

at $t = t_0^+$, which is the same equation as (7.34). Hence,

$$\psi = \hat{r} \quad \text{mod Ker } S$$

over the entire time interval since they are equal (mod ker S) at t_0^+ and are propagated by the same equations for $t > t_0^+$. This means that

$$\hat{e} = \hat{r} \quad \text{mod Ker } S, \quad \forall t,$$

which implies that

$$\hat{x} = \alpha_p \pmod{\text{Ker } S}, \forall t.$$

The optimal estimate is, thus, given by

$$\begin{aligned} S\hat{x} = SA\hat{x} + SB_1(F_2^T C^T \bar{V}^{-1} C F_2)^{-1} F_2^T C^T \bar{V}^{-1} (y - C\hat{x}) \\ + C^T (\bar{H})^T \bar{V} \bar{H} (y - C\hat{x}), \end{aligned} \quad (7.39)$$

where S is the solution of (7.26). While it is possible to generate an estimate from (7.39) in full-order form, it may not be practical since S is not invertible. We will see in the next section, however, that an easily implementable reduced-order estimator can be derived from these results.

If $F_2^T C^T \bar{V}^{-1} C F_2$ fails to be positive definite, we will still have a singular problem and our results from above will be invalid, since (7.26) requires that the inverse, $(F_2^T C^T \bar{V}^{-1} C F_2)^{-1}$, exists. We must, therefore, continue to transform our problem until it is nonsingular. The way we proceed, however, depends on the type of singularity that we are dealing with.

1. If $F_2^T C^T \bar{V}^{-1} C F_2$ is *totally* singular, i.e. equal to zero, we can repeat the Goh transformation,

$$\begin{aligned} \phi_2(t) &= \int_{t_0}^t \phi_1(\tau) d\tau, \\ \alpha_2 &= \alpha_1 - B_1 \phi_1, \\ \dot{\alpha}_2 &= A\alpha_2 + B_2 \phi_2, \\ B_2 &= AB_1 - \dot{B}_1, \end{aligned} \quad (7.40)$$

since we have the same problem that we started out with.

2. If $F_2^T C^T \bar{V}^{-1} C F_2$ is only *partially* singular, that is, singular but nonzero, we can always assume that this quantity takes the form,

$$F_2^T C^T \bar{V}^{-1} C F_2 = \begin{bmatrix} Q^a & 0 \\ 0 & 0 \end{bmatrix},$$

where Q_a is positive definite. This assumption is reasonable since we can reshuffle the state-space if needed (Moylan and Moore 1971). In fact, we can also group the nuisance input, ϕ_1 , accordingly:

$$\dot{\alpha}_1 = A\alpha_1 + B_1^a\phi_1^a + B_1^b\phi_1^b,$$

so that the game cost is singular with respect to ϕ_1^b , but not ϕ_1^a . The transformation proceeds on ϕ_1^b only:

$$\begin{aligned}\phi_2^b(t) &= \int_{t_0}^t \phi_1^b(\tau) d\tau \\ \alpha_2 &= \alpha_1 - B_1^b\phi_2^b.\end{aligned}$$

The new input matrix is then

$$B_2 = \begin{bmatrix} B_1^a & AB_1^b - \dot{B}_1^b \end{bmatrix}, \quad (7.41)$$

and the new game is formed as before.

In both cases, we can stop with the transformation process if $B_1^T C^T \bar{V}^{-1} C B_1$ is positive definite. Otherwise, we must continue the transformation in the appropriate manner. When we finally get a B_k such that $B_{k-1}^T C^T \bar{V}^{-1} C B_{k-1}$ is positive definite, the differential game will be

$$\min_{\hat{x}} \max_y \max_{\phi_k} \max_{\alpha_k(t_0)} J^* \leq 0,$$

$$\begin{aligned}J^* &= \int_{t_0}^{t_1} \left[\|\alpha_k - \hat{x}\|_{C^T H Q H C}^2 - \|y - C\alpha_k\|_{\bar{V}^{-1}}^2 \right. \\ &\quad + (y - C\alpha_k)^T \bar{V}^{-1} C B_{k-1} \phi_k + \phi_k^T B_{k-1}^T C^T \bar{V}^{-1} (y - C\alpha_k) \\ &\quad \left. - \|\phi_k\|_{B_{k-1}^T C^T \bar{V}^{-1} C B_{k-1}}^2 \right] dt - \|\alpha_k(t_0) + \bar{B}\hat{\phi}(t_0^+) - \hat{x}_0\|_{\Pi_0}^2,\end{aligned}$$

subject to

$$\dot{\alpha}_k = A\alpha_k + B_k\phi_k,$$

where

$$\alpha_k = x + \bar{B}\hat{\phi}(t_0^+).$$

\bar{B} is a matrix formed by eliminating the redundant columns of the composite matrix, $[F_2 \ \cdots \ B_{k-1}]$, and $\hat{\phi}(t_0^+)$ is the corresponding vector, $[\phi_1^T \ \cdots \ \phi_k^T]^T$, with the redundant elements eliminated. These columns and elements must be removed to avoid accounting for the same signal more than once. The potential for repeating elements exists, because in the partially singular case the columns of B_{j-1} which correspond to the nonsingular inputs (denoted B_j^a) are simply carried over unchanged to the next input matrix, B_j , e.g. (7.41).

The corresponding Goh Riccati equation for the general problem is

$$\begin{aligned} -\dot{S} = S & \left[A - B_k(B_{k-1}^T C^T \bar{V}^{-1} C B_{k-1})^{-1} B_{k-1}^T C^T \bar{V}^{-1} C \right] \\ & + \left[A - B_k(B_{k-1}^T C^T \bar{V}^{-1} C B_{k-1})^{-1} B_{k-1}^T C^T \bar{V}^{-1} C \right]^T S \\ & + C^T (H Q H - \bar{H}^T \bar{V}^{-1} \bar{H}) C + S B_k (B_{k-1}^T C^T \bar{V}^{-1} C B_{k-1})^{-1} B_{k-1}^T S \end{aligned} \quad (7.42)$$

with the boundary condition,

$$S(t_0^+) = \bar{\Pi}_0 - \bar{\Pi}_0 \bar{B} (\bar{B}^T \bar{\Pi}_0 \bar{B})^{-1} \bar{B}^T \bar{\Pi}_0. \quad (7.43)$$

The general form of the estimator is

$$\begin{aligned} S\dot{\hat{x}} = S A \hat{x} + S B_k & (B_{k-1}^T C^T \bar{V}^{-1} C B_{k-1})^{-1} B_{k-1}^T C^T \bar{V}^{-1} (y - C \hat{x}) \\ & + C^T (\bar{H})^T \bar{V}^{-1} \bar{H} (y - C \hat{x}). \end{aligned} \quad (7.44)$$

Implicit in the general form of the Goh Riccati equation is the assumption that the projector, H , will be such that $H C B_i = 0$, $\forall i < k - 1$, where k is the iteration step which leads to a nonsingular problem. If one examines the construction of H , however, he will see that this is always indeed the case. B_{k-1} is constructed by operating on the columns of the nuisance map, F_2 , with the Goh transformation until they lie outside the kernel of C

(7.13,7.40,7.41). This is the same way that the matrices, \hat{F} or $\hat{F}(t)$, from the definition of H , (6.14,6.12), are derived. Thus, one could equivalently define H as

$$H = I - CB_{k-1} \left[(CB_{k-1})^T CB_{k-1} \right]^{-1} (CB_{k-1})^T$$

and \bar{H} as

$$\bar{H} = I - CB_{k-1} \left[B_{k-1}^T C^T \bar{V}^{-1} CB_{k-1} \right]^{-1} B_{k-1}^T C^T \bar{V}^{-1}. \quad (7.45)$$

We can relate the Goh Riccati equation to our game Riccati equation and to the limiting case analysis through the following theorem taken directly from (Bell and Jacobsen 1973):

Theorem 7.1. The solution to (7.42), S , is such that

$$SB_{i-1} = 0, \quad \forall t \in [t_0, t_1], \quad (7.46)$$

$$\dot{S} + SA + A^T S + C^T (HQH - \bar{V}^{-1})C \leq 0. \quad (7.47)$$

Proof. Rewrite (7.42) as

$$\begin{aligned} \dot{S} + SA + A^T S + C^T (HQH - \bar{H}^T \bar{V}^{-1} \bar{H})C = \\ - SB_k (B_{k-1}^T C^T \bar{V}^{-1} CB_{k-1})^{-1} B_k^T S + SB_k (B_{k-1}^T C^T \bar{V}^{-1} CB_{k-1})^{-1} B_{k-1}^T C^T \bar{V}^{-1} C \\ + C^T \bar{V}^{-1} CB_{k-1} (B_{k-1}^T C^T \bar{V}^{-1} CB_{k-1})^{-1} B_k^T S. \end{aligned} \quad (7.48)$$

Using (7.45), we can expand \bar{H} in (7.48) and collect terms to get

$$\begin{aligned} \dot{S} + SA + A^T S + C^T (HQH - \bar{V}^{-1})C = - \left[SB_k - C^T \bar{V}^{-1} CB_{k-1} \right] \\ \times (B_{k-1}^T C^T \bar{V}^{-1} CB_{k-1})^{-1} \left[B_k^T S - B_{k-1}^T C^T \bar{V}^{-1} C \right]. \end{aligned} \quad (7.49)$$

Equation (7.49) clearly implies our first claim, (7.47). To prove our second claim, (7.46), we first rearrange (7.49) as

$$\begin{aligned} \dot{S} = & -SA - A^T S - C^T (HQH - \bar{V}^{-1})C - [SB_k - C^T \bar{V}^{-1}CB_{k-1}] \\ & \times (B_{k-1}^T C^T \bar{V}^{-1}CB_{k-1})^{-1} [B_k^T S - B_{k-1}^T C^T \bar{V}^{-1}C]. \end{aligned} \quad (7.50)$$

Multiply both sides of (7.50) by B_{k-1}^T and then subtract $\dot{B}_{k-1}^T S$ from both sides of the result to get

$$\begin{aligned} -B_{k-1}^T \dot{S} - \dot{B}_{k-1}^T S = & -B_{k-1}^T SA - \dot{B}_{k-1}^T S + B_{k-1}^T A^T S \\ & - B_{k-1}^T C^T \bar{V}^{-1}C - [B_{k-1}^T SB_k - B_{k-1}^T C^T \bar{V}^{-1}CB_{k-1}] \\ & \times (B_{k-1}^T C^T \bar{V}^{-1}CB_{k-1})^{-1} [B_k^T S - B_{k-1}^T C^T \bar{V}^{-1}C]. \end{aligned}$$

If we collect terms, making use of the fact that $B_k = AB_{k-1} - \dot{B}_{k-1}$, we get

$$\begin{aligned} \frac{d}{dt} [B_{k-1}^T S] = & \\ & - B_{k-1}^T S \left[A + B_k (B_{k-1}^T C^T \bar{V}^{-1}CB_{k-1})^{-1} (B_k^T S - B_{k-1}^T C^T \bar{V}^{-1}C) \right]. \end{aligned} \quad (7.51)$$

Equation (7.51) is a homogeneous differential equation in the $B_{k-1}^T S$. The boundary condition to (7.51) is derived from (7.43), where we make use of fact that $S(t_0^+)$ is a projector that maps B_{k-1} to zero since \bar{B} contains the columns of B_{k-1} :

$$B_{k-1}^T S(t_0^+) = B_{k-1}^T \bar{\Pi}_0 - B_{k-1}^T \bar{\Pi}_0 \bar{B} (\bar{B}^T \bar{\Pi}_0 \bar{B})^{-1} \bar{B}^T \bar{\Pi}_0 = 0. \quad (7.52)$$

Equations (7.51) and (7.52) together imply (7.46). ◀

The same arguments used to prove Theorem 7.1 are used in (Moylan and Moore 1971) to show that (7.46) implies $SF_2 = 0$, $\forall t \in [t_0, t_1]$. Hence, the Goh Riccati solution satisfies all of the sufficient conditions for nonpositivity.

Remark 9. Equations (7.19) and (7.52) show that the nuisance input acts impulsively at t_0 to move the error trajectory onto the singular arc defined by (7.46). The projector, H ,

restricts z to this singular arc so that the transformed game becomes the same game that was solved in Section 6.2, except restricted to the singular arc. In this sense, S is the limit of Π on the singular arc. \blacklozenge

Remark 10. The requirement that $B_i^T C^T \bar{V}^{-1} C B_i$ be invertible is the Generalized Legendre-Clebsch Condition (Bell and Jacobsen 1973). Note that taking V to zero along with γ so that γV^{-1} has a nonzero limit is crucial to satisfying this condition. \blacklozenge

7.4 The Relationship Between the Limiting Game Filter and Detection Filters

7.4.1 A Reduced-Order Detection Filter from the Limiting Game Solution

The results that we will present in this subsection are most easily derived for time-invariant systems. We will, therefore, limit ourselves to this case to simplify the presentation.

To begin, we consider the initial condition, $S(t_0)$, (7.43), to the Goh Riccati equation, (7.42). This matrix is symmetric, nonnegative definite with a nontrivial nullspace which means that there exists a nonsingular, orthonormal transformation, Γ , such that

$$\Gamma^T S(t_0) \Gamma = \begin{bmatrix} \bar{S}(t_0) & 0 \\ 0 & 0 \end{bmatrix}. \quad (7.53)$$

$\bar{S}(t_0)$ is positive definite and symmetric. Applying the same transformation to our system matrices, gives us

$$\begin{aligned} C\Gamma &= [C_1 \quad C_2], & \Gamma^T A\Gamma &= \begin{bmatrix} A_{11} & A_{12} \\ A_{21} & A_{22} \end{bmatrix}, \\ \Gamma^T B_{k-1} &= \begin{bmatrix} D_1 \\ D_2 \end{bmatrix}, & \Gamma^T B_k &= \begin{bmatrix} G_1 \\ G_2 \end{bmatrix}. \end{aligned}$$

Note that since $S B_{k-1} = 0$, applying the transformation, Γ , within the product, $S B_{k-1}$, gives us $\Gamma^T S \Gamma \Gamma^T B_{k-1} = \bar{S} D_1 = 0$, which implies that $D_1 = 0$ since \bar{S} is positive definite. Hence,

$$\Gamma^T B_{k-1} = \begin{bmatrix} 0 \\ D_2 \end{bmatrix}.$$

We can apply this transformation to the estimator state,

$$\hat{\eta} = \begin{Bmatrix} \hat{\eta}_1 \\ \hat{\eta}_2 \end{Bmatrix} = \Gamma^T \hat{x},$$

to get a reduced-order estimator by transforming (7.44):

$$\begin{aligned} \begin{bmatrix} \bar{S} & 0 \\ 0 & 0 \end{bmatrix} \begin{Bmatrix} \dot{\hat{\eta}}_1 \\ \dot{\hat{\eta}}_2 \end{Bmatrix} &= \begin{bmatrix} \bar{S} & 0 \\ 0 & 0 \end{bmatrix} \begin{bmatrix} A_{11} & A_{12} \\ A_{21} & A_{22} \end{bmatrix} \begin{Bmatrix} \hat{\eta}_1 \\ \hat{\eta}_2 \end{Bmatrix} \\ &+ \begin{Bmatrix} C_1^T \\ C_2^T \end{Bmatrix} \bar{H}^T \bar{V}^{-1} \bar{H} \left(y - \begin{bmatrix} C_1 & C_2 \end{bmatrix} \begin{Bmatrix} \hat{\eta}_1 \\ \hat{\eta}_2 \end{Bmatrix} \right) \\ &- \begin{bmatrix} \bar{S} & 0 \\ 0 & 0 \end{bmatrix} \begin{bmatrix} G_1 \\ G_2 \end{bmatrix} \left(\begin{bmatrix} 0 & D_2^T \end{bmatrix} \begin{bmatrix} C_1^T \\ C_2^T \end{bmatrix} \bar{V}^{-1} \begin{bmatrix} C_1 & C_2 \end{bmatrix} \begin{bmatrix} 0 \\ D_2 \end{bmatrix} \right)^{-1} \\ &\times \begin{bmatrix} 0 & D_2^T \end{bmatrix} \begin{bmatrix} C_1^T \\ C_2^T \end{bmatrix} \bar{V}^{-1} (y - C_1 \hat{\eta}_1 - C_2 \hat{\eta}_2). \end{aligned} \quad (7.54)$$

From (7.54), we get a pair of equations:

$$\begin{aligned} \bar{S} \dot{\hat{\eta}}_1 &= \bar{S} A_{11} \hat{\eta}_1 + \bar{S} A_{12} \hat{\eta}_2 + C_1^T (\bar{H})^T \bar{V}^{-1} \bar{H} (y - C_1 \hat{\eta}_1 - C_2 \hat{\eta}_2) \\ &- \bar{S} G_1 (D_2^T C_2^T \bar{V}^{-1} C_2 D_2)^{-1} D_2^T C_2^T \bar{V}^{-1} (y - C_1 \hat{\eta}_1 - C_2 \hat{\eta}_2), \end{aligned} \quad (7.55)$$

$$0 = C_2^T (\bar{H})^T \bar{V}^{-1} \bar{H} (y - C_1 \hat{\eta}_1 - C_2 \hat{\eta}_2). \quad (7.56)$$

Since the residual signal, $y - C_1 \hat{\eta}_1 - C_2 \hat{\eta}_2$, is arbitrary, (7.56) implies that

$$\bar{H} C_2 = 0. \quad (7.57)$$

Since $\text{Ker } S \subset \text{Ker } HC$ at t_0^+ by construction (7.29), we can take a vector, $\xi \in \text{Ker } S(t_0^+)$, and then pre- and post-multiply (7.42) by ξ^T and ξ respectively to get $\xi^T \dot{S}(t_0^+) \xi = 0$. This implies that

$$\Gamma^T \dot{S}(t_0^+) \Gamma = \begin{bmatrix} \dot{S} & 0 \\ 0 & 0 \end{bmatrix}.$$

Thus, if we apply the Goh transformation to the Goh Riccati equation, (7.42), we get three equations:

$$0 = C_2^T (HQH - \bar{H}^T \bar{V}^{-1} \bar{H}) C_2, \quad (7.58)$$

$$0 = \bar{S} \left[A_{12} - G_1 (D_2^T C_2^T \bar{V}^{-1} C_2 D_2)^{-1} D_2^T C_2^T \bar{V}^{-1} C_2 \right] + C_1^T (HQH - \bar{H}^T \bar{V}^{-1} \bar{H}) C_2, \quad (7.59)$$

$$\begin{aligned} \dot{\bar{S}} = & \bar{S} \left[A_{11} - G_1 (D_2^T C_2^T \bar{V}^{-1} C_2 D_2)^{-1} D_2^T C_2^T \bar{V}^{-1} C_1 \right] \\ & + \left[A_{11} - G_1 (D_2^T C_2^T \bar{V}^{-1} C_2 D_2)^{-1} D_2^T C_2^T \bar{V}^{-1} C_1 \right]^T \bar{S} \\ & + \bar{S} G_1 (D_2^T C_2^T \bar{V}^{-1} C_2 D_2)^{-1} G_1^T \bar{S} + C_1^T (HQH - \bar{H}^T \bar{V}^{-1} \bar{H}) C_1. \end{aligned} \quad (7.60)$$

Equation (7.60) is a reduced-order Goh Riccati equation with a boundary condition taken from (7.53). Equations (7.57) and (7.58) imply that

$$HC_2 = 0. \quad (7.61)$$

By applying (7.57,7.61) to (7.59), we find that

$$\bar{S} \left[A_{12} - G_1 (D_2^T C_2^T \bar{V}^{-1} C_2 D_2)^{-1} D_2^T C_2^T \bar{V}^{-1} C_2 \right] = 0$$

which means that

$$A_{12} - G_1 (D_2^T C_2^T \bar{V}^{-1} C_2 D_2)^{-1} D_2^T C_2^T \bar{V}^{-1} C_2 = 0, \quad (7.62)$$

since \bar{S} is positive definite. Together (7.57,7.61, and 7.62) reduce (7.55) to

$$\begin{aligned} \dot{\hat{\eta}}_1 = & A_{11} \hat{\eta}_1 + G_1 (D_2^T C_2^T \bar{V}^{-1} C_2 D_2)^{-1} D_2^T C_2^T \bar{V}^{-1} (y - C_1 \hat{\eta}_1) \\ & + \bar{S}^{-1} C_1^T (\bar{H})^T \bar{V}^{-1} \bar{H} (y - C_1 \hat{\eta}_1). \end{aligned} \quad (7.63)$$

Equations (7.57), (7.61), and (7.62) also imply that for all $t \in [t_0, t_1]$, the kernel of the Goh Riccati matrix does not increase or decrease in size. Thus, the Goh Riccati equation, (7.42), reduces to (7.60).

To get the error equation, we define

$$\eta = \begin{Bmatrix} \eta_1 \\ \eta_2 \end{Bmatrix} \triangleq \Gamma^T \alpha_k, \quad e_1 \triangleq \eta_1 - \hat{\eta}_1, \quad e_2 \triangleq \eta_2 - \hat{\eta}_2.$$

If we transform the state dynamics, (6.31), and the measurements, (6.1), we get

$$\dot{\eta}_1 = A_{11}\eta_1 + A_{12}\eta_2 + G_1\phi_k, \quad (7.64)$$

$$\dot{\eta}_2 = A_{21}\eta_1 + A_{22}\eta_2 + G_2\phi_k,$$

$$y = C\alpha_k + C\bar{B}\hat{\phi} + v = C_1\eta_1 + C_2\eta_2 + C_2D_2\phi_k + v. \quad (7.65)$$

The expression on the furthest right hand side of (7.65) results from the fact that the only columns in \bar{B} which lie outside the kernel of C are those which correspond to B_{k-1} . Using (7.63–7.65), the error equation for our reduced-order estimator is

$$\begin{aligned} \dot{e}_1 = & \left[A_{11} - G_1(D_2^T C_2^T \bar{V}^{-1} C_2 D_2)^{-1} D_2^T C_1^T \bar{V}^{-1} C_1 - \bar{S}^{-1} C_1^T (\bar{H})^T \bar{V}^{-1} \bar{H} C_1 \right] e_1 \\ & + \left[A_{12} - G_1(D_2^T C_2^T \bar{V}^{-1} C_2 D_2)^{-1} D_2^T C_2^T \bar{V}^{-1} C_2 \right] \eta_2 + G_1 \phi_k \\ & - G_1(D_2^T C_2^T \bar{V}^{-1} C_2 D_2)^{-1} D_2^T C_2^T \bar{V}^{-1} C_2 (D_2 \phi_k + v) \\ & - \bar{S}^{-1} C_1^T (\bar{H})^T \bar{V}^{-1} \bar{H} (C_2 D_2 \phi_k + v). \end{aligned} \quad (7.66)$$

By using (7.57) and (7.62), (7.66) can be further simplified to

$$\begin{aligned} \dot{e}_1 = & \left[A_{11} - G_1(D_2^T C_2^T \bar{V}^{-1} C_2 D_2)^{-1} D_2^T C_1^T \bar{V}^{-1} C_1 - \bar{S}^{-1} C_1^T (\bar{H})^T \bar{V}^{-1} \bar{H} C_1 \right] e_1 \\ & - \left[G_1(D_2^T C_2^T \bar{V}^{-1} C_2 D_2)^{-1} D_2^T C_2^T \bar{V}^{-1} C_2 + \bar{S}^{-1} C_1^T (\bar{H})^T \bar{V}^{-1} \bar{H} \right] v. \end{aligned} \quad (7.67)$$

Equation (7.67) clearly shows that the error, e_1 , is not influenced by the nuisance fault. In practice, however, we will not be able to monitor e_1 directly, since our information about the system comes from the filter residual, $(y - C\hat{\eta}_1)$, which is not free from the influence

of η_2 . The use of the projector, H , on this residual, however, will eliminate this influence. The failure signal for the reduced-order filter is then

$$z = H(y - C_1 \hat{\eta}_1).$$

It is fairly easy to show:

Theorem 7.2. The reduced-order estimator, (7.63), is asymptotically stable.

Proof. From (7.67), it is clear that the stability of the reduced-order estimator depends on the eigenvalues of the closed-loop matrix,

$$\bar{A}_{cl} = A_{11} - G_1(D_2^T C_2^T \bar{V}^{-1} C_2 D_2)^{-1} D_2^T C_1^T \bar{V}^{-1} C_1 - \bar{S}^{-1} C_1^T (\bar{H})^T \bar{V}^{-1} \bar{H} C_1. \quad (7.68)$$

We can show that \bar{A}_{cl} is Hurwitz, i.e. its eigenvalues are in the open left-half plane, by rewriting (7.60) as

$$\begin{aligned} \dot{\bar{S}} + \bar{S} \bar{A}_{cl} + \bar{A}_{cl}^T \bar{S} &= -C_1^T (H Q H + \bar{H}^T \bar{V}^{-1} \bar{H}) C_1 \\ &\quad - \bar{S} G_1 (D_2^T C_2^T \bar{V}^{-1} C_2 D_2)^{-1} G_1^T \bar{S}. \end{aligned} \quad (7.69)$$

The first term on the right-hand side of (7.69) is negative semi-definite. The second term is negative definite, since \bar{S} and $(D_2^T C_2^T \bar{V}^{-1} C_2 D_2)^{-1}$ are positive definite and G_1 has independent columns by construction. Therefore,

$$\dot{\bar{S}} + \bar{S} \bar{A}_{cl} + \bar{A}_{cl}^T \bar{S} < 0.$$

Lyapunov's Stability Theorem (Khalil 1996) then implies that \bar{A}_{cl} is Hurwitz. ◀

Remark 11. The reduced-order filter that we find here is similar to the “residual generator” introduced by Massoumnia *et al.* in (Massoumnia et al. 1989) and establishes an important link between our limiting case results and classical detection filters. A stronger link will be established shortly when we show the equivalence between the limiting solution and the unknown input observer. ◀

Remark 12. The difficulty in deriving a reduced-order filter for the time-varying case lies in finding a way to transform S so that the reduced-order estimator, (7.63), and the reduced-order Riccati equation, (7.60), remain valid over the entire time interval. Note that Theorem 7.1, Equation (7.46), gives insight on how to form the transformation matrix and (Oshman and Bar-Itzhack 1985) gives similar insights on the propagation structure. ◀

Remark 13. Taking the limit of γV^{-1} allows us to give a rigorous accounting of the measurement uncertainty, v , in the lower-dimensional subspace determined by the singular arc. The authors of (Massoumnia et al. 1989) claim that they can choose a reduced-order filter structure to deal with such issues, though their analyses do not explicitly consider sensor noise, making it unclear how such noise projects onto their reduced state-space. ◀

7.4.2 The Invariant Subspace Structure of the Limiting Case Filter

Unknown input observers work by placing the image of the nuisance failure map into the unobservable subspace. We will show that the asymptotic game filter works in the same way. Getting to this result, however, will require that we first introduce some concepts from geometric control theory (Basile and Marro 1992, Wonham 1985).

Geometric control theory gets its name from its use of abstract subspaces and operators, without specific bases, to define and solve problems in systems theory. Of particular importance in this theory are subspaces which are invariant with respect to operators. If we consider a system, (6.1,6.31), defined by the triple, (C, A, F_2) , and let \mathcal{X} denote the state-space, then a subspace $\mathcal{W} \subset \mathcal{X}$ is said to be *A-invariant* if for every $x \in \mathcal{W}$, $Ax \in \mathcal{W}$. This can be equivalently symbolized as $A\mathcal{W} \subset \mathcal{W}$. \mathcal{W} is said to be *(C,A)-invariant* if there exists an output injection feedback matrix, L , such that $(A + LC)\mathcal{W} \subset \mathcal{W}$.

Another important element in geometric control theory, and in control theory in general, is the concept of *invariant zeros*. Invariant zeros are the complex numbers, λ , which cause the matrix,

$$P(\lambda) = \begin{bmatrix} A - \lambda I & F_2 \\ C & 0 \end{bmatrix},$$

to lose column rank (Macfarlane and Karcanias 1976). Associated with each zero is an *invariant zero direction*, z , such that

$$\begin{bmatrix} A - \lambda I & F_2 \\ C & 0 \end{bmatrix} \begin{Bmatrix} z \\ w \end{Bmatrix} = 0. \quad (7.70)$$

By (Moore and Laub 1978), when (7.70) holds, the vector w is such that $w = Kz$ for some matrix K . Invariant zeros behave like multivariable analogs to the transfer function zeros of classical control theory. They play a fundamental role in determining the limits of performance for optimal control systems (Francis 1979, Kwakernaak and Sivan 1972, Shaked 1990), and they are also essential to defining special (C, A) -invariant subspaces, called (C, A) -*unobservability subspaces*, which are used in Beard-Jones Fault Detection Filters (Douglas 1993, Massoumnia 1986) and in reduced-order residual generators (see (Massoumnia et al. 1989) and Remark (7.4.2)) for design.

The following theorem tells us that $\text{Ker } S$ is a (C, A) -invariant subspace, and it also tells us something of $\text{Ker } S$'s invariant zero structure. The second claim will require the following lemma:

Lemma 7.3. Let λ and z be an invariant zero and zero direction for the triple, (C, A, F_2) . Let $\mathcal{W} \subset \mathcal{X}$ be a (C, A) -invariant subspace with the image of F_2 contained in \mathcal{W} and let L be any map such that $(A + LC)\mathcal{W} \subset \mathcal{W}$. Then $z \notin \mathcal{W}$ implies that λ is an eigenvalue of $(A + LC)$ restricted to the factor space, \mathcal{X}/\mathcal{W} .

Proof. See (Douglas 1993), Proposition 2.9 ◀

Theorem 7.4.

1. $\text{Ker } S$ is a (C, A) -invariant subspace.
2. The invariant zero directions corresponding to the right-half plane and $j\omega$ -axis zeros of (C, A, F_2) lie in $\text{Ker } S$.

Proof. Consider the “state matrix,”

$$A_{cl} = SA - SB_k(B_{k-1}^T C^T \bar{V}^{-1} C B_{k-1})^{-1} B_{k-1}^T C^T \bar{V}^{-1} C + C^T (\bar{H})^T \bar{V} \bar{H} C,$$

of the full-order estimator found from the singular game solution, (7.44). If we pre- and post-multiply A_{cl} by Γ^T and Γ respectively, we get

$$\Gamma^T A_{cl} \Gamma = \begin{bmatrix} \bar{S} & 0 \\ 0 & 0 \end{bmatrix} \begin{bmatrix} \bar{A}_{cl} & \bar{A}_{12} \\ \bar{A}_{21} & \bar{A}_{22} \end{bmatrix}, \quad (7.71)$$

where \bar{A}_{cl} is as defined in (7.68) and

$$\begin{aligned} \bar{A}_{12} &\triangleq A_{12} - G_1 (D_2^T C_2^T \bar{V}^{-1} C_2 D_2)^{-1} D_2^T C_2^T \bar{V}^{-1} C_2, \\ \bar{A}_{21} &\triangleq A_{21} - G_2 (D_2^T C_2^T \bar{V}^{-1} C_2 D_2)^{-1} D_2^T C_2^T \bar{V}^{-1} C_1, \\ \bar{A}_{22} &\triangleq A_{22} - G_2 (D_2^T C_2^T \bar{V}^{-1} C_2 D_2)^{-1} D_2^T C_2^T \bar{V}^{-1} C_2. \end{aligned}$$

From (7.62), $\bar{A}_{12} = 0$, which means that (7.71) simplifies to

$$\Gamma^T A_{cl} \Gamma = \begin{bmatrix} \bar{S} & 0 \\ 0 & 0 \end{bmatrix} \begin{bmatrix} \bar{A}_{cl} & 0 \\ \bar{A}_{21} & \bar{A}_{22} \end{bmatrix}. \quad (7.72)$$

Equation (7.72) clearly implies that $\text{Ker } S$ is (C, A) -invariant, since the error e , if it initially lies in $\text{Ker } S$, must be of the form,

$$e(t_0) = \begin{Bmatrix} 0 \\ \underline{e}(t_0) \end{Bmatrix},$$

in the basis corresponding to the transformation, Γ . In the absence of exogenous inputs, (7.72) implies that $e(t)$ will then be propagated by way of

$$\dot{e}(t) = \begin{bmatrix} \bar{S} & 0 \\ 0 & 0 \end{bmatrix} \begin{Bmatrix} 0 \\ \bar{A}_{22} \underline{e}(t) \end{Bmatrix}.$$

This clearly shows that the error trajectory will never leave $\text{Ker } S$.

The second part of our theorem follows from Lemma 7.3. Applied to our case, this lemma tells us that any zero directions which do not lie in $\text{Ker } S$ will show up as eigenvalues of the submatrix, \bar{A}_{cl} , in (7.72). We have just shown in Theorem 7.2, however, that \bar{A}_{cl} is asymptotically stable. Therefore these zero directions cannot lie outside of $\text{Ker } S$. \blacktriangleleft

Since the image of F_2 lies in $\text{Ker } S$, the following theorem implies that the limiting case game filter has the structure of an unknown input observer:

Theorem 7.5. $\text{Ker } S$ is contained in the unobservable subspace of (HC, A) , where H is the projector defined by (6.12) or (6.14).

Proof. Let ξ be a constant vector which lies in $\text{Ker } S$ at $t = t_0^+$. Define

$$\Gamma^T \xi = \begin{Bmatrix} 0 \\ \underline{\xi} \end{Bmatrix}$$

and pre- and post-multiply the Goh Riccati equation, (7.42), by ξ^T and ξ respectively to get

$$0 = \xi^T \dot{S} \xi + \xi^T C^T (H Q H - \bar{H}^T \bar{V} \bar{H}) C \xi. \quad (7.73)$$

However,

$$\xi^T \Gamma \Gamma^T \dot{S} \Gamma \Gamma^T \xi = [0 \quad \underline{\xi}^T] \begin{bmatrix} \dot{S} & 0 \\ 0 & 0 \end{bmatrix} \begin{Bmatrix} 0 \\ \underline{\xi} \end{Bmatrix} = 0, \quad (7.74)$$

which implies that

$$\xi^T C^T (H Q H - \bar{H}^T \bar{V} \bar{H}) C \xi = 0. \quad (7.75)$$

Since HC and $\bar{H}C$ project onto the same space⁴, we can define $\bar{\xi} \triangleq HC\xi = \bar{H}C\xi$ and then rewrite (7.75) as

$$\|\bar{\xi}\|_{Q-\bar{V}^{-1}}^2 = 0.$$

⁴See the discussion which follows (7.24).

So long as $Q \neq \bar{V}^{-1}$, this implies that $\|\bar{\xi}\| = 0$, which, in turn, implies that

$$\xi \in \text{Ker } HC = \text{Ker } \bar{H}C. \quad (7.76)$$

We will now consider the general case. We define the vector, ξ_k , to be

$$\xi_k \triangleq \left[A - B_k (B_{k-1}^T C^T \bar{V}^{-1} C B_{k-1})^{-1} B_{k-1}^T C^T \bar{V}^{-1} C \right]^k \xi$$

and assume that $\xi_k \in \text{Ker } S$. Note that this implies that

$$\Gamma \xi_k = \begin{Bmatrix} 0 \\ \xi_k \end{Bmatrix}$$

which, in turn, means that $\dot{S}\xi_k = 0$, since we can transform $\dot{S}\xi_k$ into a form similar to (7.74). ξ_k lying in the kernels of both S and \dot{S} then implies that ξ_k also lies in $\text{Ker } HC$ since we can pre- and post-multiply the Goh Riccati equation, (7.42), by ξ_k^T and ξ_k respectively to get

$$\xi_k^T C^T (HQH - \bar{H}^T \bar{V} \bar{H}) C \xi_k = 0.$$

Thus, if we post-multiply, (7.42) by ξ_k , the remainder,

$$\begin{aligned} 0 &= S \left[A - B_k (B_{k-1}^T C^T \bar{V}^{-1} C B_{k-1})^{-1} B_{k-1}^T C^T \bar{V}^{-1} C \right] \xi_k \\ &= S \left[A - B_k (B_{k-1}^T C^T \bar{V}^{-1} C B_{k-1})^{-1} B_{k-1}^T C^T \bar{V}^{-1} C \right]^{k+1} \xi, \end{aligned}$$

tells us that

$$\xi_{k+1} \triangleq \left[A - B_k (B_{k-1}^T C^T \bar{V}^{-1} C B_{k-1})^{-1} B_{k-1}^T C^T \bar{V}^{-1} C \right]^{k+1} \xi$$

lies in the kernel of S . The same arguments as before then lead to $\xi_{k+1} \in \text{Ker } \dot{S}$ and $\xi_{k+1} \in \text{Ker } HC$. Thus, ξ_k lying in the kernel of S implies it also lies in the kernel of HC and that ξ_{k+1} lies in the kernel of S . By induction, we can claim that this holds for all k , in particular, $k = 0, \dots, n-1$, so that

$$\begin{aligned}
HC\xi &= 0, \\
HC\left[A - B_k(B_{k-1}^T C^T \bar{V}^{-1} C B_{k-1})^{-1} B_{k-1} C^T \bar{V}^{-1} C\right]\xi &= 0, \\
&\vdots \\
HC\left[A - B_k(B_{k-1}^T C^T \bar{V}^{-1} C B_{k-1})^{-1} B_{k-1} C^T \bar{V}^{-1} C\right]^{n-1}\xi &= 0.
\end{aligned}$$

This leads us to the conclusion that our original vector, ξ , lies in the unobservable subspace of $(HC, A - B_k(B_{k-1}^T C^T \bar{V}^{-1} C B_{k-1})^{-1} B_{k-1} C^T \bar{V}^{-1} C)$. Since output injection feedback cannot change the observability of a system, ξ lies in the unobservable subspace of (HC, A) . Since ξ is an arbitrary vector in $\text{Ker } S$, this implies the proposition. \blacklozenge

Remark 14. The fault-embedding state subspace of the residual generator described by (Massoumnia et al. 1989) is a (C, A) -unobservability subspace. These subspaces are distinguished by the fact that they contain all of the invariant zero directions associated with the triple, (C, A, F_2) . This characteristic allows for complete eigenvalue assignment on both the (C, A) -unobservability subspace and the associated factor space. The authors of (Massoumnia et al. 1989) claim that this not only ensures the stability of their residual generator, but that it also enables them to address other design issues such as sensor noise rejection (see Remark 7.4.1). Our invariant subspace, $\text{Ker } S$, on the other hand, can only be said to be (C, A) -invariant, since we cannot account for all of the invariant zeros with Theorem 7.4. The game theoretic filter, however, provides the analyst the freedom to adjust his designs through the use of the weighting matrices, and it has also been shown to be asymptotic stable (Theorem 7.2). \blacklozenge

Remark 15. The proof to Theorem 7.4 is patterned after the proof to Lemma 3.1(b) from (Limebeer and Halikias 1988). It is also possible to prove the second part of Theorem 7.4 using the proof given in Part 3 of Appendix B in (Francis 1979). Other reported results concerning the null space of Riccati solutions are cited in (Saber et al. 1995). \blacklozenge

7.5 Revisited: Accelerometer Fault Detection in an F-16XL

In this section, we revisit the F-16XL example of Section 6.3.1 to demonstrate the use of the reduced-order filter of Section 7.4.1. A description of this problem is given in Section 6.3.1. The nominal failure model is

$$\dot{x} = Ax + F_{A_z}\mu_{A_z} + F_{w_g}\mu_{w_g}, \quad (7.77)$$

$$y = Cx + v, \quad (7.78)$$

$$z = H(y - C\hat{x}) \quad (7.79)$$

with the system matrices given by (6.56–6.59).

The first step is to determine the transformation matrix, Γ . This, in turn, comes from the boundary condition of the Goh Riccati equation, (7.43). In this example,

$$\bar{B} = \begin{bmatrix} F_{w_g} & AF_{w_g} \end{bmatrix}.$$

Using an initial weighting of $\Pi_0 = 10 \times I$, we get

$$\begin{aligned} S(t_0^+) &= 10 \times \left[I - \bar{B} \left(\bar{B}^T \bar{B} \right)^{-1} \bar{B}^T \right] \\ &= \begin{bmatrix} 9.9963 & 0.1269 & 0.1452 & 0 & 0 \\ 0.1269 & 5.6732 & -4.9528 & 0 & 0 \\ 0.1452 & -4.9528 & 4.3305 & 0 & 0 \\ 0 & 0 & 0 & 10 & 0 \\ 0 & 0 & 0 & 0 & 0 \end{bmatrix}. \end{aligned}$$

Using eigenvalue decomposition of $S(t_0^+)$, we get the transformation matrix,

$$\Gamma = \begin{bmatrix} -0.0000 & 0.9998 & 0 & 0.0173 & 0.0086 \\ -0.7531 & 0.0127 & 0 & -0.5896 & -0.2917 \\ 0.6579 & 0.0145 & 0 & -0.6749 & -0.3339 \\ 0 & 0 & 1 & 0 & 0 \\ 0 & 0 & 0 & 0.4434 & -0.8963 \end{bmatrix}, \quad (7.80)$$

by using the eigenvectors of $S(t_0^+)$ as the columns of Γ . By applying (7.80) to the F-16XL model (7.77–7.79) and (6.56–6.59), we get a decomposition of the system and a steady-state solution to the reduced-order Goh Riccati equation, (7.60),

$$\bar{S} = \begin{bmatrix} 0.0637 & 0.0341 & 0.8387 \\ 0.0341 & 0.0577 & 0.4814 \\ 0.8387 & 0.4814 & 11.1811 \end{bmatrix}. \quad (7.81)$$

Our choice of weightings is

$$V = \begin{bmatrix} 2 & 0 & 0 & 0 \\ 0 & 2 & 0 & 0 \\ 0 & 0 & 200 & 0 \\ 0 & 0 & 0 & 2 \end{bmatrix}, \quad Q = I.$$

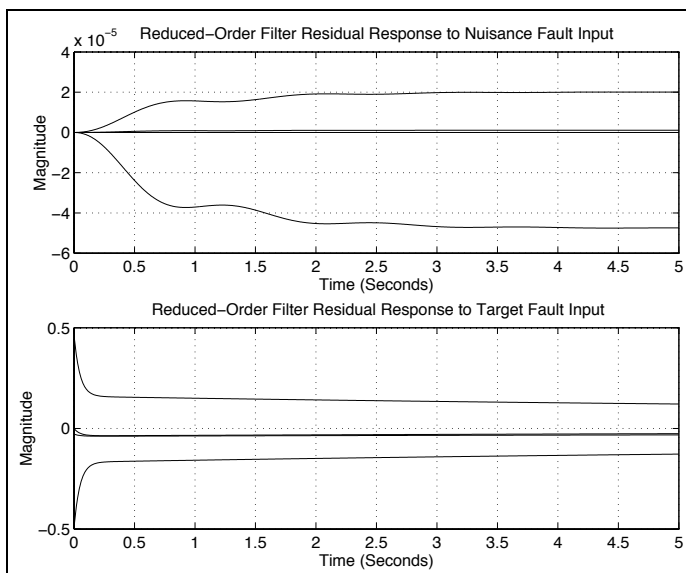


Figure 7.1: Reduced-Order Detection Filter Performance for the F-16XL Example.

Figure 7.1 shows that the resulting reduced-order filter effectively blocks the nuisance fault transmission while preserving the target fault transmission. If one compares the Goh Riccati solution, (7.81), to the game Riccati solution used in Section 6.3.1, (6.62), he will notice that the reduced-order filter does not necessarily lead to a high-gain filter. Looking

back on the discussion on high-gain feedback in Section 6.3.1, this is an important aspect of the reduced-order filter.

A Parameter Robust Game Theoretic Fault Detection Filter

A GAME THEORETIC FAULT DETECTION FILTER which is robust to uncertainty in the plant dynamics is derived and analyzed in this chapter. In Section 8.1, we discuss the various strategies that have been used to robustify detection filters. In Section 8.2, we discuss how fault detection and parameter robustness can act as competing objectives and in Section 8.3 we formulate a new disturbance attenuation problem in which plant parameter variations are modeled as additional disturbances. The parameter robust detection filter falls out from the problem solution. In Section 8.4, we analyze the limiting case properties of the new filter, and in Section 8.5 we work through an example which compares the performance of filters designed with and without an accounting of model uncertainty.

8.1 Parameter Robustness and FDI

A fundamental issue in fault detection and identification is the sensitivity of the given method to plant parameter variations. Detection filters and other analytical redundancy

techniques rely on accurate representations of the systems that they monitor. FDI under modeling error, however, is still an open question.

For unknown input observers, it has been proposed to treat model uncertainty as another disturbance, for example, (Patton and Chen 1992). Using standard design techniques, the uncertainty disturbance is then embedded in the unobservable subspace along with the other inputs in the disturbance set. In general however, it is not always possible to separate the effects of parameter variations from the target fault. Thus, some, (Ding and Frank 1989), have proposed filters which maximize the ratio of the fault transmission to disturbance transmission with model uncertainty, again, thrown into the disturbance set. Still others (Viswanadham and Minto 1988) have considered bounding the effect of model perturbations on the estimation error using stable factorization and \mathcal{H}_∞ optimization.

Beard-Jones detection filters (Douglas 1993, Massoumnia 1986, White and Speyer 1987) are difficult to robustify because of their reliance upon geometric methods. Schemes have been introduced which robustify the detection filter to ill-conditioning in the eigenstructure (Douglas and Speyer 1996) and to exogenous disturbances (Douglas and Speyer 1995); but, to date, no significant progress has been made in handling plant parameter robustness. We should note that it is possible to model plant uncertainty as an additional fault as in (Patton and Chen 1992), but this approach, as shown in Section 8.5, leads to a filter with poor performance if the plant uncertainty is not output separable from the target fault.

Approximate detection filter designs, such as the game theoretic fault detection filter, can be robustified via the method of DeSouza *et al.* Here, plant parameter variations are formulated as an additional element in the disturbance attenuation problem. The resulting filter is still an \mathcal{H}_∞ filter, but one with the added property of parameter robustness. In this chapter, we will apply the methods of (DeSouza et al. 1992) to derive a parameter robust version of the game theoretic filter introduced in Chapter 6.

Remark 16. We must acknowledge the work of Edelmayer *et al.* who derive a pair of robust \mathcal{H}_∞ detection filters in (Edelmayer et al. 1994). Their first approach uses the DeSouza method (as we will do), and their second is a modification of their original filter

which was first presented in (Edelmayer et al. 1996). We contribute further analysis on the filter which arises from the DeSouza construction, including an analysis of its asymptotic properties. We will also show that the two filters proposed by Edelmayer *et al.* are actually variations on the same theme, the second being a simplification of the first. ◀

Remark 17. The benefit of DeSouza’s approach is that it provides an easy and elegant way to incorporate parameter robustness into the design problem. Classic detection filter structures already have the freedom to incorporate features into their designs beyond basic FDI objectives (Douglas 1993, Massoumnia et al. 1989). However, it is not always clear how to make use of this freedom. An analogous situation is the well-known “ Q -parameterization” of \mathcal{H}_∞ or \mathcal{H}_2 solutions (Doyle et al. 1989). Existence of this design freedom is well-known; finding a way to use it is not. See the discussion in (Iwasake and Skelton 1994). ◀

Remark 18. A good survey of the robust FDI problem is given in (Frank 1994). ◀

8.2 Parameter Robustness versus FDI

Suppose that instead of the system described by (6.2), we have one in which there is uncertainty in the plant:

$$\dot{x} = (A + \Delta A)x + Bu + F_1\mu_1 + F_2\mu_2. \quad (8.1)$$

Clearly if we attempt to monitor (8.1) with a fault detection filter designed for the nominal model, A , the error equation ($e \triangleq x - \hat{x}$),

$$\dot{e} = (A + LC)e + \Delta Ax + F_1\mu_1 + F_2\mu_2 + Lv, \quad (8.2)$$

will be biased by the uncertainty term. Equation (8.2), however, suggests that we can deal with modeling uncertainty by simply defining $F_3 \triangleq \Delta A$ and $\mu_3 \triangleq x$. If F_3 is output separable from F_1 , conventional detection filter designs are applicable, since the effect of plant uncertainty is completely decoupled from the target fault input. In general, however, F_1 and F_3 will not be output separable, and non-output separable faults cannot be distinguished by a detection filter (Beard 1971).

Output separability is not a necessary condition, however, for approximate detection filters like the game theoretic fault detection filter (Edelmayer et al. 1996). Thus, we can still design a filter which treats the plant parameter variations as another nuisance fault, though the loss of this property eliminates the only guarantee we have that the target fault will be visible at the output (Proposition 6.1). Our only recourse, therefore, is to proceed with a design and attempt to find the best tradeoff between target fault transmission, nuisance fault attenuation, and plant parameter robustness.

8.3 A Disturbance Attenuation Problem with Parameter Variations

8.3.1 The Modified Disturbance Attenuation Problem

This section repeats the derivation and analysis of Chapter 6 with the additional element of model uncertainty. Start with a system described by (8.1) and measurements given by the additive noise model, (6.1). As before, the disturbance attenuation function is

$$D_{af} = \frac{\int_{t_0}^{t_1} \|HC(x - \hat{x})\|_Q^2 dt}{\int_{t_0}^{t_1} [\|\mu_2\|_{M^{-1}}^2 + \|v\|_{V^{-1}}^2] dt + \|x(t_0) - \hat{x}_0\|_{P_0^{-1}}^2},$$

where M, V, Q , and P_0 are weighting matrices. As in Chapter 6, the disturbance attenuation problem is to find an estimator so that for all adversaries, $\mu_2, v \in L_2[t_1, t_2]$, $x(t_0) \in \mathbb{R}^n$,

$$D_{af} \leq \gamma. \quad (8.3)$$

We solve (8.3) by converting it into a differential game,

$$\min_{\hat{x}} \max_v \max_{\mu_2} \max_{x(t_0)} J' \leq 0,$$

$$J' = \int_{t_0}^{t_1} \left[\|HC(x - \hat{x})\|_Q^2 - \gamma(\|\mu_2\|_{M^{-1}}^2 + \|v\|_{V^{-1}}^2) \right] dt - \|x(t_0) - \hat{x}_0\|_{\Pi_0}^2,$$

subject to (8.1). $\Pi_0 \triangleq \gamma P_0^{-1}$. Following DeSouza, we assume that the plant uncertainty, ΔA , can be decomposed as

$$\Delta A = F_3 \Lambda G. \quad (8.4)$$

F_3 and G are known matrices of dimension, $n \times r$ and $r \times n$, respectively. Λ is an $r \times r$ matrix whose elements are unknown $L_2[t_0, t_1]$ functions. Defining

$$\mu_3 \triangleq \Lambda Gx,$$

we get a new dynamical equation,

$$\dot{x} = Ax + Bu + F_1\mu_1 + F_2\mu_2 + F_3\mu_3. \quad (8.5)$$

Additionally, we will augment the output, z ,

$$z = \left\{ \begin{array}{c} HC(x - \hat{x}) \\ \sqrt{\epsilon}Gx \end{array} \right\},$$

so that the disturbance attenuation function is now

$$D_{af}^* = \frac{\int_{t_0}^{t_1} [\|HC(x - \hat{x})\|_Q^2 + \epsilon\|Gx\|^2] dt}{\int_{t_1}^{t_2} [\|\mu_2\|_{M^{-1}}^2 + \|\mu_3\|_{N^{-1}}^2 + \|v\|_{V^{-1}}^2] dt + \|x(t_0) - \hat{x}_0\|_{P_0^{-1}}^2}. \quad (8.6)$$

To solve the disturbance attenuation problem, we convert (8.6) into the cost function,

$$J = \int_{t_0}^{t_1} \left[\|HC(x - \hat{x})\|_Q^2 + \epsilon\|Gx\|^2 - \gamma(\|\mu_2\|_{M^{-1}}^2 + \|\mu_3\|_{N^{-1}}^2 + \|v\|_{V^{-1}}^2) \right] dt - \|x(t_0) - \hat{x}_0\|_{\Pi_0}^2,$$

where $\Pi_0 \triangleq \gamma P_0^{-1}$, and solve the differential game,

$$\min_{\hat{x}} \max_v \max_{\mu_2} \max_{\mu_3} \max_{x(t_0)} J \leq 0,$$

subject to

$$\dot{x} = Ax + F_2\mu_2 + F_3\mu_3. \quad (8.7)$$

Note that we have eliminated a pair of elements from Equation (8.5). As in Chapter 6, μ_1 is taken to be zero in the the derivation of the solution, since it is the target fault and

should not be attenuated. We also take u to be zero for convenience. When the plant model is perfectly known, it is possible to simply subtract out known signals such as u to nullify their effects. However, in the case of model uncertainty, such signals can have a significant impact upon filter performance (DeSouza et al. 1992). The inclusion of the control input is an obvious extension of the work that we present here.

The following proposition, modified from (DeSouza et al. 1992), shows that the solution to the new game also solves the original game under a mild restriction:

Proposition 8.1. If Λ is such that $\|\Lambda\|_\infty \leq \frac{1}{\sqrt{\gamma} \|N^{-\frac{1}{2}}\|_\infty}$, then for any $\epsilon > 0$,

$$\max_v \max_{\mu_2} \max_{\mu_3} \max_{x(t_0)} J' \leq \max_v \max_{\mu_2} \max_{\mu_3} \max_{x(t_0)} J.$$

Proof. If one simply compares the terms in J' and J , he would find that:

$$J = J' + \epsilon \left[\|Gx\|^2 - \gamma \|\Lambda Gx\|_{N^{-1}}^2 \right]$$

Now,

$$\begin{aligned} \gamma \|\Lambda Gx\|_{N^{-1}}^2 &= \gamma \|N^{-\frac{1}{2}} \Lambda Gx\|^2 \\ &\leq \gamma \|N^{-\frac{1}{2}} \Lambda\|_\infty^2 \|Gx\|^2 \\ &\leq \gamma \|N^{-\frac{1}{2}}\|_\infty^2 \|\Lambda\|_\infty^2 \|Gx\|^2. \end{aligned}$$

Thus, $\|\Lambda\|_\infty \leq \frac{1}{\sqrt{\gamma} \|N^{-\frac{1}{2}}\|_\infty}$ implies the proposition. ◀

As in Chapter 6, rewrite the sensor noise term, $\|v\|_{V^{-1}}^2$, as the equivalent $\|y - Cx\|_{V^{-1}}^2$:

$$\begin{aligned} J = \int_{t_0}^{t_1} \left[\|HC(x - \hat{x})\|_Q^2 + \epsilon \|Gx\|^2 - \gamma (\|\mu_2\|_{M^{-1}}^2 + \|\mu_3\|_{N^{-1}}^2 \right. \\ \left. + \|y - Cx\|_{V^{-1}}^2) \right] dt - \|x(t_0) - \hat{x}_0\|_{\Pi_0}^2, \quad (8.8) \end{aligned}$$

so that the game becomes

$$\min_{\hat{x}} \max_y \max_{\mu_2} \max_{\mu_3} \max_{x(t_0)} J \leq 0.$$

The differential game solution comes in two steps, beginning with

$$\max_{\mu_2} \max_{\mu_3} \max_{x(t_0)} J \leq 0.$$

We start by appending the system dynamics, (8.7), to the cost function, (8.8), through a Lagrange multiplier, λ^T ,

$$J = \int_{t_0}^{t_1} \left[\|HC(x - \hat{x})\|_Q^2 + \epsilon \|Gx\|^2 - \gamma (\|\mu_2\|_{M^{-1}}^2 + \|\mu_3\|_{N^{-1}}^2 + \|y - Cx\|_{V^{-1}}^2) \right. \\ \left. + \lambda^T (Ax + F_2\mu_2 + F_3\mu_3 - \dot{x}) \right] dt - \|x(t_0) - \hat{x}_0\|_{\Pi_0}^2,$$

and then integrate $\lambda^T \dot{x}$ by parts:

$$J = \int_{t_0}^{t_1} \left[\|HC(x - \hat{x})\|_Q^2 + \epsilon \|Gx\|^2 \right. \\ \left. - \gamma (\|\mu_2\|_{M^{-1}}^2 + \|\mu_3\|_{N^{-1}}^2 + \|y - Cx\|_{V^{-1}}^2) \right. \\ \left. + \lambda^T (Ax + F_2\mu_2 + F_3\mu_3) + \dot{\lambda}^T x \right] dt \\ - \|x(t_0) - \hat{x}_0\|_{\Pi_0}^2 + \lambda(t_0)^T x(t_0) - \lambda(t_1)^T x(t_1). \quad (8.9)$$

Taking the first variation of (8.9) with respect to μ_2, μ_3 and $x(t_0)$, then gives us

$$\mu_2^* = \frac{1}{\gamma} M F_2^T \lambda, \quad (8.10)$$

$$\mu_3^* = \frac{1}{\gamma} N F_3^T \lambda, \quad (8.11)$$

$$-\dot{\lambda} = A^T \lambda + \epsilon G^T Gx + C^T H Q H C (x - \hat{x}) + \gamma C^T V^{-1} (y - Cx), \quad (8.12)$$

$$\lambda(t_1) = 0, \quad (8.13)$$

$$\lambda(t_0) = \Pi_0 [x(t_0)^* - \hat{x}_0] \quad (8.14)$$

as the first-order necessary conditions for the maximization of J . The asterisk is indicative of the extremizing value of the variable. Substituting (8.10) and (8.11) into our dynamics, (8.7), and combining the result with (8.12), gives us a two point boundary value problem,

$$\begin{aligned} \begin{Bmatrix} \dot{x} \\ \dot{\lambda} \end{Bmatrix} = & \begin{bmatrix} A & \frac{1}{\gamma}(F_2MF_2^T + F_3NF_3^T) \\ -C^T(HQH - \gamma V^{-1})C - \epsilon G^TG & -A^T \end{bmatrix} \begin{Bmatrix} x \\ \lambda \end{Bmatrix} \\ & + \begin{Bmatrix} 0 \\ C^T H Q H C \hat{x} - \gamma C^T V^{-1} y \end{Bmatrix}, \end{aligned} \quad (8.15)$$

with initial conditions,

$$x^*(t_0) = \hat{x}_0 + \Pi_0^{-1}\lambda(t_0), \quad (8.16)$$

$$\lambda^*(t_1) = 0.$$

Following Chapter 6, we will assume solutions, x^* and λ^* , to (8.15) such that

$$\lambda^* = \Pi(x^* - x_p). \quad (8.17)$$

If we take

$$\Pi(t_0) = \Pi_0, \quad (8.18)$$

$$x_p(t_0) = \hat{x}_0, \quad (8.19)$$

then (8.17) is in agreement with the boundary condition for λ , (8.14), at the initial time, t_0 . In Chapter 6 we found that, in the absence of model uncertainty, x_p is equivalent to the optimal state estimate. With model uncertainty, however, x_p will act like the state variable in the second half of the game solution.

As we did in Chapter 6, we can substitute our assumed solution, (8.17), into the TPBVP, (8.15), and manipulate the equations to find that the TPBVP is solved identically if

$$\begin{aligned} -\dot{\Pi} = & A^T\Pi + \Pi A + \frac{1}{\gamma}\Pi(F_2MF_2^T + F_3NF_3^T)\Pi \\ & + C^T(HQH - \gamma V^{-1})C + \epsilon G^TG \end{aligned} \quad (8.20)$$

and

$$\Pi \dot{x}_p = \Pi A x_p + \epsilon G^T G x_p - C^T H Q H C (\hat{x} - x_p) + \gamma C^T V^{-1} (y - C x_p). \quad (8.21)$$

Equation (8.20) is an estimator Riccati equation and its boundary condition is given by (8.18). The boundary condition for (8.21) is given by (8.19). We will often need the inverse of Π in derivations and applications. Thus, we can alternatively propagate

$$\begin{aligned} \dot{\Pi}^{-1} = \Pi \Pi^{-1} + \Pi^{-1} A^T + \Pi^{-1} C^T (H Q H - \gamma V^{-1}) C \Pi^{-1} \\ + \epsilon \Pi^{-1} G^T G \Pi^{-1} + \frac{1}{\gamma} (F_2 M F_2^T + F_3 N F_3^T). \end{aligned} \quad (8.22)$$

The second half of our solution begins by substituting the game optimal values of μ_2 , μ_3 , and $x(t_0)$, (8.10,8.11,8.16), into the cost function, (8.8). The new cost, \bar{J} , is then

$$\begin{aligned} \bar{J} = \int_{t_0}^{t_1} \left[\|x - \hat{x}\|_{C^T H Q H C}^2 + \epsilon \|Gx\|^2 - \|\lambda\|_{\frac{1}{\gamma}(F_2 M F_2^T + F_3 N F_3^T)}^2 \right. \\ \left. - \gamma \|y - Cx\|_{V^{-1}}^2 \right] dt - \|\lambda(t_0)\|_{\Pi_0^{-1}}^2. \end{aligned} \quad (8.23)$$

Add the identically zero term,

$$0 = \|\lambda(t_0)\|_{\Pi(t_0)^{-1}}^2 - \|\lambda(t_1)\|_{\Pi(t_1)^{-1}}^2 + \int_{t_0}^{t_1} \frac{d}{dt} \|\lambda(t)\|_{\Pi^{-1}}^2 dt,$$

to (8.23) and use the inverse Riccati equation, (8.22), the boundary condition for Π at t_0 , (8.18), and the boundary condition for λ at t_1 , (8.13), to get

$$\begin{aligned} \bar{J} = \int_{t_0}^{t_1} \left[\|x - \hat{x}\|_{C^T H Q H C}^2 + \epsilon \|Gx\|^2 - \gamma \|y - Cx\|_{V^{-1}}^2 \right. \\ - (x - \hat{x})^T C^T H Q H C \Pi^{-1} \lambda - \lambda^T \Pi^{-1} C^T H Q H C (x - \hat{x}) - \epsilon \lambda^T \Pi^{-1} G^T G x \\ - \epsilon x^T G^T G \Pi^{-1} \lambda + (y - Cx)^T V^{-1} C \Pi^{-1} \lambda + \lambda^T \Pi^{-1} C^T V^{-1} (y - Cx) \\ \left. + \epsilon \lambda^T \Pi^{-1} G^T G \Pi^{-1} \lambda + \lambda^T \Pi^{-1} C^T (H Q H - \gamma V^{-1}) C \Pi^{-1} \lambda \right] dt. \end{aligned} \quad (8.24)$$

We can group all the terms in (8.24) into three quadratics,

$$\bar{J} = \int_{t_0}^{t_1} \left[\|(x - \hat{x}) - \Pi^{-1}\lambda\|_{C^T H Q H C}^2 + \epsilon \|x - \Pi^{-1}\lambda\|_{G^T G}^2 - \gamma \|(y - Cx) + C\Pi^{-1}\lambda\|_{V^{-1}}^2 \right] dt, \quad (8.25)$$

and then use the solution, (8.17), to replace λ in (8.25). This leaves us with

$$\bar{J} = \int_{t_0}^{t_1} \left[\|x_p - \hat{x}\|_{C^T H Q H C}^2 + \epsilon \|x_p\|_{G^T G}^2 - \gamma \|y - Cx_p\|_{V^{-1}}^2 \right] dt. \quad (8.26)$$

The game is now

$$\min_{\hat{x}} \max_y \bar{J} \leq 0,$$

subject to (8.21). As in the first subproblem, we find the solution to this game by appending the dynamics, (8.21), to the cost, (8.26), through a Lagrange multiplier, ρ^T :

$$\begin{aligned} \bar{J} = \int_{t_0}^{t_1} \left\{ \|x_p - \hat{x}\|_{C^T H Q H C}^2 + \epsilon \|x_p\|_{G^T G}^2 - \gamma \|y - Cx_p\|_{V^{-1}}^2 \right. \\ \left. + \rho^T \left[Ax_p + \epsilon \Pi^{-1} G^T G x_p - \Pi^{-1} C^T H Q H C (\hat{x} - x_p) \right. \right. \\ \left. \left. + \gamma \Pi^{-1} C^T V^{-1} (y - Cx_p) - \dot{x}_p \right] \right\} dt. \quad (8.27) \end{aligned}$$

After integrating $\rho^T \dot{x}_p$ by parts, we get

$$\begin{aligned} \delta \bar{J} = \int_{t_0}^{t_1} \left\{ \left[(x_p - \hat{x})^T C^T H Q H C + \epsilon x_p^T G^T G + \gamma (y - Cx_p)^T V^{-1} C + \rho^T A \right. \right. \\ \left. \left. + \epsilon \rho^T \Pi^{-1} G^T G + \rho^T \Pi^{-1} C^T H Q H C - \gamma \rho^T \Pi^{-1} C^T V^{-1} C + \dot{\rho}^T \right] \delta x_p \right. \\ \left. + \left[-(x_p - \hat{x})^T C^T H Q H C - \rho^T \Pi^{-1} C^T H Q H C \right] \delta \hat{x} + \left[-\gamma (y - Cx_p)^T V^{-1} \right. \right. \\ \left. \left. + \gamma \rho^T \Pi^{-1} C^T V^{-1} \right] \delta y \right\} dt + \rho^T(t_0) \delta x_p(t_0) - \rho^T(t_1) \delta x_p(t_1) \quad (8.28) \end{aligned}$$

by taking the variation of (8.27) with respect to y and \hat{x} . Note that $\delta x_p(t_0) = 0$, because x_p is fixed at t_0 by the boundary condition, (8.19). From (8.28), the first order necessary conditions to extremize (8.26) with respect to \hat{x} and y are

$$\hat{x}^* = x_p + \Pi^{-1}\rho \quad \text{mod Ker } HC, \quad (8.29)$$

$$y^* = C(x_p + \Pi^{-1}\rho), \quad (8.30)$$

$$\begin{aligned} \dot{\rho} = & \left[-(A + \epsilon\Pi^{-1}G^TG)^T - C^T(HQH - \gamma V^{-1})C\Pi^{-1} \right] \rho \\ & - C^T H Q H C (x_p - \hat{x}) - \gamma C^T V^{-1} (y - Cx_p) - \epsilon G^T G x_p, \end{aligned} \quad (8.31)$$

$$\rho(t_1) = 0. \quad (8.32)$$

If we substitute (8.29) and (8.30)¹ into (8.21) and (8.31), we get

$$\dot{x}_p = (A + \epsilon\Pi^{-1}G^TG)x_p - \Pi^{-1}C^T(HQH - \gamma V^{-1})C\Pi^{-1}\rho, \quad (8.33)$$

$$\dot{\rho} = -(A + \epsilon\Pi^{-1}G^TG)^T \rho - \epsilon G^T G x_p, \quad (8.34)$$

which is a homogeneous two-point boundary value problem in x_p and ρ with boundary conditions, (8.19) and (8.32). Using the sweep method, we take

$$\rho = Sx_p \quad (8.35)$$

and substitute (8.35) into (8.29) to get

$$\hat{x}^* = (I + \Pi^{-1}S)x_p \quad (8.36)$$

as the optimal estimate. The vector, x_p , is propagated by

$$\dot{x}_p = (A + \epsilon\Pi^{-1}G^TG - \Pi^{-1}C^T H Q H C \Pi^{-1}S)x_p + \gamma \Pi^{-1}C^T V^{-1}(y - Cx_p), \quad (8.37)$$

¹We can ignore any differences between \hat{x} and x_p that lie in $\ker HC$ since these differences will not show up at our controlled output, z .

which is the result of substituting (8.36) into (8.21). S is found by propagating

$$\begin{aligned} -\dot{S} &= (A + \epsilon\Pi^{-1}G^TG)^TS + S(A + \epsilon\Pi^{-1}G^TG) \\ &\quad - S\Pi^{-1}C^T(HQH - \gamma V^{-1})C\Pi^{-1}S + \epsilon G^TG \end{aligned} \quad (8.38)$$

from the terminal condition,

$$S(t_1) = 0. \quad (8.39)$$

Equation (8.38) is found by differentiating (8.35) and using (8.33) and (8.34) where needed. Equation (8.39) is determined from (8.32) and (8.35).

Remark 19. If we take $\epsilon = 0$, S will be identically zero since (8.38) will be an unforced differential equation with zero as its boundary condition. Thus, from (8.36), $\hat{x} = x_p$, and the robust game theoretic fault detection filter simplifies to

$$\begin{aligned} \dot{\hat{x}} &= A\hat{x} + \gamma\Pi^{-1}C^TV^{-1}(y - C\hat{x}), \\ -\dot{\Pi} &= A^T\Pi + \Pi A + \frac{1}{\gamma}\Pi(F_2MF_2^T + F_3NF_3^T)\Pi + C^T(HQH - \gamma V^{-1})C, \\ \Pi(t_0) &= \Pi_0. \end{aligned}$$

This is identical to the results of Chapter 6, except that we still have the map, F_3 , which corresponds to plant uncertainty. Thus, the filter is still robustified, though in a much simpler way. As it turns out, this is Edelmayer's alternative approach robustifying the approximate detection filter (see Remark 8.1 and (Edelmayer et al. 1994)). Our results, however, show that this "alternative" is just DeSouza's method with $\epsilon = 0$. \blacktriangleleft

8.3.2 Equivalence to the \mathcal{H}_∞ Measurement Feedback Control Problem

The robust game theoretic fault detection filter requires the solutions to two differential Riccati equations: one that is integrated forward in time, (8.20), and one that is integrated backwards in time, (8.38). This is strikingly similar to the "two Riccati" solution to the

\mathcal{H}_∞ measurement feedback problem given in (Doyle et al. 1989, Green and Limebeer 1995, Rhee and Speyer 1991). We will now show that the robust approximate detection filter problem and the \mathcal{H}_∞ measurement feedback control problem are one in the same problem.

We begin by making the following definitions:

$$\begin{aligned} \check{x} &\triangleq x_p, & \check{Q} &\triangleq \epsilon G^T G, & \check{A} &\triangleq A + \epsilon \Pi^{-1} G^T G, \\ u &\triangleq x_p - \hat{x}, & R &\triangleq C^T H Q H C, & B &\triangleq \Pi^{-1} C^T H Q H C, \\ w &\triangleq y - C x_p, & W &\triangleq \gamma V^{-1}, & \Gamma &\triangleq \gamma \Pi^{-1} C^T V^{-1}. \end{aligned}$$

Assume for argument's sake that $R = C^T H Q H C$ is invertible. Substituting these definitions into the cost function for the second half of the game, (8.26), gives us

$$\check{J} = \int_{t_0}^{t_1} \left[\|\check{x}\|_{\check{Q}}^2 + \|u\|_R^2 - \|w\|_W \right] dt.$$

If we also make these substitutions into the differential equation for x_p , (8.37), we then get

$$\dot{\check{x}} = \check{A}\check{x} + Bu + \Gamma w. \quad (8.40)$$

Our game is now given by the following which is subject to (8.40):

$$\min_u \max_w \check{J} \leq 0,$$

This is the classic, linear quadratic differential game. If we apply our definitions to the well-known feedback solution for the game (Başar and Bernhard 1995, Mageirou 1976),

$$u = -R^{-1} B^T S x, \quad (8.41)$$

$$-\dot{S} = \check{A}^T S + S \check{A} - S(BR^{-1}B^T - \Gamma^T W^{-1}\Gamma)S + Q, \quad (8.42)$$

we find that we recover the differential game solutions of Section 8.3. That is, from (8.41), we get the optimal state estimate, (8.36):

$$\begin{aligned} u &= -R^{-1} B^T S \check{x} \\ \implies x_p - \hat{x} &= -(C^T H Q H C)^{-1} (C^T H Q H C) \Pi^{-1} S x_p \\ \implies \hat{x} &= (I + \Pi^{-1} S) x_p, \end{aligned}$$

and from (8.42) we get the our second Riccati equation, (8.38):

$$\begin{aligned}
-\dot{S} &= \check{A}^T S + S \check{A} - S(BR^{-1}B^T - \Gamma W^{-1}\Gamma^T)S + Q \\
\implies -\dot{S} &= (A + \epsilon\Pi^{-1}G^T G)^T S + S(A + \epsilon\Pi^{-1}G^T G) \\
&\quad - S\left[\Pi^{-1}C^T H Q H C (C^T H Q H C)^{-1} C^T H Q H C \Pi^{-1} \right. \\
&\quad \left. - (\gamma\Pi^{-1}C^T V^{-1})(\gamma^{-1}V)(\gamma V^{-1}C\Pi^{-1})\right] S + \epsilon G^T G \\
\implies -\dot{S} &= (A + \epsilon\Pi^{-1}G^T G)^T S + S(A + \epsilon\Pi^{-1}G^T G) \\
&\quad - S\Pi^{-1}C^T (H Q H - \gamma V^{-1})C\Pi^{-1} S + \epsilon G^T G.
\end{aligned}$$

Thus, if we think of the first half of the differential game as giving us an estimator, the equivalence between the second-half and the classic linear quadratic game implies that the entire game is equivalent to \mathcal{H}_∞ measurement feedback problem.

Remark 20. The results presented here imply that the results derived by DeSouza (DeSouza et al. 1992) are also equivalent to a variation of the \mathcal{H}_∞ measurement feedback problem. This equivalence, to our knowledge, has not been recognized previously. \blacklozenge

8.4 The Robust Game Theoretic Fault Detection Filter in the Limit

In Chapter 7, it was shown that in the limit, $\gamma \rightarrow 0$, the game theoretic fault detection filter becomes an unknown input observer in that it obtains the same invariant subspace structure. In this section, we will examine whether the parameter robust filter derived in the previous section also possesses this limiting property. As in Chapter 7, we will begin by trying to find the conditions which guarantee that the game cost will be nonpositive. These fall out after we manipulate the cost function to look like a single quadratic,

$$J(\hat{x}, x(t_0), \mu_2, \mu_3, v) = \int_{t_0}^{t_1} \xi^T W \xi dt.$$

A nonpositive definite W ensures a nonpositive cost which ensures an attenuating solution.

We begin with the cost function as given by (8.8),

$$J = \int_{t_0}^{t_1} \left[\|x - \hat{x}\|_{C^T H Q H C}^2 + \|x\|_{\epsilon G^T G}^2 - \gamma \|\mu_2\|_{M^{-1}}^2 - \gamma \|\mu_3\|_{N^{-1}}^2 - \gamma \|y - Cx\|_{V^{-1}}^2 \right] dt - \|x(t_0) - \hat{x}_0\|_{\Pi_0}^2. \quad (8.43)$$

Appending the dynamic equations for x , (8.7), and x_p , (8.21), to game cost, (8.43), through the Lagrange multipliers, $(x - \hat{x})^T \Pi$ and $x_p^T S$, we get

$$J = \int_{t_0}^{t_1} \left\{ \|x - \hat{x}\|_{C^T H Q H C}^2 + \|x\|_{\epsilon G^T G}^2 - \gamma \|\mu_2\|_{M^{-1}}^2 - \gamma \|\mu_3\|_{N^{-1}}^2 - \gamma \|y - Cx\|_{V^{-1}}^2 + (x - \hat{x})^T \Pi \left[Ax + F_2 \mu_2 + F_3 \mu_3 - \dot{x} \right] + x_p^T S \left[Ax_p + \epsilon \Pi^{-1} G^T G x_p - \Pi^{-1} C^T H Q H C (\hat{x} - x_p) + \gamma \Pi^{-1} C^T V^{-1} (y - Cx_p) - \dot{x}_p \right] \right\} dt - \|x(t_0) - \hat{x}_0\|_{\Pi_0}^2. \quad (8.44)$$

Now expand some of the quadratic terms in (8.44) to introduce x_p into the cost:

$$\begin{aligned} \|x - \hat{x}\|_{C^T H Q H C}^2 &\longrightarrow \|(x - x_p) - (\hat{x} - x_p)\|_{C^T H Q H C}^2 \\ \|x\|_{\epsilon G^T G}^2 &\longrightarrow \|(x - x_p) + x_p\|_{\epsilon G^T G}^2 \\ \|y - Cx\|_{V^{-1}}^2 &\longrightarrow \|(y - Cx_p) - C(x - x_p)\|_{V^{-1}}^2. \end{aligned}$$

After we introduce these expansions into (8.44) and collect terms, we get

$$\begin{aligned} J = \int_{t_0}^{t_1} \left\{ \|x - x_p\|_{C^T (H Q H - \gamma V^{-1}) C + \epsilon G^T G}^2 + \|x_p\|_{S(A + \epsilon \Pi^{-1} G^T G) + \epsilon G^T G}^2 \right. \\ + \|\hat{x} - x_p\|_{C^T H Q H C}^2 - \gamma \|\mu_2\|_{M^{-1}}^2 - \gamma \|\mu_3\|_{N^{-1}}^2 - \gamma \|y - Cx_p\|_{V^{-1}}^2 \\ + (x - x_p)^T \left[-C^T H Q H C (\hat{x} - x_p) + \epsilon G^T G x_p + \gamma C^T V^{-1} (y - Cx_p) \right] \\ + \left[-C^T H Q H C (\hat{x} - x_p) + \epsilon G^T G x_p + \gamma C^T V^{-1} (y - Cx_p) \right]^T (x - x_p) \\ + x_p^T S \left[\Pi^{-1} C^T H Q H C (\hat{x} - x_p) + \gamma \Pi^{-1} C^T V^{-1} (y - Cx_p) - \dot{x}_p \right] \\ \left. + (x - x_p)^T \Pi \left[Ax + F_2 \mu_2 + F_3 \mu_3 - \dot{x} \right] \right\} dt - \|x(t_0) - \hat{x}_0\|_{\Pi_0}^2. \end{aligned}$$

Add and subtract $(x - x_p)^T \Pi A x_p$ and $(x - x_p)^T \Pi \dot{x}_p$ to the above and collect terms to get

$$\begin{aligned}
J = & \int_{t_0}^{t_1} \left\{ \|x - x_p\|_{\Pi A + C^T(HQH - \gamma V^{-1})C + \epsilon G^T G}^2 + \|x_p\|_{S(A + \epsilon \Pi^{-1} G^T G) + \epsilon G^T G}^2 \right. \\
& + \|\hat{x} - x_p\|_{C^T H Q H C}^2 - \gamma \|\mu_2\|_{M^{-1}}^2 - \gamma \|\mu_3\|_{N^{-1}}^2 - \gamma \|y - C x_p\|_{V^{-1}}^2 \\
& + (x - x_p)^T \left[-\Pi \dot{x}_p + \Pi A x_p - C^T H Q H C (\hat{x} - x_p) + \epsilon G^T G x_p + \gamma C^T V^{-1} (y - C x_p) \right] \\
& + \left[-C^T H Q H C (\hat{x} - x_p) + \epsilon G^T G x_p + \gamma C^T V^{-1} (y - C x_p) \right]^T (x - x_p) \\
& + x_p^T S \left[\Pi^{-1} C^T H Q H C (\hat{x} - x_p) + \gamma \Pi^{-1} C^T V^{-1} (y - C x_p) - \dot{x}_p \right] \\
& \left. + (x - \hat{x})^T \Pi (F_2 \mu_2 + F_3 \mu_3) - (x - x_p)^T \Pi (\dot{x} - \dot{x}_p) \right\} dt - \|x(t_0) - \hat{x}_0\|_{\Pi_0}^2. \quad (8.45)
\end{aligned}$$

The third line of (8.45) can be eliminated by using (8.21), which comes from the first half of the game solution derived in Section 8.3. We now integrate the terms, $(x - x_p)^T \Pi (\dot{x} - \dot{x}_p)$ and $x_p^T S \dot{x}_p$, in (8.45) by parts so that the cost now becomes

$$\begin{aligned}
J = & \int_{t_0}^{t_1} \left\{ \|x - x_p\|_{\Pi + \Pi A + C^T(HQH - \gamma V^{-1})C + \epsilon G^T G}^2 + \|\hat{x} - x_p\|_{C^T H Q H C} \right. \\
& + \left[-\Pi \dot{x}_p - C^T H Q H C (\hat{x} - x_p) + \epsilon G^T G x_p + \gamma C^T V^{-1} (y - C x_p) \right]^T (x - x_p) \\
& + (x - x_p)^T \Pi (F_2 \mu_2 + F_3 \mu_3) + \dot{x}^T \Pi (x - x_p) + \dot{x}_p^T S x_p - \gamma \|y - C x_p\|_{V^{-1}}^2 \\
& + x_p^T S \left[\Pi^{-1} C^T H Q H C (\hat{x} - x_p) + \gamma \Pi^{-1} C^T V^{-1} (y - C x_p) \right] - \gamma \|\mu_2\|_{M^{-1}}^2 \\
& \left. - \gamma \|\mu_3\|_{N^{-1}}^2 + \|x_p\|_{S + S(A + \epsilon \Pi^{-1} G^T G) + \epsilon G^T G}^2 \right\} dt + \|x_p(t_0)\|_{S(t_0)}^2 - \|x_p(t_1)\|_{S(t_1)}^2 \\
& - \|x(t_0) - \hat{x}_0\|_{\Pi_0}^2 + \|x(t_0) - x_p(t_0)\|_{\Pi(t_0)}^2 - \|x(t_1) - x_p(t_1)\|_{\Pi(t_1)}^2. \quad (8.46)
\end{aligned}$$

The first two terms on the last line of (8.46) can be combined by using the boundary condition for x_p at t_0 , (8.19). Moreover, if we insert the state equation for x , (8.7), and x_p , (8.21), into the third line of (8.46), we get

$$\begin{aligned}
J = & \int_{t_0}^{t_1} \left\{ \|x - x_p\|_{\Pi + \Pi A + C^T(HQH - \gamma V^{-1})C + \epsilon G^T G}^2 + \|\hat{x} - x_p\|_{C^T H Q H C}^2 \right. \\
& + \left[-\Pi \dot{x}_p - C^T H Q H C(\hat{x} - x_p) + \epsilon G^T G x_p + \gamma C^T V^{-1}(y - C x_p) \right]^T (x - x_p) \\
& - \gamma \|\mu_2\|_{M^{-1}}^2 - \gamma \|\mu_3\|_{N^{-1}}^2 + \|x_p\|_{\dot{S} + S(A + \epsilon \Pi^{-1} G^T G) + (A + \epsilon \Pi^{-1} G^T G)^T S + \epsilon G^T G}^2 \\
& + (x - x_p)^T \Pi (F_2 \mu_2 + F_3 \mu_3) + (A x + F_2 \mu_2 + F_3 \mu_3)^T \Pi (x - x_p) - \gamma \|y - C x_p\|_{V^{-1}}^2 \\
& + \left[-\Pi^{-1} C^T H Q H C(\hat{x} - x_p) + \gamma \Pi^{-1} C^T V^{-1}(y - C x_p) \right]^T S x_p \\
& + x_p^T S \left[-\Pi^{-1} C^T H Q H C(\hat{x} - x_p) + \gamma \Pi^{-1} C^T V^{-1}(y - C x_p) \right] \left. \right\} dt \\
& + \|x_p(t_0)\|_{\dot{S}(t_0)}^2 - \|x(t_0) - \hat{x}_0\|_{\Pi_0 - \Pi(t_0)}^2 - \|x_p(t_1)\|_{\dot{S}(t_1)}^2 - \|x(t_1) - x_p(t_1)\|_{\Pi(t_1)}^2.
\end{aligned}$$

Now, add and subtract $x_p^T A^T \Pi (x - x_p)$ to the above and collect terms so that we end up with

$$\begin{aligned}
J = & \int_{t_0}^{t_1} \left\{ \|x - x_p\|_{\Pi + \Pi A + A^T \Pi + C^T(HQH - \gamma V^{-1})C + \epsilon G^T G}^2 + \|\hat{x} - x_p\|_{C^T H Q H C}^2 \right. \\
& + \left[-\Pi \dot{x}_p + \Pi A x_p - C^T H Q H C(\hat{x} - x_p) + \epsilon G^T G x_p + \gamma C^T V^{-1}(y - C x_p) \right]^T (x - x_p) \\
& + \|x_p\|_{\dot{S} + S(A + \epsilon \Pi^{-1} G^T G) + (A + \epsilon \Pi^{-1} G^T G)^T S + \epsilon G^T G}^2 - \gamma \|\mu_2\|_{M^{-1}}^2 - \gamma \|\mu_3\|_{N^{-1}}^2 \\
& + (x - x_p)^T \Pi (F_2 \mu_2 + F_3 \mu_3) + (F_2 \mu_2 + F_3 \mu_3)^T \Pi (x - x_p) - \gamma \|y - C x_p\|_{V^{-1}}^2 \\
& + \left[-\Pi^{-1} C^T H Q H C(\hat{x} - x_p) + \gamma \Pi^{-1} C^T V^{-1}(y - C x_p) \right]^T S x_p \\
& + x_p^T S \left[-\Pi^{-1} C^T H Q H C(\hat{x} - x_p) + \gamma \Pi^{-1} C^T V^{-1}(y - C x_p) \right] \left. \right\} dt \\
& + \|x_p(t_0)\|_{\dot{S}(t_0)}^2 - \|x(t_0) - \hat{x}_0\|_{\Pi_0 - \Pi(t_0)}^2 - \|x_p(t_1)\|_{\dot{S}(t_1)}^2 - \|x(t_1) - x_p(t_1)\|_{\Pi(t_1)}^2. \quad (8.47)
\end{aligned}$$

Using (8.21), we can eliminate the second line of (8.47). The remainder can then be compactly written as

$$\begin{aligned}
J = & \int_{t_0}^{t_1} \xi^T W \xi dt + \|x_p(t_0)\|_{\dot{S}(t_0)}^2 - \|x(t_0) - \hat{x}_0\|_{\Pi_0 - \Pi(t_0)}^2 \\
& - \|x_p(t_1)\|_{\dot{S}(t_1)}^2 - \|x(t_1) - x_p(t_1)\|_{\Pi(t_1)}^2,
\end{aligned}$$

where

$$\xi = \begin{Bmatrix} (x - x_p) \\ \mu_2 \\ \mu_3 \\ x_p \\ (\hat{x} - x_p) \\ (y - Cx_p) \end{Bmatrix}.$$

The matrix, W , has the form,

$$W = \begin{bmatrix} W_1(\Pi) & 0 \\ 0 & W_2(S) \end{bmatrix},$$

in which

$$W_1(\Pi) \triangleq \begin{bmatrix} L_1(\Pi) & \Pi F_2 & \Pi F_3 \\ F_2^T \Pi & -\gamma M^{-1} & 0 \\ F_3^T \Pi & 0 & -\gamma N^{-1} \end{bmatrix}, \quad (8.48)$$

$$L_1(\Pi) \triangleq \dot{\Pi} + A^T \Pi + \Pi A + C^T (H Q H - \gamma V^{-1}) C + \epsilon G^T G$$

and

$$W_2(S) \triangleq \begin{bmatrix} L_2(S) & -S \Pi^{-1} C^T H Q H C & \gamma S \Pi^{-1} C^T V^{-1} \\ -C^T H Q H C \Pi^{-1} S & C^T H Q H C & 0 \\ \gamma V^{-1} C \Pi^{-1} S & 0 & -\gamma V^{-1} \end{bmatrix},$$

$$L_2(S) \triangleq \dot{S} + (A + \epsilon \Pi^{-1} G^T G)^T S + S (A + \epsilon \Pi^{-1} G^T G) + \epsilon G^T G.$$

Therefore, for matrices $\Pi > 0$ and $S > 0$ such that

$$W_1(\Pi) \leq 0,$$

$$W_2(S) \leq 0,$$

$$\Pi_0 - \Pi(t_0) \geq 0,$$

$$S(t_0) = 0 \text{ or } \hat{x}_0 = 0,$$

$$S(t_1) \geq 0,$$

$$\Pi(t_1) \geq 0,$$

the cost, J , will be nonpositive.

In the special case, $\epsilon = 0$, we know from Remark 8.3.1 that S will be zero, which allows us to ignore $W_2(S)$ altogether. The limiting conditions for $\gamma \rightarrow 0$ then come from (8.48) and are

$$\Pi F_2 = 0, \quad (8.49)$$

$$\Pi F_3 = 0, \quad (8.50)$$

$$L_1(\Pi) \leq 0. \quad (8.51)$$

Equations (8.49–8.51) are identical to the conditions found in Chapter 7 for the standard problem with no model uncertainty, which is what we would expect. Note that (8.49) and (8.50) clearly show that, in the limit, the Riccati matrix, Π , obtains a nontrivial null space which contains the image of the nuisance failure maps, F_2 and F_3 . This, in turn, implies that a limiting solution *does not exist* for the case, $\epsilon \neq 0$, since $W_2(S)$ requires that an inverse exist for Π . Thus, robustifying the game theoretic fault detection filter destroys the limiting property found in Chapter 7. The loss of this asymptotic property can be thought of as a vivid example of the tradeoff between fault detection and parameter robustness.

8.5 Example: Accelerometer Fault Detection in an F16XL with Model Uncertainty

8.5.1 Problem Statement

To show how the robust game theoretic detection filter can be used for fault detection and identification, we once again revisit the F-16XL example introduced in Chapter 6. In this section, we will add model uncertainty to the problem. A description of the states and the measurements is given in Section 6.3.1. The nominal failure model is given by

$$\dot{x} = Ax + F_{A_z}\mu_{A_z} + F_{wg}\mu_{wg},$$

$$y = Cx + v,$$

$$z = H(y - C\hat{x}).$$

The system matrices are given by (6.56–6.59). To complete our model, incorporate plant uncertainty into the equations. In this example, we will assume that the system eigenvalues are only known to within a certain range. The perturbation in A corresponding to this uncertainty is found by decomposing A into its eigenvalues and eigenvectors:

$$A = XDX^{-1}.$$

X is a matrix whose columns are the eigenvectors of A ; D is a diagonal matrix whose diagonal elements are the corresponding eigenvalues. ΔA is then obtained by perturbing the eigenvalues by 10%, reforming the matrix, and taking the difference from the nominal A :

$$\begin{aligned}\tilde{A} &= V(1.1 \times D)V^{-1}, \\ \Delta A &= \tilde{A} - A.\end{aligned}$$

We do not need all of the elements of ΔA , however. Since any element in the fifth column of ΔA enters the system in the same way as the nuisance fault, μ_{wg} , it is redundant to include these perturbations. Also, the fourth state, θ , is the integral of the third state, q . There is no uncertainty in this dynamic relationship (since an integral is always an integral), and so we can eliminate the corresponding element in ΔA , to get

$$\Delta A = \begin{bmatrix} -0.0067 & 0.0043 & -0.0889 & 0 & 0 \\ 0.0020 & -0.1467 & 1.6580 & 0 & 0 \\ 0.0138 & -0.1679 & -0.0682 & 0 & 0 \\ 0 & 0 & 0 & 0 & 0 \\ 0 & 0 & 0 & 0 & 0 \end{bmatrix}.$$

Now implicit in this perturbation model is a perturbation size, 10 %. We remove this assumption when we decompose ΔA into the form given by (8.4). We must also point out that we are only interested in finding the map, F_3 , since this represents the way in which the plant uncertainty drives the system. By using the singular value decomposition,

$$\Delta A = USV^T,$$

we construct F_3 from unitary matrix,

$$U = \begin{bmatrix} -0.0533 & -0.0156 & -0.9985 & 0 & 0 \\ 0.9981 & -0.0331 & -0.0528 & 0 & 0 \\ -0.0322 & -0.9993 & 0.0173 & 0 & 0 \\ 0 & 0 & 0 & 1 & 0 \\ 0 & 0 & 0 & 0 & 1 \end{bmatrix},$$

which gives an orthonormal basis for the image of ΔA and its orthogonal complement (Klema and Laub 1980). Since the first three columns of U correspond to the three nonzero singular values of ΔA , these correspond to the image of ΔA and, thus, are the only columns we will use for F_3 :

$$F_3 = \begin{bmatrix} -0.0533 & -0.0156 & -0.9985 \\ 0.9981 & -0.0331 & -0.0528 \\ -0.0322 & -0.9993 & 0.0173 \\ 0 & 0 & 0 \\ 0 & 0 & 0 \end{bmatrix}.$$

To complete the decomposition, we take G to be the least-squares solution to $F_3 G = \Delta A$,

$$G = \begin{bmatrix} 0.0020 & -0.1412 & 1.6617 & 0 & 0 \\ -0.0137 & 0.1726 & 0.0147 & 0 & 0 \\ 0.0069 & 0.0005 & 0.0000 & 0 & 0 \end{bmatrix},$$

and assume that Λ has the form,

$$\Lambda = \begin{bmatrix} \lambda_1(t) & 0 & 0 \\ 0 & \lambda_2(t) & 0 \\ 0 & 0 & \lambda_3(t) \end{bmatrix}.$$

Again, for our purposes, F_3 is the only important element of the uncertainty model. Note, also, that F_3 is not output separable from F_{A_z} , our target fault.

8.5.2 Parameter Robust Filter Design

Our ultimate objective is to design a filter which transmits the accelerometer fault input with little or no attenuation over a reasonable frequency range while simultaneously rejecting

sensor noise and the windgust disturbance. Additionally, the filter must also be insensitive to uncertainty in the eigenvalues, and it must be stable. To achieve this design goal, we have the parameters, γ and ϵ , and the weighting matrices: Q , V , M , and N .

A critical element in our design is the value chosen for the parameter, ϵ . As we discussed in Remark 8.3.1, with $\epsilon = 0$, the robust game theoretic detection filter simplifies to standard game theoretic fault detection filter of Chapter 6. With $\epsilon \neq 0$, additional elements appear in the estimator equation which bias the estimate in anticipation of variations in the plant. We will, therefore, look at two different designs: one with $\epsilon = 0$ and the other with ϵ nonzero.

After much trial and error, in which target fault transmission was traded off for nuisance fault attenuation, the following weightings,

$$V = \begin{bmatrix} 1 & 0 & 0 & 0 \\ 0 & 1 & 0 & 0 \\ 0 & 0 & 4000 & 0 \\ 0 & 0 & 0 & 1 \end{bmatrix}, \quad N = \begin{bmatrix} 10 & 0 & 0 \\ 0 & 10 & 0 \\ 0 & 0 & 10 \end{bmatrix} \quad Q = I, \quad M = 1000, \quad (8.52)$$

were used along with $\gamma = 0.0015$ and $\epsilon = 0.000005$. These values were found to give the best design for nonzero ϵ . The corresponding Riccati solutions are

$$\Pi^{-1} = 10^5 \times \begin{bmatrix} 0.4723 & -0.0065 & 0.0019 & -0.0012 & 0.0393 \\ -0.0065 & 0.0004 & 0.0006 & 0.0001 & -0.0138 \\ 0.0019 & 0.0006 & 0.0011 & 0.0000 & -0.0162 \\ -0.0012 & 0.0001 & 0.0000 & 0.0034 & -0.0002 \\ 0.0393 & -0.0138 & -0.0162 & -0.0002 & 1.0895 \end{bmatrix},$$

$$S = 10^{-5} \times \begin{bmatrix} 0.0006 & -0.0054 & -0.0010 & 0.0001 & -0.0045 \\ -0.0054 & 0.0699 & -0.0262 & -0.0011 & 0.0597 \\ -0.0010 & -0.0262 & 0.5650 & 0.0012 & -0.0597 \\ 0.0001 & -0.0011 & 0.0012 & 0.0171 & -0.0003 \\ -0.0045 & 0.0597 & -0.0597 & -0.0003 & 0.0729 \end{bmatrix}.$$

If we take $\epsilon = 0$, we find that the best results come when we keep all other parameters as before, with the exception of γ , which we change to 0.0000005. For this case, the corresponding Riccati solutions are

$$\Pi^{-1} = 10^8 \times \begin{bmatrix} 0.1406 & -0.0019 & 0.0005 & 0.0000 & 0.0134 \\ -0.0019 & 0.0000 & 0.0000 & 0.0000 & -0.0006 \\ 0.0005 & 0.0000 & 0.0000 & 0.0000 & -0.0010 \\ 0.0000 & 0.0000 & 0.0000 & 0.0010 & -0.0000 \\ 0.0134 & -0.0006 & -0.0010 & -0.0000 & 2.0780 \end{bmatrix},$$

$$S = 0.$$

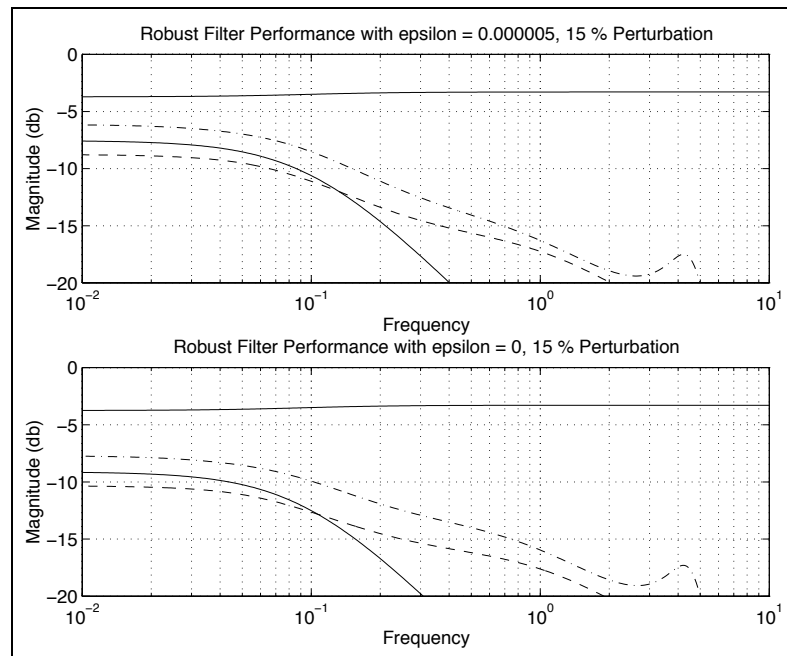


Figure 8.1: F-16XL example: signal transmission in the parameter robust game theoretic fault detection filter with a 15% Shift in eigenvalues (The accelerometer fault and nominal windgust transmission are represented by the solid line. The windgust is the lower of the two. The dash-dot line corresponds to windgust transmission when modeled eigenvalues are in error by 15%. The dashed line corresponds to transmission under a -15% modeling error).

Figure 8.1 shows the performance of both filters for the nominal plant and for a perturbed plant with a 15% shift in the eigenvalues. As we saw from before, the direct feedthrough of the target fault has a very pronounced effect on target fault transmission. There is no high frequency roll-off, and the low frequency transmission is degraded. This degradation

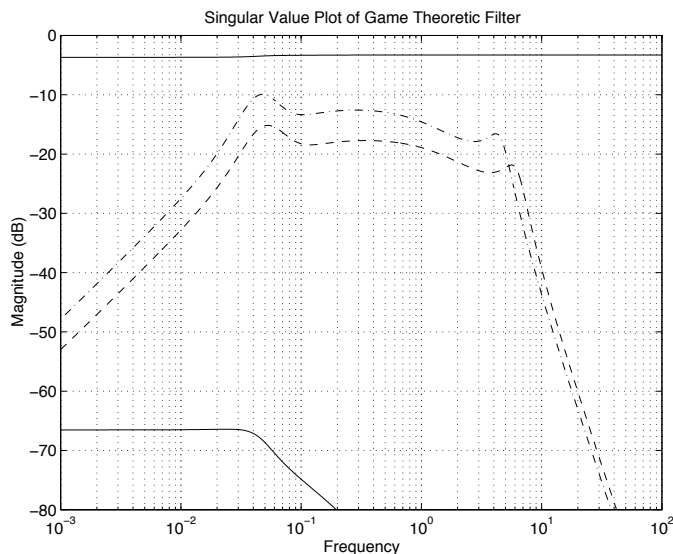


Figure 8.2: F-16XL example: signal transmission in the standard game theoretic fault detection filter with a 15% shift in eigenvalues (The accelerometer fault and nominal windgust transmission are represented by the solid line. The windgust is the lower of the two. The dash-dot line corresponds to windgust transmission when modeled eigenvalues are in error by 15%. The dashed line corresponds to transmission under a -15% modeling error).

is mitigated somewhat by choosing the particular form of weighting, V , seen in (8.52). We also note that the accelerometer fault transmission is invariant under plant parameter changes. This is because the accelerometer fault comes in through the measurements and, as a result, only drives the filter.

From Figure 8.1, we can see that the loss of the output separability property severely degrades our ability to both maintain target fault sensitivity and achieve good separation between the target fault and nuisance fault. This separation is particularly poor in the low frequency region. Experience with this example has shown that little can be done to improve the low frequency separation without severely degrading low frequency accelerometer fault transmission. Figure 8.1 also shows that the ϵ parameter has a negligible, perhaps even detrimental, effect upon the filter design. This result is due to the sensitivity of the Riccati solution, S , to the values of ϵ and γ used in the problem. It was found that S will quickly

lose its symmetry property when more aggressive values of ϵ and γ are used. This hurts the performance of the robust filter by preventing the additional elements of the filter associated with ϵ and S from having an impact on the design. It also prevents the designer from using lower values of γ to improve nominal performance.

If one compares Figure 8.1 to Figure 8.2, which shows the performance of the filter designed in Chapter 6 under a 15% perturbation, he will see that the parameter robust filter achieves its robustness at the cost of nominal performance. The original filter design from Chapter 6, in fact, has far superior low frequency performance, even under plant parameter variations. This is critical for detecting “hard failures,” which look like step inputs.

A Decentralized Fault Detection Filter

FOR MANY of the larger scale systems of interest to PATH, such as multi-car platoons, the design of a fault detection filter may best be done using a decentralized scheme, particularly for the monitoring of sensors which measure relative states between cars. By this, we refer to a filter that is formed indirectly by combining the state estimates generated by several "local" estimators to form an estimate of the overall, or "global," system. This is distinct from the standard approach, which is to design a single filter directly for the "global" system.

For large-scale systems, a decentralized filter may offer several advantages over using just a single filter. First, by decentralizing the problem one simplifies it by decomposing it down into a collection of smaller problems. Second, there are times when the decentralized point of view reflects the actual physical structure of the system, such as a platoon of automated cars. Third, the element of scalability is introduced into the fault detection filter with a decentralized approach. When a car joins the platoon, for instance, there is a step change

in the order of the problem. If the system is being monitored with a single filter, it may be impossible to make a graceful adjustment. Finally, fault tolerance can be built into the system by checking for faults in the local sensors and actuators prior to allowing their outputs to be passed onto the global level as suggested by (Kerr 1985).

9.1 Decentralized Estimation Theory and its Application to FDI

The decentralized fault detection filter is the result of combining the game theoretic fault detection filter of the Chapter 6 with the decentralized filtering algorithm introduced by Speyer in (Speyer 1979) and extended by Willsky *et al.* in (Willsky et al. 1982). For completeness, we will review the basics of decentralized estimation theory in this section. The general theory was first presented in (Chung and Speyer 1995) which was research sponsored in part by the PATH program.

9.1.1 The General Solution

Consider the following system driven by process disturbances, w , and sensor noise, v ,

$$\dot{x} = Ax + Bw, \quad x(0), x \in \mathcal{R}^n, \quad (9.1)$$

$$y = Cx + v, \quad y \in \mathcal{R}^m. \quad (9.2)$$

for which it is desired to derive an estimate of x . The standard approach is a full-order observer,

$$\dot{\hat{x}} = A\hat{x} + L(y - C\hat{x}), \quad \hat{x}(0) = 0, \quad (9.3)$$

which we will call a *centralized estimator*. An alternative to this method is to derive the estimated with a *decentralized estimator*. In the decentralized approach, \hat{x} is found by combining estimates based upon “local” models,

$$\dot{x}^j = A^j x^j + B^j w^j, \quad x^j \in \mathcal{R}^{n^j}, \quad (j = 1 \dots N), \quad (9.4)$$

$$y^j = E^j x^j + v^j, \quad y^j \in \mathcal{R}^{m^j}, \quad (j = 1 \dots N), \quad (9.5)$$

which together provide an alternate representation of the original system, (9.1, 9.2), which, as one might guess, is called the “global” system. The vector, x , is likewise called the “global” state. The number of local systems, N , is bounded above by the number of measurements in the system, i.e. $N \leq m$.

The global/local decomposition is really of only secondary importance, since, as argued by (Chung and Speyer 1995), there are no real restrictions on how one forms the global and local models. The real key to the decentralized estimation algorithm is the relationship between the global set of measurements, y , and the N local sets, y^j . The two basic assumptions are that the local sets are simply segments of the global set,

$$y = \begin{Bmatrix} y^1 \\ y^2 \\ \vdots \\ y^N \end{Bmatrix}, \quad (9.6)$$

and that the local sets can be described in terms of both the local state *and* the global state. In other words, y^j can be given by (9.5) or by

$$y^j = C^j x + v^j, \quad (j = 1 \dots N). \quad (9.7)$$

Equations (9.2), (9.6), and (9.7), consequently, imply that

$$C = \begin{bmatrix} C^1 \\ \vdots \\ C^N \end{bmatrix}$$

and that

$$v = \begin{bmatrix} v^1 \\ \vdots \\ v^N \end{bmatrix}. \quad (9.8)$$

The decentralized estimation algorithm falls out when we attempt to estimate the global state by first generating estimates of the local systems, (9.4), using the local measurement sets, y^j , and the local models, A^j :

$$\dot{\hat{x}}^j = A^j \hat{x}^j + L^j (y^j - E^j \hat{x}^j), \quad \hat{x}^j(t_0) = 0, \quad (j = 1 \dots N). \quad (9.9)$$

The global state estimate, \hat{x} , is then found via

$$\hat{x} = \sum_{j=1}^N (G^j \hat{x}^j + h^j), \quad (9.10)$$

where h^j is a measurement-dependent variable propagated by

$$\dot{h}^j = \Phi h^j + (\Phi G^j - \dot{G}^j - G^j \Phi^j) \hat{x}^j, \quad h^j(0) = 0. \quad (9.11)$$

The constituent matrices are defined as

$$\begin{aligned} \Phi &:= A - \sum_{j=1}^N G^j L^j C^j, \\ \Phi^j &:= A^j - L^j E^j. \end{aligned}$$

The G^j matrices are chosen “blending matrices”. In (Chung and Speyer 1995) it was found that in order for the decentralized estimation algorithm, (9.10,9.11), to generate the same estimate, \hat{x} , as a standard centralized estimator, (6.3), the blending matrices have to be related to the gain of the centralized estimator and the gains of the local estimators through the equation:

$$L = [G^1 \quad \dots \quad G^N] \begin{bmatrix} L^1 & 0 & \dots & 0 \\ 0 & L^2 & \dots & 0 \\ \vdots & \vdots & \ddots & \vdots \\ 0 & 0 & \dots & L^N \end{bmatrix}. \quad (9.12)$$

L is the gain for the global estimator, and L^j is the gain for the j th local estimator. This is simply the requirement that a solution exists to a linear algebraic equation. In general, however, this condition can not be met because of an insufficient number of equations with which to solve for the unknowns.

There is, however, one general class of estimator for which (9.12) is satisfied almost automatically. This class is comprised of estimators which take their gains from Riccati solutions, that is Kalman filters (Speyer 1979, Willsky et al. 1982) or H^∞ -norm bounding filters (Jang and Speyer 1994). In this case, the local gains are found from

$$L^j = P^j (E^j)^T (V^j)^{-1}, \quad (9.13)$$

where, in the case of the Kalman Filter, the matrix, P^j is the solution of the Riccati equation:

$$\begin{aligned}\dot{P}^j &= A^j P^j + P^j (A^j)^T + B^j W^j (B^j)^T - P^j (E^j)^T (V^j)^{-1} E^j P^j, \\ P^j(0) &= P_0^j.\end{aligned}$$

The initial condition, P_0^j , is chosen by the analyst based upon his knowledge of the system. In the global system, the global gain is

$$L = PC^T V^{-1}$$

where

$$\mathcal{V} = \begin{bmatrix} V^1 & 0 & \dots & 0 \\ 0 & V^2 & 0 & 0 \\ \vdots & 0 & \ddots & \vdots \\ 0 & \dots & \dots & V^N \end{bmatrix}, \quad (9.14)$$

is restricted to a block diagonal form comprised of the local weightings, V^j , and P is the solution to the global Riccati equation,

$$\dot{P} = AP + PA^T + BWB^T - PC^T \mathcal{V} CP, \quad P(0) = P_0.$$

. The blending matrix solution is then,

$$G^j = P(S^j)^T (P^j)^{-1} \quad j = 1, \dots, N, \quad (9.15)$$

where S^j is any matrix such that

$$C^j = E^j S^j. \quad (9.16)$$

One can, in fact, always take $S^j = (E^j)^\dagger C^j$ where $(E^j)^\dagger$ is the pseudo-inverse of E^j (Willsky et al. 1982). Note that the solutions for G^j will always exist for Riccati-based observers so long as P^j is invertible or, equivalently, positive-definite. This will always be the case if the triples, (C^j, A^j, B^j) , are controllable and observable for each of the local systems.

9.1.2 Implications for Detection Filters

The analysis of the previous section implies that will we be able to form a decentralized fault detection filter in the general case only if we are able to find a Riccati-based observer which is equivalent to a Beard-Jones Filter or unknown input observer. The most direct way to achieve this is to find a linear-quadratic optimization problem which is equivalent to the fault detection and identification problem. This is an analog of the famous inverse optimal control problem first posed by Kalman (Kalman 1964). In (Chung 1997), however, a counterexample was given which showed that FDI observers do not correspond one-to-one with linear-quadratic problems.

Another way to address this problem, of course, is to use the Riccati-based game theoretic fault detection filter that we have painstakingly developed in the previous three chapters. This filter is entirely suitable for use in the decentralized estimation algorithm. One might, in fact, take the following steps to use the game theoretic fault detection filter in this way:

1. Identify the sensors and actuators which must be monitored at the global level, i.e. define the target faults for the global filter.
2. Identify the faults which should be included in the global nuisance set. The remaining faults should be monitored at the local levels.
3. Derive global and local models for the system including failure maps. (Chung 1997) contains a brief discussion about this process. In Section 9.2, we will demonstrate one method in which the local models are derived from the global model via a minimum realization.
4. Design game theoretic fault detection filters for the local and global systems. Solve the corresponding Riccati equations and store the solutions for later use.
5. Determine the blending solutions, G^j , from Equation (9.15).

6. Propagate the local estimates, \hat{x}^j , and vectors, h^j , and then use the decentralized estimation algorithm (9.10) to derive a global estimate, \hat{x} .
7. Determine the global failure signal from $(y - C\hat{x})$ where y is the total measurement set, C is the global measurement matrix, and \hat{x} is the global fault detection filter estimate just derived.

We will now apply these steps in an example.

9.2 Range Sensor Fault Detection in a Platoon of Cars

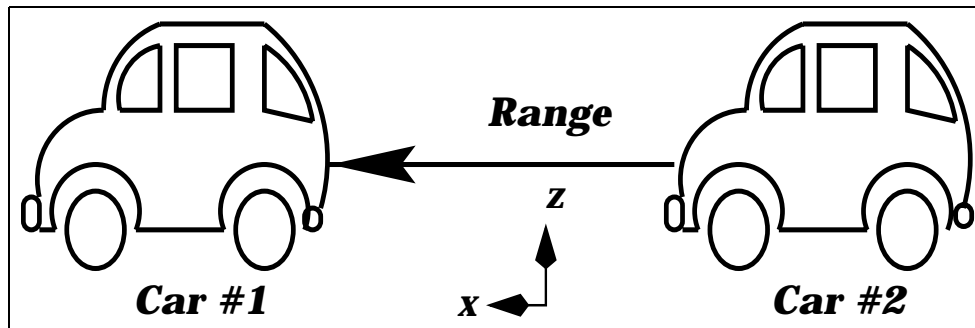


Figure 9.1: A two-car platoon with a range sensor.

9.2.1 Problem Statement

We will now examine the utility of the decentralized approach to FDI by working through an example. The problem that we will look at involves the detection of failures within a system of two cars traveling as a platoon. See Figure 9.1. The cars are controlled to maintain a uniform speed and constant separation.

The platoon is the central component of automated highway schemes in which groups of cars line up single file and travel as a unit, thereby eliminating the possibility of individual vehicles impeding one another (Douglas et al. 1995, Douglas et al. 1996). With careful coordination, these platoons will allow traffic to move with much the same order and protocol as electrical signals on the Internet. The viability of the platooning scheme, however, will depend on many factors, not the least of which are reliability and safety.

The FDI schemes that we have examined to this point are capable of monitoring individual cars, but may not be ideal for monitoring elements that deal with the interactions between cars. For example, to maintain uniform speed throughout the platoon and to keep the spacing between the cars constant, additional sensors will be needed to measure the relative speed and the relative distance, or “range”, between the cars. In order to detect a failure in the range sensor using analytic redundancy, however, it is necessary to have a dynamic relationship between the range sensor and other sensors on the vehicles. Range, however, involves the dynamics of both of the cars and so would require a higher-order model for its detection filter.

While this is not necessarily prohibitive, it does not make use of the many different state estimates that are already being propagated throughout the platoon. The sensors on each of the cars, for instance, will be monitored by detection filters, and it is more than likely that a state estimate would also be generated by the vehicles’ control loops. Given these pre-existing estimates, it seems logical to make use of the decentralized estimation algorithm to carry out range sensor fault detection.

9.2.2 System Dynamics and Failure Modeling

Our example starts with the car model used in (Douglas et al. 1995). In this model, the nonlinear, six degree-of-freedom dynamics of an representative automobile are linearized about a straight, level path at a speed of 25 meters/sec (roughly 56 miles per hour). The linearized equations are found to decouple nicely into latitudinal and longitudinal dynamics, much like an airplane. Moreover, the linearized equations can be further reduced by eliminating “fast modes” and actuator states. For simplicity, we will only use the longitudinal dynamics which we represent as

$$\begin{aligned}\dot{\underline{x}} &= A^L \underline{x}, \\ \underline{y} &= C^L \underline{x}.\end{aligned}$$

The vehicle states are

$$\underline{x} = \begin{pmatrix} m_a \\ \omega_e \\ v_x \\ v_z \\ z \\ q \\ \theta \end{pmatrix} \begin{array}{l} \text{engine air mass (kg)} \\ \text{engine speed (rad/sec)} \\ \text{long. velocity (m/sec)} \\ \text{vertical velocity (m/sec)} \\ \text{vertical position (m)} \\ \text{pitch rate (rad/sec)} \\ \text{pitch (rad)} \end{array} \quad (9.17)$$

and are propagated by the state matrix,

$$A^L = 10^3 \times \begin{bmatrix} -0.0226 & -0.0001 & 0 & 0 & 0 & 0 & 0 \\ 0.3070 & -0.0354 & 0.3974 & -0.2381 & -2.6980 & -3.7530 & -0.3311 \\ 0 & 0.0001 & -0.0008 & 0.0006 & 0.0068 & 0.0168 & 0.0015 \\ 0 & -0.0000 & 0.0000 & -0.0036 & -0.0404 & -0.0091 & -0.0008 \\ 0 & 0 & 0 & 0.0010 & 0 & 0 & 0 \\ 0 & 0 & 0 & 0 & 0 & 0 & 0.0010 \\ 0 & -0.0000 & 0.0002 & -0.0006 & -0.0072 & -0.0396 & -0.0036 \end{bmatrix}. \quad (9.18)$$

The measurements are

$$\underline{y} = \begin{pmatrix} m_a \\ \omega_e \\ \dot{v}_x \\ \dot{v}_z \\ q \\ \bar{\omega}_f \\ \bar{\omega}_r \end{pmatrix} \begin{array}{l} \text{engine air mass (kg)} \\ \text{engine speed (rad/sec)} \\ \text{long. acceleration (m/sec}^2\text{)} \\ \text{heave acceleration (m/sec}^2\text{)} \\ \text{pitch rate (rad/sec)} \\ \text{front symmetric wheel speed (rad/sec)} \\ \text{rear symmetric wheel speed (rad/sec)} \end{array} \quad (9.19)$$

with the corresponding measurement matrix,

$$C^L = \begin{bmatrix} 1 & 0 & 0 & 0 & 0 & 0 & 0 \\ 0 & 1 & 0 & 0 & 0 & 0 & 0 \\ 0 & 0.0713 & -0.8177 & 0.5934 & 6.7786 & 16.8068 & 1.5162 \\ 0 & -0.0020 & 0.0221 & -3.5646 & -40.4210 & -9.0765 & -0.8141 \\ 0 & 0 & 0 & 0 & 0 & 0 & 1 \\ 0 & 0 & 7.1220 & -4.5806 & -51.9152 & 58.8718 & 5.1944 \\ 0 & 0.0888 & 5.9738 & -3.5782 & -40.5542 & -56.4109 & -4.9773 \end{bmatrix}. \quad (9.20)$$

The rear and front symmetric wheel speeds are states that were eliminated when the fast modes were factored out of the linearized system.

In order to build a detection filter for the range sensor, we need to use (9.17–9.20) to build state space models for the platoon,

$$\begin{aligned}\dot{\eta} &= A\eta + F_1\mu_1 + F_2\mu_2, \\ y &= C\eta,\end{aligned}$$

and the two cars,

$$\begin{aligned}\dot{\eta}^1 &= A^1\eta^1 + F_1^1\mu_1^1 + F_2^1\mu_2^1, \\ y^1 &= E^1\eta^1, \\ \dot{\eta}^2 &= A^2\eta^2 + F_1^2\mu_1^2 + F_2^2\mu_2^2, \\ y^2 &= E^2\eta^2.\end{aligned}$$

We will build up our models with the following steps:

1. Using (9.17–9.20), we will derive the global state matrices, A and C .
2. Using the modelling techniques described in (Douglas 1993), we will determine the failure maps, F_i .
3. We will then obtain the local state matrices, A^i, E^i , and F_j^i , from the minimum realization of the triples (C^1, A, F_2) and (C^2, A, F_2) .

Our general strategy is to derive the global equation first and then get the local equations from decompositions based upon observability and controllability. While this is by no means the only way to obtain the global and local representations of a system, it is a logical method that can be applied to any problem.

The obvious way to get the global matrices, A and C , is to form block diagonal composite matrices with A^L and C^L repeated on the diagonal, i.e.

$$A' = \begin{bmatrix} A^L & 0 \\ 0 & A^L \end{bmatrix}, \quad C' = \begin{bmatrix} C^L & 0 \\ 0 & C^L \end{bmatrix}.$$

This, however, is not sufficient, since there is no way to describe the range, R , between the two vehicles with the given states, (9.17). Range is the relative distance between the cars,

$$R = x^1 - x^2,$$

where x^i is the longitudinal displacement of car i . Displacement, however, is not a state of the vehicle (9.17). We must, therefore, add a range state to the platoon dynamics, using the equation,

$$\dot{R} = v_x^1 - v_x^2.$$

The end result is that the platoon will be a fifteen-state system,

$$\eta = \left\{ \begin{array}{l} m_a^1 \\ \omega_e^1 \\ v_x^1 \\ v_z^1 \\ z^1 \\ q^1 \\ \theta^1 \\ m_a^2 \\ \omega_e^2 \\ v_x^2 \\ v_z^2 \\ z^2 \\ q^2 \\ \theta^2 \\ R \end{array} \right\} \begin{array}{l} \text{engine air mass (kg) - Car\#1} \\ \text{engine speed (rad/sec) - Car\#1} \\ \text{long. velocity (m/sec) - Car\#1} \\ \text{vertical velocity (m/sec) - Car\#1} \\ \text{vertical position (m) - Car\#1} \\ \text{pitch rate (rad/sec) - Car\#1} \\ \text{pitch (rad) - Car\#1} \\ \text{engine air mass (kg) - Car\#2} \\ \text{engine speed (rad/sec) - Car\#2} \\ \text{long. velocity (m/sec) - Car\#2} \\ \text{vertical velocity (m/sec) - Car\#2} \\ \text{vertical position (m) - Car\#2} \\ \text{pitch rate (rad/sec) - Car\#2} \\ \text{pitch (rad) - Car\#2} \\ \text{Range (m).} \end{array}$$

The corresponding state matrix is

$$A = \begin{bmatrix} A^L & 0 \\ 0 & A^L \\ E_1 & -E_1 \end{bmatrix}, \quad (9.21)$$

$$E_1 = [0 \ 0 \ 1 \ 0 \ 0 \ 0 \ 0 \ 0].$$

The measurement matrix is

$$C = \left[\begin{array}{c|cc} C^L & 0 & \\ \hline 0 & C^L & 0 \\ & 0 & 1 \end{array} \right] = \begin{bmatrix} C^1 & 0 \\ 0 & C^2 \end{bmatrix}, \quad (9.22)$$

where C^1 and C^2 can be inferred from (9.22). Finally, the local measurement sets are

$$y^1 = \left\{ \begin{array}{l} m_a^1 \\ \omega_e^1 \\ \dot{v}_x^1 \\ \dot{v}_z^1 \\ q^1 \\ \bar{\omega}_f^1 \\ \bar{\omega}_r^1 \end{array} \right\} \left\{ \begin{array}{l} \text{engine air mass (kg)- Car\#1} \\ \text{engine speed (rad/sec)- Car\#1} \\ \text{long. acceleration (m/sec}^2\text{)- Car\#1} \\ \text{heave acceleration (m/sec}^2\text{)- Car\#1} \\ \text{pitch rate (rad/sec)- Car\#1} \\ \text{front symmetric wheel speed (rad/sec) - Car\#1} \\ \text{rear symmetric wheel speed (rad/sec) - Car\#1.} \end{array} \right.$$

and

$$y^2 = \left\{ \begin{array}{l} m_a^2 \\ \omega_e^2 \\ \dot{v}_x^2 \\ \dot{v}_z^2 \\ q^2 \\ \bar{\omega}_f^2 \\ \bar{\omega}_r^2 \\ R \end{array} \right\} \left\{ \begin{array}{l} \text{engine air mass (kg)- Car\#2} \\ \text{engine speed (rad/sec)- Car\#2} \\ \text{long. acceleration (m/sec}^2\text{)- Car\#2} \\ \text{heave acceleration (m/sec}^2\text{)- Car\#2} \\ \text{pitch rate (rad/sec)- Car\#2} \\ \text{front symmetric wheel speed (rad/sec) - Car\#2} \\ \text{rear symmetric wheel speed (rad/sec) - Car\#2} \\ \text{range (rad/sec).} \end{array} \right.$$

Our ultimate objective is to design a filter which will detect a range sensor fault in the presence of potential failures in the other sensors.

In an actual health monitoring system, we would design the global filter to block out all of the nuisance faults that are output separable from the range sensor fault and then rely upon the local filters to monitor the remaining faults. Given the size of our example, however, the full analysis required to do a detailed design would clutter our presentation. We will, therefore, limit ourselves to constructing only one local filter and will choose simple nuisance sets at both the global and local levels.

For this example, we choose to monitor the front symmetric wheel speed sensor at the local level. The nuisance set is then chosen to be the engine air mass sensor and the heave accelerometer. At the global level, the range sensor has already been designated as the target fault. We, therefore, complete the problem definition by choosing the engine speed sensor and longitudinal accelerometer as the global nuisance set. There is no particular significance attached to any of our choices for the nuisance and target sets, aside from the choice of the range sensor as the global target fault.

For the local filters, we need the need the airmass sensor failure maps,

$$F_{m_a^1} = \begin{bmatrix} 1 & -22.5605 \\ 0 & 307.0298 \\ 0 & 0 \\ 0 & 0 \\ 0 & 0 \\ 0 & 0 \\ 0 & 0 \\ 0 & 0 \\ 0 & 0 \\ 0 & 0 \\ 0 & 0 \\ 0 & 0 \\ 0 & 0 \\ 0 & 0 \\ 0 & 0 \end{bmatrix}, \quad F_{m_a^2} = \begin{bmatrix} 0 & 0 \\ 0 & 0 \\ 0 & 0 \\ 0 & 0 \\ 0 & 0 \\ 0 & 0 \\ 0 & 0 \\ 1 & -22.5605 \\ 0 & 307.0298 \\ 0 & 0 \\ 0 & 0 \\ 0 & 0 \\ 0 & 0 \\ 0 & 0 \\ 0 & 0 \end{bmatrix},$$

and the heave accelerometer sensor failure maps,

$$F_{v_z^1} = \begin{bmatrix} 0 & 0 \\ 0 & 0 \\ -0.1767 & 0 \\ -7.8747 & 1 \\ 0.6698 & -7.8747 \\ -0.0007 & 0 \\ 0 & 0.0197 \\ 0 & 0 \\ 0 & 0 \\ 0 & 0 \\ 0 & 0 \\ 0 & 0 \\ 0 & 0 \\ 0 & 0 \\ 0 & -0.1767 \end{bmatrix}, \quad F_{v_z^2} = \begin{bmatrix} 0 & 0 \\ 0 & 0 \\ 0 & 0 \\ 0 & 0 \\ 0 & 0 \\ 0 & 0 \\ 0 & 0 \\ 0 & 0 \\ 0 & 0 \\ 0 & 0 \\ -0.1767 & 0 \\ -7.8747 & 1 \\ 0.6698 & -7.8747 \\ -0.0007 & 0 \\ 0 & 0.0197 \\ 0 & 0.1767 \end{bmatrix}.$$

Finally, to check for output separability in the local filters, we will need the front wheel

speed sensor failure maps,

$$F_{\bar{\omega}_f^1} = \begin{bmatrix} 0 & 0 \\ 0.0001 & -0.3401 \\ 0.0645 & 0.0046 \\ 14.0371 & 0.0114 \\ -1.2399 & 14.0371 \\ 0.0079 & 0 \\ 0.0000 & -0.0241 \\ 0 & 0 \\ 0 & 0 \\ 0 & 0 \\ 0 & 0 \\ 0 & 0 \\ 0 & 0 \\ 0 & 0.0645 \end{bmatrix}, \quad F_{\bar{\omega}_f^2} = \begin{bmatrix} 0 & 0 \\ 0 & 0 \\ 0 & 0 \\ 0 & 0 \\ 0 & 0 \\ 0 & 0 \\ 0 & 0 \\ 1.0000 & -22.5605 \\ 0 & 307.0298 \\ 0.0675 & 0 \\ 14.9324 & 0 \\ -1.3186 & 14.9324 \\ 0.0079 & 0 \\ 0 & -0.0087 \end{bmatrix}.$$

A quick application of (6.17) will show that all of our failure sets are output separable.

We are now in position to generate the local state equations. The local dynamics for car #1 come from the minimum realization of $(C^1, A, [F_{m_a^1} \ F_{v_z^1}])$. The corresponding matrices are

$$A^1 = 10^3 \times \begin{bmatrix} -0.0001 & -0.0000 & -0.0001 & 0.0000 & -0.0040 & -0.0426 & 0.0013 \\ -0.0000 & -0.0017 & -0.0571 & 0.0072 & 0.0263 & -0.6658 & -0.4966 \\ 0.0000 & 0.0000 & -0.0226 & -0.0001 & 0.0000 & -0.0000 & -0.0000 \\ 0.0001 & 0.0078 & 0.3017 & -0.0386 & -0.1372 & 3.6120 & 2.8167 \\ 0.0001 & -0.0001 & -0.0025 & 0.0002 & 0.0009 & -0.0191 & -0.0091 \\ 0.0009 & -0.0003 & 0.0002 & -0.0001 & -0.0004 & -0.0025 & -0.0002 \\ -0.0003 & -0.0009 & 0.0001 & -0.0002 & 0.0000 & 0.0013 & -0.0014 \end{bmatrix},$$

$$E^1 = \begin{bmatrix} 0 & 0 & -1 & 0 & 0 & 0 & 0 \\ 0.0004 & 0.1861 & 0 & -0.9825 & 0.0081 & -0.0007 & -0.0004 \\ -0.0044 & -0.0142 & 0 & -0.0903 & -0.2118 & 11.2661 & 14.3096 \\ -0.0002 & -0.0007 & 0 & -0.0048 & -4.0642 & -41.3183 & 2.4264 \\ 0.0001 & -0.9787 & 0 & -0.1854 & 0.0016 & 0.0245 & 0.0845 \\ 0.0003 & 0.0017 & 0 & 0.0069 & 1.4478 & -34.1025 & 71.3771 \\ -0.0010 & -0.0039 & 0 & -0.0192 & 2.1041 & -55.2068 & -42.9870 \end{bmatrix},$$

$$F_{m_a^1}^1 = \begin{bmatrix} 0 & 0.1213 \\ 0 & 57.1230 \\ 1 & -22.5605 \\ 0 & -301.6586 \\ 0 & 2.4980 \\ 0 & -0.2041 \\ 0 & -0.1202 \end{bmatrix}, \quad F_{\dot{v}_z^1}^1 = \begin{bmatrix} 7.9031 & -1.6879 \\ -0.0007 & -0.0213 \\ 0 & 0 \\ -0.0048 & -0.0057 \\ -0.1760 & -0.7911 \\ -0.0068 & -7.4136 \\ -0.0003 & -2.1388 \end{bmatrix}.$$

A model for Car #2 is similarly found as a minimal realization of $(C^2, A, [F_{m_a^2} \ F_{\dot{v}_z^2}])$.

The corresponding matrices are

$$A^2 = 10^3 \times$$

$$\begin{bmatrix} -0.0003 & -0.0003 & 0.0010 & -0.0000 & 0.0000 & 0.0000 & 0.0000 & -0.0000 \\ 0.0003 & 0.0003 & 0.0000 & 0.0010 & -0.0000 & -0.0000 & -0.0000 & 0.0000 \\ -0.0125 & -0.0121 & -0.0015 & -0.0008 & -0.0000 & 0.0000 & 0.0000 & 0.0000 \\ -0.0283 & -0.0275 & -0.0021 & -0.0030 & 0.0000 & 0.0081 & 0.0067 & -0.0001 \\ 0.1951 & 0.1939 & -0.0024 & 0.0389 & -0.0002 & -0.1529 & -0.1262 & 0.0027 \\ 0.0039 & 0.0046 & 0.0004 & 0.0005 & -0.0000 & -0.0213 & -0.0184 & 0.0000 \\ -0.0041 & -0.0048 & -0.0004 & -0.0005 & 0.0000 & 0.0228 & 0.0178 & -0.0000 \\ -2.6548 & -2.6391 & 0.0323 & -0.5294 & -0.3044 & 2.0805 & 1.7175 & -0.0578 \end{bmatrix},$$

$$E^2 = \begin{bmatrix} -0.0000 & 0.0000 & 1.0000 & -0.0000 & 0.0000 & 0.0000 & -0.0000 \\ -0.0004 & 0.1861 & 0 & -0.9825 & 0.0081 & -0.0007 & 0.0004 \\ 0.0044 & -0.0142 & -0.0000 & -0.0903 & -0.2118 & 11.2661 & -14.3096 \\ 0.0002 & -0.0007 & -0.0000 & -0.0048 & -4.0642 & -41.3183 & -2.4264 \\ -0.0001 & -0.9787 & 0 & -0.1854 & 0.0016 & 0.0245 & -0.0845 \\ -0.0003 & 0.0017 & 0 & 0.0069 & 1.4478 & -34.1025 & -71.3771 \\ 0.0010 & -0.0039 & 0 & -0.0192 & 2.1041 & -55.2068 & 42.9870 \end{bmatrix},$$

$$F_{m_a^2}^2 = \begin{bmatrix} 0 & 0 \\ 0 & 0 \\ 0 & 0 \\ 0 & 0 \\ 0.9973 & 0.0002 \\ 0 & 0 \\ 0 & 0 \\ 0.0733 & -307.8575 \end{bmatrix}, \quad F_{\dot{v}_z^2}^2 = \begin{bmatrix} 0 & 0 \\ 0 & 0 \\ 0 & 0 \\ 0 & 0 \\ 0 & 0 \\ -5.0327 & -4.9282 \\ 6.0961 & -6.2254 \\ 0 & 0 \end{bmatrix}.$$

With all of these system matrices in place, we can now form the residual projectors, H , (6.12) needed generate the failure signal, z . In the global filter, we define

$$\hat{F} = \begin{bmatrix} F_{\omega_e^1} & F_{v_x^1} & F_{\omega_e^2} & F_{v_x^2} \end{bmatrix}$$

so that the projector for the global filter is

$$H = I - C\hat{F} \left[(C\hat{F})^T C\hat{F} \right]^{-1} (C\hat{F})^T.$$

In the local filters, we define

$$\hat{F}^i = \begin{bmatrix} F_{m_a^i} & F_{v_z^i} \end{bmatrix} \quad i = 1, 2$$

so that the projector is

$$H^i = I - C\hat{F}^i \left[(C\hat{F}^i)^T C\hat{F}^i \right]^{-1} (C\hat{F}^i)^T.$$

We do not show either of these matrices explicitly because of their size.

9.2.3 Decentralized Fault Detection Filter Design

We will first design filters for the local systems. For simplicity, we will once again use the steady-state version of the game theoretic fault detection filter. The design process boils down to finding the design weightings which give the best tradeoff between target fault transmission and nuisance fault attenuation. For this example, it was found that

$$\begin{aligned} M^1 &= 10 \times I_7, & V^1 &= \text{diag} [1 \quad 1 \quad 10 \quad 1 \quad 1 \quad 1 \quad 1], \\ Q^1 &= I_7, & \gamma &= 0.18 \end{aligned}$$

leads to the filter for Car #1 depicted in Figure 9.2. The minimum separation over frequency is only 35 dB, but the filter has particularly good separation in the low frequency range.

For Car #2, the same weightings, adjusted for the different dimensions of the Car #2 dynamics,

$$\begin{aligned} M^2 &= 10 \times I_8, & V^2 &= \text{diag} [1 \quad 1 \quad 10 \quad 1 \quad 1 \quad 1 \quad 1 \quad 1], \\ Q^2 &= I_8, & \gamma &= 0.18, \end{aligned}$$

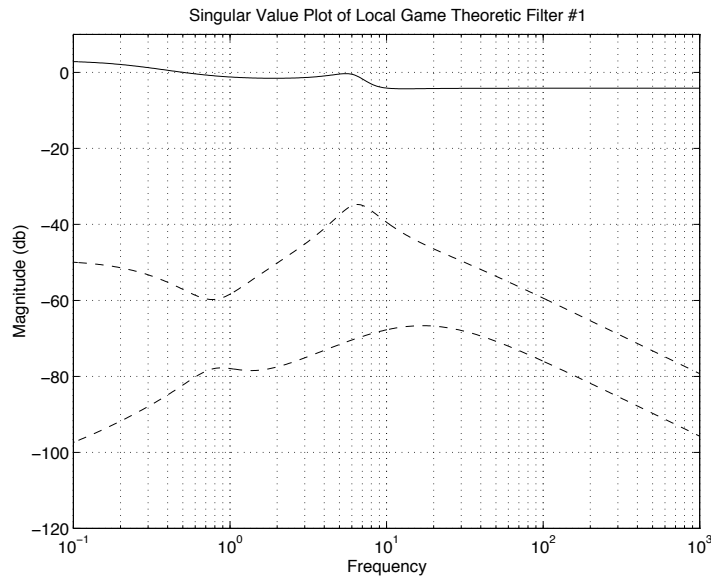


Figure 9.2: Platoon example: signal transmission in the local detection filter on car # 1 (accelerometer fault transmission shown with solid line, nuisance fault transmission shown with dashed line).

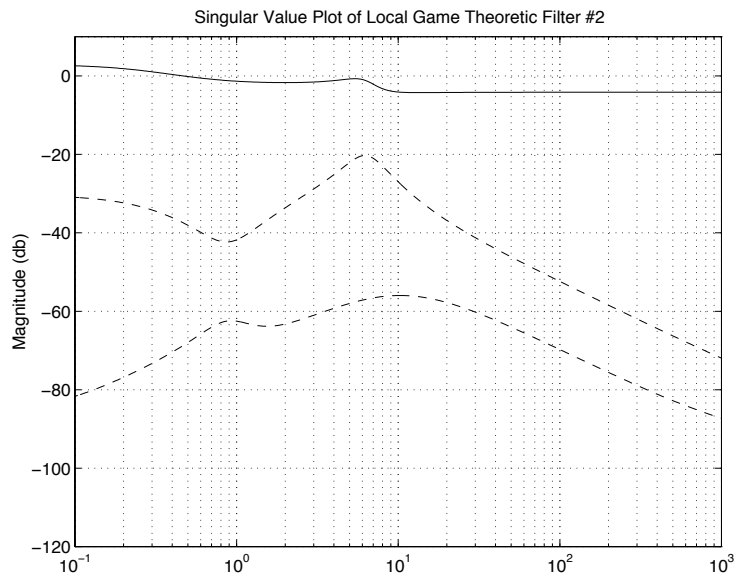


Figure 9.3: Platoon example: signal transmission in the local detection filter on car # 2 (accelerometer fault transmission shown with solid line, nuisance fault transmission shown with dashed line).

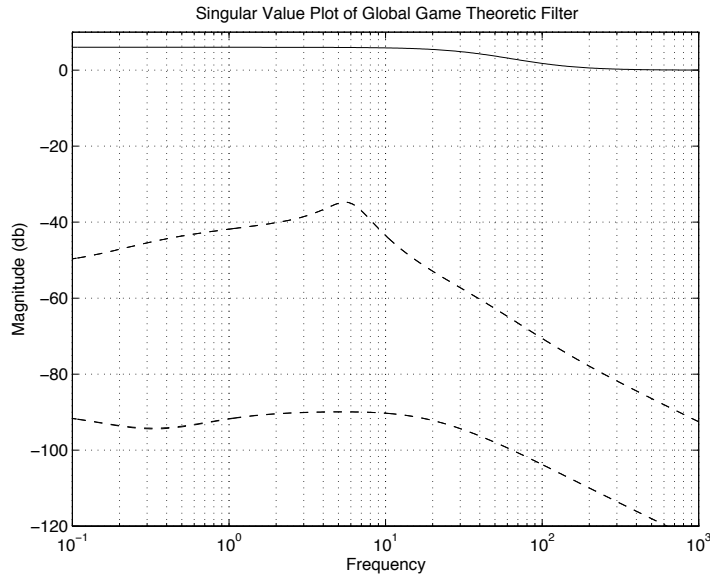


Figure 9.4: Platoon example: signal transmission in the global detection filter (position sensor fault transmission shown with solid line, nuisance fault transmission shown with dashed line).

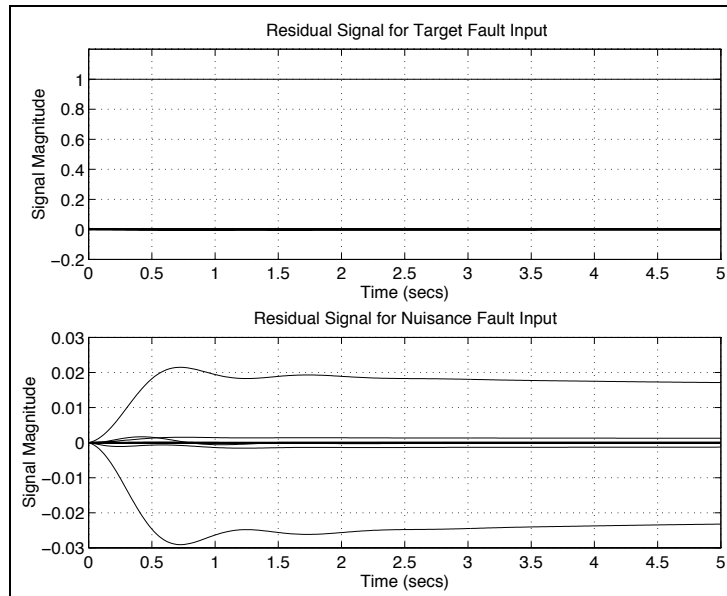


Figure 9.5: Platoon example: failure signal response of the decentralized fault detection filter (Nuisance fault is a step failure in the longitudinal accelerometer on car # 1).

lead to a filter with the performance depicted in Figure 9.3.

Finally, we turn to the global system. The decentralized fault detection filter for range sensor health monitoring in the platoon is found by solving,

$$0 = \Pi^{-1}A^T + A\Pi^{-1} + \frac{1}{\gamma}F_2MF_2^T + \Pi^{-1}C^T(HQH - \gamma V^{-1})C\Pi^{-1}, \quad (9.23)$$

which is simply a variation of (6.54). The weightings,

$$\begin{aligned} \gamma V^{-1} &= I_{17}, & Q &= I_{17}, \\ M &= 100 \times I_8, & \gamma &= 0.18. \end{aligned}$$

were used in the design. The resulting filter has the properties depicted in Figure 9.4. The decentralized estimator should also exhibit this level of performance. As a check, a simple time domain simulation was run comparing the response of the residual signal when the system is driven by the target fault (a step failure of the range sensor) to when it is driven by a nuisance fault (a step failure of the longitudinal accelerometer on Car #1). Because we are using Riccati-based estimators, the blending matrices, G^j , are given by (9.15). The connecting matrices, S^j , are taken to be the pseudo-inverses of E^j . The remaining vectors and matrices that form the decentralized estimation algorithm are as given in Section 9.1. As Figure 9.5 shows, the resulting decentralized fault detection filter does a good job of distinguishing the target fault from the nuisance fault.

It must be noted that we have assumed that the lead car will transmit its measurements, y^1 , its local state estimates, $\hat{\eta}^2$, and the vector, h^1 , back to car #2 so that the latter can form the global estimate via the decentralized estimation algorithm. Transmission issues and limitations, quite obviously, open up the potential for new problems. We have also assumed that each car will have stored on-board the needed Riccati solutions for all likely scenarios.

Multiple Model Adaptive Estimation

A CLASS OF ADAPTIVE ESTIMATION PROBLEMS is considered where an unknown system model is assumed to correspond to one of a number of specified models and the model uncertainty is summarized as a time-varying parametric uncertainty. In particular, we concern ourselves with estimation in linear stochastic systems with time-varying parameters. Early attempts to solve this problem produced the Multiple Model Adaptive Estimation (MMAE) algorithm, first proposed by (Magill 1965) then generalized by (Lainiotis 1976) to form the framework of *partitioned algorithms*. This algorithm addresses the most basic adaptive estimation problem, estimation in a linear stochastic system with time-invariant parametric uncertainty. It is a joint estimation and system identification algorithm with of a bank of Kalman filters, each matched to one hypothesis and an identification subsystem, which may be construed as the dynamics of a sub-optimal multiple hypothesis Wald's Sequential Probability Ratio Test (WSPRT). We denote the underlying dynamics of the WSPRT by F_{ki}^w , which is defined as the posterior probability of hypothesis \mathcal{H}_i conditioned

on the residual history up to t_k . The use of F_{ki}^w is motivated by the implicit assumption that we are dealing with a time-invariant parametric uncertainty. However, as stated in (Athans 1977), there is no rigorous proof that the posterior probability associated with the true model will converge to unity. Moreover, apart from being computationally intensive, this algorithm suffers from *beta dominance* (Menke and Maybeck 1995), which arises out of incorrect system modeling and leads to irregular residuals.

Recently, there have been efforts to improve the performance of the MMAE algorithm (Maybeck and Hanlon 1995). Recall that the recursive relation for the generation of F_{ki}^w does not allow for transitions from one hypothesis to another: It can be shown that if the conditional probability of a particular hypothesis becomes unity/zero, it stays at unity/zero irrespective of what the correct hypothesis is. To avoid this, the recursive relation was modified by upper and lower bounding the conditional probabilities of all hypotheses. Secondly, in an effort to remove beta dominance, the conditional density functions were altered by removing the covariance term from the denominator. The probabilities still sum to one, though the “density” functions are no longer scaled. However, there appears to be no rigorous theoretical justification for both these procedures.

We develop a new algorithm based on a *single* adaptive Kalman filter wherein the time-varying parameters are updated by feeding back the posterior probability of each hypothesis conditioned on the residual process. It is then shown that the expected value of the true posterior probability converges to unity and, under certain assumptions, the expected value of the norm of the difference between the constructed error covariance and the true posteriori error covariance converges to a lower bound. It is also shown that in the presence of modeling errors, the filter converges to the hypothesis which maximizes a certain information function. We also make a comment about the extension of the MMAE algorithm by using the dynamics F_{ki}^s of a multiple hypothesis Shiriyayev sequential probability ratio test (MHSSPRT), which explicitly allows for transitions to occur.

This chapter is organized as follows. In Section 10.1, we form the framework of the time-varying parameter estimation problem. In Section 10.2, we highlight the salient

features of the MMAE scheme. In Section 10.3, we develop the adaptive Kalman filter algorithm and in Section 10.4, we derive the properties of this scheme. In Section 10.5, we compare the two algorithms in various numerical simulations. Finally, in Section 10.6, we conclude by summarizing the adaptive Kalman filter algorithm and its theoretical properties.

10.1 Problem Statement

Consider a linear time-varying stochastic system:

$$x_{k+1} = A_k x_k + b_k + w_k \quad (10.1a)$$

$$y_k = C_k x_k + d_k + v_k \quad (10.1b)$$

wherein $x_k \in \mathbb{R}^n$ is the state, $y_k \in \mathbb{R}^s$ is the measurement, $b_k \in \mathbb{R}^n$ and $d_k \in \mathbb{R}^s$ are bias vectors. Matrices A_k and C_k have the appropriate dimensions. Under each hypothesis \mathcal{H}_i , the process noise $\{w_k\}$ and measurement noise $\{v_k\}$ sequences are white, with the following statistics:

$$v_k \sim \mathcal{N}(0, V_i) \quad A_k = A_{ki} \quad b_k = b_i \quad (10.2)$$

$$w_k \sim \mathcal{N}(0, W_i) \quad C_k = C_{ki} \quad d_k = d_i \quad (10.3)$$

Note that instead of being parameterized, the noise statistics and other model parameters are hypothesized. Clearly they are equivalent.

Now, as a particular application, we can reduce the problem of detection and isolation of the occurrence of a change in a correlated measurement sequence, by assuming an ARMA model for the measurement process. Assuming the AR-coefficients to be time-varying, we can formulate a state-space equivalent of the ARMA process as:

$$x_{k+1} = A_k x_k + b_k + w_k \quad (10.4a)$$

$$y_k = C_k x_k + d_k + v_k \quad (10.4b)$$

wherein $y_k \in \mathbb{R}^s$ is the measurement, $C_k = [y_{k-1} | \dots | y_{k-n}]$ is the measurement matrix, $x_k \in \mathbb{R}^n$ are the AR-coefficients, A_k is a given matrix and b_k and d_k are appropriate bias

vectors. Again, from (10.2–10.3), the process and sensor noise sequences are white with different statistics under different hypotheses.

The problem may be stated as follows. Identify the current system model in minimum time by detecting and isolating a change in the measurement process. As stated earlier, all existing algorithms have an embedded identification subsystem construed as the recursive relation for F_{ki}^w . It is assumed that no change occurs in the measurement process when the test is in progress. However, in our AKF algorithm, we explicitly model the probability of a transition from one hypothesis to another thereby allowing for time-varying hypotheses and using the recursive relation for F_{ki}^s (Malladi and Speyer 1996, Malladi and Speyer 1997). We also extend the MMAE algorithm to time-varying hypotheses by using this F_{ki}^s instead of the bounded F_{ki}^w . Finally, we develop sufficient conditions for the convergence of this adaptive filter structure.

10.2 MMAE Algorithm

The Multiple Model Adaptive Estimation algorithm and its variations are widely applied to linear stochastic system parameter estimation (Athans 1977, Menke and Maybeck 1995). Let there be $L + 1$ linear, discrete-time stochastic dynamic system models, each generating measurements corrupted by white noise. It follows that the available measurement sequence may be assumed to correspond to one of the m different hypotheses. The sensor and process noise statistics vary with each hypothesis. One can then construct a bank of $L + 1$ discrete-time Kalman filters, each matched to one hypothesis, generating a white residual process provided the corresponding hypothesis is the true one. The residual process becomes the input to the recursive relation for F_{ki}^w , which generates the posterior probability of each hypothesis, conditioned on the measurement sequence. This leads to a neat parallel structure shown in Figure 10.1.

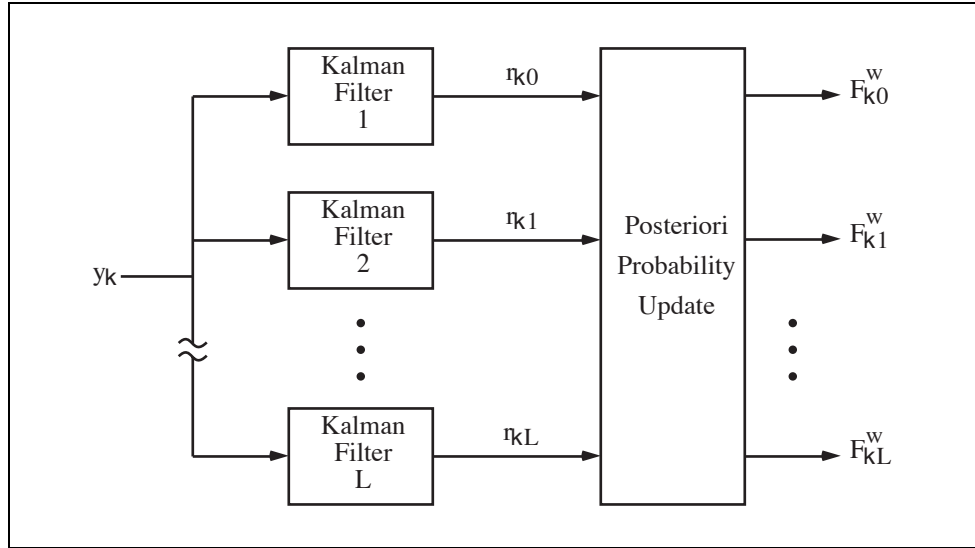


Figure 10.1: Multiple Model Adaptive Estimation - Lainiotis Filters.

The update equations for a generic Kalman filter for hypothesis \mathcal{H}_i are

$$S_{ki} = C_{ki}M_{ki}C_{ki}^T + V_i \quad (10.5a)$$

$$K_{ki} = M_{ki}C_{ki}^T S_{ki}^{-1} \quad (10.5b)$$

$$\hat{x}_{ki} = \bar{x}_{ki} + K_{ki}[y_k - C_{ki}\bar{x}_{ki} - d_{ki}] \quad (10.5c)$$

$$P_{ki} = [I - K_{ki}C_{ki}]M_{ki} \quad (10.5d)$$

$$r_{ki} = y_k - C_{ki}\bar{x}_{ki} - d_{ki} \quad (10.5e)$$

$$\mathcal{R}_{ki} \triangleq [r_{1i} \dots r_{ki}] \quad (10.5f)$$

$$\mathcal{R}_k \triangleq [\mathcal{R}_{k1} \dots \mathcal{R}_{kM}] \quad (10.5g)$$

wherein M_{ki} is the apriori error covariance matrix, P_{ki} is the posteriori covariance matrix, \bar{x}_{ki} is the apriori state estimate and \hat{x}_{ki} is the posteriori state estimate at time t_k . The propagation equations are

$$\bar{x}_{k+1,i} = A_{ki}\hat{x}_{ki} + b_{ki} \quad (10.6a)$$

$$M_{k+1,i} = A_{ki}P_{ki}A_{ki}^T + W_i \quad (10.6b)$$

In the cited literature and in the figure, F_{ki}^w is generated. However, allowing transitions from one hypothesis to another, we generate F_{ki}^s .

$$F_{kj}^s \triangleq P(\mathcal{H}_j/\mathcal{R}_k)$$

The overall posteriori state estimate and error covariance become

$$x_k^* = \sum_j \hat{x}_{kj} F_{kj}^s \quad (10.7a)$$

$$P_k^* = \sum_j \{P_{kj} + (x_k^* - \hat{x}_{kj})(x_k^* - \hat{x}_{kj})^T\} F_{kj}^s \quad (10.7b)$$

Remark 21. The noise characteristics of each filter are time-invariant. ◀

Remark 22. As the number of hypotheses grows, the algorithm becomes computationally intensive, as one needs to compute all the time-varying filter gains. To alleviate this problem, sometimes the steady-state gains of each Kalman filter are used, instead of the time-varying gains (Athans 1977). But this can lead to convergence to the wrong hypothesis. ◀

Remark 23. There is no rigorous proof that in the posterior probability associated with the correct hypothesis will converge to unity. ◀

Remark 24. The recursive relation for F_{ki}^s or F_{ki}^w assumes that the residual sequence is conditionally independent, but when \mathcal{H}_i is true, \mathcal{R}_{kj} is not conditionally independent for all $j \neq i$. Hence the generated F_{ki}^w or F_{ki}^s is always wrong no matter what the correct hypothesis is. ◀

Remark 25. Under certain circumstances (Athans 1977), the algorithm leads to the convergence to the wrong hypothesis. This phenomenon has been termed as *beta dominance* in (Menke and Maybeck 1995). ◀

10.2.1 Beta Dominance

Let \mathcal{H}_i be true. Then, one would expect the residual process r_{ki} to be small while the residuals of the mismatched Kalman filters to be large. If for some reason this doesn't

happen, for example, if the wrong noise statistics are chosen, it can be shown that the posterior probability of \mathcal{H}_i might actually decrease, depending upon S_{kj} for all j . Refer to Section 10.7.1 for the proof.

10.3 Adaptive Kalman Filter Algorithm

We formulate an algorithm based on a structure which uses a single adaptive Kalman filter in conjunction with the recursive relation for F_{ki}^s . Consider Figure 10.2. An approximate posterior probability F_{ki} of each hypothesis conditioned on the residual history is generated and fed back to the filter. All the bias vectors and system matrices, including the process and sensor noise statistics, are updated in the following way:

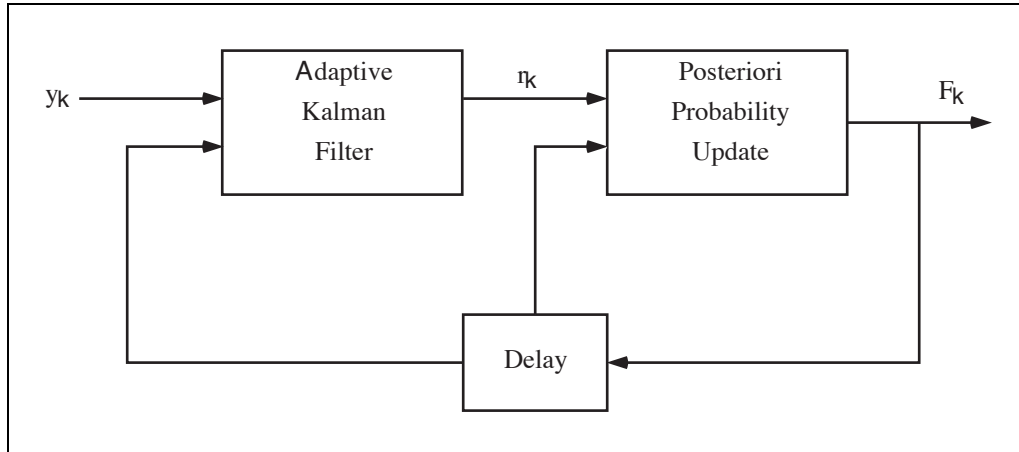


Figure 10.2: Adaptive Kalman Filter Algorithm.

$$v_k \sim \mathcal{N}(0, V_k) \quad w_k \sim \mathcal{N}(0, W_k) \quad \mathcal{R}_k \triangleq [r_0 \ r_1 \ \dots \ r_k] \quad (10.8)$$

$$F_{kj} \triangleq \text{approximate } F_{kj}^s \quad F_k \triangleq [F_{k0} \ F_{k1} \ \dots \ F_{kL}]^T \quad (10.9)$$

$$A_k = \sum_j F_{kj} A_j \quad b_k = \sum_j F_{kj} b_j \quad W_k = \sum_j F_{kj} W_j \quad (10.10)$$

$$C_k = \sum_j F_{k-1,j} C_j \quad d_k = \sum_j F_{k-1,j} d_j \quad V_k = \sum_j F_{k-1,j} V_j \quad (10.11)$$

We derive sufficient conditions for the convergence of F_{kj} to F_{kj}^s in the next section. As mentioned earlier, the structure of the MMAE algorithm never permits the exact calculation of F_{ki}^s or F_{ki}^w . Note that A_k , b_k and W_k are updated using F_{kj} , as it is already available. That is not the case for C_k , d_k and V_k . However, this does not produce any difference in the theoretical results presented later on in Section 10.4. The filter equations remain the same except that we remove the subscript i from Equations (10.5–10.6). Therefore

$$S_k = C_k M_k C_k^T + V_k \quad (10.12a)$$

$$K_k = M_k C_k^T S_k^{-1} \quad (10.12b)$$

$$\hat{x}_k = \bar{x}_k + K_k [y_k - C_k \bar{x}_k - d_k] \quad (10.12c)$$

$$P_k = [I - K_k C_k] M_k \quad (10.12d)$$

$$r_k = y_k - C_k \bar{x}_k - d_k \quad (10.12e)$$

$$\bar{x}_{k+1} = A_k \hat{x}_k + b_k \quad (10.12f)$$

$$M_{k+1} = A_k P_k A_k^T + W_k \quad (10.12g)$$

The true error covariance, \tilde{M}_k , of this sub-optimal state estimate is not computed in this algorithm as it requires the knowledge of the correct hypothesis. Instead, as shown later on, it is approximated by M_k . Of course, if \mathcal{H}_i is true, we can compute \tilde{M}_k in the following way:

$$\begin{aligned} \hat{e}_k &\triangleq x_k - \hat{x}_k & \bar{e}_k &\triangleq x_k - \bar{x}_k & \bar{m}_k^e &\triangleq E\{\bar{e}_k/\mathcal{R}_k\} \\ m_k &\triangleq E\{x_k/\mathcal{R}_k\} & \hat{m}_k^e &\triangleq E\{\hat{e}_k/\mathcal{R}_k\} & \bar{E}_k &\triangleq E\{x_k \bar{e}_k^T/\mathcal{R}_k\} \\ X_k &\triangleq E\{x_k x_k^T/\mathcal{R}_k\} & \hat{E}_k &\triangleq E\{x_k \hat{e}_k^T/\mathcal{R}_k\} & \bar{E}_k &\triangleq E\{x_k \bar{e}_k^T/\mathcal{R}_k\} \\ \tilde{P}_k &\triangleq E\{\hat{e}_k \hat{e}_k^T/\mathcal{R}_k\} & \bar{E}_k &\triangleq E\{x_k \bar{e}_k^T/\mathcal{R}_k\} & & \end{aligned} \quad (10.13)$$

The error update and propagation become

$$\hat{e}_k = (I - K_k C_k) \bar{e}_k - K_k (C_{ki} - C_k) x_k - K_k (d_{ki} - d_k) - K_k v_k \quad (10.14)$$

$$\bar{e}_{k+1} = A_k \hat{e}_k + (A_{ki} - A_k) x_k + (b_{ki} - b_k) + w_k \quad (10.15)$$

and the difference equations become

$$\begin{aligned}\tilde{P}_k &= (I - K_k C_k) \tilde{M}_k (I - K_k C_k)^T + K_k (C_{ki} - C_k) X_k (C_{ki} - C_k)^T K_k^T \\ &\quad + K_k (d_{ki} - d_k) (d_{ki} - d_k)^T K_k^T + K_k V_i K_k^T \\ &\quad - 2(I - K_k C_k) \bar{E}_k^T (C_{ki} - C_k)^T K_k^T - 2(I - K_k C_k) \bar{m}_k^e (d_{ki} - d_k)^T K_k^T\end{aligned}\quad (10.16)$$

$$\begin{aligned}\tilde{M}_{k+1} &= A_k \tilde{P}_k A_k^T + (A_{ki} - A_k) X_k (A_{ki} - A_k)^T + (b_{ki} - b_k) (b_{ki} - b_k)^T + W_i \\ &\quad + 2A_k \hat{E}_k^T (A_{ki} - A_k)^T + 2A_k \hat{m}_k^e (b_{ki} - b_k)^T \\ &\quad + 2(A_{ki} - A_k) m_k (b_{ki} - b_k)^T\end{aligned}\quad (10.17)$$

$$X_{k+1} = A_{ki} X_k A_{ki}^T + b_{ki} b_{ki}^T + W_i + 2A_{ki} m_k b_{ki}^T \quad (10.18)$$

$$\hat{E}_k = \bar{E}_k (I - K_k C_k)^T - X_k (C_{ki} - C_k)^T K_k^T - m_k K_k (d_{ki} - d_k) \quad (10.19)$$

$$\begin{aligned}\bar{E}_{k+1} &= A_{ki} \hat{E}_k A_{ki}^T + A_{ki} X_k (A_{ki} - A_k)^T + A_k \hat{m}_k^e b_{ki}^T \\ &\quad + A_{ki} m_k (b_{ki} - b_k)^T + (A_{ki} - A_k) m_k b_{ki}^T + b_{ki} (b_{ki} - b_k)^T + W_i\end{aligned}\quad (10.20)$$

$$m_{k+1} = A_{ki} m_k + b_{ki} \quad (10.21)$$

$$\hat{m}_k^e = (I - K_k C_k) \bar{m}_k^e - K_k (C_{ki} - C_k) m_k - K_k (d_{ki} - d_k) \quad (10.22)$$

$$\bar{m}_{k+1}^e = A_k \hat{m}_k^e + (A_{ki} - A_k) m_k + (b_{ki} - b_k) \quad (10.23)$$

The initial conditions become:

$$\begin{aligned}X_0 &= \tilde{P}_0 + \hat{x}_0 \hat{x}_0^T & \hat{E}_0 &= \tilde{P}_0 \\ m_0 &= \hat{x}_0 & \hat{m}_0^e &= 0\end{aligned}$$

These equations are computationally intensive, but can be computed off-line to assess the performance of the AKF algorithm for specific applications. In certain cases, the off-line computation becomes necessary to analyze the steady-state behavior of the AKF algorithm, in particular, its convergence to the correct hypothesis.

Given \mathcal{H}_i , the true distribution of r_k is

$$\tilde{f}_{ki}(r_k) \triangleq f_k(r_k / \mathcal{H}_i, \mathcal{R}_{k-1}) \quad (10.24)$$

$$E[r_k / \mathcal{H}_i, \mathcal{R}_{k-1}] = (C_{ki} - C_k) \bar{x}_k + (d_{ki} - d_k) \triangleq \tilde{b}_{ki} \quad (10.25)$$

$$E[r_k r_k^T / \mathcal{H}_i, \mathcal{R}_{k-1}] = C_{ki} \tilde{M}_k C_{ki}^T + V_i \triangleq \tilde{S}_{ki} \quad (10.26)$$

Therefore,

$$(r_k/\mathcal{H}_i, \mathcal{R}_{k-1}) \sim \mathcal{N}(\tilde{b}_{ki}, \tilde{S}_{ki}) \quad (10.27)$$

However, since the correct hypothesis is unknown, the AKF algorithm is designed to approximate the true error covariance \tilde{M}_k with the error “covariance” M_k , which is computed on-line from (10.12d) and (10.12g). In Section 10.4, this assumption is justified by showing that under certain conditions, $E\{M_k/\mathcal{H}_i\} \rightarrow M_{ki}$, where M_{ki} is the apriori error covariance corresponding to the i^{th} filter in the MMAE algorithm. It is also shown that $E\{M_k/\mathcal{H}_i\} \rightarrow M_k^*$, wherein M_k^* is the exact apriori error covariance derived from (10.7b) and $E\{M_k/\mathcal{H}_i\} \rightarrow \tilde{M}_k$. At each t_k , we assume

$$\begin{aligned} E[r_k/\mathcal{H}_i, \mathcal{R}_{k-1}] &= 0 \\ E[r_k r_k^T/\mathcal{H}_i, \mathcal{R}_{k-1}] &= C_{ki} M_k C_{ki}^T + V_i \triangleq \Lambda_{ki} \end{aligned} \quad (10.28)$$

Under the Gaussian assumption, we explicitly construct the density function $f_{ki}(\cdot)$ as

$$\begin{aligned} f_{ki}(r_k) &\triangleq \text{Approx. } \tilde{f}_{ki}(r_k) \\ (r_k/\mathcal{H}_i, \mathcal{R}_{k-1}) &\sim \mathcal{N}(0, \Lambda_{ki}) \end{aligned} \quad (10.29)$$

We make a crucial observation that $\{r_k\}$ is no longer an independent residual process. Now, F_{ki}^s requires the knowledge of the density functions $\tilde{f}_{ki}(\cdot)$. Since we approximate these functions with $f_{ki}(\cdot)$, F_{ki}^s has been approximated by F_{ki} .

Note that, by removing the parallel structure of the MMAE approach while retaining the time-varying filter gain, the AKF algorithm is computationally less intensive, especially if the number of hypotheses is large. Further, following the argument used in Section 10.7.1, it can be shown that beta dominance cannot exist in this structure as there is only one residual process here.

10.4 Performance of AKF Algorithm

The following sections consider the convergence and robustness properties of the AKF algorithm and prove the following:

- If hypothesis \mathcal{H}_i is true, then the generated posterior probability of \mathcal{H}_j (called F_{kj}) decreases monotonically in time for all $j \neq i$, that is, $F_{k+1,j} \leq F_{kj} \quad \forall j \neq i$.
- If hypothesis \mathcal{H}_i is true, then the posterior error covariance P_k of the AKF algorithm converges to P_{ki} of the “correct” filter from the MMAE algorithm.
- If hypothesis \mathcal{H}_i is true but not included in the set of probable hypotheses, $\Theta \triangleq \{\mathcal{H}_j\}$, then, the generated posterior probability converges to that hypothesis $\mathcal{H}_m \in \Theta$ which maximizes a particular information function.

10.4.1 Underlying Assumptions of MHSSPRT

We briefly rederive the MHSSPRT (Malladi and Speyer 1996, Malladi and Speyer 1997) by defining the following notation:

- $\pi_i \triangleq P(\mathcal{H}_i)$
- $\tilde{p}_i \triangleq$ Apriori probability of change from \mathcal{H}_0 to \mathcal{H}_i from t_k to t_{k+1} , for all k
- $f_{ki}(\cdot) \triangleq$ Approximate probability density function of r_k conditioned on \mathcal{H}_i and \mathcal{R}_{k-1}
- $f_{k0}(\cdot) \triangleq$ Approximate probability density function of r_k conditioned on \mathcal{H}_0 and \mathcal{R}_{k-1}
- $L + 1 \triangleq$ Number of hypotheses
- $\theta_i \triangleq$ Time of occurrence of \mathcal{H}_i

At stage t_1

$$P(\theta_i \leq t_1/r_1) = \frac{P(r_1/\theta_i \leq t_1)P(\theta_i \leq t_1)}{P(r_1)} \quad (10.30)$$

$$\begin{aligned} P(r_1) &= \sum_{i=1}^L P(r_1/\theta_i \leq t_1)P(\theta_i \leq t_1) + P(r_1/\theta_i > t_1)P(\theta_i > t_1) \\ P(\theta_i \leq t_1) &= P(\theta_i \leq t_0) + P(\theta_i = t_1/\theta_i > t_0) \\ &= \pi_i + \tilde{p}_i(1 - \pi_i) \\ P(r_1/\theta_i \leq t_1) &= f_{1i}(r_1)dr_1 \end{aligned} \quad (10.31)$$

Strictly, (10.31) denotes the probability that the measurement lies between r_1 and $r_1 + dr_1$ given the occurrence of \mathcal{H}_i at or before t_1 .

$$\sum_{i=1}^L P(\theta_i > t_1) = 1 - \sum_{i=1}^L P(\theta_i \leq t_1)$$

From (10.30), we get:

$$F_{1,i} = \frac{[\pi_i + \tilde{p}_i(1 - \pi_i)]f_{1i}(r_1)}{\sum_{i=1}^L [\pi_i + \tilde{p}_i(1 - \pi_i)]f_{1i}(r_1) + [1 - \sum_{i=1}^L \pi_i + \tilde{p}_i(1 - \pi_i)]f_{10}(r_1)}$$

At stage t_2

$$P(\theta_i \leq t_2/\mathcal{R}_2) = \frac{P(\mathcal{R}_2/\theta_i \leq t_2)P(\theta_i \leq t_2)}{P(\mathcal{R}_2)} \quad (10.32)$$

$$P(r_2/\theta_i \leq t_2, r_1) = f_{2i}(r_2)dr_2 \quad (10.33)$$

$$P(r_1/\theta \leq t_2) = \frac{P(\theta_i \leq t_2/r_1)P(r_1)}{P(\theta_i \leq t_2)} \quad (10.34)$$

$$P(\mathcal{R}_2) = P(r_2/r_1)P(r_1) \quad (10.35)$$

Since from (10.29), we know the density function $f_k(r_k/\mathcal{H}_i, \mathcal{R}_{k-1})$ for all k , from (10.32):

$$P(\theta_i \leq t_2/\mathcal{R}_2) = \frac{P(r_2/\theta_i \leq t_2, r_1)P(r_1/\theta_i \leq t_2)P(\theta_i \leq t_2)}{P(\mathcal{R}_2)}$$

Now, from (10.33), (10.34) and (10.35) we have

$$P(\theta_i \leq t_2/\mathcal{R}_2) = \frac{f_{2i}(r_2)P(\theta_i \leq t_2/r_1)dr_2}{P(r_2/r_1)} \quad (10.36)$$

$$P(\theta_i \leq t_2/r_1) = P(\theta_i \leq t_1/r_1) + P(\theta_i = t_2/\theta_i > t_0, r_1) \quad (10.37)$$

$$= F_{1,i} + \tilde{p}_i(1 - F_{1,i})$$

$$\begin{aligned} P(r_2/r_1) &= \sum_{i=1}^L P(r_2/\theta_i \leq t_2, r_1)P(\theta_i \leq t_2/r_1) + P(r_2/\theta_i, r_1 > t_2)P(\theta_i > t_2/r_1) \\ &= \sum_{i=1}^L [F_{1,i} + \tilde{p}_i(1 - F_{1,i})] f_{2i}(r_2)dr_2 \\ &\quad + \left[1 - \sum_{i=1}^L F_{1,i} + \tilde{p}_i(1 - F_{1,i}) \right] f_{20}(r_2)dr_2 \end{aligned} \quad (10.38)$$

Clearly, by induction, we can now write the recursive relation for $F_{k+1,i}$ in terms of $F_{k,i}$ as

$$F_{k+1,i} = \frac{[F_{k,i} + \tilde{p}_i(1 - F_{k,i})] f_{k+1,i}(r_{k+1})}{\sum_{i=1}^L [F_{k,i} + \tilde{p}_i(1 - F_{k,i})] f_{k+1,i}(r_{k+1}) + \left[1 - \sum_{i=1}^L F_{k,i} + \tilde{p}_i(1 - F_{k,i})\right] f_{k+1,0}(r_{k+1})} \quad (10.39)$$

$$F_{0,i} = \pi_i \quad (10.40)$$

Nowhere have we made any assumptions about the independence of the residual process. From (10.29), we explicitly construct $f_{ki}(\cdot)$ for all i and at each t_k . This approximates F_{ki}^s by F_{ki} as mentioned in the earlier section. In the next section, we derive sufficient conditions for the convergence of F_{ki} and the associated error covariance.

10.4.2 Convergence of the Posterior Probability

We seek to prove that when \mathcal{H}_i is true, the posterior probabilities of all hypotheses \mathcal{H}_j for all $j \neq i$ decrease. We define the following:

$$\mathcal{F} \triangleq \{f(r/\mathcal{H}) : \mathcal{H} \in \Theta\} \quad (10.41)$$

$$\mathcal{J}_{ji}(k) \triangleq E[\ln\{f_{kj}(r_k)\} / \mathcal{H}_i, \mathcal{R}_{k-1}] \quad (10.42)$$

$$\rho_{jmi} \triangleq \max_k E \left[\left[\frac{f_{kj}(r_k)}{f_{km}(r_k)} \right]^t / \mathcal{H}_i, \mathcal{R}_{k-1} \right] \quad \text{for some } t \in (0, 1) \quad (10.43)$$

$$\triangleq \max_k \rho_{jmi}(\mathcal{R}_{k-1})$$

Assumption 10.1. The family of density functions \mathcal{F} is identifiable, that is,

$$f(r/\mathcal{H}_i) = f(r/\mathcal{H}_j) \quad \Leftrightarrow \quad \theta_i = \theta_j \quad \forall r$$

This assumption is invoked to prove Claim 10.1.

Claim 10.1. By Assumption 10.1, beta dominance cannot exist in the AKF algorithm.

Proof. Refer to Section 10.7.2. ◀

In an effort to illustrate the classes of problems for which \mathcal{J}_{ji} is an information function, we consider a time-varying ARMA process of order n , wherein the measurement noise is different for each hypothesis. Therefore under each hypothesis \mathcal{H}_i , the process noise $\{w_k\}$ and measurement noise $\{v_k\}$ sequences are white, with the following statistics:

$$\begin{aligned} v_k &\sim \mathcal{N}(0, V_i) & A_k &= A_k & b_k &= b_k \\ w_k &\sim \mathcal{N}(0, W_k) & C_k &= C_k & d_k &= d_k \end{aligned} \quad (10.44)$$

wherein $C_k = [y_{k-1} | \dots | y_{k-n}]$ is the measurement matrix. We now prove the following lemma.

Lemma 10.2. Let \mathcal{H}_i be true. Then, for the ARMA process shown in (10.44):

- If $V_i > V_k$ and $\tilde{M}_k \geq M_k$, then $\tilde{M}_{k+1} > M_{k+1} \quad \forall k$.
- If $V_i < V_k$ and $\tilde{M}_k \leq M_k$, then $\tilde{M}_{k+1} < M_{k+1} \quad \forall k$.

Proof. From (10.16), (10.17), (10.12d) and (10.12g)

$$\begin{aligned} \tilde{P}_k &= (I - K_k C_k) \tilde{M}_k (I - K_k C_k)^T + K_k V_i K_k^T \\ P_k &= (I - K_k C_k) M_k (I - K_k C_k)^T + K_k V_k K_k^T \\ \tilde{M}_{k+1} &= A_k \tilde{P}_k A_k^T + W_k \\ M_{k+1} &= A_k P_k A_k^T + W_k \end{aligned}$$

Therefore

$$\begin{aligned} \tilde{P}_k - P_k &= (I - K_k C_k) (\tilde{M}_k - M_k) (I - K_k C_k)^T + K_k (V_i - V_k) K_k^T \\ \tilde{M}_{k+1} - M_{k+1} &= A_k (\tilde{P}_k - P_k) A_k \end{aligned}$$

from which the conclusion follows

$$\begin{aligned} V_i > V_k, \tilde{M}_k \geq M_k &\Rightarrow \tilde{M}_{k+1} > M_{k+1} \quad \forall k \\ V_i < V_k, \tilde{M}_k \leq M_k &\Rightarrow \tilde{M}_{k+1} < M_{k+1} \quad \forall k \end{aligned}$$

As a consequence, from (10.12a), (10.26) and (10.28)

$$\begin{aligned} V_i > V_j &\Rightarrow \Lambda_{kj} < \Lambda_{ki} < \tilde{S}_{ki} & \forall k \\ V_i < V_j &\Rightarrow \Lambda_{kj} > \Lambda_{ki} > \tilde{S}_{ki} & \forall k \end{aligned} \quad (10.45)$$

We could consider another class of problems similar to (10.44) wherein the hypotheses differ only in the process noise statistics, that is, under \mathcal{H}_i

$$w_k \sim \mathcal{N}(0, W_i) \quad (10.46)$$

We now prove the following lemma.

Lemma 10.3. Let \mathcal{H}_i be true. Then, for the process shown in (10.46)

- If $W_i > W_k$ and $\tilde{M}_k \geq M_k$, then $\tilde{M}_{k+1} > M_{k+1} \quad \forall k$.
- If $W_i < W_k$ and $\tilde{M}_k \leq M_k$, then $\tilde{M}_{k+1} < M_{k+1} \quad \forall k$.

Proof. The proof is very similar to the one of Lemma 10.2. From (10.16), (10.17), (10.12d) and (10.12g)

$$\begin{aligned} \tilde{P}_k &= (I - K_k C_k) \tilde{M}_k (I - K_k C_k)^T + K_k V_k K_k^T \\ P_k &= (I - K_k C_k) M_k (I - K_k C_k)^T + K_k V_k K_k^T \\ \tilde{M}_{k+1} &= A_k \tilde{P}_k A_k^T + W_i \\ M_{k+1} &= A_k P_k A_k^T + W_k \end{aligned}$$

Therefore

$$\begin{aligned} \tilde{P}_k - P_k &= (I - K_k C_k) (\tilde{M}_k - M_k) (I - K_k C_k)^T \\ \tilde{M}_{k+1} - M_{k+1} &= A_k (\tilde{P}_k - P_k) A_k^T + (W_i - W_k) \end{aligned}$$

from which the conclusion follows

$$\begin{aligned} W_i > W_k, \tilde{M}_k \geq M_k &\Rightarrow \tilde{M}_{k+1} > M_{k+1} & \forall k \\ W_i < W_k, \tilde{M}_k \leq M_k &\Rightarrow \tilde{M}_{k+1} < M_{k+1} & \forall k \end{aligned}$$



So, from (10.12a), (10.26) and (10.28):

$$\begin{aligned} W_i > W_j &\Rightarrow \Lambda_{kj} < \Lambda_{ki} < \tilde{S}_{ki} & \forall k \\ W_i < W_j &\Rightarrow \Lambda_{kj} > \Lambda_{ki} > \tilde{S}_{ki} & \forall k \end{aligned}$$

These results are used in proving the following claim.

Claim 10.4. If the state estimate bias is sufficiently small and

$$\Lambda_{kj} < \Lambda_{ki} < \tilde{S}_{ki} \quad \text{or} \quad \Lambda_{kj} > \Lambda_{ki} > \tilde{S}_{ki} \quad \forall k$$

then \mathcal{J}_{ji} is an information function. Therefore, when \mathcal{H}_i is true:

$$\mathcal{J}_{ii}(k) > \mathcal{J}_{ji}(k) \quad \forall j \neq i, \quad \forall k \quad (10.47)$$

Proof. See Section 10.7.3. ◀

Remark 26. Claim 10.4 assumes that convergence to the wrong hypothesis has occurred and proves that under certain conditions, the filter cannot remain in the wrong hypothesis. The conditions spelt out are sufficient but not necessary. Moreover for the processes shown in (10.44) and (10.46), the state estimate is unbiased and from Lemmas 10.2 and 10.3, Claim 10.4 is always valid. ◀

Lemma 10.5. Let \mathcal{H}_i be true and $\mathcal{H}_m \in \Theta$ be such that:

$$\mathcal{J}_{mi}(k) \triangleq \max_j \mathcal{J}_{ji}(k) \quad \forall \mathcal{H}_j \in \Theta \quad \forall k \quad (10.48)$$

Then

$$\rho_{jmi} < 1 \quad \forall j \neq m$$

Proof. See Section 10.7.4. ◀

For the classes of problems that we consider, in view of Claim 10.4 and Lemma 10.5, if $\mathcal{H}_i \in \Theta$ then $\mathcal{H}_i \equiv \mathcal{H}_m$ and

$$\rho_{jii} < 1 \quad (10.49)$$

From now on, we only consider the classes of problems for which Claim 10.4 is valid. We now proceed to prove the following theorem.

Theorem 10.6. Let the family \mathcal{F} be identifiable and $\mathcal{H}_i \in \Theta$ be true. Then

$$E[F_{k,j}/\mathcal{H}_i] < E[F_{k-1,j}/\mathcal{H}_i] \quad \forall j \neq i \quad (10.50)$$

Proof. Let hypothesis $\mathcal{H}_i \in \Theta$ be true. Since $F_{kj} \leq 1$, we have

$$F_{kj} \leq F_{kj}^t \quad \text{for some } t \in (0, 1) \quad (10.51)$$

This is a crucial observation and is invoked to use $\rho_{jii} < 1$ from (10.49). All the terms in the denominator of the recursive relation (10.40) are positive. Therefore we get

$$\begin{aligned} F_{kj} &\leq \frac{[F_{k-1,j} + \tilde{p}_j(1 - F_{k-1,j})] f_{kj}(r_k)}{[F_{k-1,i} + \tilde{p}_i(1 - F_{k-1,i})] f_{ki}(r_k)} \\ \phi_{ji} &\triangleq \frac{F_{k-1,j} + \tilde{p}_j(1 - F_{k-1,j})}{F_{k-1,i} + \tilde{p}_i(1 - F_{k-1,i})} \end{aligned} \quad (10.52)$$

We note that the density functions $f_{kj}(\cdot)$ are the approximate conditional density functions as defined in (10.29). Assume that $\tilde{p}_j = \tilde{p}$ for all j . Let

$$F_{k-1,j} \geq F_{k-1,i} \quad \forall j \neq i, \forall k \leq N$$

Then

$$\begin{aligned} \phi_{ji} &= \frac{\tilde{p} + (1 - \tilde{p})F_{k-1,j}}{\tilde{p} + (1 - \tilde{p})F_{k-1,i}} \\ &= \frac{F_{k-1,j}}{F_{k-1,i}} \cdot \frac{(1 - \tilde{p}) + \frac{\tilde{p}}{F_{k-1,j}}}{(1 - \tilde{p}) + \frac{\tilde{p}}{F_{k-1,i}}} \\ &\leq \frac{F_{k-1,j}}{F_{k-1,i}} \end{aligned} \quad (10.53)$$

From (10.51), (10.52), (10.53):

$$\begin{aligned}
F_{kj} &\leq \left[\frac{F_{k-1,j}}{F_{k-1,i}} \right]^t \left[\frac{f_{kj}(r_k)}{f_{ki}(r_k)} \right]^t \\
&\leq \left[\frac{F_{k-2,j}}{F_{k-2,i}} \right]^t \left[\frac{f_{k-1,j}(r_{k-1})}{f_{k-1,i}(r_{k-1})} \right]^t \left[\frac{f_{kj}(r_k)}{f_{ki}(r_k)} \right]^t \\
&\leq \left[\frac{\pi_j}{\pi_i} \right]^t \left[\frac{f_{1j}(r_1)}{f_{1i}(r_1)} \right]^t \cdots \left[\frac{f_{kj}(r_k)}{f_{ki}(r_k)} \right]^t
\end{aligned} \tag{10.54}$$

We note that $f_{ki}(r_k)$ are the constructed density functions $f_k(r_k/\mathcal{H}_i, \mathcal{R}_{k-1})$ in (10.26). Take the expectation conditioned on \mathcal{H}_i

$$\begin{aligned}
E[F_{kj}/\mathcal{H}_i] &\leq \left[\frac{\pi_j}{\pi_i} \right]^t E \left[\left[\frac{f_{1j}(r_1)}{f_{1i}(r_1)} \right]^t \cdots \left[\frac{f_{kj}(r_k)}{f_{ki}(r_k)} \right]^t / \mathcal{H}_i \right] \\
&= \left[\frac{\pi_j}{\pi_i} \right]^t \int \left[\frac{f_{1j}(r_1)}{f_{1i}(r_1)} \right]^t \cdots \left[\frac{f_{kj}(r_k)}{f_{ki}(r_k)} \right]^t \tilde{f}_{ki}(\mathcal{R}_k/\mathcal{H}_i) d\mathcal{R}_k \\
&\triangleq \left[\frac{\pi_j}{\pi_i} \right]^t I_k
\end{aligned} \tag{10.55}$$

where I_k is the integral. Now

$$\begin{aligned}
\tilde{f}_{ki}(\mathcal{R}_k/\mathcal{H}_i) &= \tilde{f}_{ki}(r_k/\mathcal{R}_{k-1}, \mathcal{H}_i) \tilde{f}_{k-1,i}(r_{k-1}/\mathcal{R}_{k-2}, \mathcal{H}_i) \cdots \tilde{f}_{1i}(r_1/\mathcal{H}_i) \\
I_k &= \int \left[\frac{f_{1j}(r_1)}{f_{1i}(r_1)} \right]^t \cdots \left[\frac{f_{k-1,j}(r_{k-1})}{f_{k-1,i}(r_{k-1})} \right]^t \tilde{f}_{k-1,i}(\mathcal{R}_{k-1}/\mathcal{H}_i) d\mathcal{R}_{k-1} \\
&\quad \times \int \left[\frac{f_{kj}(r_k)}{f_{ki}(r_k)} \right]^t \tilde{f}_{ki}(r_k/\mathcal{R}_{k-1}, \mathcal{H}_i) dr_k \\
&= \int \left[\frac{f_{1j}(r_1)}{f_{1i}(r_1)} \right]^t \cdots \left[\frac{f_{k-1,j}(r_{k-1})}{f_{k-1,i}(r_{k-1})} \right]^t \tilde{f}_{k-1,i}(\mathcal{R}_{k-1}/\mathcal{H}_i) d\mathcal{R}_{k-1} \rho_{jii}(\mathcal{R}_{k-1}) \\
&\leq I_{k-1} \rho_{jii}
\end{aligned}$$

Therefore, from (10.55):

$$E[F_{k,j}/\mathcal{H}_i] \leq \left[\frac{\pi_j}{\pi_i} \right]^t \rho_{jii}^k \tag{10.56}$$

From Claim 10.4 and Lemma 10.5, $\rho_{jii} < 1$. Hence, the posterior probability rapidly decreases as $k \rightarrow \infty$ and the assumption of $F_{k-1,j} \geq F_{k-1,i}$ for all $j \neq i$ and for all k is no

longer valid. Let $F_{k-1,j} \leq F_{k-1,i}$ for all $j \neq i$ and for all $k \geq N$. Then

$$\begin{aligned}
\phi_{ji} &= \frac{F_{k-1,j}}{F_{k-1,i}} \cdot \frac{1 + \tilde{p}(1/F_{k-1,j} - 1)}{1 + \tilde{p}(1/F_{k-1,i} - 1)} \\
&\leq \frac{F_{k-1,j}}{F_{k-1,i}} [1 + \tilde{p}(1/F_{k-1,j} - 1)] \\
&\leq \frac{F_{k-1,j}}{F_{k-1,i}} + \tilde{p} \frac{(1 - F_{k-1,j})}{F_{k-1,i}} \\
&\leq \frac{F_{k-1,j}}{F_{k-1,i}} + \tilde{p}
\end{aligned} \tag{10.57}$$

Following the argument used above, we get:

$$\begin{aligned}
F_{kj}^t &\leq \left(\frac{F_{k-1,j}}{F_{k-1,i}} + \tilde{p} \right)^t \left[\frac{f_{kj}(r_k)}{f_{ki}(r_k)} \right]^t \\
&\leq \left[\left(\frac{F_{k-1,j}}{F_{k-1,i}} \right)^t + \tilde{p}^t \right] \left[\frac{f_{kj}(r_k)}{f_{ki}(r_k)} \right]^t \\
\left(\frac{F_{k-1,j}}{F_{k-1,i}} \right)^t &\leq \left[\left(\frac{F_{k-2,j}}{F_{k-2,i}} \right)^t + \tilde{p}^t \right] \left[\frac{f_{k-1,j}(r_{k-1})}{f_{k-1,i}(r_{k-1})} \right]^t
\end{aligned}$$

Therefore:

$$F_{kj}^t \leq \left[\frac{F_{k-2,j}}{F_{k-2,i}} \right]^t \left[\frac{f_{kj}(r_k) f_{k-1,j}(r_{k-1})}{f_{ki}(r_k) f_{k-1,i}(r_{k-1})} \right]^t + \tilde{p}^t \left[\frac{f_{kj}(r_k) f_{k-1,j}(r_{k-1})}{f_{ki}(r_k) f_{k-1,i}(r_{k-1})} \right]^t + \tilde{p}^t \left[\frac{f_{kj}(r_k)}{f_{ki}(r_k)} \right]^t \tag{10.58}$$

Again, taking an expectation conditioned on \mathcal{H}_i and from (10.43)

$$E[F_{kj}/\mathcal{H}_i] \leq E \left[\left[\frac{F_{Nj}}{F_{Ni}} \right]^t / \mathcal{H}_i \right] \rho_{jii}^{k-N} + \tilde{p}^t \left(\rho_{jii} + \rho_{jii}^2 + \dots + \rho_{jii}^{k-N} \right) \tag{10.59}$$

$$\triangleq \epsilon_k$$

$$\epsilon_{k+1} - \epsilon_k = \rho_{jii}^{k-N} E \left[\left(\frac{F_{Nj}}{F_{Ni}} \right)^t / \mathcal{H}_i \right] (\rho_{jii} - 1) + \rho_{jii}^{k+1-N} \tilde{p}^t \tag{10.60}$$

$$< 0 \quad \forall k \geq N_k$$

Hence

$$\epsilon < \dots < \epsilon_{k+1} < \epsilon_k < \epsilon_{k-1} < \dots \quad \forall k \geq N_k \tag{10.61}$$

Clearly, for the WSPRT, $\tilde{p} = 0$, and hence, the lower bound $\epsilon = 0$. ◀

Corollary 10.7. Let the family \mathcal{F} be identifiable, $\mathcal{H}_i \notin \Theta$ be true. Then

$$E[F_{k,j}/\mathcal{H}_i] < E[F_{k-1,j}/\mathcal{H}_i] \quad \forall j \neq m \quad (10.62)$$

where \mathcal{H}_m maximizes the information function defined in (10.48).

Proof. The proof remains essentially the same as at appropriate places we replace the subscript i by m , except that now $\rho_{jmi} < 1$. The corollary is relevant to the robustness issues associated with any multiple model adaptive estimation scheme. \blacklozenge

10.4.3 Convergence of the Posterior Error Covariance

Let \mathcal{H}_i be true. We now compare the posterior error covariance matrices of the adaptive filter and the “true” filter matched to \mathcal{H}_i in the MMAE algorithm. From (10.5–10.6) and (10.12a–10.12g)

$$P_{ki} = (I - K_{ki}C_{ki})M_{ki} \quad (10.63)$$

$$P_k = (I - K_kC_k)M_k \quad (10.64)$$

$$M_k - M_{ki} = A_{k-1}P_{k-1}A_{k-1}^T - A_{k-1,i}P_{k-1,i}A_{k-1,i}^T + (W_{k-1} - W_i) \quad (10.65)$$

Therefore

$$\begin{aligned} P_k - P_{ki} &= (I - K_kC_k)(M_k - M_{ki})(I - K_{ki}C_{ki})^T \\ &\quad + (I - K_kC_k)M_kC_{ki}^TK_{ki}^T - K_kC_kM_{ki}(I - K_{ki}C_{ki})^T \\ &= (I - K_kC_k)(M_k - M_{ki})(I - K_{ki}C_{ki})^T + G_{ki} \end{aligned} \quad (10.66)$$

Now from the definitions of K_k and K_{ki} in (10.5b) and (10.12b)

$$\begin{aligned} G_{ki} &= K_{ki}C_{ki}M_k - K_kC_kM_kC_{ki}^TK_{ki}^T - K_kC_kM_{ki} + K_{ki}C_{ki}M_{ki}C_k^TK_k^T \\ &= M_{ki}C_{ki}^TS_k^{-1}C_{ki}M_k - M_kC_k^TS_k^{-1}C_kM_kC_{ki}^TS_k^{-1}C_{ki}M_{ki} - \\ &\quad M_kC_k^TS_k^{-1}C_kM_{ki} + M_{ki}C_{ki}^TS_k^{-1}C_{ki}M_{ki}C_k^TS_k^{-1}C_kM_k \\ &= M_{ki} [C_{ki}^TS_k^{-1}C_{ki} - C_kS_k^{-1}C_k - C_{ki}^TS_k^{-1}C_{ki} (M_k - M_{ki}) C_k^TS_k^{-1}C_k] M_k \end{aligned}$$

Now

$$C_{ki}^TS_k^{-1}C_{ki} - C_kS_k^{-1}C_k = C_{ki}^T(S_{ki}^{-1} - S_k^{-1})C_k - (C_k^TS_k^{-1} + C_{ki}^TS_{ki}^{-1})(C_k - C_{ki})$$

Therefore

$$\begin{aligned}
G_{ki} &= M_{ki} C_{ki}^T [S_{ki}^{-1} - S_k^{-1} - S_{ki}^{-1} C_{ki} (M_k - M_{ki}) C_k^T S_k^{-1}] C_k M_k \\
&\quad - M_{ki} (C_k^T S_k^{-1} + C_{ki}^T S_{ki}^{-1}) (C_k - C_{ki}) M_k \\
&= M_{ki} C_{ki}^T S_{ki}^{-1} [S_k - S_{ki} - C_{ki} (M_k - M_{ki}) C_k^T] S_k^{-1} C_k M_k \\
&\quad - M_{ki} (C_k^T S_k^{-1} + C_{ki}^T S_{ki}^{-1}) (C_k - C_{ki}) M_k \\
&= K_{ki} (C_k M_k C_k^T + V_k - C_{ki} M_{ki} C_{ki}^T - V_i - C_{ki} M_k C_k^T + C_{ki} M_{ki} C_k^T) K_k \\
&\quad - M_{ki} (C_k^T S_k^{-1} + C_{ki}^T S_{ki}^{-1}) (C_k - C_{ki}) M_k \\
&= K_{ki} (V_k - V_i) K_k + K_{ki} (C_k - C_{ki}) (M_k C_k^T + C_{ki} M_{ki}) K_k^T \\
&\quad - M_{ki} (C_k^T S_k^{-1} + C_{ki}^T S_{ki}^{-1}) (C_k - C_{ki}) M_k
\end{aligned} \tag{10.67}$$

Similarly from (10.65)

$$\begin{aligned}
M_k - M_{ki} &= A_{k-1} (P_{k-1} - P_{k-1,i}) A_{k-1,i}^T \\
&\quad + (A_{k-1,i} P_{k-1,i} + A_{k-1} P_{k-1}) (A_{k-1} - A_{k-1,i})^T + (W_{k-1} - W_i)
\end{aligned}$$

and from (10.65–10.67)

$$\begin{aligned}
P_k - P_{ki} &= (I - K_k C_k) A_{k-1} (P_{k-1} - P_{k-1,i}) A_{k-1,i}^T (I - K_{ki} C_{ki})^T \\
&\quad + (I - K_k C_k) (A_{k-1,i} P_{k-1,i} + A_{k-1} P_{k-1}) (A_{k-1} - A_{k-1,i})^T (I - K_{ki} C_{ki})^T \\
&\quad + (I - K_k C_k) (W_{k-1} - W_i) (I - K_{ki} C_{ki})^T + K_{ki} (V_k - V_i) K_k \\
&\quad + K_{ki} (C_k - C_{ki}) (M_k C_k^T + C_{ki} M_{ki}) K_k^T \\
&\quad - M_{ki} (C_k^T S_k^{-1} + C_{ki}^T S_{ki}^{-1}) (C_k - C_{ki}) M_k
\end{aligned} \tag{10.68}$$

The filter equations are

$$\begin{aligned}
\hat{x}_{ki} &= (I - K_{ki} C_{ki}) A_{k-1,i} \hat{x}_{k-1,i} + K_{ki} (y_k - C_{ki} b_{k-1,i} - d_{ki}) \\
\hat{x}_k &= (I - K_k C_k) A_{k-1} \hat{x}_{k-1} + K_k (y_k - C_k b_{k-1} - d_k)
\end{aligned}$$

Denote the state transition matrices as

$$\begin{aligned}
\Phi_i(k, k-1) &\triangleq (I - K_{ki}C_{ki})A_{k-1,i} \\
\Phi(k, k-1) &\triangleq (I - K_kC_k)A_{k-1} \\
\Psi_{ki} &\triangleq (I - K_kC_k)(A_{k-1,i}P_{k-1,i} + A_{k-1}P_{k-1})(A_{k-1} - A_{k-1,i})^T(I - K_{ki}C_{ki})^T \\
&\quad + (I - K_kC_k)(W_{k-1} - W_i)(I - K_{ki}C_{ki})^T + K_{ki}(V_k - V_i)K_k \\
&\quad + K_{ki}(C_k - C_{ki})(M_kC_k^T + C_{ki}M_{ki})K_k^T \\
&\quad - M_{ki}(C_k^T S_k^{-1} + C_{ki}^T S_{ki}^{-1})(C_k - C_{ki})M_k
\end{aligned} \tag{10.69}$$

Therefore:

$$\begin{aligned}
\delta P_{ki} &\triangleq P_k - P_{ki} \\
&= \Phi(k, k-1)\delta P_{k-1,i}\Phi_i^T(k, k-1) + \Psi_{ki}
\end{aligned} \tag{10.70}$$

We now prove the following theorem:

Theorem 10.8. If the system in (10.1a–10.3) is uniformly completely controllable and uniformly completely observable, and if $\{\Psi_{ki}\}$ is uniformly bounded and decreasing, then

$$E[\|\delta P_{ki}\|/\mathcal{H}_i] \leq \mathcal{L}_{ki}$$

where

$$\mathcal{L}_i < \dots < \mathcal{L}_{k+1,i} < \mathcal{L}_{ki} < \mathcal{L}_{k-1,i} < \dots \quad \forall k \geq N_k \tag{10.71}$$

Proof. From (10.70)

$$\delta P_{ki} = \Phi(k, 0)\delta P_{0i}\Phi_i^T(k, 0) + \sum_{l=1}^k \Phi(k, l)\Psi_{li}\Phi_i^T(k, l)$$

so that

$$E[\delta P_{ki}/\mathcal{H}_i] = \Phi(k, 0)\delta P_{0i}\Phi_i^T(k, 0) + \sum_{l=1}^k \Phi(k, l)E[\Psi_{li}/\mathcal{H}_i]\Phi_i^T(k, l) \tag{10.72}$$

Since the system is uniformly completely controllable and observable

$$\begin{aligned}\|\Phi(k, l)\| &\leq C_1 e^{-c_2(k-l)} \\ \|\Phi_i(k, l)\| &\leq C_3 e^{-c_4(k-l)} \quad \forall C_1, C_2, c_3, c_4 > 0\end{aligned}\quad (10.73)$$

Further

$$\begin{aligned}\|W_{k-1} - W_i\| &= \left\| \sum_{j=0}^{L-1} F_{k-1,j} W_j - W_i \right\| \\ &\leq \|(1 - F_{k-1,i})W_a - (1 - F_{k-1,i})W_i\| \quad \text{where } W_a = \max_j W_j \\ &\leq F_{k-1,a} \|W_a - W_i\|\end{aligned}\quad (10.74)$$

Similarly

$$\begin{aligned}\|A_{k-1} - A_i\| &\leq F_{k-1,b} \|A_b - A_i\| \quad \text{where } A_b = \max_j A_j \\ \|V_k - V_i\| &\leq F_{k-1,c} \|V_c - V_i\| \quad \text{where } V_c = \max_j V_j \\ \|C_k - C_i\| &\leq F_{k-1,d} \|C_d - C_i\| \quad \text{where } C_d = \max_j C_j\end{aligned}\quad (10.75)$$

From (10.69), (10.74) and (10.75)

$$E[\|\Psi_{ki}\|/\mathcal{H}_i] \leq \|\Psi\| \|\epsilon_{ki}\| \quad (10.76)$$

wherein from Theorem 10.6 and (10.61), $\{\epsilon_{ki}\}$ is monotonically decreasing for all $k \geq N_k$ and bounded from below, and Ψ is some matrix defined from (10.69). From (10.72–10.76)

$$\begin{aligned}E[\|\delta P_{ki}\|/\mathcal{H}_i] &\leq \|C_1\| \|\delta P_{0i}\| \|C_3\| e^{-(c_2+c_4)k} + \|C_1\| \|\Psi\| \left[\sum_{l=1}^k e^{-(c_2+c_4)(k-l)} \|\epsilon_{li}\| \right] \|C_3\| \\ &\triangleq \mathcal{L}_{ki} \\ \mathcal{L}_{k+1,i} - \mathcal{L}_{ki} &= \|C_1\| \|\delta P_{0i}\| \|C_3\| e^{-(c_2+c_4)k} [e^{-(c_1+c_2)} - 1] \\ &\quad + \|C_1\| \|\Psi\| \|\epsilon_{1i}\| \|C_3\| e^{-(c_2+c_4)k} \\ &\quad + \|C_1\| \|\Psi\| \left[\sum_{l=1}^k e^{-(c_2+c_4)(k-l)} (\|\epsilon_{l+1,i}\| - \|\epsilon_{li}\|) \right] \|C_3\|\end{aligned}$$

so that

$$\mathcal{L}_{k+1,i} - \mathcal{L}_{ki} < 0 \quad \forall k \geq N_k$$

Hence

$$\mathcal{L}_i < \dots < \mathcal{L}_{k+1,i} < \mathcal{L}_{ki} < \mathcal{L}_{k-1,i} < \dots \quad \forall k \geq N_k$$

◀

Remark 27. Note that the lower bound is governed by the factor $\tilde{\rho}$ of the MHSSPRT as it controls the lower bound of the sequence $\{\epsilon_{ki}\}$, as shown in Theorem 10.6. This theorem, based upon our adaptive filter structure, shows that the apriori “covariance” assumed for the conditional density function of the residual $f_{ki}(r_k)$ approaches the true apriori error covariance, that is, $E\{M_k/\mathcal{H}_i\} \rightarrow M_{ki}$. As a special case, consider the Wald SPRT, where $\tilde{\rho} = 0$. From Theorem 10.6, it can be seen that for $\rho < 1$

$$\epsilon_k \sim \epsilon \rho^k$$

so that

$$E[\|\delta P_{ki}\|/\mathcal{H}_i] \leq \|C_1\| \|\delta P_{0i}\| \|C_3\| e^{-(c_2+c_4)k} + \|C_1\| \|\Psi\| \left[\frac{\rho^{k+1} e^{(c_2+c_4)(k+1)} - e^{(c_2+c_4)k}}{\rho e^{c_2+c_4} - 1} \right] \|C_3\|$$

and

$$E[\|\delta P_{ki}\|/\mathcal{H}_i] = 0 \quad \text{as } k \rightarrow \infty \quad (10.77)$$

So, for the Wald SPRT, $\mathcal{L}_i = 0$. The adaptive filter converges exactly to the “true” filter of the MMAE scheme. ◀

The assumptions in the AKF algorithm may be justified in yet another way, by looking at the exact expressions for the overall state estimate and posteriori error covariance, as

developed in the MMAE algorithm. Recall from (10.7a) and (10.7b)

$$\begin{aligned} x_k^* &= \sum_j x_{kj} F_{kj} \\ P_k^* &= \sum_j [P_{kj} + (x_k^* - x_{kj})(x_k^* - x_{kj})^T] F_{kj} \end{aligned}$$

Let

$$\delta P_k^* \triangleq P_k^* - P_k \quad (10.78)$$

We now show that the expected value of δP_k^* conditioned on any hypothesis decreases as $k \rightarrow \infty$.

Theorem 10.9. If the system in (10.1a–10.3) is uniformly completely controllable and uniformly completely observable, then

$$E[\|\delta P_k^*\|/\mathcal{H}_i] \leq \mathcal{L}_{ki}^* \quad \forall \mathcal{H}_i$$

where

$$\mathcal{L}_i^* < \dots < \mathcal{L}_{k+1,i}^* < \mathcal{L}_{ki}^* < \mathcal{L}_{k-1,i}^* < \dots \quad \forall k \geq N_k$$

Proof. From the above equations

$$\begin{aligned} \delta P_k^* &= \sum_j [(P_{kj} - P_k) + (x_k^* - x_{kj})(x_k^* - x_{kj})^T] F_{kj} \\ &= \sum_j [\delta P_{kj} + (x_k^* - x_{kj})(x_k^* - x_{kj})^T] F_{kj} \\ &= \sum_{j \neq i} [\delta P_{kj} + (x_k^* - x_{kj})(x_k^* - x_{kj})^T] F_{kj} \\ &\quad + [\delta P_{ki} + (x_k^* - x_{ki})(x_k^* - x_{ki})^T] F_{ki} \end{aligned} \quad (10.79)$$

Taking the norm and using an analysis similar to (10.75)

$$\begin{aligned} \delta P_k^* &\leq \sum_{j \neq i} [\|\delta P_{kj}\| + \|(x_k^* - x_{kj})(x_k^* - x_{kj})^T\|] F_{kj} \\ &\quad + [\|\delta P_{ki}\| + \|(x_k^* - x_{ki})(x_k^* - x_{ki})^T\|] F_{ki} \end{aligned}$$

$$\begin{aligned}
\|\delta P_{kj}\| &= \|P_{kj} - P_k\| \\
&= \|P_{kj} - P_{ki} + P_{ki} - P_k\| \\
&\leq \|\delta P_{kji}\| + \|\delta P_{ki}\| \leq \|\delta P_{ji}\| + \|\delta P_{ki}\| \quad j \neq i
\end{aligned} \tag{10.80}$$

$$\begin{aligned}
\|\delta X_{kj}\| &\triangleq \|(x_k^* - x_{kj})(x_k^* - x_{kj})^T\| \\
&\leq (1 - F_{kj})^2 \|x_{km} - x_{kj}\|^2, \quad m \neq j \\
&\leq (1 - F_{kj})^2 \|\delta X_j\|
\end{aligned} \tag{10.81}$$

so that

$$\begin{aligned}
\delta P_k^* \leq \sum_{j \neq i} [\|\delta P_{ki}\| + \|\delta P_{ji}\| + (1 - F_{kj})^2 \|\delta X_j\|] F_{kj} \\
+ [\|\delta P_{ki}\| + (1 - F_{ki})^2 \|\delta X_i\|] F_{ki}
\end{aligned} \tag{10.82}$$

From Theorem 10.6 and Theorem 10.8, for all $k \geq N_k$

$$\begin{aligned}
E[F_{k+1,j}/\mathcal{H}_i] &\leq E[F_{kj}/\mathcal{H}_i] \\
E[\|\delta P_{k+1,i}\|/\mathcal{H}_i] &\leq E[\|\delta P_{ki}\|/\mathcal{H}_i] \\
E[F_{k+1,i}/\mathcal{H}_i] &\geq E[F_{ki}/\mathcal{H}_i]
\end{aligned} \tag{10.83}$$

Therefore:

$$\begin{aligned}
E[\delta P_k^*/\mathcal{H}_i] &\leq E \left[\sum_{j \neq i} [\|\delta P_{ki}\| + \|\delta P_{ji}\| + (1 - F_{kj})^2 \|\delta X_j\|] F_{kj}/\mathcal{H}_i \right] \\
&\quad + E [\|\delta P_{ki}\| + (1 - F_{ki})^2 \|\delta X_i\|] F_{ki}/\mathcal{H}_i \\
&= E \left[\sum_{j \neq i} [\|\delta P_{ji}\| + (1 - F_{kj})^2 \|\delta X_j\|] F_{kj}/\mathcal{H}_i \right] \\
&\quad + E [(1 - F_{ki})^2 \|\delta X_i\| F_{ki}/\mathcal{H}_i] + E [\|\delta P_{ki}\|/\mathcal{H}_i] \\
&\triangleq \mathcal{L}_{ki}^*
\end{aligned}$$

Now

$$\begin{aligned}
\mathcal{L}_{k+1,i}^* - \mathcal{L}_{ki}^* &= \sum_{j \neq i} \|\delta P_{ji}\| E [(F_{k+1,j} - F_{kj})/\mathcal{H}_i] + E [(\|\delta P_{k+1,i}\| - \|\delta P_{ki}\|)/\mathcal{H}_i] \\
&\quad + \sum_j \|\delta X_j\| E [(1 - F_{k+1,j})^2 F_{k+1,j} - (1 - F_{kj})^2 F_{kj}/\mathcal{H}_i]
\end{aligned} \tag{10.84}$$

Consider the function:

$$\begin{aligned} E[(1 - F_{kj})^2 F_{kj} / \mathcal{H}_i] &= E[F_{kj} / \mathcal{H}_i] + E[F_{kj}^3 / \mathcal{H}_i] - 2E[F_{kj}^2 / \mathcal{H}_i] \\ &\leq 2E[F_{kj} / \mathcal{H}_i] - 2E[F_{kj}^2 / \mathcal{H}_i] \end{aligned}$$

Now

$$E[F_{kj}^2 / \mathcal{H}_i] \geq (E[F_{kj} / \mathcal{H}_i])^2$$

which implies that

$$\begin{aligned} E[(1 - F_{kj})^2 F_{kj} / \mathcal{H}_i] &\leq 2 \{E[F_{kj} / \mathcal{H}_i] - (E[F_{kj} / \mathcal{H}_i])^2\} \\ &\triangleq \varphi(E[F_{kj} / \mathcal{H}_i]) \end{aligned}$$

Since $\varphi(\cdot)$ is an increasing function in the interval $[0, 1/2)$ and a decreasing function in the interval $(1/2, 1]$, it follows from (10.83) and (10.84) that

$$\begin{aligned} E[(1 - F_{k+1,j})^2 F_{k+1,j} / \mathcal{H}_i] &\leq E[(1 - F_{kj})^2 F_{kj} / \mathcal{H}_i] \quad \forall j \neq i \\ E[(1 - F_{k+1,i})^2 F_{k+1,i} / \mathcal{H}_i] &\leq E[(1 - F_{ki})^2 F_{ki} / \mathcal{H}_i] \end{aligned}$$

so that

$$\mathcal{L}_{k+1,i}^* - \mathcal{L}_{ki}^* \leq 0 \quad k \geq N_k \quad (10.85)$$

and

$$\mathcal{L}_i^* < \dots < \mathcal{L}_{k+1,i}^* < \mathcal{L}_{ki}^* < \mathcal{L}_{k-1,i}^* < \dots \quad \forall k \geq N_k$$

Clearly the posteriori “covariance” of the AKF algorithm approaches the exact posteriori error covariance as computed in the MMAE algorithm.

Finally, we analyze the difference between the assumed error “covariance” P_k and the exact error covariance \tilde{P}_k . Let \mathcal{H}_i be true. From (10.12d), (10.16) and (10.17)

$$\delta \tilde{P}_{ki} \triangleq P_k - \tilde{P}_k \quad (10.86)$$

$$\begin{aligned} &= (I - K_k C_k) A_k (P_{k-1} - \tilde{P}_{k-1}) A_k^T (I - K_k C_k)^T + \tilde{\Psi}_k \\ &= \Phi(k, k-1) \delta \tilde{P}_{k-1} \Phi(k, k-1)^T + \tilde{\Psi}_k \end{aligned} \quad (10.87)$$

wherein:

$$\begin{aligned}
\tilde{\Psi}_k = & K_k[(V_k - V_i) - (C_k - C_{ki})X_k(C_k - C_{ki})^T + (d_k - d_{ki})(d_k - d_{ki})^T \\
& + 2(C_k - C_{ki})m_k(d_{ki} - d_k)^T]K_k^T \\
& - (I - K_k C_k)[2\bar{E}_k^T(C_k - C_{ki})^T - 2\bar{m}_k^e(d_k - d_{ki})^T]K_k^T \\
& + (I - K_k C_k)[(W_{k-1} - W_i) - (A_{k-1} - A_{k-1,i})X_{k-1}(A_{k-1} - A_{k-1,i})^T \\
& - (b_{k-1,i} - b_{k-1})(b_{k-1,i} - b_{k-1})^T + 2A_{k-1}\hat{E}_{k-1}^T(A_{k-1} - A_{k-1,i})^T \\
& + 2A_{k-1}\hat{m}_{k-1}^e(b_{k-1} - b_{k-1,i})^T \\
& - 2(A_{k-1} - A_{k-1,i})m_{k-1}(b_{k-1} - b_{k-1,i})^T](I - K_k C_k)^T
\end{aligned}$$

We now prove that the expected value of $\delta\tilde{P}_{ki}$ conditioned on \mathcal{H}_i decreases as $k \rightarrow \infty$.

Theorem 10.10. If the system in (10.1a–10.3) is uniformly completely controllable and uniformly completely observable, then

$$E[\|\delta\tilde{P}_{ki}\|/\mathcal{H}_i] \leq \tilde{\mathcal{L}}_{ki}, \quad \forall \mathcal{H}_i$$

wherein:

$$\tilde{\mathcal{L}}_i < \dots < \tilde{\mathcal{L}}_{k+1,i} < \tilde{\mathcal{L}}_{ki} < \tilde{\mathcal{L}}_{k-1,i} < \dots \quad \forall k \geq N_k$$

Proof. From (10.87)

$$\delta\tilde{P}_{ki} = \Phi(k, 0)\delta\tilde{P}_{0i}\Phi^T(k, 0) + \sum_{l=1}^k \Phi(k, l)\tilde{\Psi}_{li}\Phi^T(k, l)$$

so that

$$E[\delta\tilde{P}_{ki}/\mathcal{H}_i] = \Phi(k, 0)\delta\tilde{P}_{0i}\Phi^T(k, 0) + \sum_{l=1}^k \Phi(k, l)E[\tilde{\Psi}_{li}/\mathcal{H}_i]\Phi^T(k, l)$$

The rest of the proof follows that of Theorem 10.8. ◀

This concludes our analysis to justify the structure of the AKF algorithm. Under \mathcal{H}_i , we derived sufficient conditions for the convergence of F_{ki} to F_{ki}^s and P_k to \tilde{P}_k , P_{ki} , and P_k^* . In the next section, we test the AKF algorithm in a few numerical simulations

10.5 Simulations

10.5.1 Example 1

Consider a scalar dynamic system:

$$\begin{aligned}x_{k+1} &= A_k x_k + b_k + w_k \\ y_k &= C_k x_k + d_k + v_k\end{aligned}$$

wherein under each hypothesis

$$\begin{aligned}\mathcal{H}_0 : \quad & A_k = -0.5, & b_k = 0.0, & C_k = 1.0, & d_k = 0.0 \\ & v_k \sim \mathcal{N}(0, 1.0), & w_k \sim \mathcal{N}(0, 0.001) \\ \mathcal{H}_1 : \quad & A_k = -0.6, & b_k = 0.25, & C_k = 1.25, & d_k = 0.25 \\ & v_k \sim \mathcal{N}(0, 2.0), & w_k \sim \mathcal{N}(0, 0.001) \\ \mathcal{H}_2 : \quad & A_k = -0.7, & b_k = 0.50, & C_k = 1.50, & d_k = 0.50 \\ & v_k \sim \mathcal{N}(0, 3.0), & w_k \sim \mathcal{N}(0, 0.001)\end{aligned}$$

The Adaptive Kalman Filter algorithm was compared to the MMAE algorithm. In the MMAE approach, F_{ki}^w was replaced by F_{ki}^s to allow for transitions from one hypothesis to another. Of course, from our earlier discussion, it is clear that the recursive relation is not strictly F_{ki}^s but an approximation to it. In order to design the AKF algorithm, it is essential to consider scenarios when a particular hypothesis is true and the filter is “matched” to the wrong hypothesis. An off-line computation of the true residual error covariance was conducted for all scenarios. It is seen from Figure 10.3 that when \mathcal{H}_i is true and the filter is matched to \mathcal{H}_j , either $\Lambda_{kj} < \Lambda_{ki} < \tilde{S}_{ki}$ or $\Lambda_{kj} > \Lambda_{ki} > \tilde{S}_{ki}$. Moreover the matrix B_{ki} in the exponential term is always positive definite and so, from Section 10.7.3, the system satisfies Claim 10.4. This implies that the filter cannot remain matched to \mathcal{H}_j .

We now test the AKF algorithm. At $t = 40$ sec, the hypothesis was changed from \mathcal{H}_0 to \mathcal{H}_1 . The posterior probabilities of the three hypotheses are shown in Figure 10.4. The bold line denotes the AKF approach while the dotted line denotes the MMAE approach.

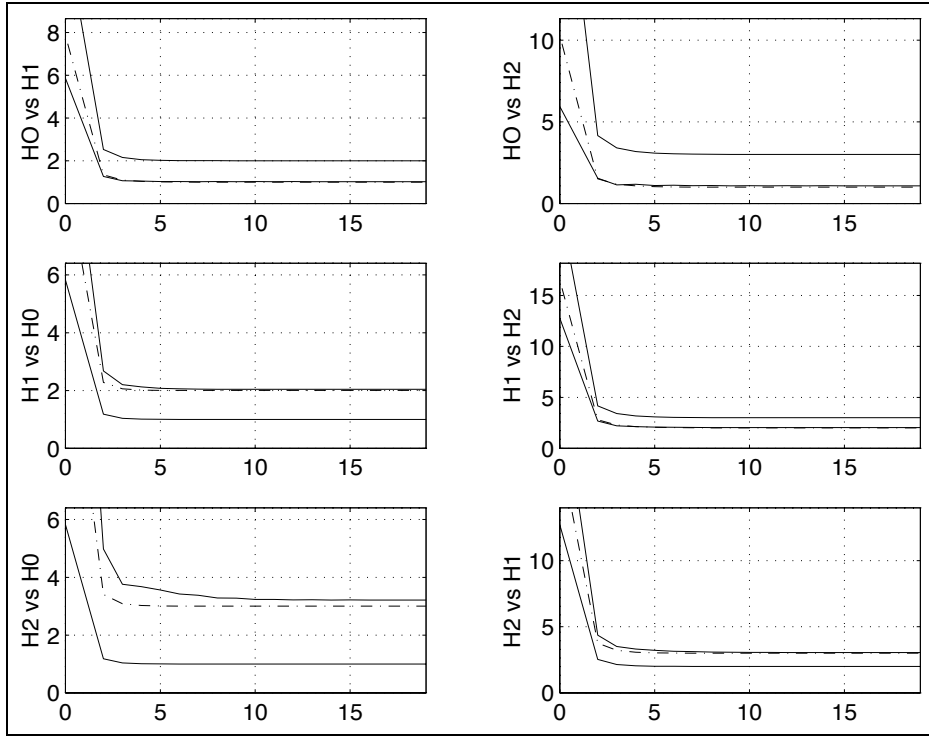


Figure 10.3: Off-line computation of Λ_{kj} , Λ_{ki} and S_{ki} : H_i vs H_j denotes H_i is true while the filter is matched to H_j ; Λ_{ki} is shown by the dotted line.

However, the computational time taken by the MMAE approach is much larger than the AKF approach. These plots have been averaged over ten different realizations.

Figure 10.5 shows the normed differences between the posteriori error covariance matrix of the AKF and each of the Lainiotis filters. For $t \leq 40$ seconds, \mathcal{H}_0 is true. As proved in Theorem 10.8, $E[\|\delta P_{k0}\|/\mathcal{H}_0] \rightarrow 0$ while $E[\|\delta P_{k1}\|/\mathcal{H}_0]$ and $E[\|\delta P_{k2}\|/\mathcal{H}_0]$ are high. For $t > 40$ seconds, \mathcal{H}_1 is true. Therefore $E[\|\delta P_{k1}\|/\mathcal{H}_1] \rightarrow 0$ while $E[\|\delta P_{k0}\|/\mathcal{H}_1]$ and $E[\|\delta P_{k2}\|/\mathcal{H}_1]$ are high.

10.5.2 Example 2

Consider another dynamic system wherein under each hypothesis:

$$\begin{aligned} \mathcal{H}_0 : \quad & A_k = 0.5, & b_k = 0.00, & C_k = 1.00, & d_k = 0.00 \\ & v_k \sim \mathcal{N}(0, 1.0), & w_k \sim \mathcal{N}(0, 0.001) \end{aligned}$$

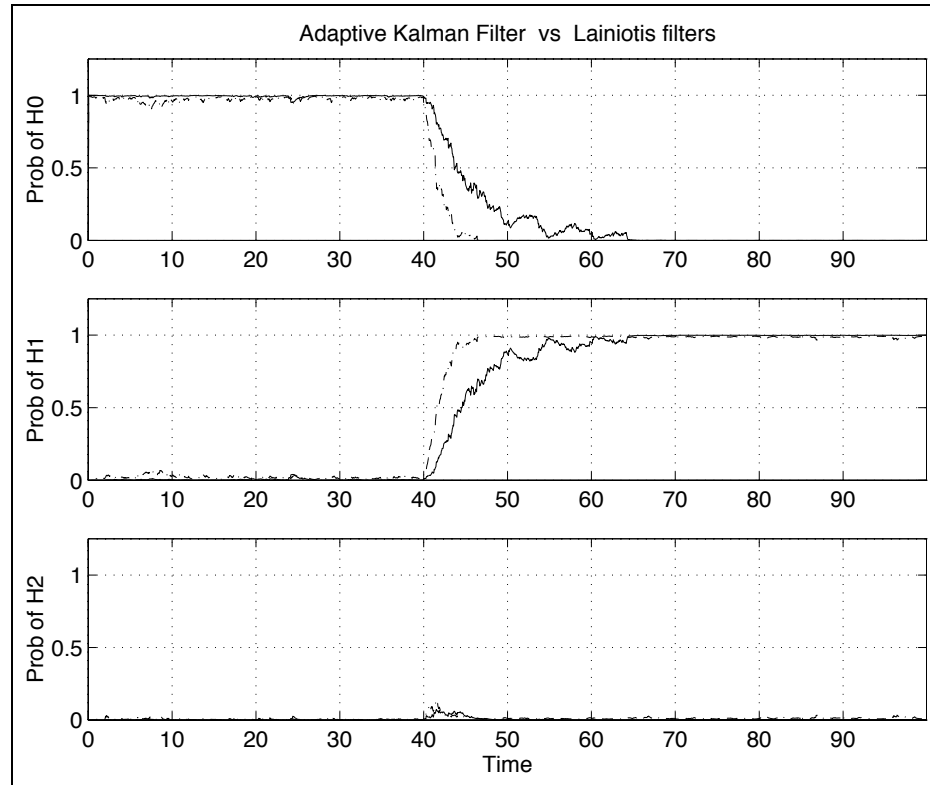
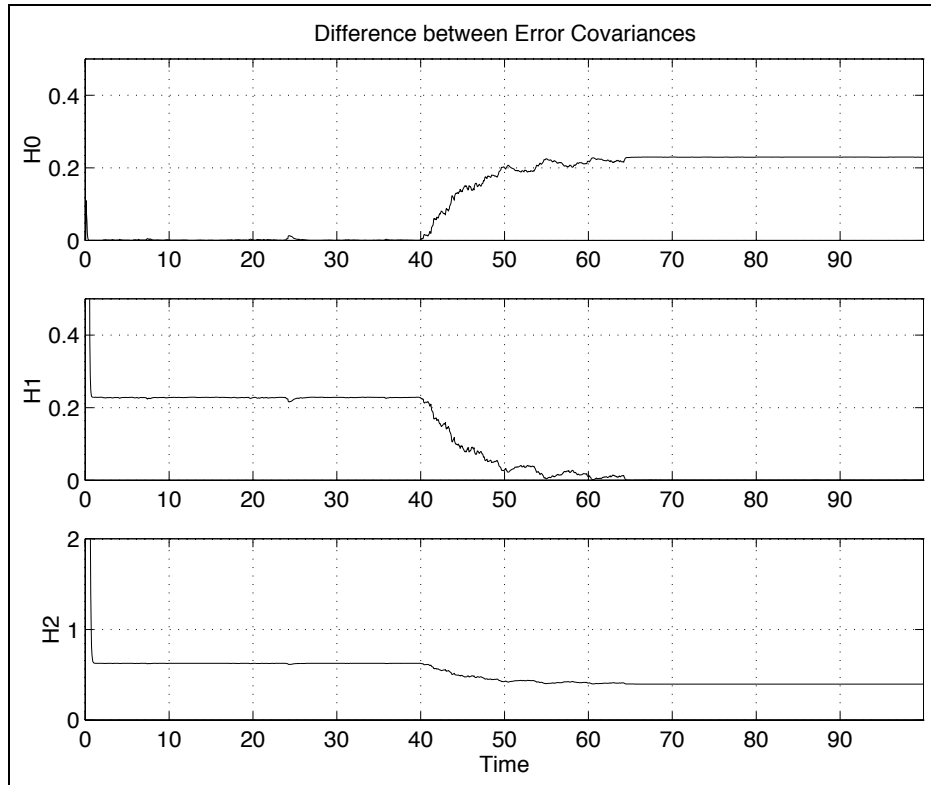


Figure 10.4: Adaptive Kalman Filter Performance - Change from H_0 to H_1 .

$$\begin{aligned}
 \mathcal{H}_1 : \quad & A_k = 0.6, & b_k = 0.25, & C_k = 1.25, & d_k = 0.25 \\
 & v_k \sim \mathcal{N}(0, 1.5), & w_k \sim \mathcal{N}(0, 0.001) \\
 \mathcal{H}_2 : \quad & A_k = 0.7, & b_k = 0.50, & C_k = 1.50, & d_k = 0.50 \\
 & v_k \sim \mathcal{N}(0, 2.0), & w_k \sim \mathcal{N}(0, 0.001)
 \end{aligned}$$

Again, we compared the Adaptive Kalman Filter to the MMAE algorithm. At $t = 3$ sec, the hypothesis was changed from \mathcal{H}_0 to \mathcal{H}_2 . The posterior probabilities of the three hypotheses are shown in Figure 10.6. The plots have been averaged over ten different realizations.

Figure 10.7 shows the normed differences between the posteriori error covariance matrix of the AKF and each of the Lainiotis filters.

Figure 10.5: $E[|\delta P_{ki}|]$ vs. t_k .

10.5.3 Example 3

Consider three hypotheses wherein:

$$\mathcal{H}_0 : v_k \sim \mathcal{N}(0, 1.0)$$

$$\mathcal{H}_1 : v_k \sim \mathcal{N}(0, 1.5)$$

$$\mathcal{H}_2 : v_k \sim \mathcal{N}(0, 2.0)$$

A fourth order ARMA measurement process was simulated thus:

$$y_k = 0.1 \cdot [y_{k-1} - y_{k-2} + y_{k-3} - y_{k-4}] + v_k$$

Since the order of the ARMA process typically is unknown, a fifth order ARMA model was assumed for the measurement process. The assumed system model is the same as

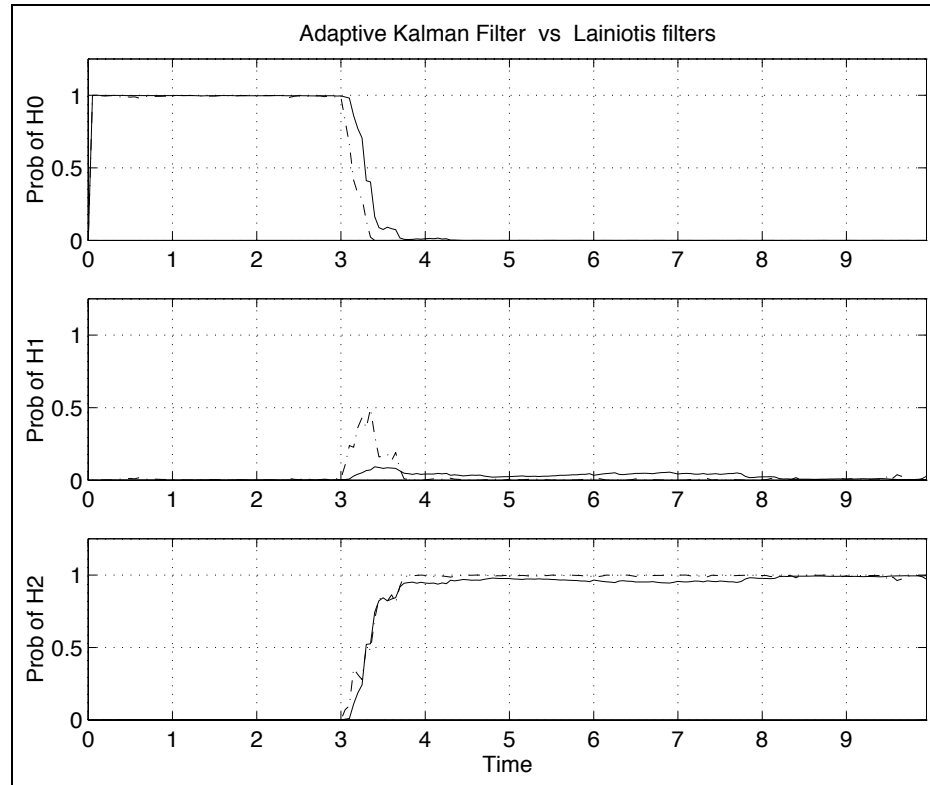
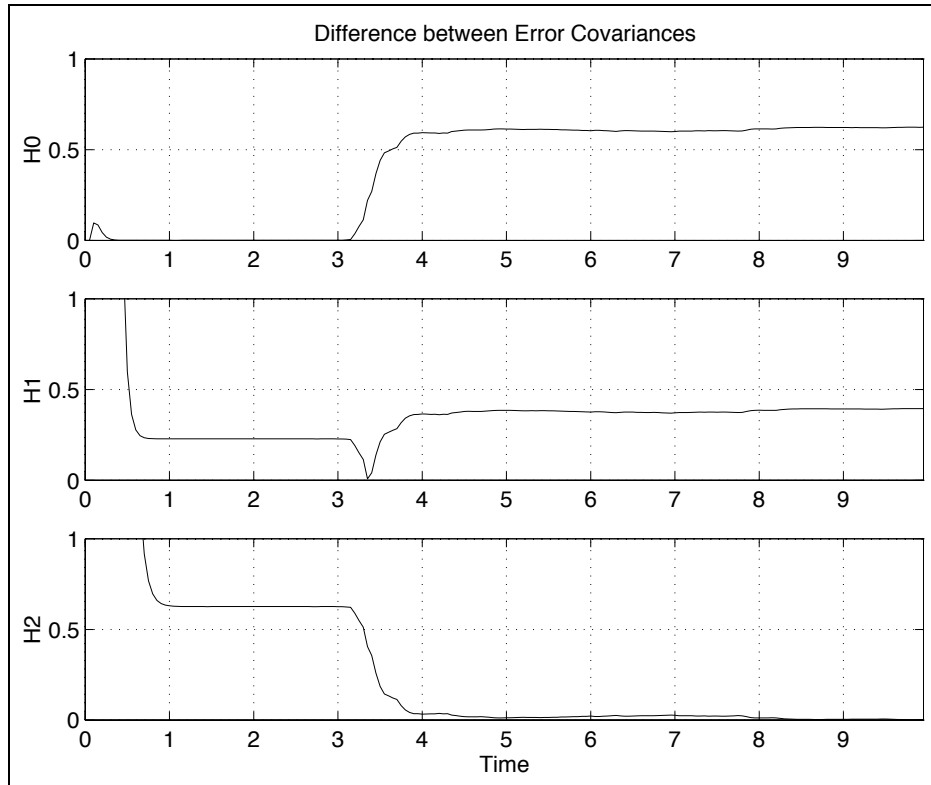


Figure 10.6: Adaptive Kalman Filter Performance - Change from H_0 to H_2 .

(10.1a–10.3) and for all \mathcal{H}_j

$$\begin{aligned}
 A &= I & W_j &= 0.001 * I & d &= 0 \\
 C_k &= [y_{k-1} | \dots | y_{k-5}] & b &= [0 \ 0 \ 0 \ 0 \ 0]^T
 \end{aligned}$$

Recall from Lemma 10.2 and Section 10.7.3 that for ARMA processes, Claim 10.4 is always valid thereby obviating any off-line computation. At $t = 40$ sec, the hypothesis was changed from \mathcal{H}_0 to \mathcal{H}_1 . The posterior probabilities of the three hypotheses are shown in Figure 10.8. The plots have been averaged over ten different realizations. Figure 10.9 shows the normed differences between the posteriori error covariance matrix of the AKF and each of the Lainiotis filters.

Figure 10.7: $E[|\delta P_{ki}|]$ vs. t_k .

10.5.4 Example 4

For the same system, the hypothesis was changed from \mathcal{H}_0 to \mathcal{H}_2 at $t = 40$ seconds. The posterior probabilities of the three hypotheses are shown in Figure 10.10. Again the plots have been averaged over ten different realizations. Figure 10.11 shows the normed differences between the posteriori error covariance matrix of the AKF and each of the Lainiotis filters.

10.6 Conclusions

An AKF algorithm and sufficient conditions for its convergence have been developed for adaptive estimation in linear time-varying stochastic dynamic systems. In the simulated examples, it performs comparably to the modified MMAE algorithm, while significantly

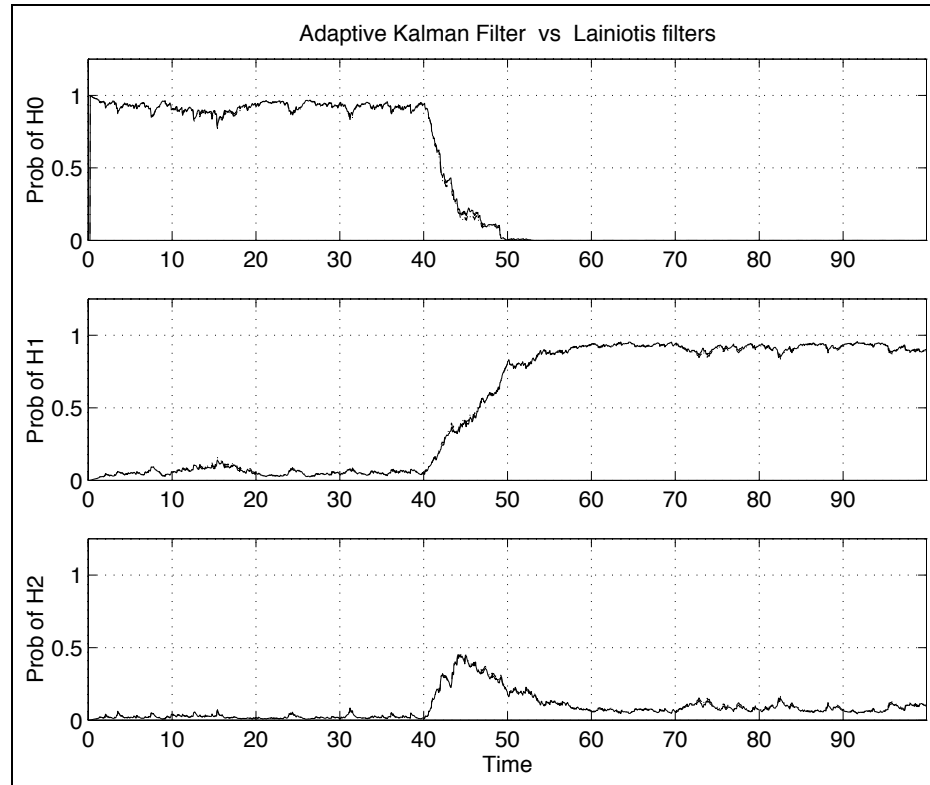
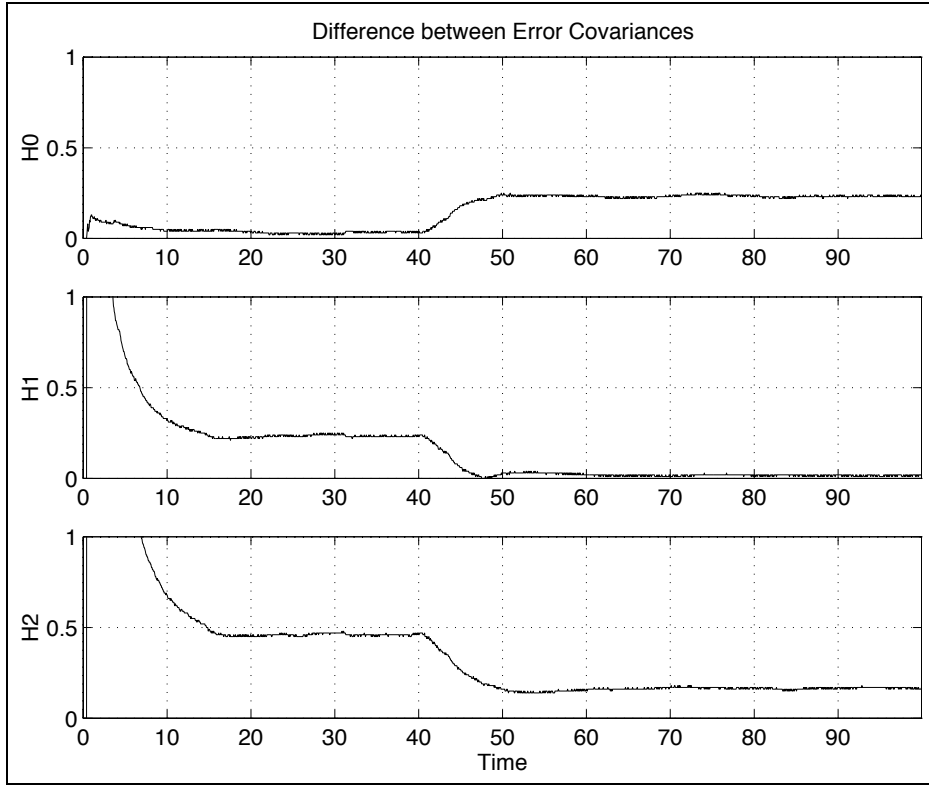


Figure 10.8: Adaptive Kalman Filter Performance - Change from H_0 to H_1 .

reducing the computational intensity. It has also been shown that for a class of problems, the expected value of the true posterior probability conditioned on the residual history converges to unity. In its most general form, an off-line computation is necessary to investigate the convergence of the true posterior probability. Under assumptions of uniform complete controllability and observability, the expected value of the norm of the difference between the constructed error covariance and the true posterior error covariance converges to a lower bound. This lower bound is determined by the a priori probability of change from one hypothesis to another in the MHSSPRT. In the presence of modeling errors, the AKF algorithm has been shown to converge to the hypothesis which maximizes a particular information function, while the MMAE algorithm might show beta dominance.

Figure 10.9: $E[|\delta P_{ki}|]$ vs. t_k .

10.7 Proofs

Proofs of some results developed in this chapter are presented in this section.

10.7.1 Proof A

From (10.40), for the MMAE scheme:

$$\begin{aligned}\phi_{ki} &\triangleq F_{k,i} + \tilde{p}_i(1 - F_{k,i}) \\ f_{k+1,i}(r_{k+1,i}) &= \frac{1}{(2\pi)^{s/2} \|S_{k+1,i}\|^{1/2}} \exp\left(-\frac{1}{2} r_{k+1,i} S_{k+1,i}^{-1} r_{k+1,i}\right) \triangleq \beta_{k+1,i} \alpha_{k+1,j} \\ F_{k+1,i} &= \frac{\phi_{ki} f_{k+1,i}(r_{k+1,i})}{\sum_{j=0}^m \phi_{kj} f_{k+1,j}(r_{k+1,j})} = \frac{\phi_{ki} \beta_{k+1,i} \alpha_{k+1,i}}{\sum_{j=0}^m \phi_{kj} \beta_{k+1,j} \alpha_{k+1,j}} \\ F_{k+1,i} - F_{ki} &= \frac{\phi_{ki}(1 - F_{ki}) \beta_{k+1,i} \alpha_{k+1,i} - \sum_{j \neq i} \phi_{kj} \beta_{k+1,j} \alpha_{k+1,j} F_{ki}}{\sum_{j=0}^m \phi_{kj} \beta_{k+1,j} \alpha_{k+1,j}}\end{aligned}$$

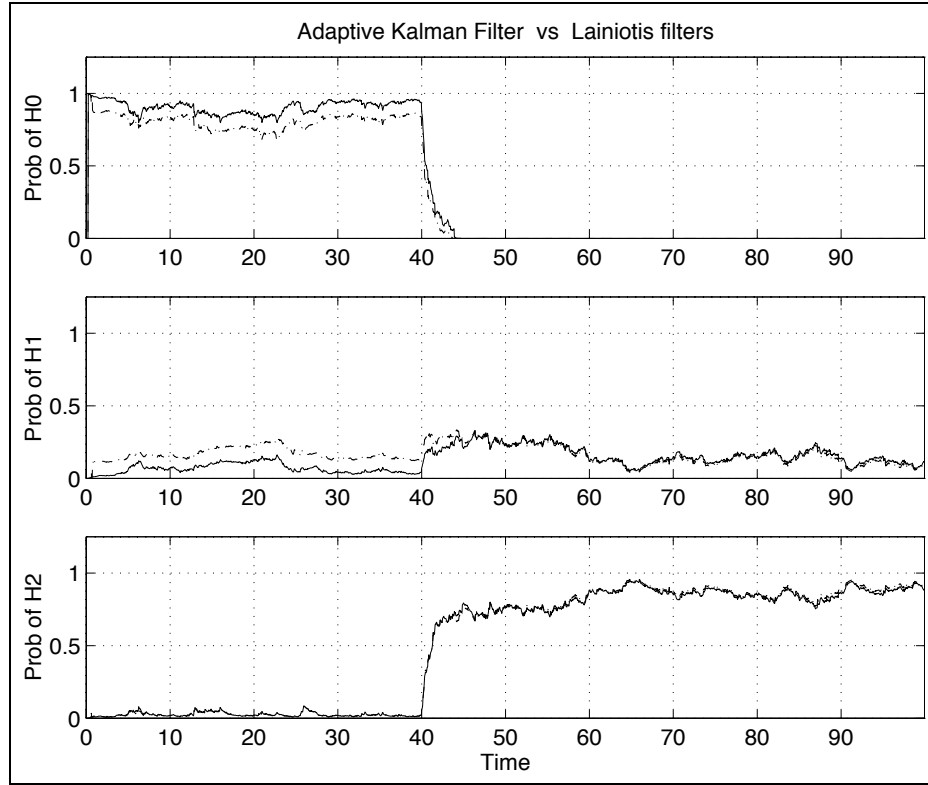


Figure 10.10: Adaptive Kalman Filter Performance - Change from H_0 to H_2 .

If \mathcal{H}_i is true, then we would expect:

$$\alpha_{k+1,j} \approx 0 \quad \forall j \neq i$$

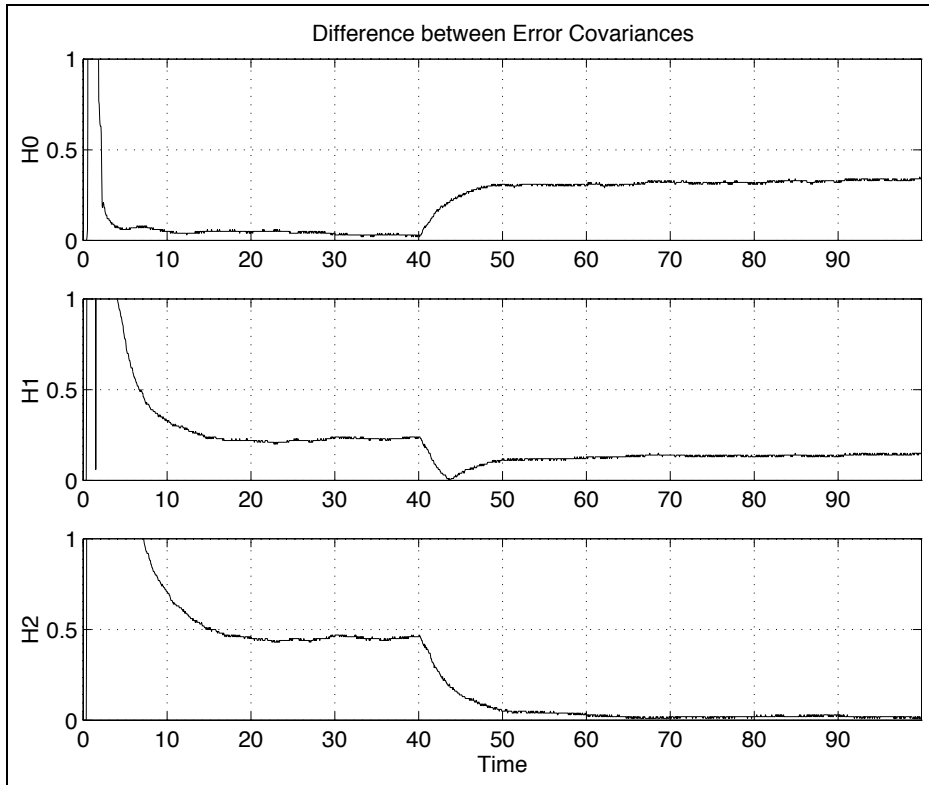
so that

$$F_{k+1,i} - F_{ki} \geq 0$$

However, if for some unknown reason, $\alpha_{kj} \approx \alpha \forall j$ for a prolonged sequence of measurements then

$$F_{k+1,i} - F_{ki} = \frac{(1 - \tilde{p}) \sum_{j \neq i} F_{kj} (\beta_{k+1,i} - \beta_{k+1,j}) F_{ki} + \tilde{p} \sum_{j \neq i} (\beta_{k+1,i} - \beta_{k+1,j}) F_{ki}}{\sum_{j=0}^m \phi_{kj} \beta_{k+1,j}}$$

If $\beta_{ki} < \beta_{kj} \forall j \neq i$, then the posterior probability corresponding to the dominant β increases irrespective of the true hypothesis.

Figure 10.11: $E[|\delta P_{ki}|]$ vs. t_k .

10.7.2 Proof B1

For the AKF algorithm, there is only one residual process. Hence, if for some reason, $\alpha_{kj} \approx \alpha$ for all j for a prolonged sequence of measurements this implies that

$$r_{k+1}^T [S_{k+1,i} - S_{k+1,j}] r_{k+1} = 0$$

and

$$S_{k+1,i} \equiv S_{k+1,j} \quad \forall k$$

This violates the identifiability assumption of the family \mathcal{F} . Moreover, since now $\beta_{ki} \equiv \beta_{kj} \forall j$, one β cannot dominate over the other.

10.7.3 Proof B2

From (10.42):

$$\mathcal{J}_{ji}(k) \triangleq E [\ln \{f_{kj}(r_k)\} / \mathcal{H}_i, \mathcal{R}_{k-1}]$$

Let \mathcal{H}_i be true. Then

$$\mathcal{J}_{ji}(k) - \mathcal{J}_{ii}(k) = \int \ln \left\{ \frac{f_{kj}(r_k)}{f_{ki}(r_k)} \right\} \tilde{f}_{ki}(r_k) dr_k$$

Since $\ln x \leq x - 1$

$$\begin{aligned} \mathcal{J}_{ji}(k) - \mathcal{J}_{ii}(k) &\leq \int \left\{ \frac{f_{kj}(r_k)}{f_{ki}(r_k)} - 1 \right\} \tilde{f}_{ki}(r_k) dr_k \\ &\leq \left\{ \int \left\{ \frac{f_{kj}(r_k)}{f_{ki}(r_k)} \right\} \tilde{f}_{ki}(r_k) dr_k \right\} - 1 \quad \forall j \neq i \\ &\triangleq I_k - 1 \end{aligned}$$

From (10.25), (10.26) and (10.28),

$$I_k \triangleq \frac{\|\Lambda_{ki}\|^{1/2} \|\Lambda_k\|^{1/2}}{\|\Lambda_{kj}\|^{1/2} \|\tilde{S}_k\|^{1/2}} \exp \left\{ -\frac{a_{ki}}{2} \right\}$$

where

$$\begin{aligned} a_{ki} &\triangleq \tilde{b}_{ki}^T [\tilde{S}_{ki} + (\Lambda_{kj}^{-1} - \Lambda_{ki}^{-1})^{-1}]^{-1} \tilde{b}_{ki} \\ &= \tilde{b}_{ki}^T B_{ki} \tilde{b}_{ki} \end{aligned}$$

and

$$\Lambda_k^{-1} \triangleq \tilde{S}_k^{-1} + \Lambda_{kj}^{-1} - \Lambda_{ki}^{-1}$$

with $\Lambda_k^{-1} > 0$ for the integral to exist.

Now, it must be true that either $\Lambda_{kj} < \Lambda_{ki} < \tilde{S}_{ki}$ or $\Lambda_{kj} > \Lambda_{ki} > \tilde{S}_{ki}$ for all k . Clearly, the integral always exists and $\Lambda_k > 0$. Since the bias terms are small, neglect the exponential term a_{ki} . However, note that if

$$\begin{aligned} \Lambda_{kj} < \Lambda_{ki} &\Rightarrow B_{ki} > 0 \\ &\Rightarrow a_{ki} > 0 \quad \forall b_{ki} \\ &\Rightarrow \exp \left\{ -\frac{a_{ki}}{2} \right\} < 1 \end{aligned}$$

Hence, in certain cases, the bias terms need not be small. Anyway, by removing the exponential term from I_k , we can show that

$$\begin{aligned} I_k &= \|\Lambda_{ki}^{-1}\Lambda_{kj} + \Lambda_{ki}^{-1}\tilde{S}_k - \Lambda_{ki}^{-1}\Lambda_{kj}\Lambda_{ki}^{-1}\tilde{S}_k\|^{-1/2} \\ &\leq 1 \end{aligned}$$

with the equality sign if and only if $\Lambda_{ki} = \Lambda_{kj}$ or $\Lambda_{ki} = \tilde{S}_k$ for all k . The former situation violates the identifiability assumption while the latter assumes that $M_k = \tilde{M}_k$ for all k in which case the algorithm has already converged. Therefore:

$$\mathcal{J}_{ji}(k) - \mathcal{J}_{ii}(k) \leq 0$$

Now, the equality sign in holds if and only if $f_{ki}(\cdot) = f_{kj}(\cdot)$ almost everywhere. Since we assumed the family \mathcal{F} to be identifiable, the $\mathcal{J}_{ji}(k)$ is strictly less than $\mathcal{J}_{ii}(k) \forall j \neq i$ and $\forall k$.

10.7.4 Proof B3

The proof follows the analysis in (Liporace 1971). Let $\mathcal{H}_i \notin \Theta$ be true. We first prove that whenever $\mathcal{J}_{ji}(k) < \mathcal{J}_{mi}(k) \quad \forall k$ the following holds true

$$E \left[\left\{ \frac{f_{kj}(r_k)}{f_{km}(r_k)} \right\}^t / \mathcal{H}_i, \mathcal{R}_{k-1} \right] \triangleq \rho_{jmi}(\mathcal{R}_{k-1}) < 1 \quad \text{forsomet} \in (0, 1) \quad \forall k$$

By definition:

$$\begin{aligned} \mathcal{J}_{ji}(k) - \mathcal{J}_{mi}(k) &= E \left[\ln \left\{ \frac{f_{kj}(r_k)}{f_{km}(r_k)} \right\} / \mathcal{H}_i, \mathcal{R}_{k-1} \right] \\ &= E \left[\lim_{t \rightarrow 0} \left(\left\{ \frac{f_{kj}(r_k)}{f_{km}(r_k)} \right\}^t - 1 \right) t^{-1} / \mathcal{H}_i, \mathcal{R}_{k-1} \right] \end{aligned}$$

Using the Lebesgue dominated convergence theorem, the limit and expectation may be interchanged. Therefore, for any $\delta \in (0, 1)$, there exists a $t \in (0, 1)$ such that

$$\begin{aligned} \lim_{t \rightarrow 0} t^{-1} \left(E \left[\left\{ \frac{f_{kj}(r_k)}{f_{km}(r_k)} \right\}^t / \mathcal{H}_i, \mathcal{R}_{k-1} \right] - 1 \right) &\leq [\mathcal{J}_{ji}(k) - \mathcal{J}_{mi}(k)] (1 - \delta) \\ E \left[\left\{ \frac{f_{kj}(r_k)}{f_{km}(r_k)} \right\}^t / \mathcal{H}_i, \mathcal{R}_{k-1} \right] &\leq 1 + t(1 - \delta) [\mathcal{J}_{ji}(k) - \mathcal{J}_{mi}(k)] \\ &< 1 \end{aligned}$$

The same analysis can be carried out $\forall k$, that is, for any realization of \mathcal{R}_k

$$\begin{aligned}\rho_{jmi}(\mathcal{R}_{k-1}) &< 1 \quad \forall k \\ \Rightarrow \rho_{jmi} &\stackrel{\Delta}{=} \max_k \rho_{jmi}(\mathcal{R}_{k-1}) < 1\end{aligned}$$

Fault Detection and Identification Using Linear Quadratic Optimization

A NEW APPROACH to the residual generation problem for fault detection and identification based on linear quadratic optimization is presented. A quadratic cost encourages the input observability of a fault that is to be detected and the unobservability of disturbances, sensor noise and a set of faults that are to be isolated. Since the filter is not constrained to form unobservability subspace structures, adjustment of the quadratic cost could realize improved performance as reduced sensor noise and dynamic disturbance components in the residual and reduced sensitivity to parametric variations. In the present form, the filter detects a single fault so the structure could also be described as that of an unidentified input observer. A bank of filters are constructed when multiple faults are to be detected.

11.1 Problem Formulation

Consider a dynamic system described by the equations

$$\dot{x} = Ax + B_1u_1 + B_2u_2; \quad x(t_0) = x_0 \quad (11.1)$$

$$y = Cx + w \quad (11.2)$$

In (11.1) and (11.2), y is a $p \times 1$ measurement vector, w is the $p \times 1$ measurement error, and u_1 and u_2 are unknown disturbance inputs representing faults. Our goal is to derive a fault detection filter which processes the measurement $y(t)$ and produces a scalar output $h(t)$ which is small if u_1 is zero and large only if u_1 is different from zero. Thus the filter should respond to a non zero input u_1 , but not to the inputs u_2 , w , and x_0 . In this development we shall consider filters in the form:

$$h(t_1) = f^T \left[y(t_1) - \int_{t_0}^{t_1} CM^T(\tau, t_1)y(\tau)d\tau \right] \quad (11.3)$$

Procedures for choosing the matrix $f(t_1)$ and the $p \times n$ matrix $M(\tau, t_1)$ are developed below. A filter with the properties described above can be used to detect a fault corresponding to u_1 . The roles of u_1 and u_2 can be interchanged to detect faults corresponding to u_2 .

Introduce an $n \times n$ square matrix $Z(t; t_1)$ satisfying

$$\frac{d}{dt}Z(t; t_1) = -A^T Z(t; t_1) + C^T M(t; t_1); \quad Z(t_1; t_1) = I \quad (11.4)$$

Form $Z^T x$ and differentiate with respect to t .

$$\begin{aligned} \frac{d}{dt}(Z^T x) &= \dot{Z}^T x + Z^T \dot{x} \\ &= [-\cancel{Z}^T A + M^T C]x + Z^T [\cancel{A}x + B_1u_1 + B_2u_2] \\ &= M^T Cx + Z^T B_1u_1 + Z^T B_2u_2 \end{aligned} \quad (11.5)$$

Substitute (11.2) into (11.5).

$$\frac{d}{dt}(Z^T x) = M^T(y - w) + Z^T B_1u_1 + Z^T B_2u_2 \quad (11.6)$$

Integrate (11.6) from t_0 to t_1 .

$$\begin{aligned} Z^T(t_1; t_1)x(t_1) - Z^T(t_0; t_1)x(t_0) \\ = \int_{t_0}^{t_1} M^T(\tau; t_1)y(\tau)d\tau - \int_{t_0}^{t_1} M^T(\tau; t_1)w(\tau)d\tau \\ + \int_{t_0}^{t_1} Z^T(\tau; t_1)B_1u_1d\tau + \int_{t_0}^{t_1} Z^T(\tau; t_1)B_2u_2d\tau \end{aligned} \quad (11.7)$$

Using $Z(t_1; t_1) = I$ and rearranging (11.7) we get

$$\begin{aligned} x(t_1) - \int_{t_0}^{t_1} M^T(\tau; t_1)y(\tau)d\tau = Z^T(t_0; t_1)x(t_0) - \int_{t_0}^{t_1} M^T(\tau; t_1)w(\tau)d\tau \\ + \int_{t_0}^{t_1} Z^T(\tau; t_1)B_1u_1d\tau + \int_{t_0}^{t_1} Z^T(\tau; t_1)B_2u_2d\tau \end{aligned} \quad (11.8)$$

Multiply (11.8) from the left by $f^T C$ where f is a vector to be determined. For the time being, regard f as given. Later we will have more to say about choosing f .

$$\begin{aligned} f^T C x(t_1) - f^T \int_{t_0}^{t_1} C M^T w d\tau &= f^T [y(t_1) - w(t_1)] - f^T \int_{t_0}^{t_1} C M^T w d\tau \\ &= h(t_1) - f^T w(t_1) \\ &= f^T C Z^T(t_0; t_1)x(t_0) - \int_{t_0}^{t_1} f^T C M^T w d\tau \\ &\quad + \int_{t_0}^{t_1} f^T C Z^T B_1 u_1 d\tau + \int_{t_0}^{t_1} f^T C Z^T B_2 u_2 d\tau \end{aligned} \quad (11.9)$$

Thus

$$\begin{aligned} h(t_1) &= f^T C Z^T(t_0; t_1)x(t_0) + f^T w(t_1) \\ &\quad + \int_{t_0}^{t_1} [f^T C Z^T(\tau, t_1)(B_1 u_1 + B_2 u_2) - f^T C M^T(\tau, t_1)w] d\tau \end{aligned} \quad (11.10)$$

Note that $h(t_1)$ in Equation (11.9) is a scalar. We want to choose f and M such that $h(t_1)$ is responsive to u_1 , but not to u_2 , w and x_0 . To accomplish this, set up the cost function

$$J = \frac{f^T C \left\{ Z^T(t_0; t_1)WZ(t_0) + \int_{t_0}^{t_1} [Z^T B_2 Q_2 B_2^T Z + M^T R M] d\tau \right\} C^T f + f^T V f}{f^T C \left\{ \int_{t_0}^{t_1} Z^T B_1 Q_1 B_1^T Z dt \right\} C^T f} \quad (11.11)$$

Equation (11.11) is subject to

$$\frac{d}{dt}Z(t; t_1) = -A^T z(t; t_1) + C^T M(t; t_1); \quad Z(t_1; t_1) = I \quad (11.12)$$

The cost function J penalizes the impulse response of $h(t_1)$ due to the input u_2 , but seeks to maximize the impulse response of $h(t_1)$ due to the input u_1 . The cost function also penalizes impulse response of the filter itself, and the response due to initial conditions. We want to choose M and f such that J is minimized.

In subsequent work it will be useful to express J in a slightly different form. To this end, add and subtract to the numerator of (11.12) γ^2 times the denominator of (11.12). Thus

$$\begin{aligned}
 J &= \\
 & \frac{f'C \left\{ Z'(t_0; t_1)WZ(t_0; t_1) + \int_{t_0}^{t_1} [Z'QZ + M'RM] d\tau + \gamma^2 \int_{t_0}^{t_1} Z'B_1Q_1B_1'Zd\tau \right\} C'f + f'Vf}{f'C \left[\int_{t_0}^{t_1} Z'B_1Q_1B_1'Zd\tau \right] C'f} \\
 &= \gamma^2 + \frac{f'Vf + f'C \left\{ Z'(t_0; t_1)WZ(t_0; t_1) + \int_{t_0}^{t_1} [Z'QZ + M'RM] d\tau \right\} C'f}{f'C \left[\int_{t_0}^{t_1} Z'B_1Q_1B_1'Ad\tau \right]} \quad (11.13)
 \end{aligned}$$

where

$$Q = B_2Q_2B_2^T - \gamma^2B_1Q_1B_1^T \quad (11.14)$$

Equation (11.1) can be cast into a still more convenient form by introducing a symmetric $n \times n$ matrix $P(t)$ which satisfies the matrix Riccati equation:

$$\dot{P} = PA^T + AP - PC^TR^{-1}CP + Q; \quad P(t_0) = W \quad (11.15)$$

Next form Z^TPZ and differentiate. Using (11.12) and (11.15) one obtains

$$\begin{aligned}
 \frac{d}{dt}(Z^TPZ) &= Z^TQZ + M^TCPZ \\
 &+ Z^TPC^TM - Z^TPC^TR^{-1}CPZ \quad (11.16)
 \end{aligned}$$

Integrating both sides of (11.16) leads to

$$\begin{aligned}
 Z^T(t_0; t_1)P(t_1)Z(t_0; t_1) - Z^T(t_0; t_1)P(t_0)Z(t_0; t_1) &= \\
 \int_{t_0}^{t_1} [Z^TQZ + M^TCPZ + Z^TPC^TM - Z^TPC^TR^{-1}CPZ] dt \quad (11.17)
 \end{aligned}$$

After some rearrangement, (11.17) can be written as

$$\begin{aligned} Z^T(t_0; t_1)WZ(t_0; t_1) + \int_{t_0}^{t_1} (Z^T QZ + M^T R M) dt = \\ Z^T(t_1; t_1)P(t_1)Z(t_1; t_1) + \int_{t_0}^{t_1} [M - R^{-1}CPZ]^T R [M - R^{-1}CPZ] dt \end{aligned} \quad (11.18)$$

Comparing (11.1) and (11.18) and using the fact that $Z(t_1; t_1) = I$ we see that J becomes

$$\begin{aligned} J &= \gamma^2 + \frac{f^T C \left\{ P(t_1) + \int_{t_0}^{t_1} [M - R^{-1}CPZ]^T R [M - R^{-1}CPZ] d\tau \right\} C^T f + f^T V f}{f' C \left\{ \int_{t_0}^{t_1} Z' B_1 Q_1 B_1' Z d\tau \right\} C' f} \\ &= \gamma^2 + \frac{f' [CP(t_1)C' + V] f}{f' C \left\{ \int_{t_0}^{t_1} Z' B_1 Q_1 B_1' Z d\tau \right\} C' f} \\ &\quad + \frac{f' C \left\{ \int_{t_0}^{t_1} [M - R^{-1}CPZ]' R [M - R^{-1}CPZ] d\tau \right\} C' f}{f' C \left\{ \int_{t_0}^{t_1} Z' B_1 Q_1 B_1' Z d\tau \right\} C' f} \end{aligned} \quad (11.19)$$

There are three quantities to be chosen in evaluating (11.19). They are γ^2 , $M(\tau, t_1)$ and f . For any particular values of f and γ^2 which are selected, J is minimized by choosing $M(\tau, t_1)$ to satisfy

$$M(\tau; t_1) = R^{-1}CP(\tau)Z(\tau; t_1) \quad (11.20)$$

With this choice J becomes:

$$J = \gamma^2 + \frac{f' [CP(t_1)C' + V] f}{f' C \left[\int_{t_0}^{t_1} Z' B_1 Q_1 B_1' z d\tau \right] C' f} \quad (11.21)$$

Now let's work on simplifying the demonimator of (11.21). Introduce $S(t)$ defined as

$$S(t) \triangleq \int_{t_0}^t Z'(\tau; t) B_1 Q_1 B_1' Z(\tau, t) dt \quad (11.22)$$

It can be shown (see Section 11.4) that $S(t)$ is the solution of the time varyng Lyapunov equation

$$\dot{S}(t) = A_{CL}(t)S(t) + S(t)A'_{CL}(t) + B_1 Q_1 B_1' \quad (11.23)$$

$$S(t_0) = 0 \quad (11.24)$$

$$A_{CL}(t) = A - K(t)C; \quad K(t) = P(t)C'R^{-1} \quad (11.25)$$

Using $S(t)$, J can be expressed as

$$J = \gamma^2 + \frac{f' [CP(t_1)C' + V] f}{f' CS(t_1)C' f} \quad (11.26)$$

Recall that this expression for J assumes that $M(\tau; t_1)$ has been chosen to satisfy (11.20).

Only γ^2 and f remain to be chosen. These parameters may be determined by a numerical search procedure which may be summarized as follows:

1. Select a value for γ^2 starting with $\gamma^2 = 0$ and gradually increasing γ^2 .
2. For each value of γ^2 start with $P(t_0) = W$, and solve the Riccati equation forward in time to obtain $P(t)$, $t_0 \leq t \leq t_1$. $P(t_1)$ is also determined in this step.
3. Using $P(t)$ from step 2, determine $A_{CL}(t)$ from (11.25). Then use $A_{CL}(t)$ to solve Equations (11.23 – 11.24) for $S(t_1)$.
4. Form the real symmetric matrices $N_1 = CP(t_1)C' + V$, $N_2 = CS(t_1)C'$, J may be expressed as

$$J = \gamma^2 + \frac{f' N_1 f}{f' N_2 f}$$

Solve the generalized eigenvalue problem

$$[N_1 + \lambda_i^2 N_2] \xi_i = 0$$

Choose f as the eigenvector corresponding to the smallest eigenvalue of this system, and normalize f such that $f' N_2 f = 1$. Then $f' N_1 f = \lambda_{\min}^2$, and

$$J = \gamma^2 + \lambda_{\min}^2$$

5. Gradually increase γ^2 and repeat steps 1-4 until one of the following two events occurs:
 - a. The eigenvalues of the Hamiltonian (i.e., the filter eigenvalues) move onto the imaginary axis. When this occurs γ^2 cannot be increased further because the filter would then become unstable.

- b. J passes through a smooth minimum ($dJ/d\gamma^2 = 0$) at which point one of the eigenvalues found in step 4 becomes zero. In this case f is chosen such that

$$f^T CP(t_1)C^T f = 0$$

Thus,

$$J = \gamma^2$$

The value of γ which results in either (a) or (b) will lead to the minimum value of J .

6. Once the minimizing value of γ^2 has been found, use this value to compute Q and hence $P(t)$. See (11.14), (11.12). Then using (11.12) and (11.20), the equation for $Z(t; t_1)$ becomes

$$\dot{Z}(t; t_1) = [-A' + C'R^{-1}CP(t)] Z(t, t_1); \quad Z(t_1; t_1) = I$$

Solve (6) backward in time to obtain $Z(\tau; t_1)$, $t_0 \leq t \leq t_1$.

7. Let

$$M(\tau, t_1) = R^{-1}CP(\tau)Z(\tau, t_1)$$

8. Using f from step 4, construct the filter as

$$h^o(t_1) = f^T \left[y(t_1) - \int_{t_0}^{t_1} CM'(\tau, t_1)y(\tau)d\tau \right] \quad (11.27)$$

11.2 On Line Filter

To develop an online version of the filter, let

$$\xi(t) \triangleq \int_{t_0}^t M^T(\tau, t)y(\tau)d\tau \quad (11.28)$$

where

$$M(\tau, t) = R^{-1}CP(\tau)Z(\tau, t) \quad (11.29)$$

$$\frac{dZ(\tau, t)}{d\tau} = (-A^T + C^T R^{-1} C P(\tau)) Z(\tau, t) \quad (11.30)$$

$$Z(t, t) = I \quad (11.31)$$

After some manipulation it can be shown [AM-1, Appendix B] that ξ satisfies the equation

$$\dot{\xi} = A\xi + PC^T R^{-1}[y - C\xi]; \quad \xi(t_0) = 0 \quad (11.32)$$

Thus, the filter given in (11.27) can also be expressed as

$$h^o(t_1) = f^T [y(t_1) - C\xi(t_1)] \quad (11.33)$$

where $\xi(t_1)$ is obtained from (11.32).

11.3 The Steady State Filter

In most cases, the fault detection filter will be implemented as a steady state filter, i.e., a linear filter in which the coefficient matrices are constant. Assume the pair (A, C) is detectable and that

$$\lim_{t_0 \rightarrow -\infty} P(t_0) = 0 \quad (11.34)$$

The steady state filter is then obtained as

$$h^o(t_1) = f^T [y(t_1) - C\xi(t_1)] \quad (11.35)$$

$$\dot{\xi} = A\xi + PC^T R^{-1}[y - C\xi]; \quad \xi(t_0) = 0 \quad (11.36)$$

In (11.35) and (11.36), P satisfies

$$PA^T + AP - PC^T R^{-1} CP + Q = 0 \quad (11.37)$$

and f is chosen as described in step 4 of section 2.

It is often instructive to look at a frequency domain expression for the steady state filter. To obtain such an expression, take the Laplace transform of (11.36). This yields:

$$s\xi = [A - PC^T R^{-1}C] \xi + PC^T R^{-1}y \quad (11.38)$$

Letting

$$K \triangleq PC^T R^{-1} \quad (11.39)$$

this becomes

$$\xi = (sI - A + KC)^{-1}Ky \quad (11.40)$$

Substitute (11.40) into the transform of (11.29).

$$h = f^t [I - C(sI - A + KC)^{-1}K] y \quad (11.41)$$

After defining Φ as

$$\Phi \triangleq (sI - A)^{-1} \quad (11.42)$$

Equation (11.41) can be written:

$$h = f^T (I + C\Phi K)^{-1}y \quad (11.43)$$

The frequency domain expression for y is:

$$y = C\Phi B_1 u_1 + C\Phi B_2 u_2 + w \quad (11.44)$$

Thus,

$$\begin{aligned} h = & f^T (I + C\Phi K)^{-1} C\Phi B_1 u_1 \\ & + f^T (I + C\Phi K)^{-1} C\Phi B_2 u_2 + f^T (I + C\Phi K)^{-1} w \end{aligned} \quad (11.45)$$

Equation (11.45) can be used to study the frequency response functions from u_1 , u_2 , and w to h . This will be illustrated by two examples.

11.4 Proofs

Proofs of some results developed in this chapter are presented in this section.

Proof A

Given

$$S(t) \triangleq \int_{t_0}^t Z'(\tau; t) B_1 Q_1 B_1' Z(\tau; t) d\tau \quad (11.46)$$

The derivative of S with respect to t becomes

$$\begin{aligned} \dot{S}(t) &= Z'(t; t) B_1 Q_1 B_1'(t, t) \\ &+ \int_{t_0}^t \frac{d}{dt} [Z'(\tau; t)] B_1 Q_1 B_1' Z(\tau; t) + Z'(\tau; t) B_1 Q_1 B_1' \frac{d}{dt} Z(\tau; t) dt \end{aligned} \quad (11.47)$$

Using (11.12) and (11.20) we obtain

$$\frac{d}{dt} Z(t; t_1) = -[A' - C'R^{-1}CP(t)] Z(t; t_1); \quad Z(t_1; t_1) = I \quad (11.48)$$

Let

$$K(t) \triangleq P(t)C'R^{-1} \quad (11.49)$$

$$A_{CL}(t) \triangleq A(t) - K(t)C \quad (11.50)$$

Then

$$\frac{d}{dt} Z(t; t_1) = -A'_{CL}(t)Z(t; t_1); \quad A(t_1; t_1) = I \quad (11.51)$$

$Z(t, t_1)$ is a transition matrix. Thus,

$$\begin{aligned} Z(t_1, t)Z(t; t_1) &= I \\ \dot{Z}(t_1; t)Z(t; t_1) + Z(t_1; t)\dot{Z}(t; t_1) &= 0 \\ \dot{Z}(t_1; t)Z(t; t_1) - Z(t_1; t)A'_{CL}(t)Z(t; t_1) &= 0 \\ \dot{Z}(t_1, t) &= Z(t_1, t)A'_{CL}(t) \\ \dot{Z}(t_1, t) &= A_{CL}(t)Z'(t_1, t) \end{aligned} \quad (11.52)$$

Substitution of τ for t_1 gives:

$$\frac{d}{dt}Z'(\tau, t) = A_{CL}(\tau)Z'(\tau, t) \quad (11.53)$$

$$\frac{d}{dt}Z(\tau, t) = Z(\tau, t)A'_{CL}(\tau) \quad (11.54)$$

Substitute (11.53) and (11.54) into (11.47) and note that $Z(t, t) = I$. This yields:

$$\begin{aligned} \dot{S}(t) &= B_1Q_1B'_1 + \int_{t_0}^t A_{CL}(\tau)Z'(\tau, t)B_1Q_1B'_1Z(\tau, t)d\tau \\ &\quad + \int_{t_0}^t Z'(\tau, t)B_1Q_1B'_1Z'(\tau, t)B_1Q_1B'_1Z(\tau, t)A'_{CL}(\tau)d\tau \\ &= B_1Q_1B'_1 + A_{CL}(t)S(t) + S(t)A'_{CL}(t) \end{aligned} \quad (11.55)$$

Hence, $S(t)$ is the solution of the equation

$$\begin{aligned} \dot{S}(t) &= A_{CL}(t)S(t) + S(t)A'_{CL}(t) + B_1Q_1B'_1 \\ S(t_0) &= 0 \end{aligned} \quad (11.56)$$

Proof B

$$\dot{\xi}(t) = M^T(t, t)y(t) + \int_{t_0}^t \frac{d}{dt}M^T(\tau, t)y(\tau)d\tau \quad (11.57)$$

$$M(t; t) = R^{-1}CP(t)Z(t; t) = R^{-1}CP(t) \quad (11.58)$$

$$\frac{d}{dt}M'(\tau, t) = \frac{d}{dt}Z'(\tau, t)P(\tau)C'R^{-1} \quad (11.59)$$

Since $Z(\tau, t)$ is a transition matrix,

$$Z(\tau, t)Z(t, \tau) = I \quad (11.60)$$

so

$$\frac{d}{dt}Z(\tau, t)Z(t, \tau) + z(\tau, t)\frac{d}{dt}Z(t, \tau) = 0 \quad (11.61)$$

Using (11.4) we get

$$\frac{d}{dt}Z(\tau, t)Z(t, \tau) + Z(\tau, t) [-A'Z(t, \tau) + C'M(t, \tau)] = 0 \quad (11.62)$$

$$\frac{d}{dt}Z(\tau, t)Z(t, \tau) - Z(\tau, t)A'Z(t, \tau) + Z(\tau, t)C'R^{-1}CP(t)Z(t, \tau) = 0 \quad (11.63)$$

$$\begin{aligned} \frac{d}{dt}Z(\tau, t) &= Z(\tau, t)A' - Z(\tau, t)C'R^{-1}CP(t) \\ &= Z(\tau, t) [A' - C'R^{-1}CP(t)] \end{aligned} \quad (11.64)$$

From (11.59) and (11.64),

$$\frac{d}{dt}M'(\tau, t) = [A - P(t)C'R^{-1}C] Z'(\tau, t)P(\tau)C'R^{-1} \quad (11.65)$$

Substitute (11.58) and (11.65) into (11.57)

$$\begin{aligned} \dot{\xi}(t) &= P(t)C'R^{-1}y(t) + \int_{t_0}^t [A - P(t)C'R^{-1}C] Z'(\tau, t)P(\tau)C'R^{-1}y(\tau)d\tau \\ &= A \int_{t_0}^t Z'(\tau, t)P(\tau)C'R^{-1}y(\tau)d\tau \\ &\quad + P(t)C'R^{-1} \left[y(t) - C \int_{t_0}^t Z'(\tau, t)P(\tau)C'R^{-1}y(\tau)d\tau \right] \\ &= A \int_{t_0}^t M'(\tau, t)y(\tau)d\tau - P(t)C'R^{-1} \left[y(t) - C \int_{t_0}^t M'(\tau, t)y(\tau)d\tau \right] \\ &= A\xi - PC'R^{-1}[y - C\xi] \end{aligned} \quad (11.66)$$

$$h = f_1'y = \int_{t_0}^{t_1} f_2'CM'y d\tau$$

$$\dot{Z} = -A'Z + C'M; \quad Z(t_1) = I$$

$$x(t_1) - \int M'y d\tau = Z'(t_0)x(t_0) - \int_{t_0}^{t_1} M'wd\tau + \int_{t_0}^{t_1} Z'B_1u_1d\tau + \int_{t_0}^{t_1} Z'B_2u_2d\tau$$

$$\begin{aligned} f_2' C x(t_1) &- \int_{t_0}^{t_1} f_2' C M' y d\tau + f_1' y - f_1' y \\ &= f_2' Z'(t_0) x(t_0) - \int_{t_0}^{t_1} f_2' C M' w d\tau + \int_{t_0}^{t_1} f_2' C Z' B_1 u_1 d\tau + \int_{t_0}^{t_1} f_2' C Z' B_2 u_2 d\tau \\ &= f_2' (y - w) - f_1' y + f_1' y - \int_{t_0}^{t_1} f_2' C M' y d\tau \\ &= h(t_1) - f_2' w + (f_2' - f_1') y \\ h(t_1) &= f_2' w + \underline{(f_2' - f_1') y} + f_2' Z'(t_0) x(t_0) \end{aligned}$$

CHAPTER 12

Model Input Reduction

TWO EXAMPLES of linear system input-order reduction problems are control blending and disturbance direction identification problems. In control blending problems, system input dimension is reduced to facilitate control design and implementation. Typically, the system has dynamically redundant actuators which are to be mapped to a smaller set of generalized controls and an associated control mapping.

In disturbance decoupling problems where the disturbance is meant to model neglected higher-order or nonlinear dynamics, determination of the direction from first principles is not always possible or practical. When the disturbance direction is found empirically, typically several directions are found, each one associated with a different operating point, and a suitable representative direction must be chosen. The problem is complicated further when the rank of the disturbance map is not known, that is, when it is not clear how many directions should be chosen from the empirically derived set.

One approach to model input reduction, appealing at first, is to inspect, pairwise, the angle between each rank one input direction. If all the angles are small it might seem

reasonable to choose any one direction or an average of all of them as a rank-one direction representative of the set (Patton and Chen 1992). However, given that the input directions form a linearly independent set, the angles depend on the chosen state-space basis. For $m \leq n$ linearly independent input directions where n is the dimension of the state-space, state transformations may be found that make the pairwise angles between the directions arbitrarily close to zero or 90 deg. It is, therefore, not clear whether the rank of the input map should be 1 or m or something in between.

A second approach is to group the input directions into a single multi-input mapping and to consider the singular values of this map (Sobel and Lallman 1989). If B_i is a linear system input map and $B = [B_1, \dots, B_m]$ an aggregate mapping, a reduced rank map is formed by combining the left singular vectors associated with the largest singular values of B , that is, once a threshold is chosen for what is to be considered a small singular value. However, this approach amounts to the first since the left singular vectors and singular values of B depend on the basis chosen for the state-space unless, of course, only unitary transformations on the state-space are allowed.

The underlying difficulty with both approaches is that the dynamics and input-output characteristics of the system are neglected. The following section introduces some notation. Section 12.2 presents an approach to model input reduction based on maximizing a system Hankel norm. Section 12.3 illustrates an application to a disturbance direction identification problem. A numerical example is included. Section 12.4 discusses an extension to input and output order reduction as applied to an internal feedback loop parameter variation model.

12.1 Notation

Let G be a linear time-invariant system with k inputs

$$\begin{aligned}\dot{x} &= Ax + B_1u_1 + \dots + B_ku_k \\ y &= Cx\end{aligned}$$

All system variables belong to real vector spaces $x \in \mathcal{X}$, $u_i \in \mathcal{U}_i$ and $y \in \mathcal{Y}$ with $n = \dim \mathcal{X}$, $m_i = \dim \mathcal{U}_i$ and $p = \dim \mathcal{Y}$. Define an aggregate control $u \in \mathcal{U} = \mathcal{U}_1 \oplus \dots \oplus \mathcal{U}_k$ and control

mapping $B = [B_1, \dots, B_k]$ where $m = \dim \mathcal{U}$. Also, define a reduced-input system $G(q)$ as

$$\begin{aligned}\dot{x} &= Ax + Bq\bar{u} \\ y &= Cx\end{aligned}$$

where $q : \mathbb{R} \mapsto \mathbb{R}^m$ and $\|q\| = 1$.

12.2 Input-Output Mappings and Model Input Reduction

The following sections build towards a Hankel norm maximization approach to model input reduction. Section 12.2.1 considers only the system output dynamic characteristics, that is, the pair (C, A) in forming a model input reduction problem. Section 12.2.2 considers only the system input dynamic characteristics, that is, the pair (A, B) . Section 12.2.3 considers both system input and output characteristics in the triple (C, A, B) and a Hankel norm cost function is formed.

12.2.1 Output Point of View

Consider the output of the system $y(t)$ for $t \in [0, \infty)$ generated only by a state initial condition $x(0) = x_0$. The \mathcal{L}_2 norm of $y(t)$ is given by

$$\|y\|_{\mathcal{L}_2[0, \infty)}^2 = \int_0^\infty x_0^T e^{A^T \tau} C^T C e^{A \tau} x_0 d\tau = x_0^T L_o x_0$$

where L_o , the observability gramian, is found as a solution to a steady-state Lyapunov equation

$$0 = A^T L_o + L_o A + C^T C$$

Now, define a reduced-order input map as $\bar{B} = Bq$ where $q : \mathbb{R} \mapsto \mathbb{R}^m$ and $\|q\| = 1$, that is, a dimension m input is to be reduced to a dimension one input. If the state initial condition x_0 is restricted to $\text{Im } B$ as $x_0 = Bq$, a model input reduction problem is to find q that maximizes $\|y\|$

$$\begin{aligned}\max_q J^o &= q^T B^T \int_0^\infty e^{A^T \tau} C^T C e^{A \tau} d\tau Bq \\ &= q^T B^T L_o Bq\end{aligned}\tag{12.1}$$

This is solved as an eigenvalue problem

$$J_{\max}^o = \lambda_{\max}(B^T L_o B)$$

with q taken to be the associated eigenvector. Since only the observability of the system pair (C, A) is considered, no weighting is given to the control energy required to reach the initial state x_0 .

12.2.2 Input Point of View

Having found an initial state direction $x_0 \in \text{Im } B$, note that the control energy required to reach x_0 by applying a control $\omega(t)$ over $t \in (-\infty, 0]$ could be arbitrarily large. A well-known result (Doyle et al. 1989) is that for a given state x_0 , the smallest signal $\omega \in \mathcal{L}(-\infty, 0]$ that produces x_0 has a norm given by

$$\inf_{\omega} \{\|\omega\|^2 | x(0) = x_0\} = x_0^T L_c^{-1} x_0$$

where L_c is the controllability gramian,

$$L_c = \int_{-\infty}^0 e^{-A\tau} B B^T e^{-A^T \tau} d\tau$$

also found as a solution to a steady-state Lyapunov equation

$$0 = A L_c + L_c A^T + B B^T$$

A best initial state x_0 is considered here as one requiring the smallest signal $\omega \in \mathcal{L}_2(-\infty, 0]$.

$$\sup_{\omega} \frac{\|x_0\|_{R^n}^2}{\|\omega\|_{L_2(-\infty, 0]}^2} = \max_{x_0} \frac{x_0^T x_0}{x_0^T L_c^{-1} x_0} = \lambda_{\max}(L_c)$$

where $\lambda_{\max}(L_c)$ is the largest eigenvalue of L_c and x_0 is the associated eigenvector

$$L_c x_0 = \lambda_{\max} x_0$$

A model input reduction problem that follows is to find q , $\|q\| = 1$ and the reduced-input map $\bar{B} = Bq$ by solving the following maximization problem

$$\begin{aligned} J_{\max}^c &= \max_q \max_{x_0} \frac{x_0^T x_0}{x_0^T \left[\int_{-\infty}^0 e^{-A\tau} B q q^T B^T e^{-A^T \tau} d\tau \right]^{-1} x_0} \\ &= \max_q \max_{x_0} \frac{x_0^T \int_{-\infty}^0 e^{-A\tau} B q q^T B^T e^{-A^T \tau} d\tau x_0}{x_0^T x_0} \end{aligned} \quad (12.2)$$

subject to $\|q\| = 1$ which is equivalent to

$$J_{\max}^c = \max_q \max_{x_0} x_0^T \int_{-\infty}^0 e^{-A\tau} B q q^T B^T e^{-A^T \tau} d\tau x_0 \quad (12.3)$$

subject to $\|q\| = 1$ and $\|x_0\| = 1$. The maximization problem (12.3) may be solved by adjoining the two constraints to the cost using Lagrange multipliers as in

$$J_{\max}^c = \max_q \max_{x_0} x_0^T \int_{-\infty}^0 e^{-A\tau} B q q^T B^T e^{-A^T \tau} d\tau x_0 - \lambda_x (x_0^T x_0 - 1) - \lambda_q (q^T q - 1)$$

The first-order variation of J^c with respect to x_0 and q ,

$$\begin{aligned} \delta J^c = & \left(x_0^T \int_{-\infty}^0 e^{-A\tau} B q q^T B^T e^{-A^T \tau} d\tau - \lambda_x x_0^T \right) \delta x_0 \\ & + \left(q^T B^T \int_{-\infty}^0 e^{-A^T \tau} x_0 x_0^T e^{-A\tau} d\tau B - \lambda_q q^T \right) \delta q \end{aligned}$$

provides a pair of eigenvalue problems as necessary conditions for J^c maximization

$$\begin{aligned} \int_{-\infty}^0 e^{-A\tau} B q q^T B^T e^{-A^T \tau} d\tau x_0 &= \lambda_x x_0 \\ B^T \int_{-\infty}^0 e^{-A^T \tau} x_0 x_0^T e^{-A\tau} d\tau B q &= \lambda_q q \end{aligned} \quad (12.4)$$

Furthermore, since $\|q\| = \|x_0\| = 1$, it follows that $\lambda_x = \lambda_q = J^c$. Thus J_{\max}^c is the largest eigenvalue of (12.4) and the necessary condition for maximizing J^c is

$$\int_{-\infty}^0 e^{-A\tau} B q q^T B^T e^{-A^T \tau} d\tau x_0 = \lambda_{\max_x} x_0 \quad (12.5a)$$

$$B^T \int_{-\infty}^0 e^{-A^T \tau} x_0 x_0^T e^{-A\tau} d\tau B q = \lambda_{\max_q} q \quad (12.5b)$$

There is no known closed form solution to (12.2.2) but a convergent iterative solution is to solve (12.5a) for x_0 while holding q fixed, then to solve (12.5b) for q while holding x_0 fixed and repeat. The convergence of the proposed iteration can be shown as follows. First, the cost (12.2.2), either $J_k^c = \lambda_{\max_{x,k}}$ or $J_k^c = \lambda_{\max_{q,k}}$, increases monotonically with each iteration since the eigenvalue problems (12.2.2) may be expressed as maximization problems. First, holding q fixed, (12.5a) gives λ_{\max_x} for iteration k as

$$\lambda_{\max_{x,k}} = \max_{x_0} \frac{x_0^T \int_{-\infty}^0 e^{-A\tau} B q q^T B^T e^{-A^T \tau} d\tau x_0}{x_0^T x_0} \quad (12.6)$$

Now, holding x_0 fixed, (12.5b) gives λ_{\max_q} for iteration $k + 1$ as

$$\begin{aligned}\lambda_{\max_q, k+1} &= \max_q \frac{q^T B^T \int_{-\infty}^0 e^{-A^T \tau} x_0 x_0^T e^{-A \tau} d\tau B q}{x_0^T x_0} \\ &= \max_q \frac{x_0^T \int_{-\infty}^0 e^{-A \tau} B q q^T B^T e^{-A^T \tau} d\tau x_0}{x_0^T x_0}\end{aligned}\quad (12.7)$$

Therefore,

$$\lambda_{\max_q, k+1} \geq \lambda_{\max_x, k} \geq \lambda_{\max_q, k-1} \geq \cdots \geq \lambda_{\max_x, 1}$$

Clearly, as long as $\|q\| = \|x_0\| = 1$, the cost J_k^c is bounded above. Thus J_k^c approaches a limit and the iteration must converge.

$$\lim_{k \rightarrow \infty} J_k^c = J_{\max}^c$$

While the uniqueness of the limit is not guaranteed, the experience of the authors has shown that in several practical applications the limit achieved is close to the upper bound given by $\lambda_{\max}(L_c)$ of the full-input system.

This approach is a dual to that of Section 12.2.1 in the sense that only the controllability of the system pair (A, B) is considered. No weight is given to the energy required to reconstruct the initial state x_0 from the output pair (C, A) .

12.2.3 Output and Input Point of View

Both input (12.1) and output (12.2.2) considerations are combined by maximizing the Hankel norm of the system triple $G \triangleq (C, A, Bq)$ as in

$$\begin{aligned}J_{max} &= \max_q \Gamma_G(q) \\ &= \max_q \sup_{\omega} \frac{\|y\|_{L_2[0, \infty)}^2}{\|\omega\|_{L_2(-\infty, 0]}^2} \\ &= \max_q \max_{x_0} \frac{x_0^T L_o x_0}{x_0^T \left[\int_{-\infty}^0 e^{-A \tau} B q q^T B^T e^{-A^T \tau} d\tau \right]^{-1} x_0} \\ &= \max_q \max_{x_0} \frac{x_0^T \int_{-\infty}^0 e^{-A \tau} B q q^T B^T e^{-A^T \tau} d\tau x_0}{x_0^T L_o^{-1} x_0}\end{aligned}$$

Necessary conditions for this problem are a pair of eigenvalue problems similar to (12.2.2) but with the premultiplication of an observability gramian

$$L_o \int_{-\infty}^0 e^{-A\tau} B q q^T B^T e^{-A^T \tau} d\tau x_0 = \lambda_{max_x} x_0 \quad (12.8a)$$

$$B^T \int_{-\infty}^0 e^{-A^T \tau} x_0 x_0^T e^{-A\tau} d\tau B q = \lambda_{max_q} q \quad (12.8b)$$

An iterative solution to (12.8) that is similar to that for (12.2.2) has been successfully applied.

12.3 Application to Disturbance Direction Estimation

Parametric uncertainties in a linear system model can often be modeled as scalar or low dimensional unknown inputs. Given the disturbance direction, a disturbance decoupling or bounding controller may be constructed to provide robustness to variations in the unknown system parameters. In practice, identifying this direction has its own uncertainty in the sense that usually a set of directions is formed from which a representative direction is chosen. For the purpose of illustration, an observer based method (Patton and Chen 1992) for identifying a disturbance direction is outlined below.

Consider a linear time invariant system with a scalar disturbance d

$$\dot{x} = Ax + Bu + Ed$$

The vector E is unknown and represents the direction of uncertainty acting on the system model. The direction E may be estimated by defining $Ed = w$, and forming an observer to estimate w . First, assume that w is a slowly time varying vector of dimension n . Then append it to the state vector to form a $2n$ -dimensional system

$$\begin{bmatrix} \dot{x} \\ \dot{w} \end{bmatrix} = \begin{bmatrix} A & I \\ 0 & 0 \end{bmatrix} \begin{bmatrix} x \\ w \end{bmatrix} + \begin{bmatrix} B \\ 0 \end{bmatrix} u \quad (12.9)$$

Since (12.9) is a system *model*, full state information may be assumed so that the observation relation is

$$y = [I \ 0] \begin{bmatrix} x \\ w \end{bmatrix} \quad (12.10)$$

An observer based on the model (12.9, 12.10) is used to estimate w . The measurements provided to the observer are from the full higher-order or nonlinear system or simulation. It is assumed that constant controls u are applied so that the observer eventually reaches a steady-state and an estimate for w , that is \hat{w} , becomes a constant. The disturbance direction E is a normalized \hat{w} . In general, the direction E found will depend on the size and direction of the control vector u applied to the nonlinear plant. Thus a system model with several disturbance directions is formed as

$$\dot{x} = Ax + Bu + \begin{bmatrix} E_1 & E_2 & \dots & E_m \end{bmatrix} \begin{bmatrix} d1 \\ d2 \\ \vdots \\ d_m \end{bmatrix}$$

The problem now is to determine an appropriate reduced dimension and range for the disturbance distribution matrix $[E_1, E_2, \dots, E_m]$.

A numerical example follows from the longitudinal dynamics of an automobile linearized as the vehicle is driven on a straight and level road at a constant speed 25 m/s. A small slope in the road appears as a disturbance in the dynamics. Thus the model becomes

$$\begin{aligned} \dot{x} &= Ax + Bu + E_1d_1 + E_2d_2 + E_3d_3 + E_4d_4 \\ y &= Cx \end{aligned}$$

The states are engine manifold air mass, engine speed, longitudinal and vertical velocity, vertical position, the sum of two front wheel speeds and the sum of two rear wheel speeds. The control inputs are throttle and brake commands. The disturbance directions $E = [E_1, E_2, E_3, E_4]$ are found for road slopes of -1 , -2 , -3 and 0 degrees respectively when the brake is held fixed at the trim value and the throttle is held fixed slightly away from the trim value. Data for the system are as follows.

$$A = \begin{bmatrix} -0.0521 & -0.2213 & 0.2681 & -0.0121 & 0.0136 & 0.0084 & -0.0078 \\ -0.3007 & -8.0277 & 19.0734 & -1.1013 & 0.0795 & 0.2471 & 0.0378 \\ -0.3263 & -19.7571 & -51.0638 & -3.2675 & -4.8766 & -2.4258 & 0.0040 \\ 0.0454 & 2.4036 & 15.7922 & -2.1857 & 6.4655 & -0.2062 & 0.0495 \\ 0.0219 & 1.1136 & 8.6428 & -7.1817 & -0.6526 & -0.2171 & 0.9316 \\ 0.0116 & 0.5928 & 3.8335 & -1.0926 & -0.6513 & -0.9851 & 5.9628 \\ 0.0154 & 0.7868 & 4.8494 & -1.4900 & -1.0329 & -6.5688 & -2.5996 \end{bmatrix}$$

$$\begin{aligned}
 B &= \begin{bmatrix} 0.0362 & 0.0711 & 0.0976 & 0.0164 \\ 0.0786 & 0.1585 & 0.2222 & 0.0343 \\ 0.2191 & 0.3765 & 0.4450 & 0.1128 \\ 0.0404 & 0.0452 & 0.0628 & 0.0419 \\ 0.1057 & 0.1292 & 0.1559 & 0.0943 \\ 0.3199 & 0.2969 & 0.2822 & 0.3294 \\ -0.9107 & -0.8492 & -0.7970 & -0.9310 \end{bmatrix} \\
 E &= \begin{bmatrix} 0.0362 & 0.0711 & 0.0976 & 0.0164 \\ 0.0786 & 0.1585 & 0.2222 & 0.0343 \\ 0.2191 & 0.3765 & 0.4450 & 0.1128 \\ 0.0404 & 0.0452 & 0.0628 & 0.0419 \\ 0.1057 & 0.1292 & 0.1559 & 0.0943 \\ 0.3199 & 0.2969 & 0.2822 & 0.3294 \\ -0.9107 & -0.8492 & -0.7970 & -0.9310 \end{bmatrix} \\
 C &= \begin{bmatrix} 0.0075 & 0.4605 & 0.3710 & 0.1023 & 0.0513 & 0.0340 & -0.0137 \\ 0.7318 & 2.7938 & -2.8640 & 0.1680 & -0.0415 & -0.0491 & -0.0029 \\ 0.0028 & 0.1711 & -0.2654 & 0.0765 & -0.0161 & 0.0093 & -0.0008 \\ 0.0000 & -0.0007 & -0.0005 & -0.0216 & -0.0496 & -0.0438 & 0.0697 \\ -0.0000 & -0.0024 & 0.0050 & 0.0111 & 0.0205 & -0.0027 & 0.0009 \\ 0.4214 & -0.1440 & 0.0371 & 0.2203 & -0.1764 & -0.0129 & 0.1051 \\ 0.4211 & 0.1318 & -0.4410 & -0.2741 & -0.0304 & -0.0734 & 0.0585 \end{bmatrix}
 \end{aligned}$$

Using the iterative approach of Section 12.2.3, it is found that the maximum Hankel norm of the reduced-input system is 1.343161 where

$$q = [0.2816 \quad 0.5588 \quad 0.7699 \quad 0.1252]^T$$

and is found in two iteration steps. The Hankel norm of the full-input system is 1.343171. By considering the Hankel norm and system eigenvectors, the original and reduced-input systems appear to be quite similar in their input-output properties. This might seem a bit surprising given that the four disturbance directions are, pairwise, 24.26, 17.91, 17.52, 11.08, 6.85 and 6.64 degrees apart.

12.4 Extension to Parameter Variation Model Reduction

This section discusses an extension to input and output order reduction as applied to an internal feedback loop parameter variation model (Tahk and Speyer 1987, Doyle 1982).

Within the context of an uncertain parameter block variation model Δ of the form

$$\begin{aligned}\dot{x} &= Ax + Bu + B_\omega \omega \\ y &= Cx \\ z &= C_z x \\ \omega &= \Delta z\end{aligned}$$

consider a model input and output reduction problem posed as follows. Find q_ω and q_z with $\|q_\omega\| = \|q_z\| = 1$ such that the system triple

$$G \triangleq (q_z^T C_z, A, B_\omega q_\omega)$$

maximizes the Hankel norm

$$\begin{aligned}J_{\max} &= \max_{q_\omega} \max_{q_z} \Gamma_G(q_\omega, q_z) \\ &= \max_{q_\omega} \max_{q_z} \max_{x_0} \frac{x_0^T L_o x_0}{x_0^T L_c^{-1} x_0} \\ &= \max_{q_\omega} \max_{q_z} \lambda_{\max}(L_c L_o)\end{aligned}$$

where

$$\begin{aligned}L_c &= \int_{-\infty}^0 e^{-A\tau} B_\omega q_\omega q_\omega^T B_\omega^T e^{-A^T \tau} d\tau \\ L_o &= \int_0^\infty e^{A^T \tau} C_z^T q_z q_z^T C_z e^{A\tau} d\tau\end{aligned}$$

This problem is also solved iteratively. First, hold q_z fixed and solve for q_ω , then hold q_ω fixed and solve for q_z . The former problem is the same problem as that in Section 12.2.3; the latter is the dual. Necessary conditions that follow are

$$L_o L_c x_{01} = \lambda_{\max x_{01}} x_{01} \quad (12.11a)$$

$$B_\omega^T \int_{-\infty}^0 e^{-A^T \tau} x_{01} x_{01}^T e^{-A\tau} d\tau B_\omega q_\omega = \lambda_{\max q_\omega} q_\omega \quad (12.11b)$$

and

$$L_c L_o x_{02} = \lambda_{\max x_{02}} x_{02} \quad (12.12a)$$

$$C_z \int_0^\infty e^{A\tau} x_{02} x_{02}^T e^{A^T \tau} d\tau C_z^T q_z = \lambda_{\max q_z} q_z \quad (12.12b)$$

The proposed iteration is to solve (12.11a) and (12.11b) holding q_z fixed until x_{01} and q_ω are found. Then, holding q_ω fixed, solve (12.12a) and (12.12b) iteratively for x_{02} and q_z . The stopping condition is when $J_{max} = \lambda_{max_{x_{01}}} = \lambda_{max_{x_{02}}}$ within some tolerance. Note that with both q_ω and q_z as one-dimensional mappings, Δ is a scalar.

12.5 Conclusions

A reduced-input system problem is formed from the point of view of preserving system input-output properties. Necessary conditions for maximizing a reduced-input system Hankel norm are stated and an iterative solution is proposed. An application to disturbance direction identification is illustrated with a numerical example. Finally, an extension to include applications to internal feedback loop parameter variation models is developed.

CHAPTER 13

Conclusions

ANALYTIC REDUNDANCY continues to be a viable approach to vehicle health monitoring. The fault detection filters and parity equations developed here as a point design for the longitudinal mode are tested in a high-fidelity vehicle simulation where nonlinearities and road variations are significant. The designed static patterns emerge clearly and quickly in response to a fault. The residual processor, a multiple hypothesis Shirayayev sequential probability ratio test, examines the filter and parity equation residuals and generates the probability of the presence of a fault. This system also works well, responding to soft failures in the presence of dynamic disturbances and vehicle nonlinearities. Sensor noise has been omitted pending development of higher fidelity sensor models.

The design as presented is intended to be packaged as a module of a comprehensive health monitoring and reconfiguration system under development at UC Berkeley. Further development of this module should involve testing with empirically derived data and the design and implementation of a software interface compatible with the system at Berkeley.

A preliminary design of a range sensor fault monitoring system is sketched as an application of a new decentralized fault detection filter structure. This system combines dynamic state information already generated by the existing filter designs with inter-vehicle analytic redundancy. This approach will be more fully tested as a high-fidelity multi-vehicle simulation becomes available.

APPENDIX A

Fault Detection Filter Design Data

THE REDUCED-ORDER longitudinal linearized system matrices used for fault detection filter design are

$$A = \begin{bmatrix} -22.56 & -0.12 & 0 & 0 & 0 & 0 & 0 & 0 \\ 307.03 & -35.41 & 396.80 & -2698.58 & -238.10 & 1901.28 & -432.86 & -0.08 \\ 0 & 0.07 & -0.76 & 4.87 & 0.43 & -3.29 & 0.87 & -0.00 \\ 0 & 0 & 0.00 & 0 & 1.00 & -25.00 & 0 & 0 \\ 0 & -0.00 & -0.01 & -39.72 & -3.50 & 78.91 & 24.20 & 0.00 \\ 0 & 0 & 0 & 0 & 0 & 0 & 1.00 & 0 \\ 0 & -0.02 & 0.22 & -7.19 & -0.61 & -25.26 & -3.73 & 0.00 \\ 0 & 0 & 0 & 0 & 0 & 0 & 0 & -1.25 \end{bmatrix}$$

$$B = \begin{bmatrix} 2.35 & 0 & -0.12 \\ 0 & 0 & 1.66 \\ 0 & 0 & 0 \\ 0 & 0 & 0 \\ 0 & 0 & 0 \\ 0 & 0 & 0 \\ 0 & 0 & 0 \\ 0 & 1.25 & 0 \end{bmatrix}$$

$$C = \begin{bmatrix} 1.00 & 0 & 0 & 0 & 0 & 0 & 0 & 0 \\ 0 & 1.00 & 0 & 0 & 0 & 0 & 0 & 0 \\ 0 & 0 & 1.00 & 0 & 0 & 0 & 0 & 0 \\ 0 & 0.07 & -0.76 & 4.87 & 0.43 & -3.29 & 0.87 & -0.00 \\ 0 & -0.00 & -0.01 & -39.72 & -3.50 & 78.91 & 24.20 & -0.00 \\ 0 & 0 & 7.10 & -45.34 & -4.00 & 146.48 & 2.83 & -0.00 \\ 0 & 0.09 & 5.96 & -40.56 & -3.58 & 28.58 & -6.51 & -0.00 \end{bmatrix}$$

$$D = \begin{bmatrix} 0 & 0 & 0 \\ 0 & 0 & 0 \\ 0 & 0 & 0 \\ 0 & 0 & 0 \\ 0 & 0 & 0 \\ 0 & 0 & 0 \\ 0 & 0 & 0 \end{bmatrix}$$

The filter gain L and the output projection matrices \hat{H}_{u_α} , $\hat{H}_{u_{T_b}}$, $\hat{H}_{y_{m_a}}$ and $\hat{H}_{y_{T_m}}$ for the first fault detection filter are as follows.

$$L = \begin{bmatrix} 19.56 & 0.12 & 0.00 & 0.00 & -0.00 & -0.00 & 0.00 \\ -307.03 & 523.06 & -334.41 & -6277.18 & 8.39 & 3.99 & -832.46 \\ -0.00 & 11.97 & -11.36 & -156.00 & 0.20 & 0.10 & -18.91 \\ 0.00 & 0.00 & -1.96 & -0.10 & -0.06 & 0.19 & 0.03 \\ 0.00 & -0.07 & -7.21 & -0.00 & -1.17 & -0.08 & 0.83 \\ -0.00 & -0.00 & 0.01 & -0.01 & -0.02 & -0.02 & 0.03 \\ 0.00 & -3.51 & 1.38 & 46.16 & -0.26 & 0.32 & 5.26 \\ -0.00 & -60.65 & 19.39 & 784.64 & -2.29 & 0.07 & 96.37 \end{bmatrix}$$

$$\hat{H}_{u_\alpha} = \begin{bmatrix} 0.93 & 0.07 & -0.02 & 0.11 & 0.16 & -0.10 & -0.11 \\ 0.07 & 0.01 & -0.00 & 0.01 & 0.00 & 0.03 & -0.05 \\ -0.02 & -0.00 & 0.99 & 0.04 & 0.05 & -0.03 & -0.04 \\ 0.11 & 0.01 & 0.04 & 0.16 & -0.28 & -0.12 & -0.18 \\ 0.16 & 0.00 & 0.05 & -0.28 & 0.62 & 0.23 & 0.28 \\ -0.10 & 0.03 & -0.03 & -0.12 & 0.23 & 0.73 & -0.35 \\ -0.11 & -0.05 & -0.04 & -0.18 & 0.28 & -0.35 & 0.55 \end{bmatrix}$$

$$\hat{H}_{u_{T_b}} = \begin{bmatrix} 0 & 0.00 & 0 & 0.00 & -0.00 & 0 & 0.00 \\ 0.00 & 0.01 & 0 & -0.07 & 0.00 & 0 & -0.09 \\ 0 & 0 & 1.00 & 0 & 0 & 0 & 0 \\ 0.00 & -0.07 & 0 & 1.00 & 0.00 & 0 & -0.01 \\ -0.00 & 0.00 & 0 & 0.00 & 1.00 & 0 & 0.00 \\ 0 & 0 & 0 & 0 & 0 & 1.00 & 0 \\ 0.00 & -0.09 & 0 & -0.01 & 0.00 & 0 & 1.00 \end{bmatrix}$$

$$\hat{H}_{y_{m_a}} = \hat{H}_{y_{T_m}} = \begin{bmatrix} 0 & 0 & 0 & 0 & 0 & 0 & 0 \\ 0 & 0.08 & -0.02 & 0.13 & 0.16 & -0.07 & -0.16 \\ 0 & -0.02 & 1.00 & 0.00 & 0.00 & -0.00 & -0.00 \\ 0 & 0.13 & 0.00 & 0.35 & -0.02 & -0.28 & -0.36 \\ 0 & 0.16 & 0.00 & -0.02 & 0.97 & 0.01 & 0.03 \\ 0 & -0.07 & -0.00 & -0.28 & 0.01 & 0.86 & -0.19 \\ 0 & -0.16 & -0.00 & -0.36 & 0.03 & -0.19 & 0.74 \end{bmatrix}$$

The filter gain L and the output projection matrices $\hat{H}_{y_{\omega_e}}$, $\hat{H}_{y_{a_x}}$, $\hat{H}_{y_{\omega_f}}$ for the second fault detection filter are as follows.

$$L = \begin{bmatrix} 18.56 & 0.12 & -0.00 & 0.00 & 0.00 & -0.00 & 0.00 \\ -307.03 & 38.32 & -0.00 & -0.00 & -0.00 & 0.00 & -66.53 \\ 0.01 & -0.00 & -3.00 & -1.00 & 0.00 & 0.00 & 0.00 \\ 0.75 & 0.01 & 0.16 & -0.04 & 0.04 & 0.21 & -0.13 \\ 2.16 & -0.00 & 4.11 & -0.01 & -0.61 & -0.00 & -0.08 \\ -0.01 & -0.00 & -0.13 & -0.02 & -0.03 & -0.02 & 0.05 \\ 0.54 & 0.03 & 0.02 & 0.36 & -0.12 & 0.33 & -0.38 \\ 0.01 & -95.97 & 32.35 & 1230.72 & -3.58 & 0.10 & 151.14 \end{bmatrix}$$

$$\hat{H}_{y_{\omega_e}} = \begin{bmatrix} 1.00 & -0.00 & -0.00 & 0.00 & 0.00 & -0.00 & -0.00 \\ -0.00 & 1.00 & -0.00 & 0.00 & 0.00 & 0.00 & -0.00 \\ -0.00 & -0.00 & 0.99 & 0.00 & 0.09 & -0.00 & -0.02 \\ 0.00 & 0.00 & 0.00 & -0.00 & 0.00 & -0.00 & -0.00 \\ 0.00 & 0.00 & 0.09 & 0.00 & 0.01 & -0.00 & -0.00 \\ -0.00 & 0.00 & -0.00 & -0.00 & -0.00 & 0.00 & 0.00 \\ -0.00 & -0.00 & -0.02 & -0.00 & -0.00 & 0.00 & 0.00 \end{bmatrix}$$

$$\hat{H}_{y_{a_x}} = \begin{bmatrix} 1.00 & 0.00 & 0.00 & -0.04 & 0.06 & -0.00 & -0.06 \\ 0.00 & 0.00 & -0.00 & 0.00 & 0.00 & -0.00 & -0.00 \\ 0.00 & -0.00 & 1.00 & 0.00 & -0.00 & -0.00 & 0.00 \\ -0.04 & 0.00 & 0.00 & 0.03 & 0.18 & -0.00 & -0.03 \\ 0.01 & 0.00 & -0.00 & 0.18 & 0.94 & -0.00 & -0.17 \\ -0.00 & -0.00 & -0.00 & -0.00 & -0.00 & 0.00 & 0.00 \\ -0.01 & -0.00 & 0.00 & -0.03 & -0.17 & 0.00 & 0.03 \end{bmatrix}$$

$$\hat{H}_{y_{\omega_f}} = \begin{bmatrix} 1.00 & -0.00 & 0.00 & 0.00 & -0.01 & 0.03 & -0.04 \\ -0.00 & -0.00 & -0.00 & -0.00 & 0.00 & 0.00 & 0.00 \\ 0.00 & -0.00 & 0.99 & 0.00 & 0.05 & -0.05 & -0.02 \\ 0.00 & -0.00 & 0.00 & 0.00 & -0.00 & -0.00 & -0.00 \\ -0.01 & 0.00 & 0.05 & -0.00 & 0.58 & 0.47 & 0.15 \\ 0.03 & 0.00 & -0.05 & -0.00 & 0.47 & 0.39 & 0.12 \\ -0.04 & 0.00 & -0.02 & -0.00 & 0.15 & 0.12 & 0.04 \end{bmatrix}$$

The filter gain L and the output projection matrices $\hat{H}_{y_{vx}}$, $\hat{H}_{y_{\alpha z}}$, $\hat{H}_{y_{\omega_f}}$ for the third fault detection filter are as follows.

$$L = \begin{bmatrix} 1.96 & 0.12 & -0.00 & 0.00 & -0.00 & -0.00 & 0.00 \\ -307.03 & 38.32 & -0.00 & 0.01 & -0.00 & 0.00 & -66.53 \\ -0.00 & 0.00 & -3.01 & -1.01 & 0.00 & -0.00 & 0.00 \\ 0.00 & 0.07 & -1.11 & -0.52 & -0.06 & 0.34 & -0.10 \\ 0.00 & 0.38 & -0.02 & -3.38 & -1.14 & 0.56 & 0.01 \\ -0.00 & -0.00 & -0.24 & -0.06 & -0.03 & -0.04 & 0.05 \\ 0.00 & 0.03 & 0.26 & 0.39 & -0.15 & 0.36 & -0.35 \\ 0.00 & -94.97 & 14.68 & 1234.19 & -3.10 & 1.68 & 151.15 \end{bmatrix}$$

$$\hat{H}_{y_{vx}} = \begin{bmatrix} 1.00 & -0.00 & -0.00 & 0.00 & -0.00 & -0.00 & 0.00 \\ -0.00 & 0.00 & -0.00 & -0.03 & 0.00 & -0.01 & 0.00 \\ -0.00 & -0.00 & 1.00 & 0.00 & -0.00 & -0.00 & 0.00 \\ 0.00 & -0.03 & 0.00 & 0.90 & -0.00 & 0.30 & -0.00 \\ -0.00 & 0.00 & -0.00 & -0.00 & -0.00 & -0.00 & -0.00 \\ -0.00 & -0.01 & -0.00 & 0.30 & -0.00 & 0.10 & -0.00 \\ 0.00 & 0.00 & 0.00 & -0.00 & -0.00 & -0.00 & -0.00 \end{bmatrix}$$

$$\hat{H}_{y_{\alpha z}} = \begin{bmatrix} 1.00 & 0.00 & 0.00 & 0.00 & -0.00 & 0.00 & 0.00 \\ 0.00 & 0.03 & -0.00 & -0.08 & 0.02 & 0.16 & -0.00 \\ 0.00 & -0.00 & -0.00 & 0.00 & -0.00 & -0.00 & -0.00 \\ 0.00 & -0.08 & 0.00 & 0.99 & 0.07 & 0.00 & 0.00 \\ -0.00 & 0.02 & -0.00 & 0.07 & 0.03 & 0.16 & -0.00 \\ 0.00 & 0.15 & -0.00 & 0.00 & 0.16 & 0.95 & -0.00 \\ 0.00 & -0.00 & -0.00 & 0.00 & -0.00 & -0.00 & -0.00 \end{bmatrix}$$

$$\hat{H}_{y_{\omega_f}} = \begin{bmatrix} 1.00 & -0.00 & 0.00 & -0.00 & -0.00 & 0.0 & 0.00 \\ -0.00 & 1.00 & 0.00 & -0.00 & 0.00 & 0.00 & 0.00 \\ 0.00 & 0.00 & -0.00 & -0.00 & -0.00 & -0.00 & -0.00 \\ -0.00 & -0.00 & -0.00 & 0.99 & -0.00 & 0.01 & 0.12 \\ -0.00 & 0.00 & -0.00 & -0.00 & 0 & -0.00 & -0.00 \\ 0.00 & 0.00 & -0.00 & 0.01 & -0.00 & 0.00 & 0.00 \\ 0.00 & 0.00 & -0.00 & 0.12 & -0.00 & 0.00 & 0.01 \end{bmatrix}$$

References

- Athans, M. 1977. The Stochastic Control of the F-8C Aircraft using a Multiple Model Adaptive Control Method : Equilibrium Flight. *IEEE Transactions on Automatic Control*, Vol. 5:768–780.
- Başar, T. and P. Bernhard 1995. \mathcal{H}_∞ Control and Other Minimax Problems. Birkhäuser, New York, 2nd edition.
- Banavar, R. N. and J. L. Speyer 1991. An Linear-Quadratic Game Approach to Estimation and Smoothing. In *Proceedings of the American Control Conference*, pages 2818–2822.
- Basile, G. and G. Marro 1992. *Controlled and Conditioned Invariants in Linear System Theory*. Prentice-Hall.
- Beard, R. V. 1971. *Failure Accomodation in Linear Systems through Self-Reorganization*. PhD thesis, Department of Aeronautics and Astronautics, Massachusetts Institute of Technology, Cambridge, MA.

- Bell, D. J. and D. H. Jacobsen 1973. *Singular Optimal Control*. Academic Press.
- Bryson, A. E. and Y. C. Ho 1975. *Applied Optimal Control*. New York: Hemisphere.
- Bryson, A. E. and D. Johansen 1965. Linear Filtering for Time-Varying Systems Using Measurements Containing Colored Noise. *IEEE Transactions on Automatic Control*, Vol. AC-10, No. 1:4–10.
- Chichka, D. F. and J. L. Speyer 1995. An Adaptive Controller Based on Disturbance Attenuation. *IEEE Transactions on Automatic Control*, Vol. AC-40, No. 7:1220–1233.
- Chung, W. H. 1997. *Game Theoretic and Decentralized Estimation for Fault Detection*. PhD thesis, University of California, Los Angeles.
- Chung, W. H. and J. L. Speyer 1995. A General Framework for Decentralized Estimation. In *Proceedings of the 1995 American Controls Conference*, Seattle, WA. ACC.
- Chung, W. H. and J. L. Speyer 1996. A Game Theoretic Filter for Fault Detection and Isolation. In *Proceedings of the 13th Triennial IFAC World Congress*.
- Chung, W. H. and J. L. Speyer 1998. A Game Theoretic Fault Detection Filter. To be published in the *IEEE Transactions on Automatic Control*.
- Clements, D. J. and B. D. O. Anderson 1978. *Singular Optimal Control: The Linear-Quadratic Problem*, volume 5 of *Lecture Notes in Control and Information Sciences*. Springer-Verlag.
- DeSouza, C., U. Shaked, and M.-Y. Fu 1992. Robust \mathcal{H}_∞ Filtering with Parametric Uncertainty and Deterministic Input Signal. In *Proceedings of the 31st Conference on Decision and Control*, pages 2305–2310, Tuscon, AZ.
- Ding, X. and P. M. Frank 1989. Fault Detection via Optimally Robust Detection Filters. In *Proceedings of the 28th Conference on Decision and Control*, pages 1767–1772, Tampa, FL. IEEE.

- Douglas, R. K. 1993. *Robust Fault Detection Filter Design*. PhD thesis, The University of Texas at Austin, Austin, TX.
- Douglas, R. K. and J. L. Speyer 1995. An \mathcal{H}_∞ Bounded Fault Detection Filter. In *Proceedings of the American Controls Conference*.
- Douglas, R. K. and J. L. Speyer 1996. Robust Fault Detection Filter Design. *AIAA Journal of Guidance, Control, and Dynamics*, Vol. 19, No. 1:214–218.
- Douglas, R. K., J. L. Speyer, D. L. Mingori, R. H. Chen, D. P. Malladi, and W. H. Chung 1995. Fault Detection and Identification with Application to Advanced Vehicle Control Systems. Research Report UCB-ITS-PRR-95-26, University of California, Los Angeles, MAE Dept. and California PATH.
- Douglas, R. K., J. L. Speyer, D. L. Mingori, R. H. Chen, D. P. Malladi, and W. H. Chung 1996. Fault Detection and Identification with Application to Advanced Vehicle Control Systems: Final Report. Research Report UCB-ITS-PRR-96-25, University of California, Los Angeles, MAE Dept. and California PATH.
- Doyle, J. C. 1982. Analysis of Feedback Systems with Structured Uncertainties. In *Proceedings of the IEE*. Part D, No. 6.
- Doyle, J. C., K. Glover, P. P. Khargonekar, and B. A. Francis 1989. State-Space Solutions to Standard \mathcal{H}_2 and \mathcal{H}_∞ Control Problems. *IEEE Transactions on Automatic Control*, Vol. AC-34, No. 8:831–847.
- Edelmayer, A., J. Bokor, and L. Keviczky 1994. An \mathcal{H}_∞ Filtering Approach to Robust Detection of Failures in Dynamical Systems. In *Proceedings of the 33rd IEEE Conference on Decision and Control*, Lake Buena Vista, Florida.
- Edelmayer, A., J. Bokor, and L. Keviczky 1996. \mathcal{H}_∞ Detection Filter Design for Linear Systems: Comparison of Two Approaches. In *Proceedings of the 13th Triennial IFAC World Congress*, San Francisco, California.

- Francis, B. A. 1979. The Optimal Linear-Quadratic Time-Invariant Regulator with Cheap Control. *IEEE Transactions on Automatic Control*, Vol. 24, No. 4:616–621.
- Frank, P. M. 1990. Fault Diagnosis in Dynamic Systems Using Analytical and Knowledge-based Redundancy – A Survey and Some New Results. *Automatica*, Vol. 26, No. 3:459–474.
- Frank, P. M. 1994. Enhancement of Robustness in Observer-Based Fault Detection. *International Journal of Control*, Vol. 59, No. 4:955–981.
- Ghaoui, L. E., A. Carrier, and A. E. Bryson 1992. Linear Quadratic Minimax Controllers. *AIAA Journal of Guidance, Control, and Dynamics*, Vol. 15, No. 4:953–961.
- Green, M. and D. J. N. Limebeer 1995. *Linear Robust Control*. Prentice-Hall.
- Iwasake, T. and R. E. Skelton 1994. All Controllers for the General \mathcal{H}_∞ Control Problem: LMI Existence Conditions and State Space Formulas. *Automatica*, Vol. 30, No. 8:1307–1317.
- Jacobson, D. H. 1971. Totally Singular Quadratic Optimization Problems. *IEEE Transactions on Automatic Control*, Vol. AC-16, No. 6:651–658.
- Jacobson, D. H. and J. L. Speyer 1971. Necessary and Sufficient Conditions for Optimality for Singular Control Problems: A Limit Approach. *Journal of Mathematical Analysis and Applications*, Vol. 34, No. 2:239–266.
- Jang, J. and J. L. Speyer 1994. Decentralized Game-Theoretic Filters. In *Proceedings of the American Control Conference*, pages 3379–3384, Baltimore, MD. ACC.
- Jones, H. L. 1973. *Failure Detection in Linear Systems*. PhD thesis, Department of Aeronautics and Astronautics, Massachusetts Institute of Technology, Cambridge, MA.
- Kalman, R. E. 1964. When is a Linear Control System Optimal. *Transactions of the ASME, Journal of Basic Engineering, Series D*, Vol. 86:51–50.

- Kerr, T. 1985. Decentralized Filtering and Redundancy Management/Failure Detection for Multisensor Integrated Navigation Systems. In *Proceedings of the ION National Technical Meeting*. Institute of Navigation.
- Khalil, H. K. 1996. *Nonlinear Systems*. Prentice-Hall Inc., 2nd edition.
- Klema, V. C. and A. J. Laub 1980. The Singular Value Decomposition: Its Computation and Some Applications. *IEEE Transactions on Automatic Control*, Vol. AC-25, No. 2.
- Kwakernaak, H. and R. Sivan 1972. The Maximally Achievable Accuracy of Linear Optimal Regulators and Linear Optimal Filters. *IEEE Transactions on Automatic Control*, Vol. AC-17, No. 1:79–86.
- Lainiotis, D. G. 1976. Partitioning : A Unified Framework for Adaptive Systems : Estimation. *Proceedings of the IEEE*, Vol. 64:1126–1143.
- Lee, G. H. 1994. *Least-Squares and Minimax Methods for Filtering, Identification and Detection*. PhD thesis, University of California, Los Angeles.
- Limebeer, D. and G. Halikias 1988. A Controller Degree Bound for Hinf Problems of the Second Kind. *SIAM Journal of Control and Optimization*, Vol. 26, No. 3:646–677.
- Limebeer, D. J. N., B. D. O. Anderson, P. P. Khargoneger, and M. Green 1992. A Game Theoretic Approach to \mathcal{H}_∞ Control for Time-Varying Systems. *SIAM Journal of Control and Optimization*, Vol. 30, No. 2:262–283.
- Liporace, L. A. 1971. Variance of Bayes Estimates. *IEEE Transactions on Information Theory*, Vol. 17:665–669.
- Macfarlane, A. G. J. and N. Karcanias 1976. Poles and Zeros of Linear Multivariable Systems: A Survey of the Algebraic, Geometric and Complex-variable Theory. *International Journal of Control*, Vol. 24, No. 1:33–74.
- Mageirou, E. F. 1976. Values and Strategies for the Infinite Time Linear Quadratic Games. *IEEE Transactions on Automatic Control*, Vol. 21, No. 9:547–550.

- Magill, D. T. 1965. Optimal Adaptive Estimation of Sampled Processes. *IEEE Transactions on Automatic Control*, Vol. 10:434–439.
- Malladi, D. P. and J. L. Speyer 1996. A Generalized Shiriyayev Sequential Probability Ratio Test for Change Detection and Isolation. In *Proceedings of the 35th Conference on Decision and Control*. IEEE.
- Malladi, D. P. and J. L. Speyer 1997. A Generalized Shiriyayev Sequential Probability Ratio Test for Change Detection and Isolation. Submitted for publication in the *IEEE Transactions on Automatic Control*.
- Mangoubi, R. S. 1995. *Robust Estimation and Failure Detection for Linear Systems*. PhD thesis, Department of Aeronautics and Astronautics, Massachusetts Institute of Technology, Cambridge, MA.
- Mangoubi, R. S., B. D. Appleby, and G. C. Verghese 1994. Stochastic Interpretation of \mathcal{H}_∞ and Robust Estimation. In *Proceedings of the 33rd Conference on Decision and Control*, pages 3943–3948. IEEE.
- Massoumnia, M.-A. 1986. A Geometric Approach to the Synthesis of Failure Detection Filters. *IEEE Transactions on Automatic Control*, Vol. AC-31, No. 9:839–846.
- Massoumnia, M.-A., G. C. Verghese, and A. S. Willsky 1989. Failure Detection and Identification. *IEEE Transactions on Automatic Control*, Vol. AC-34, No. 3:316–321.
- Maybeck, P. S. and P. D. Hanlon 1995. Performance Enhancement of a Multiple Model Adaptive Estimator. *IEEE Transactions on Aerospace and Electronic Systems*, Vol. 31:1240–1253.
- Mehra, R. K. and A. E. Bryson 1968. Linear Smoothing Using Measurements Containing Correlated Noise with an Application to Inertial Navigation. *IEEE Transactions on Automatic Control*, Vol. AC-13, No. 5:496–503.

- Menke, T. E. and P. S. Maybeck 1995. Sensor/Actuator Failure Detection in the Vista F-16 by Multiple Model Adaptive Estimation. *IEEE Transactions on Aerospace and Electronic Systems*, Vol. 31:1218–1228.
- Mills, R. A. and A. E. Bryson 1994. Calculus of Variations Derivation of the Minimax Linear-Quadratic (\mathcal{H}_∞) Controller. *AIAA Journal of Guidance, Control, and Dynamics*, Vol. 17, No. 1:153–160.
- Moore, B. C. and A. J. Laub 1978. Computation of Supremal (A,B)-Invariant and Controllability Subspaces. *IEEE Transactions on Automatic Control*, Vol. AC-23, No. 5.
- Moylan, P. J. and J. B. Moore 1971. Generalizations of Singular Optimal Control Theory. *Automatica*, Vol. 7:591–598.
- Oshman, Y. and I. Y. Bar-Itzhack 1985. Eigenfactor Solution of the Matrix Riccati Equation - A Continuous Square Root Algorithm. *IEEE Transactions on Automatic Control*, Vol. AC-30, No. 10:971–978.
- Ozçetin, H., A. Saberi, and P. Sannuti 1992. Design for \mathcal{H}_∞ Almost Disturbance Decoupling Problem with Internal Stability via State or Measurement Feedback - Singular Perturbation Approach. *International Journal of Control*, Vol. 55, No. 4:901–944.
- Patton, R. J. and J. Chen 1992. Robust Fault Detection of Jet Engine Sensor Systems Using Eigenstructure Assignment. *AIAA Journal of Guidance, Control, and Dynamics*, Vol. 15, No. 6.
- Rhee, I. and J. L. Speyer 1991. A Game Theoretic Approach to a Finite-Time Disturbance Attenuation Problem. *IEEE Transactions on Automatic Control*, Vol. AC-36, No. 9:1021–1032.
- Rugh, W. J. 1996. *Linear System Theory*. Prentice-Hall Inc., 2nd edition.

- Saberi, A., Z. Lin, and A. A. Stoorvogel 1995. \mathcal{H}_2 Almost Disturbance Decoupling Problem with Internal Stability. In *Proceedings of the American Control Conference*, pages 3414–3418, Seattle, WA.
- Saif, M. and Y. Guan 1993. A New Approach to Robust Fault Detection and Identification. *IEEE Transactions on Aerospace and Electronic Systems*, Vol. AES-29, No. 3:685–695.
- Schumacher, J. M. 1983. The Role of the Dissipation Matrix in Singular Optimal Control. *System and Control Letters*, Vol. 2, No. 3:262–266.
- Schumacher, J. M. 1985. A Geometric Approach to the Singular Filtering Problem. *IEEE Transactions on Automatic Control*, Vol. AC-30, No. 11:1075–1082.
- Shaked, U. 1990. \mathcal{H}_∞ -Minimum Error State Estimation of Linear Stationary Processes. *IEEE Transactions on Automatic Control*, Vol. AC-35, No. 5.
- Sobel, K. M. and F. J. Lallman 1989. Eigenstructure Assignment for the Control of Highly Augmented Aircraft. *AIAA Journal of Guidance, Control, and Dynamics*, Vol. 12, No. 3.
- Speyer, J. L. 1979. Computation and Transmission Requirements for a Decentralized Linear-Quadratic-Gaussian Control Problem. *IEEE Transactions on Automatic Control*, Vol. AC-24, No. 2.
- Stoorvogel, A. A. 1991. The Singular \mathcal{H}_∞ Control Problem with Dynamic Measurement Feedback. *SIAM Journal of Control and Optimization*, Vol. 29, No. 1:160–184.
- Sutton, G. P. 1986. *Rocket Propulsion Elements: An Introduction to the Engineering of Rockets*. Wiley-Interscience, 5th edition.
- Tahk, M. and J. L. Speyer 1987. Modeling of Parameter Variations and Asymptotic LQG Synthesis. *IEEE Transactions on Automatic Control*, Vol. AC-32, No. 9.

- Viswanadham, N. and K. D. Minto 1988. Robust Observer Design with Application to Fault Detection. In *Proceedings of the American Controls Conference*, pages 1393–1399, Atlanta, GA.
- White, J. E. and J. L. Speyer 1987. Detection Filter Design: Spectral Theory and Algorithms. *IEEE Transactions on Automatic Control*, Vol. AC-32, No. 7:593–603.
- Willems, J., A. Dittapçı, and L. M. Silverman 1986. Singular Optimal Control: A Geometric Approach. *SIAM Journal of Control and Optimization*, Vol. 24, No. 2:323–337.
- Willems, J. C. 1981. Almost Invariant Subspaces: An Approach to High Gain Feedback Design – Part I: Almost Controlled Invariant Subspaces. *IEEE Transactions on Automatic Control*, Vol. AC-26, No. 1:235–252.
- Willsky, A. S., M. G. Bello, D. A. Castanon, B. C. Levy, and G. C. Verghese 1982. Combining and Updating of Local Estimates and Regional Maps Along Sets of One-Dimensional Tracks. *IEEE Transactions on Automatic Control*, Vol. AC-27, No. 4:799–813.
- Wonham, W. M. 1985. *Linear Multivariable Control: A Geometric Approach*. Springer-Verlag, New York, 3rd edition.
- Yaesh, I. and U. Shaked 1993. Game Theory Approach to Finite-Time Horizon Optimal Estimation. *IEEE Transactions on Automatic Control*, Vol. 38, No. 6:957–963.